

AD-A043 977

TERRA TEK INC SALT LAKE CITY UTAH

F/G 18/3

MATERIAL PROPERTIES OF NEVADA TEST SITE TUFF AND GROUT - WITH E--ETC(U)

NOV 76 S W BUTTERS, R K DROPEK, A H JONES

DNA001-75-C-0260

UNCLASSIFIED

TR-76-63

DNA-4235F

NL

1 OF 5
AD
A043977



ADA 043977

12

DNA 4235F

MATERIAL PROPERTIES OF NEVADA TEST SITE TUFF AND GROUT-WITH EMPHASIS ON THE MIGHTY EPIC EVENT

Terra Tek, Inc.
University Research Park
420 Wakara Way
Salt Lake City, Utah 84108

November 1976

Final Report for Period 1 April 1975—31 July 1976

CONTRACT No. DNA 001-75-C-0260

APPROVED FOR PUBLIC RELEASE;
DISTRIBUTION UNLIMITED.

THIS WORK SPONSORED BY THE DEFENSE NUCLEAR AGENCY
UNDER RDT&E RMSS CODE K400075462 J45GAXYX97308 H2590D.

Prepared for
Director
DEFENSE NUCLEAR AGENCY
Washington, D. C. 20305

DDC FILE COPY

DDC
RECEIVED
SEP 12 1977
RECEIVED
B

Destroy this report when it is no longer
needed. Do not return to sender.



UNCLASSIFIED

SECURITY CLASSIFICATION OF THIS PAGE (When Data Entered)

19 REPORT DOCUMENTATION PAGE		READ INSTRUCTIONS BEFORE COMPLETING FORM
1. REPORT NUMBER DNA 4235F	2. GOVT ACCESSION NO.	3. RECIPIENT'S CATALOG NUMBER
4. TITLE (and Subtitle) MATERIAL PROPERTIES OF NEVADA TEST SITE TUFF AND GROUT — WITH EMPHASIS ON THE MIGHTY EPIC EVENT.		5. TYPE OF REPORT & PERIOD COVERED Final Report for Period 1 Apr 75 — 31 Jul 76
7. AUTHOR(s) S. W./Butters, A. H./Jones R. K./Dropek		6. PERFORMING ORG. REPORT NUMBER TR-76-63
9. PERFORMING ORGANIZATION NAME AND ADDRESS Terra Tek, Inc. 420 Wakara Way, University Research Park Salt Lake City, Utah 84108		8. CONTRACT OR GRANT NUMBER(s) DNA 001-75-C-0260
11. CONTROLLING OFFICE NAME AND ADDRESS Director Defense Nuclear Agency Washington, D.C. 20305		10. PROGRAM ELEMENT, PROJECT, TASK AREA & WORK UNIT NUMBERS Subtask J45GAXYX973-08
14. MONITORING AGENCY NAME & ADDRESS (if different from Controlling Office)		12. REPORT DATE November 1976
		13. NUMBER OF PAGES 428
		15. SECURITY CLASS (of this report) UNCLASSIFIED
		15a. DECLASSIFICATION DOWNGRADING SCHEDULE
16. DISTRIBUTION STATEMENT (of this Report) Approved for public release; distribution unlimited.		
17. DISTRIBUTION STATEMENT (of the abstract entered in Block 20, if different from Report)		
18. SUPPLEMENTARY NOTES This work sponsored by the Defense Nuclear Agency under RDT&E RMSS Code K400075462 J45GAXYX97308 H2590D.		
19. KEY WORDS (Continue on reverse side if necessary and identify by block number) Nuclear Experiment Uniaxial Strain Hydrostatic Grout Load Pressure Tuff Tests		
20. ABSTRACT (Continue on reverse side if necessary and identify by block number) Material properties testing has been conducted for the Defense Nuclear Agency Field Command. The testing was in support of the Nevada Test Site nuclear test program and covered the period 1 April 1975 through 31 July 1976. The contract number was DNA001-75-C-0260 with Mr. J. W. LaComb as the Contracting Officer Representative. other side		

DD FORM 1 JAN 73 1473

EDITION OF 1 NOV 65 IS OBSOLETE

UNCLASSIFIED

SECURITY CLASSIFICATION OF THIS PAGE (When Data Entered)

389 155

UNCLASSIFIED

SECURITY CLASSIFICATION OF THIS PAGE(When Data Entered)

20. ABSTRACT (Continued)

→ The primary task during this period was material evaluations for the Mighty Epic event (both preshot and postshot). Tuff, grout, sand, concrete, concrete-steel interfaces and steel were tested. Other material evaluations and analyses during this period were for 1) the "two-in-one concept" -- a proposed plan to use a common tunnel and equipment for two nuclear events, 2) determining the influence of fracturing on ultrasonic velocities to help explain field seismic and sonic velocity results, 3) obtaining the angles-of-internal-friction in the tuff as a function of confining pressure for use in material modeling, 4) determining and evaluating methods for extracting pore water for subsequent chemical analysis, 5) measuring the effect of hydrostatic pressure (i.e. grain size distributions, cohesion, etc.) on sand-water mixtures, 6) evaluating currently used and proposed methods for obtaining the elastic moduli needed to determine *in situ* stress from tuff overcore samples, and 7) evaluating the possibility of resaturating dry tuff core samples for obtaining material properties representative of the original saturated material and for evaluating the likelihood of water invasion into core samples during the field coring process. ↗

UNCLASSIFIED

SECURITY CLASSIFICATION OF THIS PAGE(When Data Entered)

PREFACE

The authors would like to express their thanks for the guidance of Mr. J. W. LaComb and to Mr. C. N. Snow for his assistance with geology and core samples.

ACCESSION for	
NTIS	White Section <input checked="" type="checkbox"/>
DOC	Buff Section <input type="checkbox"/>
UNANNOUNCED	<input type="checkbox"/>
JUL 1 1964	
BY	
DISTRIBUTION/AVAILABILITY CODES	
Date	
SPECIAL	
A	

TABLE OF CONTENTS

	<u>Page</u>
Preface	1
Table of Contents	2
Introduction	5
Mighty Epic Event	11
Material Properties for Mighty Epic Interface Experiment	13
Some Comments on Mighty Epic Material Properties	35
Physical and Mechanical Properties of Several Grout Mixtures	47
Material Properties on Samples from Mighty Epic Drill Holes U12n.10 UG#4, U12n.10 UG#6a and U12n.10 UG#7	53
Some Material Properties on Core Samples from Several Drill Holes Relating to the Mighty Epic Event	79
Some Mechanical Properties of Concrete, Steel and Concrete- Steel Interfaces Used in Mighty Epic Structures	117
Characterization of Tuff and Development of Grouts for Mighty Epic Structures Program	143
Properties of U12n.10 MH#2 and MH#3 Core Samples	205
Miscellaneous Mighty Epic Properties	213
Ming Blade Event	243
Miscellaneous Core Sample Properties	245
Investigation of the Effect of Fracturing on the Ultrasonic Velocities in Ash-Fall Tuff	255
Nevada Test Site "Two-In-One Concept" Evaluation: Comparison of Preshot and Postshot Material Properties	291
Determination of the Angle-of-Internal Friction for NTS Tuffs	351
Water Extraction from Nevada Test Site Tuffs	367

	<u>Page</u>
Hydrostatic Response of a Water Saturated Sand	389
Laboratory Determination of the Elastic Modulus of Stress-Relief Overcores	399
Specific Moisture Retention of Nevada Test Site Tuffs	437

INTRODUCTION

The Defense Nuclear Agency (DNA) nuclear test program at the Nevada Test Site requires, among many things, the mechanical and physical properties of the construction material and rock at the test location. The material properties are needed primarily for the purpose of evaluating the potential for successful stemming and containment of the nuclear tests. They are also used in modeling material behavior in subsequent ground motion calculations for predicting and evaluating experimental programs.

This report summarizes material evaluations conducted by Terra Tek over a period of 16 months (April 1975 through July 1976) for DNA Test Command. The primary task during this period was material evaluations for the Mighty Epic event (both preshot and postshot). Tuff, grout, sand, concrete, concrete-steel interfaces and steel were tested. Other material evaluations and analyses during this period were for 1) the "two-in-one concept" -- a proposed plan to use a common tunnel and equipment for two nuclear events, 2) determining the influence of fracturing on ultrasonic velocities to help explain field seismic and sonic velocity results, 3) obtaining the angles-of-internal-friction in the tuff as a function of confining pressure for use in material modeling, 4) determining and evaluating methods for extracting pore water for subsequent chemical analysis, 5) measuring the effect of hydrostatic pressure (i.e. grain size distributions, cohesion, etc.) on sand-water mixtures, 6) evaluating currently used and proposed methods for obtaining the elastic moduli needed to determine *in situ* stress from tuff overcore samples, and 7) evaluating the possibility of resaturating dry tuff core samples for obtaining material properties representative of the original saturated material and for evaluating the likelihood of water invasion into core samples during the field coring

process. During the contract period, reports were distributed on each of these tasks. All those reports are reproduced here as originally distributed. As an introduction a synopsis (in some cases, the abstract from the report) of the testing and analysis for each task is provided here.

Mighty Epic Event: The Mighty Epic event included, in addition to the standard "Line-of-Site-Pipe", a number of structures and an experiment to evaluate movement along a material discontinuity (this discontinuity has been referred in the past as the "interface"). The discontinuity was a change from tuff material to a much harder and competent paleozoic material. The structures experiment required extensive tuff characterization, both for design of the experiments and to facilitate development of a grout which closely matched selected tuff properties. Other structures materials evaluated were concrete, concrete/steel and steel. For the interface experiment, direct shear tests were conducted to define the frictional properties. Magnetic characterization of core samples were also needed to assist in analyzing post-shot movement at the interface.

Reports describing the above work are:

Material Properties for Mighty Epic Interface Experiment, June 1975,
TR 75-36

Some Comments on Mighty Epic Material Properties, August 1975, TR
75-42

Physical and Mechanical Properties of Several Grout Mixtures, August
1975, TR 75-45

Material Properties on Samples from Mighty Epic Drill Holes U12n.10
UG#4, U12n.10 UG#6a and U12n.10 UG#7, September 1975, TR 75-50

Some Material Properties on Core Samples from Several Drill Holes
Relating to the Mighty Epic Event, November 1975, TR 75-64

Some Mechanical Properties of Concrete, Steel and Concrete-Steel
Interfaces Used in Mighty Epic Structures, July 1976, TR 76-14

Characterization of Tuff and Development of Grouts for Mighty Epic Structures Program, April 1976, TR 76-21

Letters or data forwarded which were not contained in the above reports

The report entitled "Characterization of Tuff and Development of Grouts for Mighty Epic Structures Program" is a summary of much of the Mighty Epic testing and contains the average material properties of the structures region along with the properties of the tuff matching grout -- ME8-11.

Investigation of the Effect of Fracturing on the Ultrasonic Velocities in Ash-Fall Tuff: The effect of fracturing on ultrasonic velocities in rock have been investigated. The material was an ash-fall tuff taken from the Nevada Test Site, Area 12. Fractures were generated in uniaxial load (compression) tests and direct shear tests. The results, in general, show the same trend as reported in other rock types: i.e., a decrease in both the p-wave (longitudinal) and s-wave (shear) velocities resulting from fracture initiation, extension and growth. The maximum observed change for the p-wave was ~25 percent, and ~10 percent for the s-wave.

Comparison of Preshot and Postshot Material Properties at the Nevada Test Site for the "Two-In-One Concept": This concept is one of locating a nuclear event in the same main drift but several hundred feet in the portal direction from a previous event. The concept results in substantial cost savings through reuse of a considerable amount of equipment (gas seal doors, cable access drifts, etc.)

Early evaluation of the concept required a close look at the tuff properties as a function of preshot versus postshot status and as a function of distance from the working points (i.e. the properties of the preshot tuff, at say 300 feet, were compared with the properties of postshot tuff at 300

feet). This comparison was necessary to evaluate potential "second event" locations and insure that the material surrounding this "second event" were effective for stemming and containment.

Determination of the Angle-Of-Internal-Friction for NTS Tuffs: Discussions with Joe LaComb, DNA Field Command, and inquiries from those doing calculations for design for tunnel structures in the tuffs have led to consideration of "Angle-of-Internal-Friction Models". Intuitive reasoning as well as data available indicate the ambiguity related to any estimate of angle-of-internal-friction for the intact tuffs. This brief write-up is an attempt to clarify the angle-of-internal-friction model for the tuffs and to help suggest what tests might be most suited to provide an adequate model.

Water Extraction from Nevada Test Site Tuffs: The hydrology of the Rainier Mesa, specifically "T" tunnel area at the Nevada Test Site, is of interest to the nuclear test program. Terra Tek has been actively developing methods for extracting water from core samples for subsequent chemical and mineralogical analysis. The development of consistent water data is dependent upon both the method of water extraction and sanitary laboratory conditions. The extraction method is critical since the bounded waters within the tuff may be extracted at different energy levels.

Hydrostatic Response of a Water Saturated Sand: Mixtures of sand and water have a number of Nevada Test Site applications, the majority of which directly relate to the stemming and containment of nuclear tests. Specific applications required knowing the affect on the sand water mixture of a hydrostatic pressure cycle.

Mixtures were subjected to a 4 kilobar hydrostatic pressure cycle followed by measurements of the sand grain size distribution and observations regarding the cohesion of the mixture (i.e. existence of "welding").

State of Stress Effects on Laboratory Determination of the Elastic Modulus of Stress-Relief Overcores: The U.S. Geological Survey has conducted *in situ* stress determinations under Rainier Mesa using the U.S. Bureau of Mines three-component borehole deformation overcore technique. The calculated *in situ* stress states are used to better quantify and understand containment phenomena. Since laboratory determined overcore elastic moduli are used for *in situ* stress calculations, a study of state of stress effects on the overcore elastic modulus was conducted. Normal tuff overcore laboratory testing has involved biaxial loading (radial pressurization with $\sigma_z = 0$) in which radial pressures of only 3.45 MPa (34.5 bars) were obtainable due to sample failure. Since Rainier Mesa *in situ* stresses have been calculated as being as high as 6.9 MPa (69 bars), testing techniques were evaluated which incorporated axial stresses to achieve 6.9 MPa radial pressure. Modulus errors caused by sample nonlinearity and a suggested laboratory technique are also discussed.

Specific Moisture Retention of Nevada Test Site Tuffs: Moisture was reintroduced into dry Nevada Test Site tuff core chips through placement in a high humidity (~95 to 100 percent) chamber at room temperature (~23°C) and atmospheric pressure (~650 mm). A minimum of 29 days was required for the dry samples to equal or exceed what was considered their *in situ* saturation levels (these *in situ* saturation levels were obtained from adjacent samples). Mechanical tests conducted subsequent to resaturation suggest that dried-resaturated samples can be used to obtain representative material properties for virgin saturated tuff.

Tuff samples, immediately sealed at the Nevada Test Site on removal from a core barrel, were subjected to the same environment to assist in analyzing the invasion of the drilling water. Test results to date are inconclusive.

Each report has been reproduced as originally distributed. Page numbers have been changed for continuity in this final report.

MIGHTY EPIC EVENT

Material Properties for Mighty Epic Interface Experiment

Some Comments on Mighty Epic Material Properties

Physical and Mechanical Properties of Several Grout Mixtures

Material Properties on Samples from Mighty Epic Drill Holes U12n.10 UG#4,
U12n.10 UG#6a and U12n.10 UG#7

Some Material Properties on Core Samples from Several Drill Holes
Relating to the Mighty Epic Event

Some Mechanical Properties of Concrete, Steel and Concrete-Steel
Interfaces Used in Mighty Epic Structures

Characterization of Tuff and Development of Grouts
for Mighty Epic Structures Program

Properties of U12n.10 MH#2 and MH#3 Core Samples

Miscellaneous Mighty Epic Properties

NOT
Preceding Page BLANK - FILMED

Progress Report One

MATERIAL PROPERTIES FOR MIGHTY EPIC INTERFACE EXPERIMENT

by

S. W. Butters
S. J. Green

Submitted to

Field Command
Defense Nuclear Agency
Nevada Test Site
Mercury, Nevada

Attn: Mr. J. W. LaComb

TR 75-36
June 1975

SUMMARY

Some physical and mechanical properties have been determined for material in the horizontal plane (along the LOS tunnel) and above and below the working point for the Mighty Epic Event in Area 12 at the Nevada Test Site. These tests were primarily used for site stemming and containment evaluation, and most of these data were included in a previous Terra Tek Report, TR 75-7 (January 1975).

At the meeting at the Nevada Test Site 16 June 1975, further material property tests were outlined to define better the "interface", and to determine the shear strength and the elastic constants (mainly velocities) for the material below the working point, down through the "interface" and on below. Once these data have been obtained, a better friction model for the interface and possible "layer configurations" to be used for calculations can be determined.

TABLE OF CONTENTS

Summary	14
List of Figures	16
List of Tables	16
Material Property Data Available	17
Best Estimate of Geologic Configuration	27
Material Property Data Needed for Interface Calculation	30
References	33

LIST OF FIGURES

<u>Figure</u>	<u>Description</u>	<u>Page</u>
1a	Plan View of Mighty Epic Region, Area 12, "N" Tunnel Complex	18
1b	Section View along the Mighty Epic Main Drift	18
1c	Section View along Mighty Epic Bypass Drift	18
2	Tests for Stemming and Containment Evaluation	19
3	Physical and Mechanical Properties Versus Drill Hole Footage Showing Lithological Zones for the UE12n #9 Drill Hole	22
4	Physical and Mechanical Properties Versus Drill Hole Footage Showing Lithological Zones for the U12n.10 UG#2 Drill Hole	23
5	Physical and Mechanical Properties Versus Drill Hole Footage Showing Lithological Zones for the U12n.10 UG#3 Drill Hole	24
6	Plan View of Mighty Epic Site Showing Location of Cross-Sections	27
7	Geology Shown in Cross-Section along the Mighty Epic Main Drift (Reference 4)	28
8	Geology Shown in Cross-Section Perpendicular to Mighty Epic Main Drift and through the Working Point (Reference 4)	28
9a	Anticipated Layer Configuration for a Section along the Mighty Epic Main Drift	31
9b	Anticipated Layer Configuration for a Section through the Working Point and Perpendicular to the Mighty Epic Main Drift	31

LIST OF TABLES

<u>Table</u>	<u>Description</u>	<u>Page</u>
1	Tabulated Test Data for Stemming and Containment Evaluation	20
2	Tabulated Test Data for Preliminary Evaluation	25
3	Terra Tek Core Sample Inventory	32

MATERIAL PROPERTY DATA AVAILABLE

Location of Drill Holes: A first set of data were generated primarily for exploratory stemming and containment site evaluation, while a second set of data were a preliminary evaluation of the material below the working point. The drill holes from which samples were obtained for the two sets of data were: (1) U12n.05 UG#4, U12n.10 UG#1 and UE12n #8, and (2) U12n.10 UG#2, U12n.10 UG#3 and UE12n #9, respectively. The approximate locations of these drill holes are indicated on the map of the Mighty Epic region in the "N" Tunnel complex of Area 12, as shown in Figure 1.¹

The drill holes U12n.05 UG#4 and U12n.10 UG#1 are horizontal drill holes in the plane of the working point, and UE12n #8 and UE12n #9 are vertical drill holes from the mesa surface. The U12n.10 UG#2 and UG#3 drill holes were collared back from the working point in the main drift and extended downward to make contact with the beds below the working point. A drill hole designated U12n.10 UG#5 was drilled downward, from the bypass drift at a lesser angle than the UG#2 and UG#3 to give an indication of the layering below and past the working point. No physical or mechanical properties data have been generated to date from this drill hole.

Tests on Cores: The U12n.05 UG#4, U12n.10 UG#1 and UE12n #8 core samples were tested in September 1974, January 1975, and December 1973 respectively.² The UE12n #9, U12n.10 UG#2 and U12n.10 UG#3 core samples were all tested in May 1975.

Tests for this first set of data for the U12n.05 UG#4, U12n.10 UG#1 and UE12n #8 core samples include hydrostatic compression tests, uniaxial strain tests, ultrasonic velocity measurement and physical property measurements as shown in Figure 2 and Table 1. Tests for the second set of data

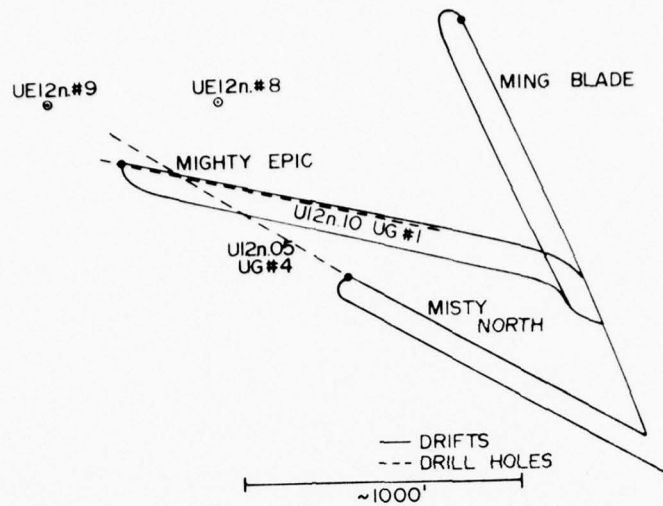


Figure 1a. Plan View of Mighty Epic Region, Area 12, "N" Tunnel Complex

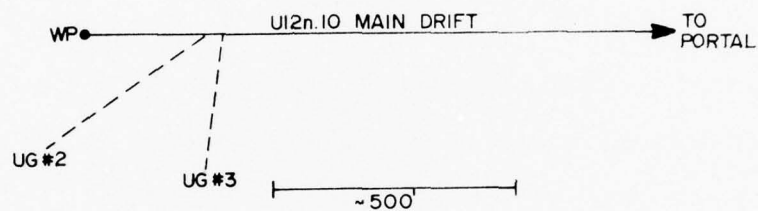


Figure 1b. Section View along the Mighty Epic Main Drift

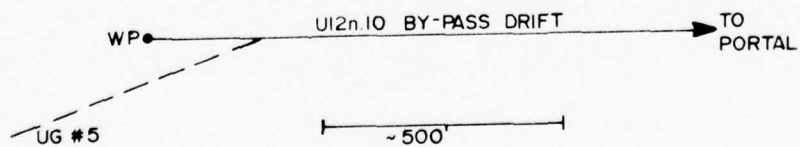


Figure 1c. Section View along Mighty Epic Bypass Drift

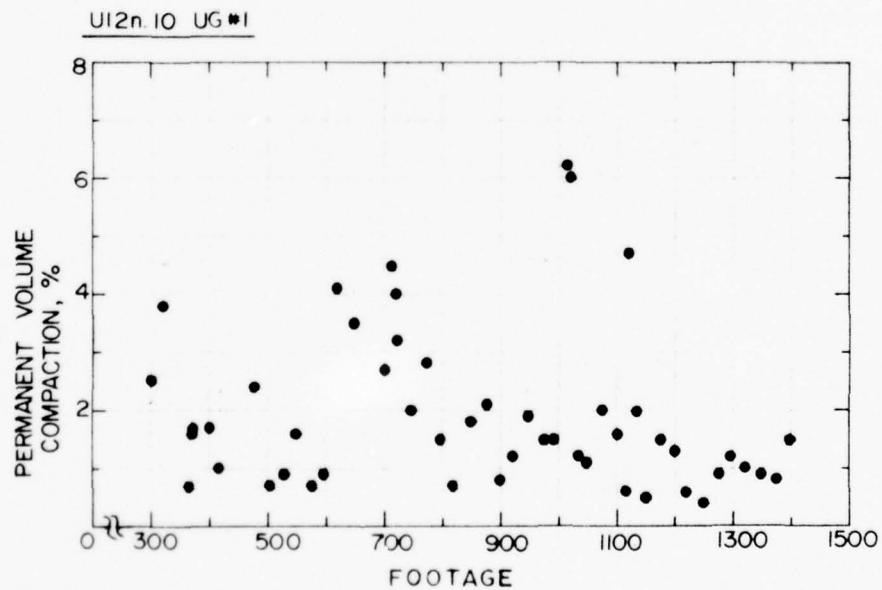
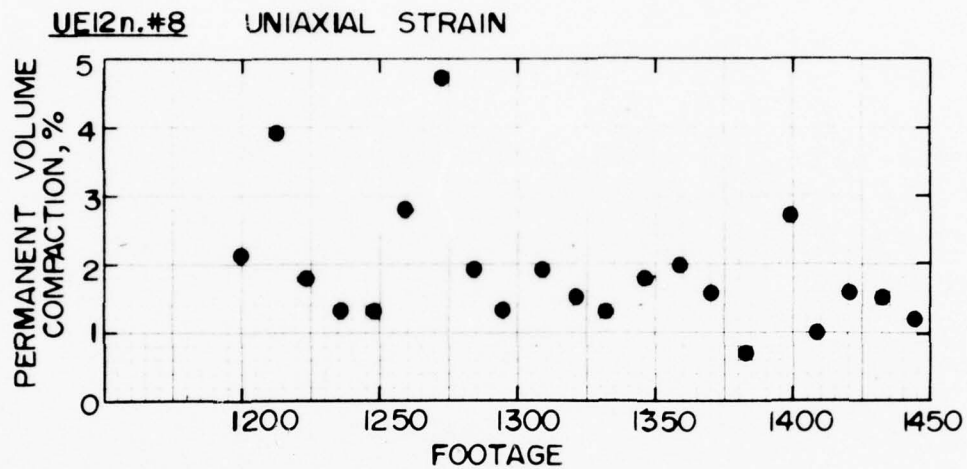
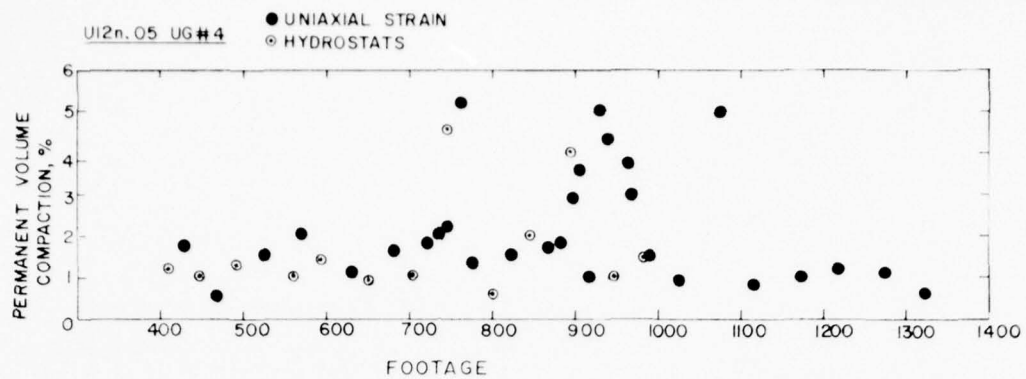


Figure 2. Tests for Stemming and Containment Evaluation

TABLE 1. TABULATED TEST DATA FOR STEMMING AND CON-TAINMENT EVALUATION

DRILL HOLE FOOTAGE	AS- RECEIVED	DENSITY (gm/cc)		WATER BY WET WEIGHT (%)	POROSITY (%)	SATURATION (%)	CALC AIR VOIDS (%)	MEAS PERMANENT COMP (%)	VELOCITY (ft/sec)	
		DRY	GRAIN						LONG	SHEAR
1200	1.98	1.61	2.43	19	34	100	0	2.1	1,510	3,080
1212	1.89	1.59	2.43	16	34	86	4.8	3.9	11,780	5,580
1224	1.95	1.68	2.43	14	31	87	3.9	1.8	9,320	4,130
1236	1.96	1.62	2.35	17	31	100	0	1.3	10,040	5,590
1247	1.95	1.56	2.33	20	33	100	0	1.3	8,660	3,710
1259	1.84	1.48	2.39	19	38	94	2.2	2.8	10,790	5,710
1272	1.79	1.40	2.42	22	42	93	2.9	4.7	8,470	3,710
1284	1.87	1.52	2.36	18	35	98	0.9	1.9	10,630	5,810
1295	1.80	1.44	2.39	20	40	90	4.0	1.9	9,560	3,970
1309	1.86	1.50	2.42	20	38	100	0	1.9	9,090	3,900
1321	1.95	1.58	2.43	19	35	100	0	1.5	8,830	4,000
1333	2.04	1.71	2.45	16	30	100	0	1.8	6,730	3,410
1346	1.91	1.50	2.48	21	39	100	0	2.0	8,590	4,070
1358	1.92	1.48	2.42	22	39	100	0	1.6	8,760	3,710
1371	1.90	1.48	2.42	22	39	100	0	1.6	8,760	3,710
1383	1.84	1.45	2.43	21	40	96	1.6	0.7	11,160	5,770
1397	1.85	1.48	2.41	20	39	96	1.7	2.7	9,840	5,150
1408	1.82	1.45	2.41	20	38	96	1.7	2.7	9,840	5,150
1421	1.86	1.49	2.40	20	38	98	0.7	1.6	8,890	4,430
1433	1.93	1.60	2.42	17	34	98	0.6	1.5	9,220	3,800
1445	1.93	1.59	2.45	18	35	98	0.8	1.2	8,630	3,350

DRILL HOLE FOOTAGE	AS- RECEIVED	DENSITY (gm/cc)		WATER BY WET WEIGHT (%)	POROSITY (%)	SATURATION (%)	CALC AIR VOIDS (%)	MEAS PERMANENT COMP (%)	VELOCITY (ft/sec)	
		DRY	GRAIN						LONG	SHEAR
1026.05 (Unstrained)	1.78	1.35	2.41	24	44	99	0.7	1.7	9600	4130
430	1.82	1.41	2.42	23	45	99	1.0	1.5	12200	5870
576	1.82	1.42	2.42	23	45	99	1.0	1.5	12200	5870
572	1.93	1.62	2.44	16	34	94	2.2	2.0	9350	4400
634	1.88	1.50	2.47	20	39	97	1.2	1.1	8630	3900
693	1.97	1.51	2.41	19	37	95	1.7	1.6	9470	4580
754	1.84	1.47	2.46	20	40	93	3.0	2.0	8450	4330
738	1.84	1.47	2.46	20	40	93	3.0	2.0	8450	4330
748	1.86	1.54	2.42	18	36	89	4.2	5.2	8200	3350
761	1.84	1.51	2.43	18	38	89	4.2	5.2	8660	4460
777	1.83	1.47	2.45	22	42	94	2.5	1.3	8630	4040
824	1.84	1.47	2.41	20	39	94	2.3	1.5	9840	5080
872	1.89	1.55	2.45	18	37	94	2.4	1.7	9380	4000
883	1.87	1.53	2.44	18	37	92	3.1	1.8	9640	4860
895	1.90	1.58	2.44	17	35	91	3.2	2.9	10170	4690
907	1.75	1.37	2.40	22	43	90	4.5	3.6	7513	3980
918	1.95	1.63	2.45	16	33	96	1.3	1.0	10830	6200
931	1.76	1.36	2.43	22	44	90	4.3	5.0	8690	4000
940	1.79	1.42	2.40	21	41	91	3.5	4.3	9940	5120
963	1.76	1.31	2.48	25	47	94	2.7	3.7	7410	3820
964	1.82	1.42	2.48	22	43	94	2.4	3.7	9550	4790
968	1.92	1.60	2.45	16	35	92	2.9	3.0	10370	5510
996	1.82	1.41	2.46	22	43	95	2.2	1.5	8960	4480
1023	2.01	1.71	2.45	14	30	99	0.2	0.9	10310	5110
1095	1.76	1.41	2.38	20.0	41	86	5.6	6.0	7800	3976
1119	1.95	1.63	2.43	16.4	33	97	1.0	0.8	10531	5786
1175	1.96	1.64	2.44	16.7	33	97	0.9	1.0	12499	6927
1212	1.92	1.58	2.43	18.0	36	96	1.4	1.1	10464	5446
1273	1.93	1.59	2.45	18.0	37	96	1.4	1.1	10827	5451
1322	1.96	1.67	2.47	15.0	32	94	2.0	0.6	10991	6113

DRILL HOLE FOOTAGE	AS- RECEIVED	DENSITY (gm/cc)		WATER BY WET WEIGHT (%)	POROSITY (%)	SATURATION (%)	CALC AIR VOIDS (%)	MEAS PERMANENT COMP (%)	VELOCITY (ft/sec)	
		DRY	GRAIN						LONG	SHEAR
1026.10 (Unstrained)	1.86	1.50	2.42	19.9	38	99	0.6	2.5	10,010	3,440
324	1.83	1.45	2.42	20.8	40	95	1.9	5.5	5,540	2,640
327	2.00	1.69	2.47	15.7	35	99	0.2	0.7	10,240	5,120
374	1.94	1.53	2.46	19.6	38	99	0.2	1.7	8,650	2,920
375	1.91	1.53	2.46	19.3	37	99	0.5	1.6	8,270	3,220
406	1.89	1.49	2.49	21.0	40	99	0.3	1.7	7,540	2,360
419	1.96	1.66	2.47	15.3	33	92	2.7	1.0	8,100	2,890
457	1.95	1.61	2.45	17.1	34	97	1.2	2.4	9,740	5,080
507	1.95	1.61	2.45	17.1	34	97	1.2	2.4	9,740	5,080
527	1.93	1.58	2.47	18.1	36	96	0.6	0.7	10,490	5,740
551	1.88	1.54	2.46	18.1	38	91	3.5	1.6	11,140	6,820
558	1.97	1.64	2.53	17.5	35	99	0.4	1.6	8,100	4,040
598	1.97	1.64	2.53	17.5	35	99	0.4	1.6	10,890	5,510
619	1.78	1.35	2.49	24.2	42	94	2.2	0.9	8,560	3,970
651	1.90	1.56	2.48	17.9	37	91	3.3	1.6	10,280	5,270
703	1.82	1.39	2.49	17.8	43	98	1.0	2.7	8,160	3,870
715	1.71	1.40	2.40	21.2	42	97	3.2	3.5	8,285	4,509
722	1.85	1.51	2.42	18.5	38	97	0.7	1.0	10,110	5,410
725	1.81	1.43	2.48	20.9	42	90	4.4	4.0	9,280	4,650
748	1.85	1.42	2.52	23.3	44	99	0.6	2.0	8,530	3,870
775	1.87	1.44	2.52	23.3	44	99	0.9	2.8	10,970	6,170
799	2.02	1.68	2.55	16.8	34	99	0.9	0.9	8,430	3,920
824	2.08	1.78	2.57	14.6	31	97	0.3	0.3	11,860	6,720
849	1.91	1.53	2.49	19.8	38	99	0.8	1.8	8,990	3,920
875	1.84	1.39	2.57	24.7	46	99	0.5	2.1	9,840	3,940
901	1.92	1.52	2.56	21.0	41	99	0.5	2.8	8,430	3,920
926	1.85	1.58	2.52	19.4	37	99	0.3	1.9	10,170	5,180
950	1.88	1.55	2.42	17.4	36	91	3.3	1.9	10,170	5,180
975	1.88	1.49	2.51	21.2	41	98	0.9	1.5	8,690	3,610
993	1.91	1.58	2.46	18.3	38	98	0.8	1.5	8,894	4,318
995	1.80	1.46	2.41	19.1	40	87	5.3	---	9,510	4,530
1016	1.77	1.42	2.40	20.0	41	87	5.3	6.2	8,207	3,993
1024	1.82	1.47	2.45	19.3	40	88	4.9	6.0	8,273	3,870
1034	1.94	1.61	2.46	17.0	35	96	1.5	1.2	10,184	5,474
1050	1.87	1.48	2.49	20.9	40	97	1.4	1.1	8,230	3,800
1076	1.80	1.37	2.49	24.0	45	96	1.9	2.0	8,270	4,200
1103	1.86	1.57	2.57	19.9	39	99	0.2	1.6	9,550	4,720
1113	1.86	1.57	2.57	19.9	39	99	0.2	1.6	11,086	6,098
1126	1.76	1.38	2.43	27.6	43	88	5.4	4.7	11,250	4,260
1136	1.84	1.48	2.46	19.5	40	90	3.9	2.0	9,365	4,818
1149	1.82	1.45	2.45	25.9	43	96	1.3	0.5	11,150	6,330
1171	1.80	1.45	2.45	25.9	43	96	1.3	0.5	11,150	6,330
1201	1.80	1.53	2.46	15.6	36	97	1.2	1.5	10,230	5,160
1221	1.96	1.65	2.44	15.6	32	94	1.8	0.6	10,509	5,733
1255	2.02	1.72	2.45	24.1	45	98	0.7	---	10,700	5,760
1276	1.85	1.44	2.46	22.5	42	98	0.4	0.4	9,710	4,460
1299	1.93	1.57	2.47	18.8	37	99	0.4	1.2	9,350	4,860

for the UE12n #9, U12n.10 UG#2 and U12n.10 UG#3 core samples include uniaxial strain tests, physical property measurements and ultrasonic velocity measurements. These data are shown in Figures 3 through 5 and Table 2.

Variation through Beds: Figures 3 through 5 have been plotted such that the variation in several of the material properties can be seen as a function of distance along the drill hole. The different lithological beds along the drill hole are estimated from inspection of the cores (3), and are shown as dashed lines on the figures. The descriptions of each "layer" were those used at the meeting on 16 June at NTS. The next section discusses the layers in more detail.

UE12n#9

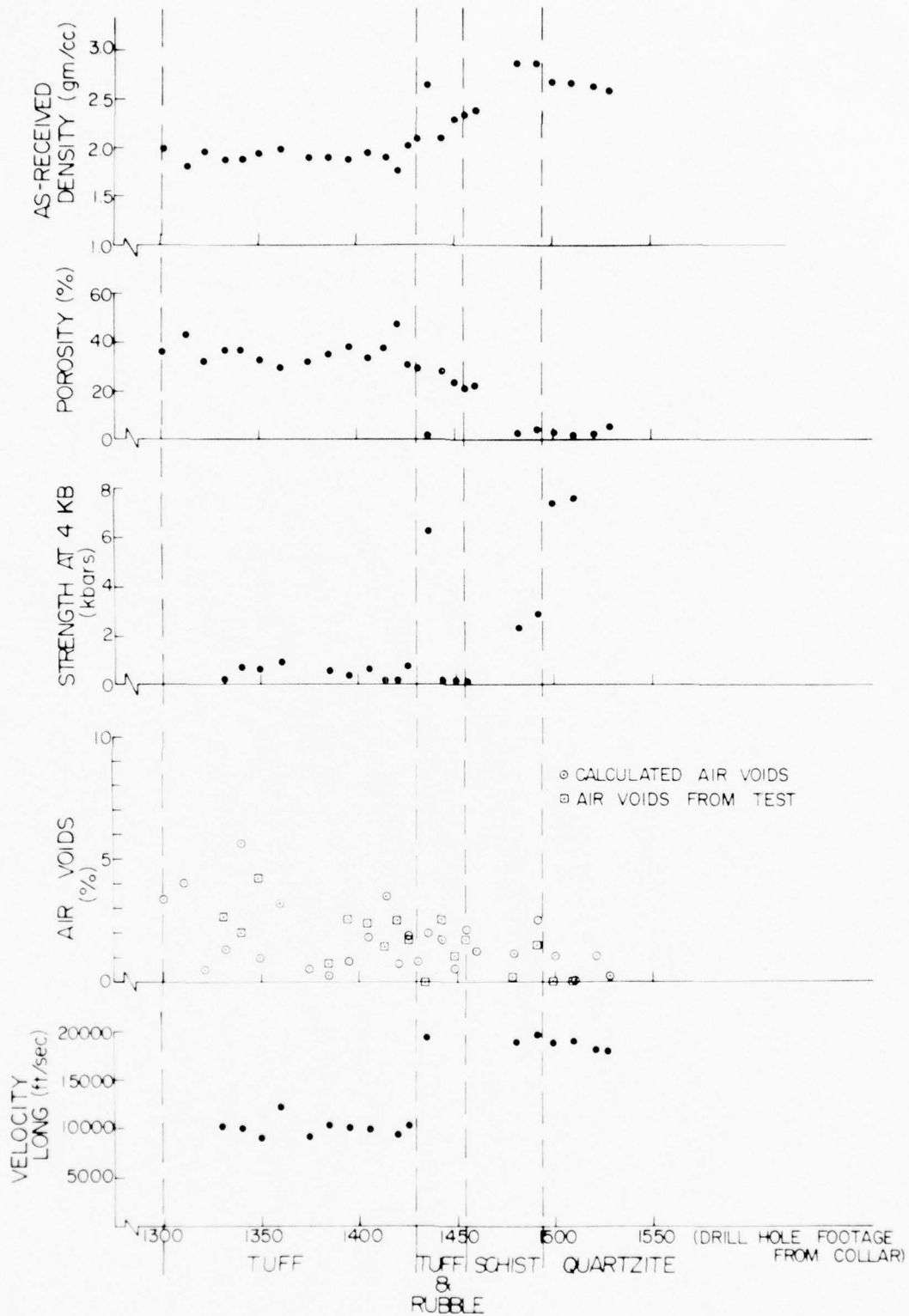


Figure 3. Physical and Mechanical Properties Versus Drill Hole Footage Showing Lithological Zones for the UE12n #9 Drill Hole

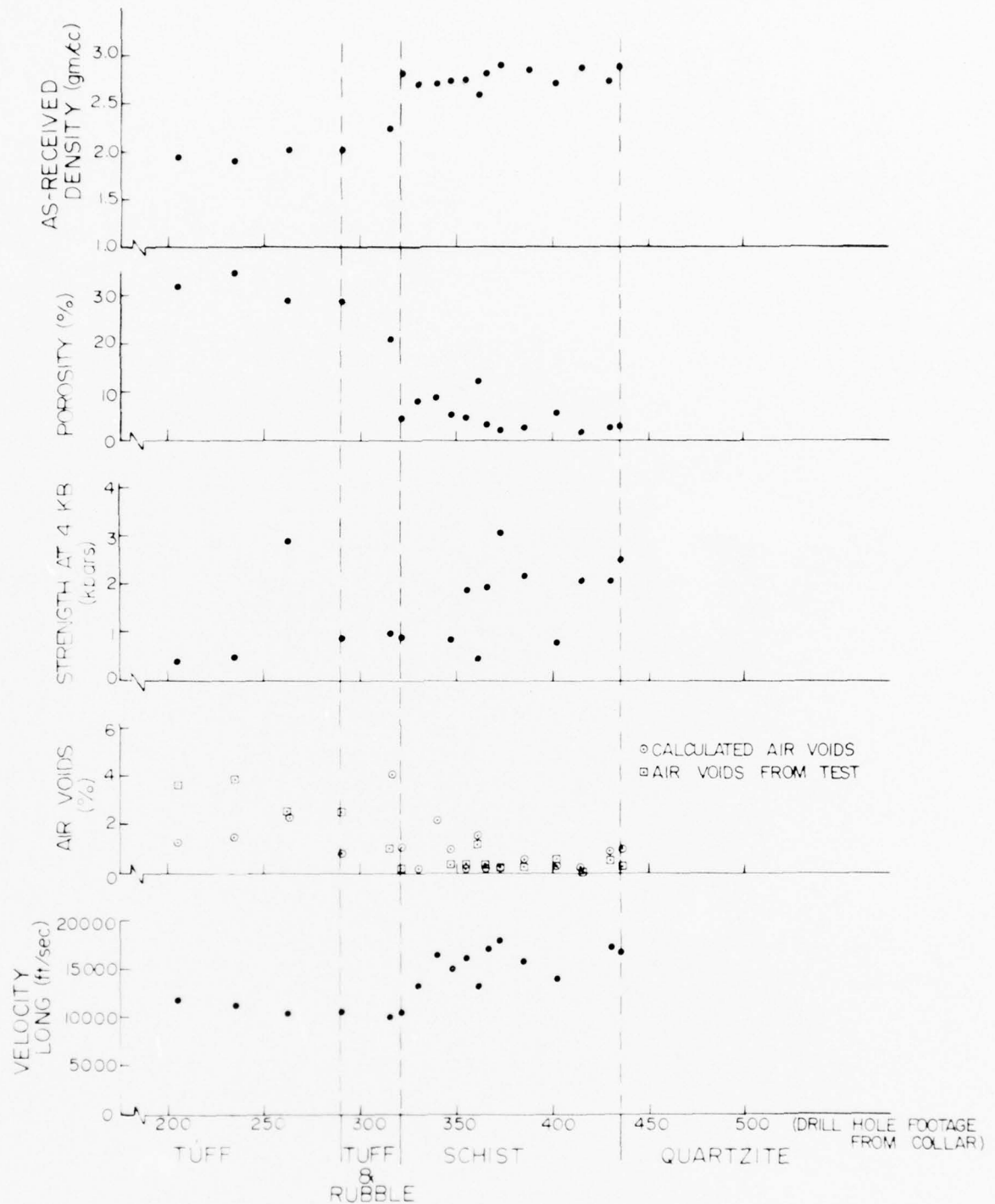


Figure 4. Physical and Mechanical Properties Versus Drill Hole Footage Showing Lithological Zones for the U12n.10 UG#2 Drill Hole

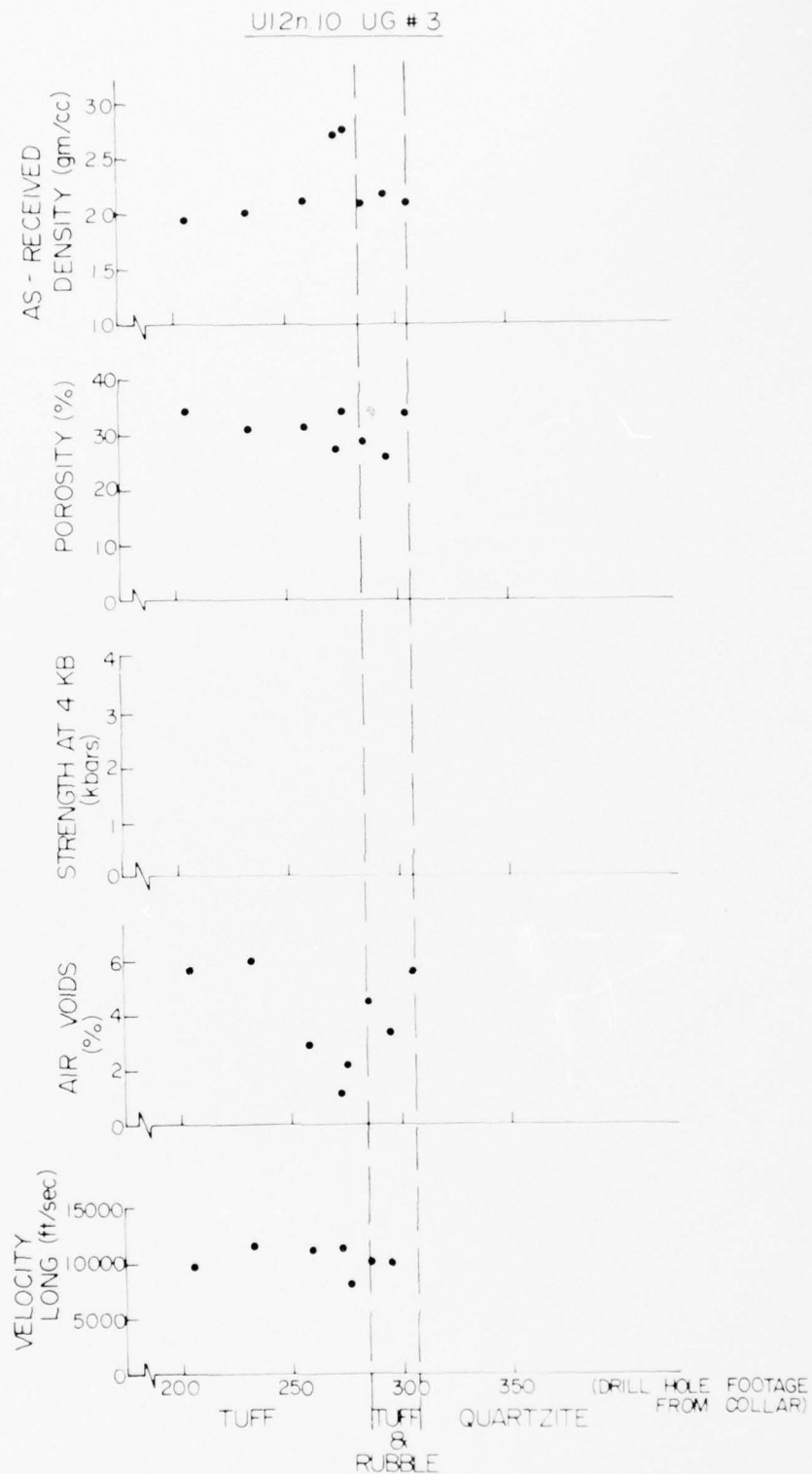


Figure 5. Physical and Mechanical Properties Versus Drill Hole Footage Showing Lithological Zones for the U12n.10 UG#3 Drill Hole

TABLE 2. TABULATED TEST DATA FOR PRELIMINARY EVALUATION.

UE12n #9

SAMPLE LOCATION (feet)	ROCK UNIT	DENSITY (g/cc)			POROSITY %	MOISTURE (Wet Wt. %)	SATURATION %	AIR Voids %	PERMANENT CONTRACTION %		ULTRASONIC VELOCITY ft./sec.		PERMEABILITY (darcies)	ATTENUATION LIMITS			STRENGTH AT 4 KB CONFINING PRESSURE
		As-Received	Dry	Grain					HYDRO	I-D	LONG	SHEAR		LL	PL	PI	
48	Tmr	2.23	2.07	2.50	17	7.4	96	0.7			11360	5680	0.01				
111		1.65	1.33			19.9							0.97				
146		1.85	1.44	2.48	42	22.4	99	0.6					1.35				
193				2.43		22.5											
222		1.57	1.14	2.31	50	27.3	85	7.5	10.3				2.18				.09
255		1.70	1.30	2.34	44	23.1	88	5.1					0.67				
275		1.83	1.42	2.36	37	19.0	94	2.4					0.77				
304		1.74	1.47	2.37	38	15.9	72	10.6					0.27				
327		1.88	1.53	2.36	35	18.5	99	0.4	4.5		6630	2250	0.65				.24
350		1.59	1.21	2.36	49	24.1	79	10.3					1.51				
372	Tt5	1.80	1.49	2.37	37	17.0	83	6.4	7.8				1.02				.26
396		1.72	1.30	2.39	46	24.8	93	3.1			7010	2440	1.46				
424		1.91	1.51	2.61	42	20.5	93	3.0					0.44				
451		1.55	1.12	2.35	53	28.1	83	8.8	5.4				1.11				.11
476		1.71	1.35	2.38	43	21.2	84	7.1	6.8				3.10				.14
510		1.89	1.58	2.39	34	16.5	93	2.5	3.5				0.89				.26
533		1.82	1.50	2.44	38	17.5	83	6.5					3.48				
564		1.86	1.49	2.38	37	20.0	99	0.2									
593		1.87	1.49	2.49	40	20.7	96	1.6					0.21				
616		1.64	1.11	2.46	55	32.6	98	1.0					0.22				
642	Tt4	1.71	1.30	2.37	45	24.2	92	3.8					4.00				
665		1.52	1.01	2.30	56	33.5	90	5.4					0.21				
690		1.57	1.21	2.31	48	22.9	76	11.6					0.40				
716		1.36	0.95	2.30	59	30.7	71	17.1					0.78				
746		1.50	1.00	2.33	57	33.2	87	7.5					0.85				
766		1.54	1.06	2.31	54	31.3	89	5.9					0.39				
790		1.61	1.19	2.39	50	26.1	84	8.1			5430	2320	0.39				
817		1.83	1.39	2.47	43	23.7	99	0.1			6170		0.20				
844		1.77	1.31	2.45	47	26.0	98	0.8					0.80				
899		1.79	1.42	2.49	43	20.9	87	5.5			10350	4490	0.36				
949	Tt3	1.55	1.20	2.39	50	22.9	72	14.2					0.27				
1000		1.57	1.07	2.41	56	30.6	84	8.9			6610	1960	0.41				
1050		1.80	1.40	2.45	43	22.2	94	2.7			12090	6050	0.23				
1106		1.55	1.62	2.50	35	17.3	95	1.7			9220	4670	0.01				
1154		1.78	1.51	2.43	38	15.4	72	10.5			8000	5440	0.23				
1205		1.82	1.37	2.52	46	24.7	98	0.7									
1253		1.99	1.69	2.47	32	14.9	94	2.1			8980	4240	0.01				
1300		1.98	1.65	2.57	36	16.4	91	3.3					6.70				
1311		1.80	1.42	2.45	43	21.7	92	4.0									
1321		1.95	1.63	2.40	32	16.3	98	0.5									
1331	Tt2	1.87	1.51	2.40	37	19.1	97	1.3	2.60		10160	5270					.19
1340		1.87	1.55	2.46	37	16.7	85	5.6	1.95		10350	5700					.68
1349		1.95	1.63	2.44	33	16.7	97	0.9	4.15		9060	4360					.62
1360		1.99	1.73	2.47	30	13.2	88	3.1	3.15		12200	6990					.93
1374		1.94	1.62	2.38	32	15.9	98	0.5			9230	4630					
1385		1.94	1.59	2.44	35	18.0	99	0.2	.70		10440	5510					.55
1395		1.88	1.51	2.43	38	19.7	98	0.8	2.50		10020	5000					.39
1405		1.94	1.62	2.44	34	16.4	95	1.8	2.35		10010	5470					.66
1413		1.89	1.54	2.49	38	18.3	91	3.4	1.40								.09
1419		1.76	1.28	2.48	48	27.1	99	0.7	2.50		9330	4120					.11
1425	Tuffa Rubble	2.02	1.73	2.51	31	14.6	94	1.8	1.60		10270	5140					.72
1430		2.11	1.81	2.59	30	13.9	97	0.8									
1436		2.66	2.66	2.72	2	00.2		1.9	0		19370	12490					6.28
1442		2.10	1.84	2.54	28	12.4	94	1.7	2.50								.18
1448		2.30	2.07	2.72	24	10.2	97	0.5	1.05								.19
1454		2.35	2.17	2.73	21	7.9	90	2.1	1.75								.10
1460		2.39	2.18	2.82	23	9.0	95	1.2									
1467				2.88		8.1											
1481		2.88	2.85	2.95	3	0.63	60	1.1	.20		18770	11920					2.28
1491		2.89	2.87	2.99	4	0.49	36	2.5	.15		19600	11400					2.88
1498	pale-ozotic (pEs)	2.68	2.65	2.75	3	0.93	70	1.0	0		18770	12470					7.40
1509		2.67	2.66	2.69	1	0.38	100	0	0		18920	12730					7.58
1521		2.64	2.63	2.69	2	0.37	60	1.0			17990	9780					
1527		2.58	2.53	2.67	5	1.89	95	0.2			17920	11320					

TABLE 2 (CONT)

U12n.10 UG#2

SAMPLE LOCATION (feet)	ROCK UNIT	DENSITY gm/cc			POROSITY %	MOISTURE CONTENT % (wet wt.)	SATURATION %	AIR VOIDS %	PERMANENT COMPACTION %		ULTRASONIC VELOCITY ft./sec.		PERMEABILITY (darcies)	ATTITUDE LIMITS			STRENGTH AT 4 yd CONFINING PRESSURE
		As-Received	Dry	Grain					HYDRO	I-D	LONG	SHEAR		LL	PL	PI	
29	Tt3	1.94	1.64	2.50	35	15.6	87	4.4		3.00	9020	4040					0.42
71		1.97	1.73	2.43	29	12.0	82	5.2		0.50	12200	6850					2.50
111		1.90	1.55	2.46	37	18.4	94	2.1		1.60	8910	3470					0.36
141		1.94	1.58	2.51	37	18.7	93	0.7		3.00	10650	5180					
170		2.15	1.98	2.46	20	8.1	88	2.4		0.70	13450	7920					1.65
206	Tt1	1.96	1.65	2.44	32	15.7	96	1.3		3.60	11830	6910					0.41
236		1.93	1.60	2.45	35	17.1	96	1.5		3.90	11340	5420					0.50
262		2.01	1.74	2.46	29	13.3	92	2.4		2.50	10470	4810					2.90
290		2.03	1.75	2.47	29	13.8	97	0.8		0.50	10670	6510					0.92
316		2.26	2.08	2.65	21.0	7.8	81	4.1		1.00	10150	4990					1.00
321	Tuff & Rubble	2.82	2.79	2.92	4.4	1.2	75	1.1		0.15	16380	9090					0.93
330		2.71	2.63	2.86	8.0	2.9	98	0.2			13410	5620					
339		2.73	2.66	2.91	8.7	2.4	75	2.2			16640	9080					
347		2.75	2.71	2.85	5.0	1.5	80	1.0		0.35	15010	9010					0.90
355		2.76	2.72	2.85	4.7	0.6	96	0.2		0.25	16170	9230					1.90
361	Schist (Ewc)	2.61	2.51	2.85	12.0	4.1	88	1.6		1.20	13470	8770					0.47
366		2.83	2.80	2.89	3.0	1.0	98	0.1		0.20	17340	10160					1.95
373		2.91	2.89	2.95	2.0	0.6	88	0.2		0.15	18040	9890					3.10
385		2.86	2.84	2.91	2.6	0.7	77	0.6		0.25	15870	8910					2.20
401		2.73	2.67	2.84	5.7	2.0	95	0.3		0.50	14130	7290					0.80
414	quartzite (pfs)	2.88	2.86	2.91	1.7	0.6	91	0.2		0.07	17490	9920					2.10
430		2.75	2.73	2.91	2.6	0.6	64	0.9		0.05	17560	10170					2.10
435		2.89	2.87	2.96	2.8	0.6	62	1.0		0.20	16890	9050					2.52
481				2.94													

U12n.10 UG#3

SAMPLE LOCATION (feet)	ROCK UNIT	DENSITY gm/cc			POROSITY %	MOISTURE CONTENT % (wet wt.)	SATURATION %	AIR VOIDS %	PERMANENT COMPACTION %		ULTRASONIC VELOCITY ft./sec.		PERMEABILITY (darcies)	ATTITUDE LIMITS			STRENGTH AT 4 yd CONFINING PRESSURE
		As-Received	Dry	Grain					HYDRO	I-D	LONG	SHEAR		LL	PL	PI	
29	Tt3	1.85	1.50	2.42	38	19.0	92	2.9			8810	4270					
62		2.03	1.79	2.39	25	11.9	95	1.1			11280	6580					
90		1.96	1.62	2.48	35	17.1	97	1.1			8090	4320					
122		2.00	1.69	2.47	32	15.7	99	0.3			10360	4920					
152		1.88	1.53	2.45	37	18.4	93	2.6			8540	3960					
170	Tt1	2.00	1.65	2.57	36	17.4	97	1.0			9580	3920					
205		1.96	1.68	2.54	34	14.4	84	5.6			9860	4050					
233		2.02	1.77	2.55	31	12.1	80	6.0			11540	6230					
258		2.13	1.85	2.68	31	13.3	91	2.9			11240	5680					
272		2.23	1.97	2.69	27	11.6	96	1.1			11440	5930					
276	Tuff & Rubble	2.03	1.71	2.60	34	15.8	94	2.2			8230	3700					
286		2.11	1.86	2.63	29	11.7	84	4.5			10270	5200					
294		2.18	1.95	2.64	26	10.4	87	3.4			10210	5140					
305		2.12	1.84	2.77	34	13.2	83	5.6									

BEST ESTIMATE OF GEOLOGIC CONFIGURATION

The geologic materials present below the working point, as indicated earlier in Figures 3 through 5, are tuff or tuffaceous sandstone (Tt_2), tuff and rubble, micaceous schist (ϵwc) and sterling quartzite ($p\epsilon s$).³ The tuff is a competent material with few fractures and little or no variation with depth. The tuff and rubble zone is a tuffaceous sandstone containing rubble, from millimeter to meter size, of quartzite and schist fragments. The micaceous schist layer is composed of an upper layer (approximately 10 to 15 feet) of highly weathered and fractured schist with reddish, silt-like material filling the cracks while the lower portion is much more competent and contains some tight fractures. The quartzite zone contains a considerable amount of fracturing, but most are considered tight with little or no filler material.

A plan view of the "Mighty Epic" site, Figure 6, shows the location and orientation of the two cross-sections shown in Figures 7 and 8. These

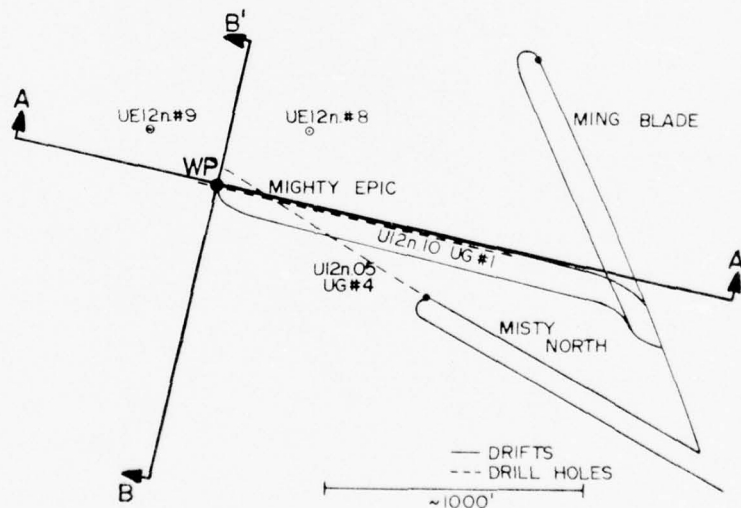
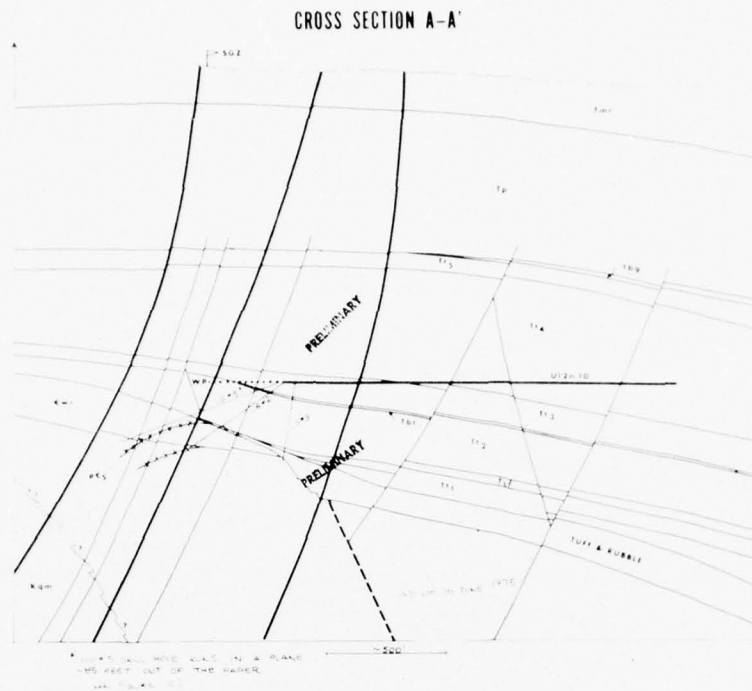


Figure 6. Plan View of Mighty Epic Site Showing Location of Cross-Sections



cross-sections were produced by United States Geological Survey⁴ and were preliminary as of 16 June 1975. More recent data from an exploratory drill hole,⁴ U12n.10 UG#5, suggests that the schist and quartzite layers dip to the north (approximately) -- see dashed and crossed line in Figure 7 -- contrary to what was initially presented.

MATERIAL PROPERTY DATA NEEDED FOR INTERFACE CALCULATION

Data Necessary: The purpose of the laboratory tests is to define the mechanical and physical properties of the various rock units (tuff, tuff and rubble, etc.) to then allow a recommendation of a layer configuration such as shown in Figure 9. The laboratory tests necessary on samples from each of the rock units are hydrostatic, triaxial compression, and possibly other load path tests, ultrasonic velocity measurements, and physical property measurements including densities and porosity. For the "interface", different tests will be needed to define a friction model, including direct-shear tests. Some of these data have already been generated. Further tests are necessary, however, to define the average *in situ* properties, especially in the case of the tuff and rubble and the upper schist zone. The tests will require special care in preparing test samples from the "worst" to the "best" material to subsequently define the average and the lower and upper bounds of the material properties.

Cores Required: A survey was made to determine what portion of the original core samples received at Terra Tek were available for added testing. Table 3 gives a list of this information. There are adequate core samples in the tuff, lower schist and the quartzite layers, but essentially no samples in the "tuff and rubble" and the upper schist layers. A minimum of three 12-inch long core samples in each of these two regions are considered necessary to characterize the material.

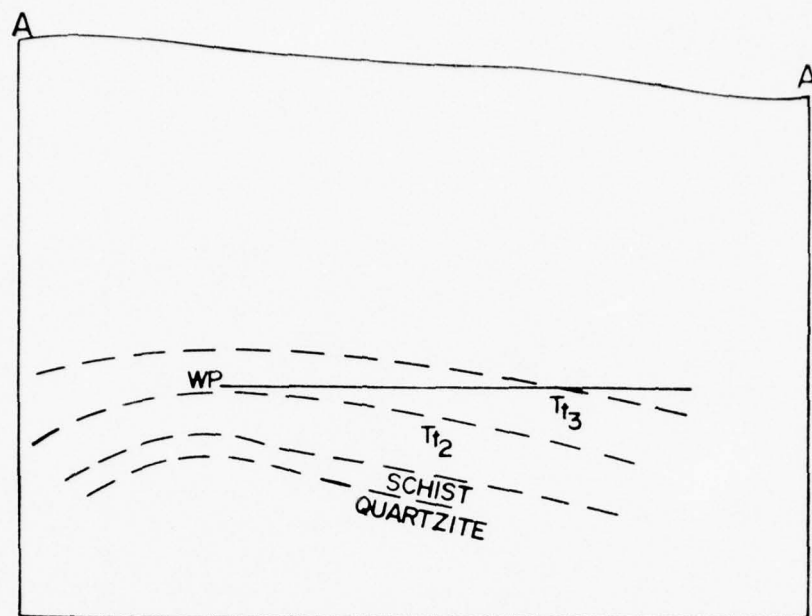


Figure 9a. Anticipated Layer Configuration for a Section along the Mighty Epic Main Drift

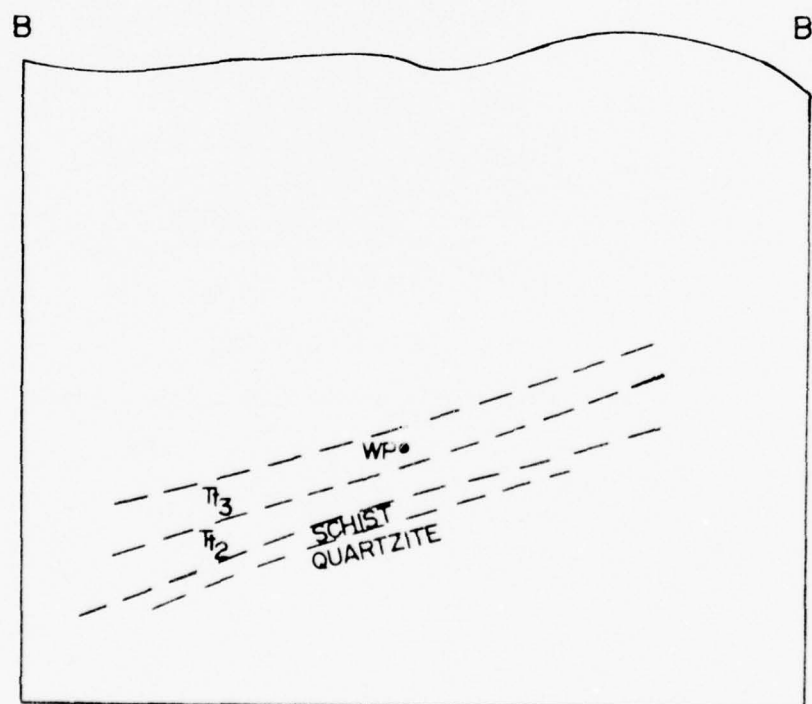


Figure 9b. Anticipated Layer Configuration for a Section through the Working Point and Perpendicular to the Mighty Epic Main Drift

TABLE 3. TERRA TEK CORE SAMPLE INVENTORY

Drill Hole	Rock Unit	Drill Hole Footage (feet)	Length (inches)	Number of Test Samples
U#12N #9	Tuff & Rubble	1436	2	none
		1442	0	none
	Schist	1454	2	none
		1481	4	1
	Paleozoic	1491	11	4
		1509	2	none
U12n.10 UG#2	Tt ₂	290	11	4
	Tuff & Rubble	316	3	1
		321	4	none
	Schist	330	0	none
		339	6	2
		347	2	none
		355	2	none
		361	7	2
		366	7	2
		374	6	2
		385	5	2
		402	3	1
		414	5	2
		431	0	none
		435	5	2
U12n.10 UG#3	Tt ₁	259	8	3
		273	7	2
		277	9	3
		286	12	4
	Tuff & Rubble	295	7	2
		305	5	1

REFERENCES

1. Communication with Cliff Snow, Nevada Test Site, Mercury, Nevada, January 1975-June 1975.
2. S. W. Butters, A. H. Jones, S. J. Green, "Properties of Quartzite from Area 12 of the Nevada Test Site", Terra Tek Report TR 75-7, January 1975.
3. Data provided by G. Fairier, United States Geological Survey; and J. W. LaComb, Nevada Test Site; May 1975.
4. Meeting at Nevada Test Site, Mercury, Nevada, 16 June 1975.

NOT
Preceding Page BLANK - FILMED

SOME COMMENTS ON
MIGHTY EPIC MATERIAL PROPERTIES

S. J. Green
S. W. Butters
J. N. Johnson
A. H. Jones

Submitted to:

Field Command
Defense Nuclear Agency
Nevada Test Site

Attn: Mr. Joseph LaComb

Contract DNA 001-75-C-0260

From

Terra Tek, Inc.
420 Wakara Way
Salt Lake City, Utah 84108

TR 75-42
August 1975

PREFACE

Some comments are made with regard to the Mighty Epic site material properties and to the associated structures calculational effort. These comments are made after meetings at NV00 on August 1, at Headquarters, DNA, August 8, and after discussions with Cliff McFarland and Kent Goering on August 12.

GENERAL DISCUSSION

Discussions between Ivan Sandler and Jim Johnson led to the presentation given by Ivan Sandler at the DNA meeting on August 8. The discussions between Jim and Ivan were conducted following the general ground rule that a "PW Capped Model" would be used to fit the Mighty Epic site tuffs for the "structure calculations". During the discussions between Jim and Ivan, representative stress-strain curves available on tunnel-bed tuffs from other sites were used for reference in the formulation of the cap model¹. Jim indicated that the Mighty Epic site had not yet been characterized and that more test data would be passed on to Ivan as they became available.

The cap model was developed knowing that certain phenomena, particularly those occurring after reaching the failure surface, would not be handled correctly. For example, the model was not intended to fit the apparent loss of strength which occurs as a test sample is unloaded via a constant axial strain path². (This is known to be an effect caused by the pore pressure³.) Secondly, it was intended that as more material property data for the Mighty Epic site became available, the parameters in the cap model would be readjusted to best represent the average properties of the site over the region of interest.

There are known phenomena that the "cap model formulated" does not fit, or handle properly. These include:

- details of the elastic-limit where crush-up begins⁴, which is complicated here by not knowing the *in situ* stress
- the difference between the apparent elastic constants obtained from the seismic velocities and from the slopes of the laboratory stress-strain curves⁵, i.e. the elastic constants obtained from the [longitudinal] seismic velocity and guessing the shear-wave velocity are "faired" into the elastic constants obtained from the slopes of the stress-strain curves
- pore pressure effects are not accounted for adequately^{2,3}
- the laboratory stress-strain curves are not fit beyond an initial loading (and to some extent unloaded) cycle^{2,6}
- the tensile and extension strength is not adequately handled⁷

The reason for not handling the above phenomena is probably due to a lack of material property data, rather than to any "shortcoming" of the cap model.

Some material property data on the Mighty Epic site has been presented previously in Terra Tek reports^{8,9}. Surprisingly, some cores from the region of the structures experiments exhibit quite high shear strength, up to 1.0 - 1.5 kilobars stress difference at multi-kilobar confining pressures; typical tunnel-bed tuffs show stress difference of about 0.3 kilobars at 1 kilobar confining pressure⁹. It is not clear why so many cores exhibit this high strength; Joe LaComb does not seem concerned with this, and I believe he feels that there may be relatively "thin" beds of this strong tuff.

At the NV00 meeting, some data were presented by Joe LaComb suggesting a low seismic velocity over parts of the Mighty Epic site. I believe Joe attributes this to stress relaxation surrounding the main and structures experiment tunnels¹⁰. Joe indicated he intends to conduct additional seismic surveys as well as hydraulic-fracturing and over-coring experiments to obtain more information about the *in situ* stress. The exact program he was going to conduct was not clear from the NV00 meeting, and no subsequent discussion was held. If this relaxation phenomenon is correct then the stresses around the structures tunnel is unknown. The *in situ* stress a few feet away from the scaled structures will not be well defined.

The "pressure range" for which the structures calculations will be most sensitive to the material properties (right around the structure) appears to be the following. For the spherical structures, collapse will likely occur at high pressures (maybe one kilobar) if at all; for the SRI structures, the porous concrete will collapse at stresses as low as about 0.1 kilobar (based on discussions at NV00). Therefore, "more detailed" strength of the tuff and the grout around the structures should be obtained over these pressure ranges.

Strength of the grout (to be used around the structures) is such that it will not match the strength of the tuff over pressure ranges from 0.1 to 1.0 kilobars^{11,12}. That is, if the angle of internal friction

of the grout is matched to that of the tuff in the zero to one or two-hundred bar pressure region, then the strength of the grout at higher confining pressures will be 1/2 to 1/3 that of the tuff (assuming the tuff strength is about 0.3 kilobars stress difference). On the other hand, if the angle of internal friction of the grout matches the tuff at the higher confining pressures, i.e. 0.5 - 1.0 kilobars pressure, then the strength of the grout at low pressure (one hundred bars) will be much greater than the tuff.

The differences in strength was discussed at the NVOO meeting, and it was Joe's opinion (I believe) that an economical (and pumpable) grout should be used to reasonably match the tuff. The strength of whatever grout used would be determined, and no further effort would be conducted to produce a "tuff matching" grout.

It is our feeling that because of the high water content in the grouts, the micro-mechanisms for deformation are different than in the tuff. In the tuffs, for example, we believe that through-going fracture-planes occur and sliding on the fracture-plane results. In the grout, a general collapse of the sample occurs without producing a through-going fracture-plane. This difference in micro-mechanisms leads us to believe that it is unlikely that pumpable grouts (50% water or thereabouts) can ever be made to match the tuff's strength properties over all pressure ranges.

Concretes used in the structures will undoubtedly behave as other cement-type materials do--reference, for example, the previous Terra Tek report on plain concrete¹³. The concretes will undoubtedly show increase in strength with confining pressure, collapse of the porous matrix, and complex post-maximum stress behavior. Furthermore, the concretes are likely to be strain-rate sensitive, exhibiting maybe a factor of two increase in strength for rapid loading as opposed to standard testing rate loadings¹⁴.

RECOMMENDATIONS

Terra Tek recommends the following with respect to the Mighty Epic Experiment materials characterization:

1. Some added tests should be performed to better characterize the tuffs from the working point out to the structures, and particularly in the regions of a few feet around the structures tunnels. These tests would determine the failure envelope and the stress-strain response up to about 1 kilobar.
2. For any calculations, the most representative material property data should be used to formulate the parameters in the cap model. This will probably not cost any more, and will provide the best material properties for the Mighty Epic site.
3. The grout used around the structures should be characterized to the extent of determining the failure envelope and the stress-strain response to selected loadings up to about 1 kilobar. This will provide data to indicate the difference between the grout and the tuff over pressure ranges up to about 1 kilobar.

4. The concrete used in the different structures should be characterized to the extent of determining the failure envelope, the stress-strain response, and some limited information on its dynamic (rapid loading) response.
5. Some information should be obtained on the "bond strength factor" for the concrete-to-steel. This can be done by running one or two direct shear tests where concretes used in the structures are sheared along steel plates - i.e., a direct shear test at several normal stresses¹⁵. It is not suggested that an extensive program be conducted, but that some indication of bond strength be obtained to serve as guidance for the calculators.
6. Some added material property tests are still needed for the "interface" calculation, and those proposed in Terra Tek report TR 75-36 should be performed as cores become available.

REFERENCES

1. S. J. Green, S. W. Butters, and R. M. Griffin, "High Pressure Mechanical Properties of the U12n.05 and U12t.02 Test Sites," Terra Tek Report TR 72-19, July 1972.
2. S. W. Butters, S. J. Green, and A. H. Jones, "Laboratory Tests on Rocks to Simulate Shock Wave Load-Unload From a Nuclear Explosion," Terra Tek Report TR 72-82, May 1974.
3. J. N. Johnson, S. W. Butters, W. F. Brace, A. H. Jones, and S. J. Green, "Plasticity Theory for Partially and Fully Saturated Porous Geological Materials," Terra Tek Report TR 74-53, October 1974.
4. S. W. Butters, "Selected Tests for Teleseismic Program," July 1975.
5. S. W. Butters, "Determination of Elastic Constants," Terra Tek Research Task Report, May 1975, and L. M. Barker, R. Lingle, and R. R. Hendrickson, "Interferometric Measurement of Transverse Strain for Determination of Low-Pressure Elastic Moduli of Rocks," Terra Tek Report TR 75-30, June 1975.
6. R. J. Reid, "Recoverable Dilatancy on Tuffs and Sandstones," February 1973, and S. J. Green, S. W. Butters, and A. H. Jones, "Recoverable Dilatancy Exhibited by Rocks," Transactions, American Geophysical Union, Vol. 54, Number 4, April 1973.
7. S. W. Butters, J. N. Johnson, H. S. Swolfs, and A. H. Jones, "Modeling and Properties for Welded Tuff from Mt. Helen - Sandia Test Range, Nevada," Terra Tek Report 75-9, January 1975.
8. S. W. Butters, A. H. Jones, and S. J. Green, "Properties of Quartzite from Area 12 of the Nevada Test Site," Terra Tek Report TR 75-7, January 1975.
9. S. W. Butters and S. J. Green, "Progress Report One - Material Properties for Mighty Epic Interface Experiment," Terra Tek Report TR 75-36, June 1975, and Terra Tek letter, subject: "Response to Request for Properties for Tuff Surrounding the Mighty Epic Working Point," dated February 5, 1975, from S. W. Butters to Jim Drake.
10. R. Lingle, R. S. Rosso and L. M. Buchholdt, "An Investigation to Determine the Effect of Fracture on the Ultrasonic Velocities in Ash-Fall Tuff," Terra Tek Report 75-20, May 1975.
11. W. F. Brace, S. J. Green, A. H. Jones, and S. W. Butters, "Determination of the Angle of Internal Friction," Terra Tek Report TR 75-38, July 1975.
12. S. W. Butters, J. N. Johnson, and S. J. Green, "Mechanical Behavior of MTS Grout," Terra Tek Report TR 74-40, August 1974.

13. S. J. Green, "Final Report - Constitutive Relations for Concrete at Intermediate Pressure Levels," Terra Tek Report 71-34, October 1971.
14. H. E. Read and C. J. Maiden, "The Dynamic Behavior of Concrete," Systems, Science and Software Report 3SR-707, August 1971.
15. H. R. Pratt and A. D. Black, "Strength, Deformation and Friction of *In Situ* Rock," Terra Tek Report TR 73-68, December 1973; and R. S. Rosso, "Rock Strength and Joint Property Data for the Mahoning Dam Site," Terra Tek Report TR 75-34, June 1975.

NOT
Preceding Page BLANK - FILMED

PHYSICAL AND MECHANICAL
PROPERTIES OF SEVERAL GROUT MIXTURES

By

S. W. Butters
A. H. Jones
S. J. Green

Submitted to:

Field Command
Defense Nuclear Agency
Nevada Test Site
Mercury, Nevada

Attn: Mr. J. W. LaComb

TR 75-45
August 1975

SUMMARY

Physical and mechanical properties tests have been conducted on several batches of grout supplied by Waterways Experiment Station. The grouts are used for gage implacement and containment of structures experiments during nuclear events at the Nevada Test Site and the grout properties are required to insure the proper grout selection. The grouts were designated HPRM-1, HPRM-2, HPRM-3, HPRM-4, HPRM-5, HPSL-16, HPNS-1 and HPNS-3C.

The properties determined for the grouts at 14, 28 and 56 day age are: physical properties (densities, porosities, water content, etc.), ultrasonic velocities and mechanical properties (shear strength, stress-strain response) from triaxial compression and uniaxial strain tests. The entire test program is not complete and the data reported is preliminary.

The data is reported in the form of tables which contain the physical properties and velocities at each of the three ages (with the exception of the HPNS-3C) and plots showing the shear strength as a function of confining pressure and the permanent compaction resulting from uniaxial strain load-unload tests.

Table 1: Physical Properties and Ultrasonic Velocities at 14 Day Age.

DRILL HOLE FOOTAGE	DENSITY (gm/cc)			WATER BY WET WEIGHT (%)	POROSITY (%)	SATURATION (%)	CALC AIR VOIDS (%)	MEAS PERMANENT COMP. (%)		VELOCITY (ft/sec)	
	AS- RECEIVED	DRY	GRAIN							LONG	SHEAR
Grout 14 Day								Hyd. 1-D			
HPRM-1	2.06	1.65	2.97	20.1	44	93	3.0	2.1 2.3		9478	5274
HPRM-2	2.04	1.64	3.01	19.8	46	89	5.1	2.2 2.25		9166	5022
HPRM-3	2.07	1.58	3.11	23.6	49	99	0.5	1.5 1.6		8366	4472
HPRM-4	2.01	1.55	3.06	22.9	49	94	3.2	3.1 3.5		9084	4640
HPRM-5	1.92	1.46	3.02	23.9	52	88	5.9	3.5 4.0		7910	3753
HPSL-16	1.86	1.37	2.94	26.5	54	92	4.3	2.4 2.5		6579	2459
HPNS-1	2.04	1.51	3.35	25.9	55	96	2.05	1.8 1.8		7213	3427
HPRM-3C	2.10	1.71		18.9				2.4 2.6		9850	5333

Table 2: Physical Properties and Ultrasonic Velocities at 28 Day Age.

DRILL HOLE FOOTAGE	DENSITY (gm/cc)			WATER BY WET WEIGHT (%)	POROSITY (%)	SATURATION (%)	CALC AIR VOIDS (%)	MEAS PERMANENT COMP. (%)		VELOCITY (ft/sec)	
	AS- RECEIVED	DRY	GRAIN							LONG	SHEAR
Grout 28 Day								Hyd. 1-D			
HPRM-1	2.02	1.56	2.97	22.9	48	97	1.3	2.2 2.8		10,259	5696
HPRM-2	2.04	1.61	3.01	21.0	46	93	3.3	1.7 2.7		11,591	6363
HPRM-3	2.08	1.61	3.11	22.7	48	98	1.0	1.5 1.9		8,871	4695
HPRM-4	1.98	1.53	3.06	22.9	50	91	4.5	3.5 3.9		9,058	4678
HPRM-5	1.94	1.45	3.02	27.4	52	95	2.6	2.9 3.0		7,707	3796
HPSL-16	1.86	1.36	2.94	27.0	54	93	3.7	2.4 2.7		6,303	2717
HPNS-1	2.05	1.51	3.35	26.7	55	99	0.2	2.0 2.5		7,519	3619

Table 3: Physical Properties and Ultrasonic Velocities at 56 Day Age.

DRILL HOLE FOOTAGE	DENSITY (gm/cc)			WATER BY WET WEIGHT (%)	POROSITY (%)	SATURATION (%)	CALC AIR VOIDS (%)	MEAS PERMANENT COMP. (%)		VELOCITY (ft/sec)	
	AS- RECEIVED	DRY	GRAIN							LONG	SHEAR
Grout 56 Day								Hyd. 1-D			
HPRM-1	2.05	1.63	2.97	20.5	45	93	3.2	2.5 3.0		10,269	5,545
HPRM-2	2.02	1.57	3.01	22.4	48	94	2.7	1.5 2.9		11,591	6,368
HPRM-3	2.10	1.65	3.11	21.2	47	95	2.5	1.6 2.5		9,672	5,230
HPRM-4	1.96	1.49	3.06	24.1	51	92	4.3	4.3 4.4		8,215	3,976
HPRM-5	1.97	1.48	3.02	24.8	51	96	2.0	2.5 2.7		8,064	4,117
HPSL-16	1.85	1.34	2.94	27.4	54	93	3.6	2.3 3.0		8,291	3,819
HPNS-1	2.09	1.58	3.35	24.2	53	96	2.2	2.1 2.6		8,015	4,006

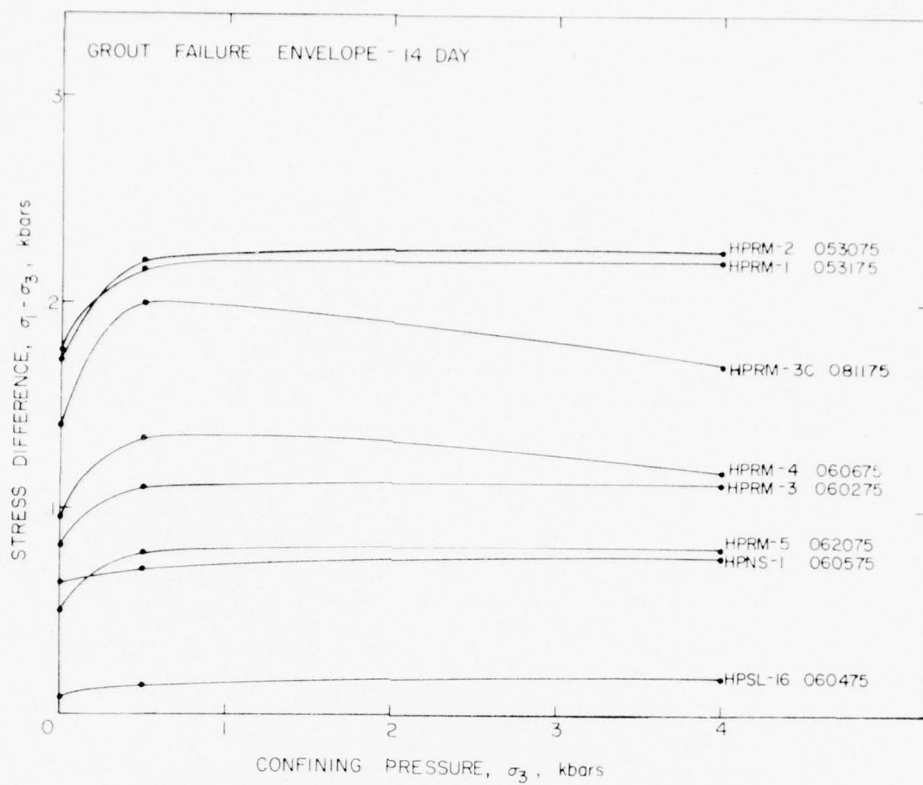


Figure 1: Failure Envelope at 14 Day Age

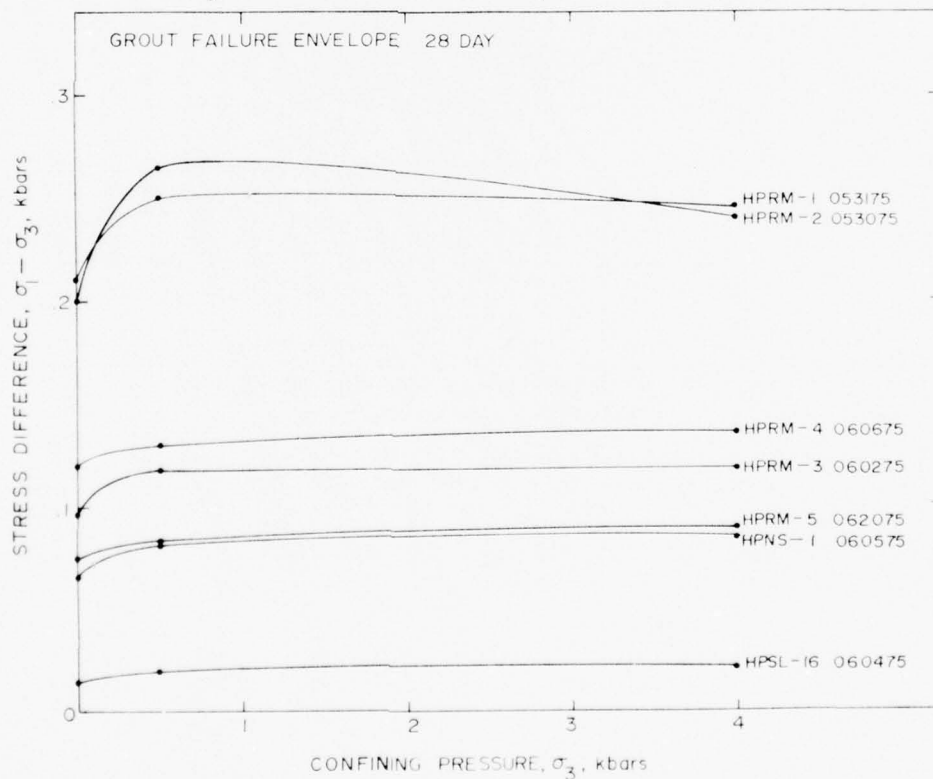


Figure 2: Failure Envelope at 28 Day Age

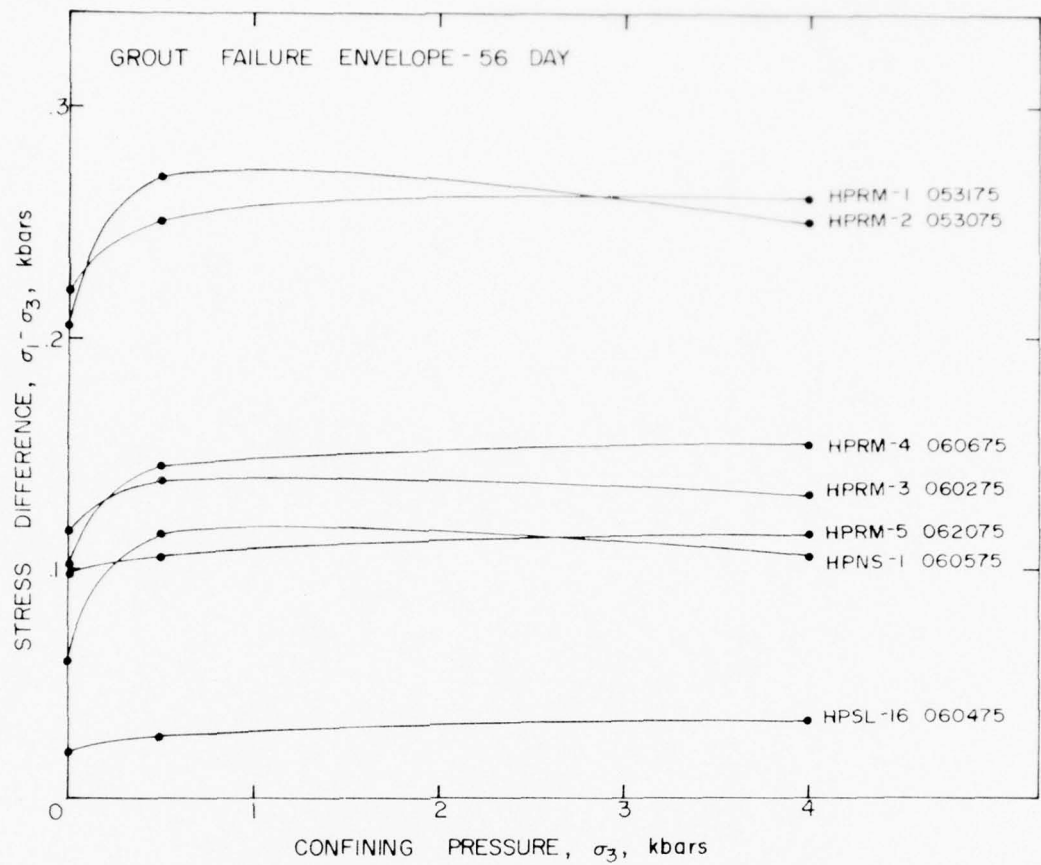


Figure 3: Failure Envelope at 56 Day Age

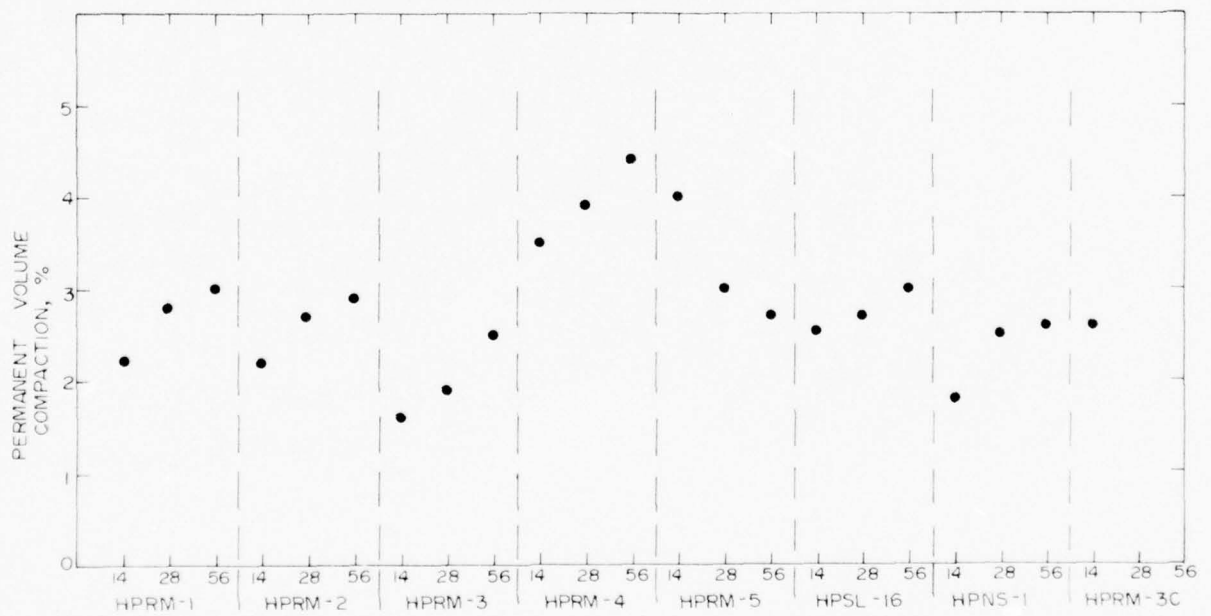


Figure 4: Permanent Volume Compaction from Uniaxial Strain Tests

NOT
Preceding Page BLANK - FILMED

PROGRESS REPORT III

MATERIAL PROPERTIES ON SAMPLES FROM MIGHTY EPIC

DRILL HOLES U12n.10 UG #4, U12n.10 UG #6a and U12n.10 UG #7

by

S. W. Butters
A. H. Jones
S. J. Green

Submitted to

Commander, Field Command
Defense Nuclear Agency
Albuquerque, New Mexico

Attn: Mr. J. W. LaComb
Mercury, Nevada

Contract Number DNA001-75-C-0260

Terra Tek, Inc.
University Research Park
420 Wakara Way
Salt Lake City, Utah 84108

TR 75-50
September 1975

PREFACE

Mighty Epic pretest planning require material properties for both shock wave propagation and rock/structural interaction calculations. In response to this requirement, Terra Tek has performed testing and reported properties in the following reports:

Progress Report I - Material Properties for the Mighty Epic Interface Experiment TR 75-36

Determination of Coefficient of Internal Friction TR 75-38

Some Comments on the Mighty Epic Material Properties TR 75-42

Physical and Mechanical Properties of Several Grout Mixtures (Preliminary) TR 75-45

Testing is continuing and properties from the U12n.10 UG #4, U12n.10 UG #6a and U12n.10 UG #7 core samples are included herein.

TABLE OF CONTENTS

Preface	54
Table of Contents	55
List of Figures	56
List of Tables	56
Introduction	57
Test Results	58
Discussion	65
References	66
Appendix	67

LIST OF FIGURES

Figure 1.	Plan View of the Mighty Epic Tunnels and Selected Drill Holes	57
Figure 2.	Selected Data from U12n.10 UG #4 Drill Hole Samples vs. the Footage Along the Drill Hole	60
Figure 3.	Selected Data from U12n.10 UG #6a Drill Hole Samples vs. the Footage Along the Drill Hole	61
Figure 4.	Selected Data from U12n.10 UG #7 Drill Hole Samples vs. the Footage Along the Drill Hole	62
Figure 5.	Triaxial Compression Test on U12n.10 UG #4 257' Sample	63
Figure 6.	Triaxial Compression Test on U12n.10 UG #6a 116' Sample	63
Figure 7.	Triaxial Compression Test on U12n.10 UG #4 and U12n.10 UG #6a Samples	64
Figure 8.	Stress-Strain Response on U12n.10 UG #4 and U12n.10 UG #6a Samples at a Confining Pressure of 50 Bars	64

LIST OF TABLES

Table 1.	Physical Properties, Permanent Volume Compaction and Ultrasonic Velocities on Core Samples from U12n.10 UG #4	59
Table 2.	Physical Properties, Permanent Volume Compaction and Ultrasonic Velocities on Core Samples from U12n.10 UG #6a	59
Table 3.	Physical Properties, Permanent Volume Compaction and Ultrasonic Velocities on Core Samples from U12n.10 UG #7	59

INTRODUCTION

Material properties have been determined on core samples from three drill holes in the Mighty Epic region at the Nevada Test Site, Mercury, Nevada. The testing was conducted on core samples from drill holes U12n.10 UG #4 and U12n.10 UG #6a, which are both located in the structures area as shown in Figure 1, and U12n.10 UG #7 which is in between the bypass drift and the main drift and was drilled toward the working point. All three of the drill holes are in the horizontal plane of the working point.

The material properties measured are physical properties (as-received density, dry density, percentage water and etc.) and longitudinal and shear velocities. In addition to tests for measuring the permanent volume compaction resulting from compaction in uniaxial strain to 4 kilobars lateral stress, further mechanical characterizations were obtained through triaxial compression tests. The confining pressures ranged from 0 (unconfined compression) to 4 kilobars but concentrating on the 0 to 500 bars range.

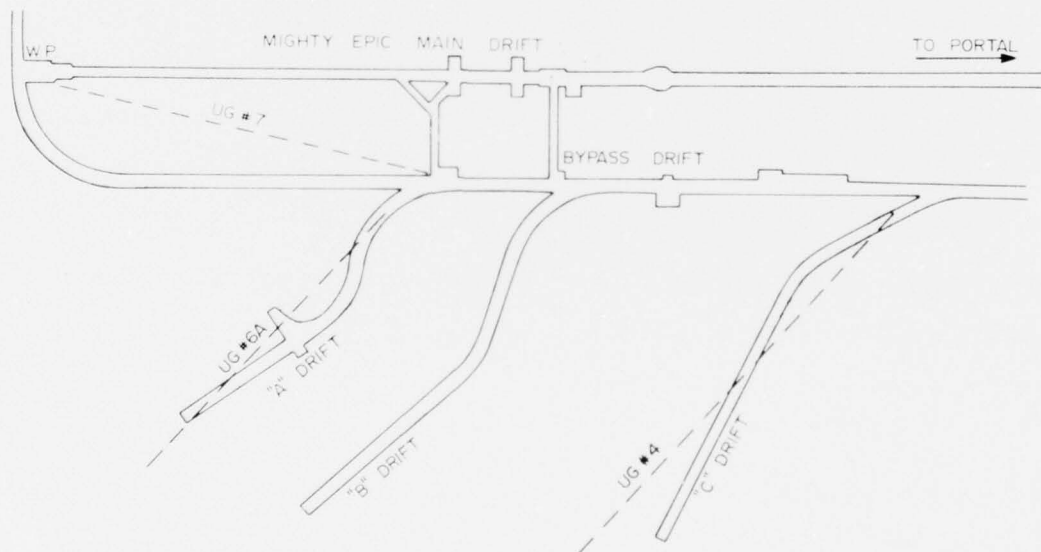


Figure 1. Plan View of the Mighty Epic Tunnels and Selected Drill Holes

TEST RESULTS

The U12n.10 UG #4, U12n.10 UG #6a and U12n.10 UG #7 drill hole samples physical properties, permanent volume compaction and ultrasonic velocities are listed in Tables 1, 2, and 3 respectively. Selected physical and mechanical properties have been plotted vs. the drill hole footage for each of the three drill holes in Figures 2, 3 and 4. The data has been plotted in this manner with the intent of indicating average properties (dashed line) and the amount of scatter in these properties as a function of drill hole footage.

Individual test curves plotted as axial stress vs. volume change and stress difference vs. confining pressure are contained in the appendix. Uniaxial strain tests curves for samples from drill holes U12n.10 UG #4 and U12n.10 UG #6a were plotted as axial stress vs. volume change such that the constrained modulus could be scaled from the slopes of the curves. The U12n.10 UG #7 test data is plotted in the usual manner -- mean normal stress vs. volume change.

The detailed triaxial compression tests on samples 257 feet from U12n.10 UG #4 and on the sample at 116 feet from U12n.10 UG #6a are shown in Figures 5 and 6. These results are plotted as stress difference vs. confining pressure through the confining pressure range of 0 to 100 bars. The same data is extended out to a confining pressure of 4 kilobars in Figure 7 and plotted as stress difference vs. axial shortening in Figure 8 for the test at a confining pressure of 50 bars.

Table 1. Physical Properties, Permanent Volume Compaction and Ultrasonic Velocities on Core Samples from U12n.10 UG #4

DRILL HOLE FOOTAGE	DENSITY (gm/cc)			WATER BY WET WEIGHT (%)	POROSITY (%)	SATURATION (%)	CALC. AIR VOIDS (%)	MEAS. PERMANENT COMP. (%)	VELOCITY (ft/sec)	
	AS-RECEIVED	DRY	GRAIN						LONG	SHEAR
U12n.10 UG #4								Hyd. 1-0		
227	1.86	1.52	2.44	18.6	38	91	3.2	1.4	9,469	4596
251	1.99	1.69	2.41	14.8	30	98	0.5	1.3	10,751	5761
254	1.95	1.65	2.39	15.4	31	96	1.3	1.8	10,009	5095
257	1.89	1.54	2.42	18.4	36	95	1.8			
263	1.97	1.65	2.50	16.2	34	94	1.9		9,694	4094
282	1.96	1.64	2.45	16.3	33	97	0.9	1.3	9,370	4104
307	2.01	1.73	2.41	14.0	28	99	0.2	0.9	9,557	6555
327	1.78	1.42	2.38	20.0	49	88	4.8		13,061	5154
331	1.74	1.37	2.36	21.2	42	88	5.2	1.2	10,548	4695
336	1.77	1.42	2.39	20.1	41	87	5.3	1.5	13,205	7523
339	1.77	1.38	2.38	22.1	42	93	2.7			

Table 2. Physical Properties, Permanent Volume Compaction and Ultrasonic Velocities on Core Samples from U12n.10 UG #6a

DRILL HOLE FOOTAGE	DENSITY (gm/cc)			WATER BY WET WEIGHT (%)	POROSITY (%)	SATURATION (%)	CALC. AIR VOIDS (%)	MEAS. PERMANENT COMP. (%)	VELOCITY (ft/sec)	
	AS-RECEIVED	DRY	GRAIN						LONG	SHEAR
U12n.10 UG #6a								Hyd. 1-0		
84	1.99	1.69	2.43	14.8	30	97	0.6	1.3	10,200	4809
109	1.97	1.69	2.36	14.0	28	98	0.7	0.7	11,227	5675
113	1.93	1.59	2.41	17.4	34	99	0.4		9,226	4505
116	1.98	1.72	2.38	12.9	28	93	1.9			
136	1.93	1.60	2.42	17.1	34	97	1.0	1.0	9,802	4563
161	1.97	1.68	2.41	15.0	31	97	1.0	1.1	10,305	4737
189	1.94	1.65	2.38	14.7	31	95	1.6	1.1	9,947	4895
192	2.01	1.80	2.35	10.4	23	90	2.4	0.6	11,603	6046
216	2.03	1.82	2.34	10.2	22	95	1.1	0.6	12,342	7306
220	1.96	1.65	2.41	15.6	31	97	1.1		10,561	4859
231	2.01	1.75	2.41	13.0	22	96	1.1			
247	2.00	1.75	2.35	12.4	25	98	0.6	0.6	13,094	7549

Table 3. Physical Properties, Permanent Volume Compaction and Ultrasonic Velocities on Core Samples from U12n.10 UG #7

DRILL HOLE FOOTAGE	DENSITY (gm/cc)			WATER BY WET WEIGHT (%)	POROSITY (%)	SATURATION (%)	CALC. AIR VOIDS (%)	MEAS. PERMANENT COMP. (%)	VELOCITY (ft/sec)	
	AS-RECEIVED	DRY	GRAIN						LONG	SHEAR
U12n.10 UG #7										
7	1.87	1.53	2.37	18.0	35	95	1.7	1.4	9478	4888
26	1.88	1.55	2.40	17.4	36	91	1.1	1.8	10377	5444
36	1.80	1.42	2.44	21.7	43	90	4.7	4.2	7207	4576
71	1.90	1.54	2.40	17.8	35	97	1.2	1.5	10423	5410
98			2.37	18.1					12545	6276
99	1.91	1.61	2.35	15.1	31	95	1.5	1.5	9298	4370
124	1.86	1.51	2.39	18.5	35	94	2.2	2.3	9039	4416
149	1.91	1.68	2.39	14.7	30	97	1.1	0.9	10547	5294
155	1.97	1.69	2.40	14.5	30	96	1.2	0.9	10453	5620
162	1.88	1.53	2.38	18.6	36	96	0.9	1.5	9859	4944
180	1.94	1.60	2.40	16.6	33	97	1.0	0.9	10513	5479
197	1.99	1.71	2.43	14.1	30	95	2.4	1.9	9311	4065
208	2.01	1.73	2.44	13.8	29	95	2.5	1.3	9632	3816
226	1.97	1.68	2.39	14.7	30	96	1.2	0.9	10515	5479
232	1.88	1.53	2.38	18.6	36	97	0.7	1.0	9547	3824
239	1.78	1.48	2.41	17.3	38	78	8.1	6.4	17520	6692
247	1.89	1.55	2.34	18.0	37	90	1.0	1.4	9288	4181
256	1.96	1.63	2.40	16.6	34	95	1.4	1.5	9413	4516
270	1.95	1.62	2.42	17.1	35	96	1.4		9473	3489
271	1.94	1.64	2.40	16.7	33	95	1.4	2.0	8917	4111
281	1.91	1.56	2.40	18.6	37	95	1.8	1.0	9537	4573
286	1.89	1.55	2.42	17.4	35	89	4.7	1.5	10410	5000
298	1.91	1.58	2.40	17.1	34	96	1.1	1.8	10272	4665
309	1.99	1.70	2.42	14.7	31	96	1.1	1.5	10944	5440

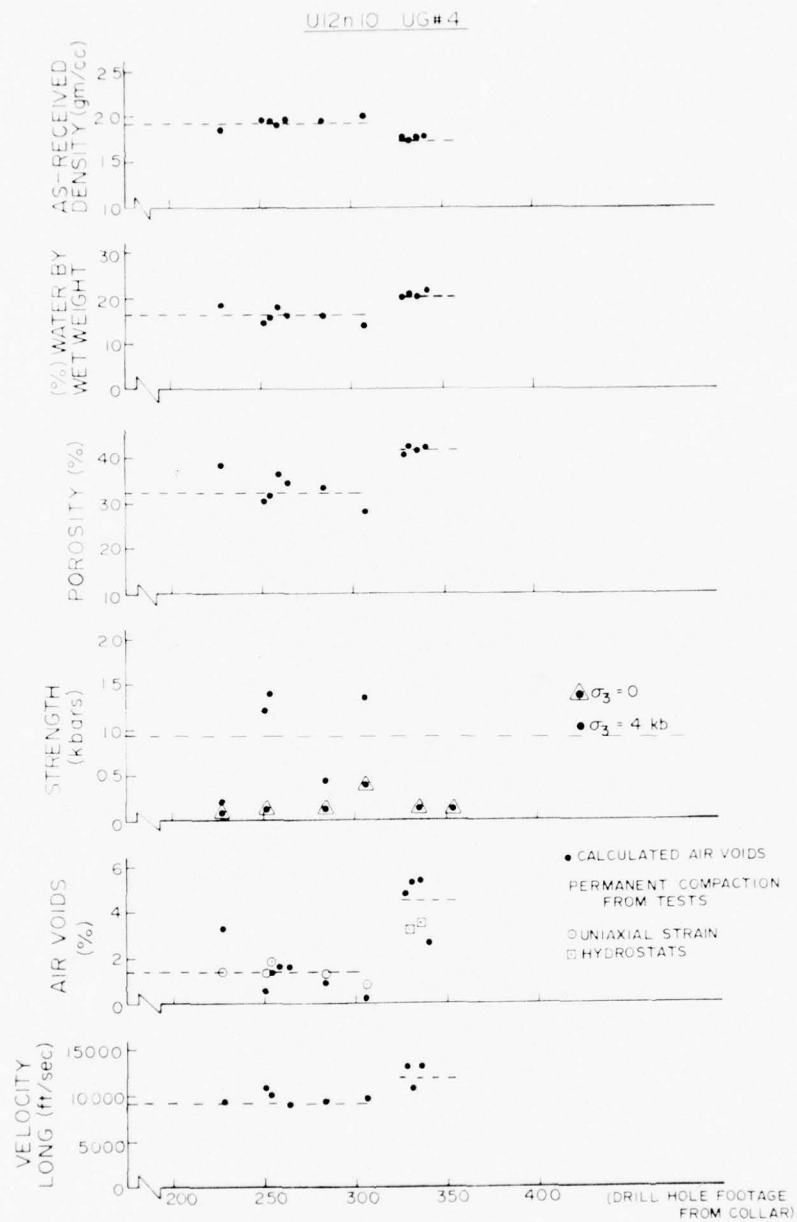


Figure 2. Selected Data from U12n.10 UG #4 Drill Hole Samples vs. the Footage Along the Drill Hole

U12n.10 UG#6A

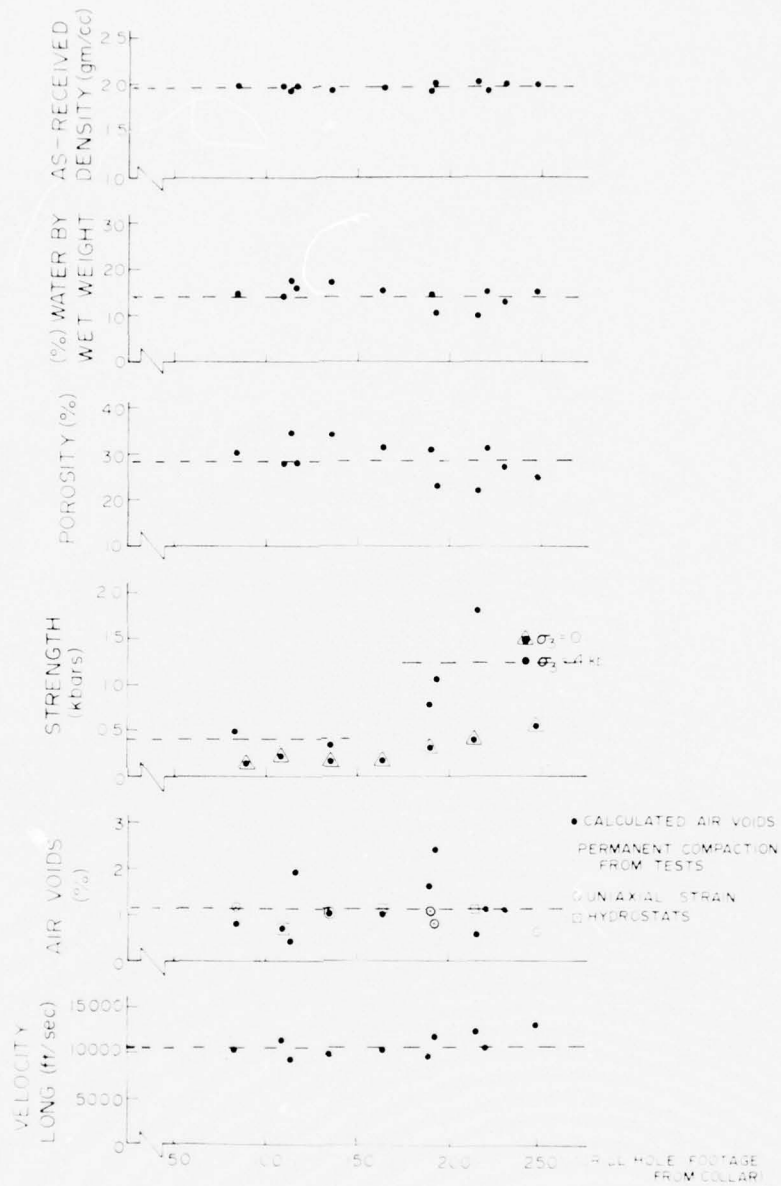


Figure 3. Selected Data from U12n.10 UG #6a Drill Hole Samples vs. the Footage Along the Drill Hole

U12n.10 UG # 7

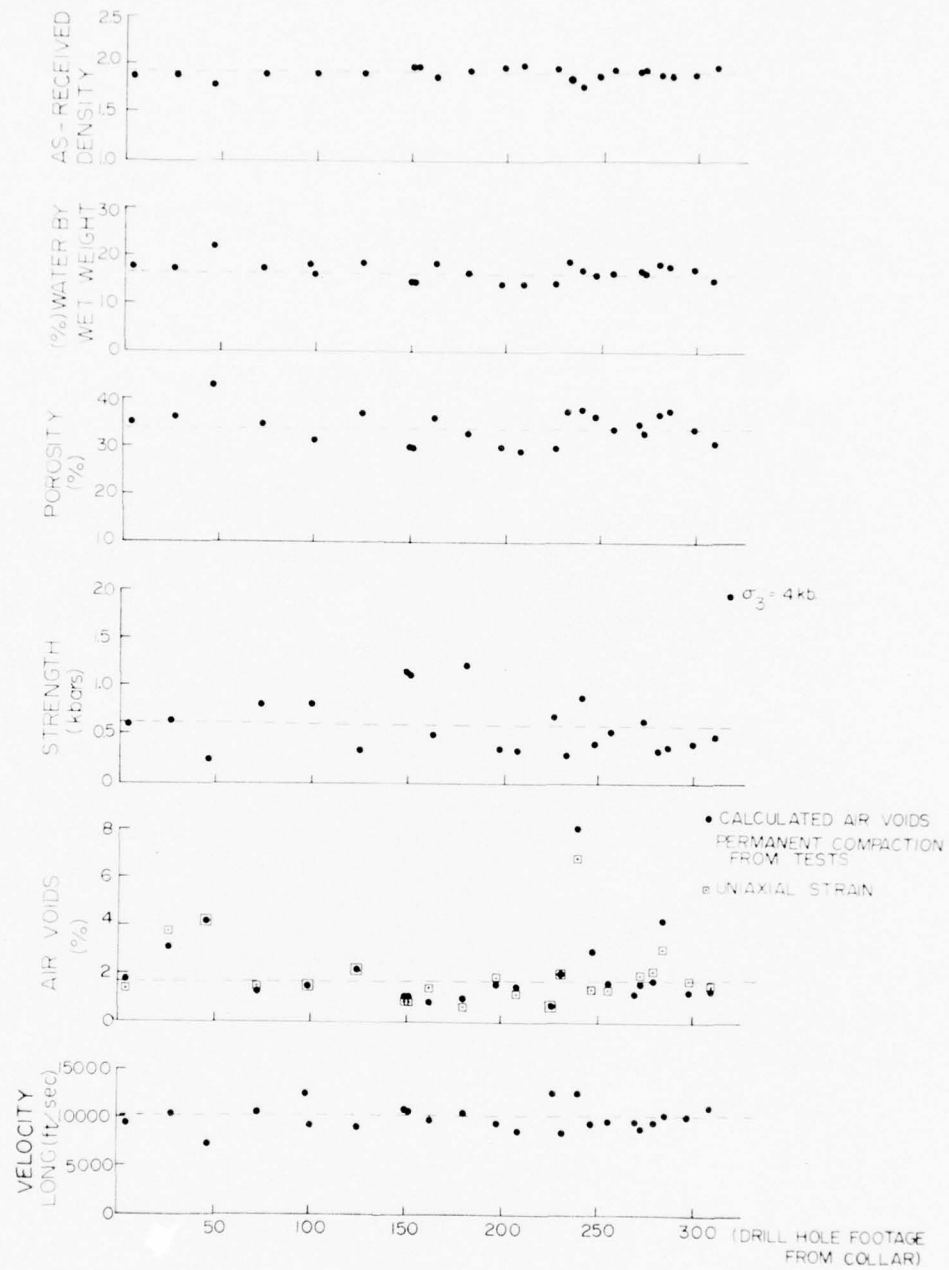


Figure 4. Selected Data from U12n.10 UG #7 Drill Hole Samples vs. the Footage Along the Drill Hole

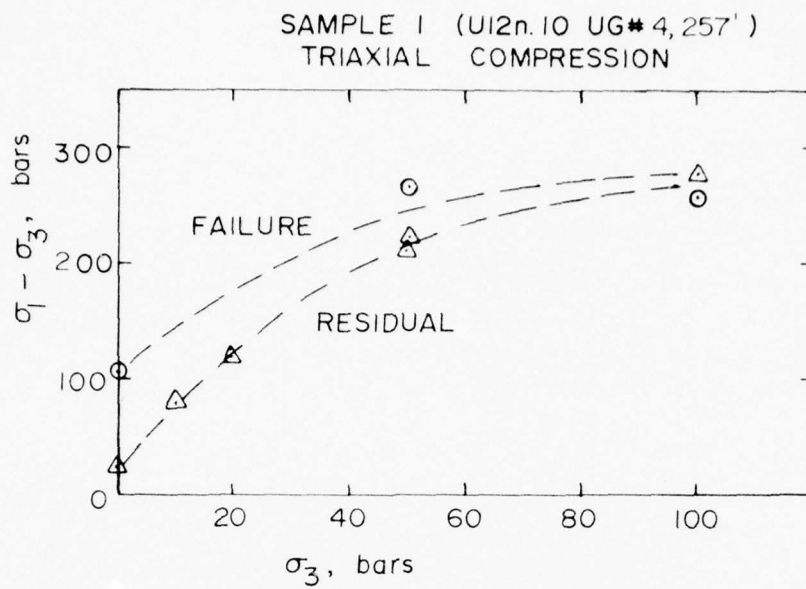


Figure 5. Triaxial Compression Test on U12n.10 UG #4 257' Sample

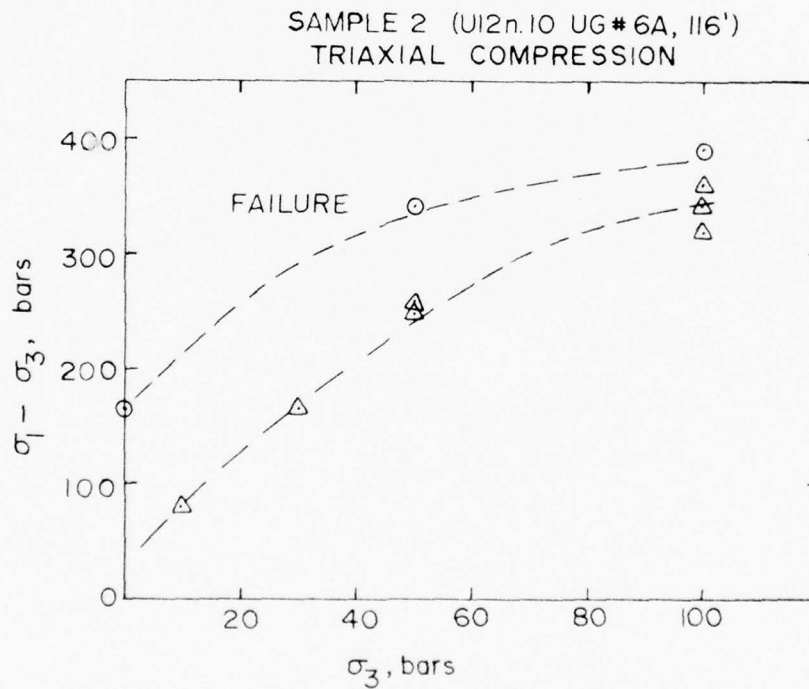


Figure 6. Triaxial Compression Test on U12n.10 UG #6a 116' Sample

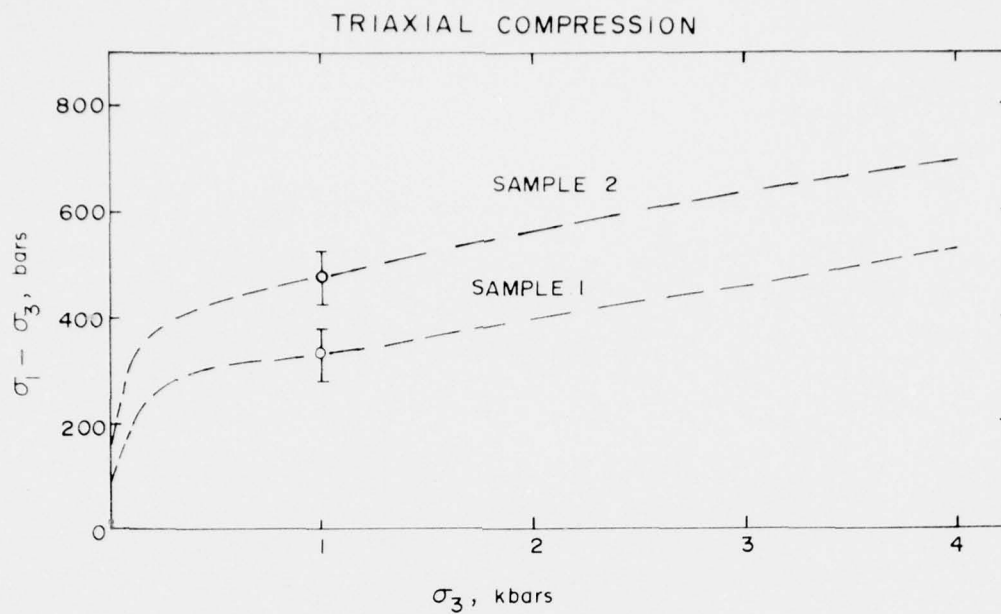


Figure 7. Triaxial Compression Test on U12n.10 UG #4 and U12n.10 UG #6a Samples

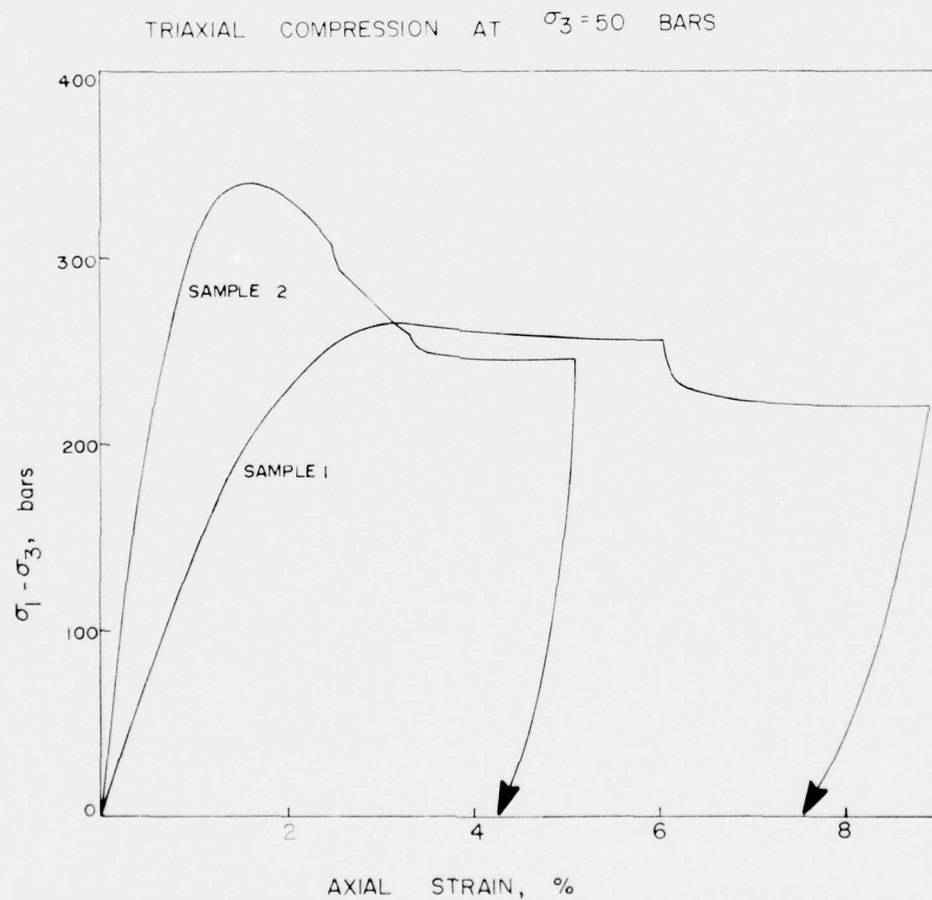


Figure 8. Stress-Strain Response on U12n.10 UG #4 and U12n.10 UG #6a Samples at a Confining Pressure of 50 Bars

DISCUSSION

The material properties show trends expected as the various lithological beds are penetrated by the drill holes. However, the Mighty Epic regions portrayed by the UG #4, UG #6a and UG #7 drill holes, on the average, indicate higher as-received densities, shear strengths and ultrasonic velocities (Figures 2, 3 and 4) than "typical" ash fall tuff^{1,2}. The porosities, air void contents and water contents are about the same.

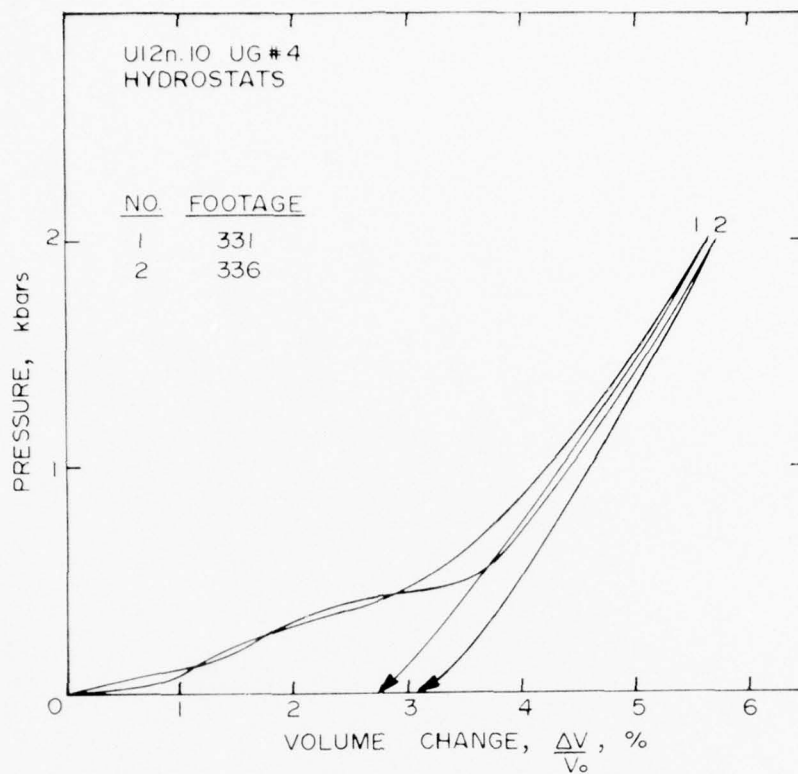
The triaxial compression tests on the two samples from UG #4 and UG #6a (Figures 5-8) were for the purpose of estimating the tuff failure envelope for comparison to grout mixtures. The difficulties in producing a "tuff matching" grout is in matching the failure envelope over a range of pressure. The grout tends to show lower strength increase with pressure than the tuff.

Additional triaxial compression tests are planned on selected samples to further characterize the tuff material in the immediate vicinity of the structures experiments.

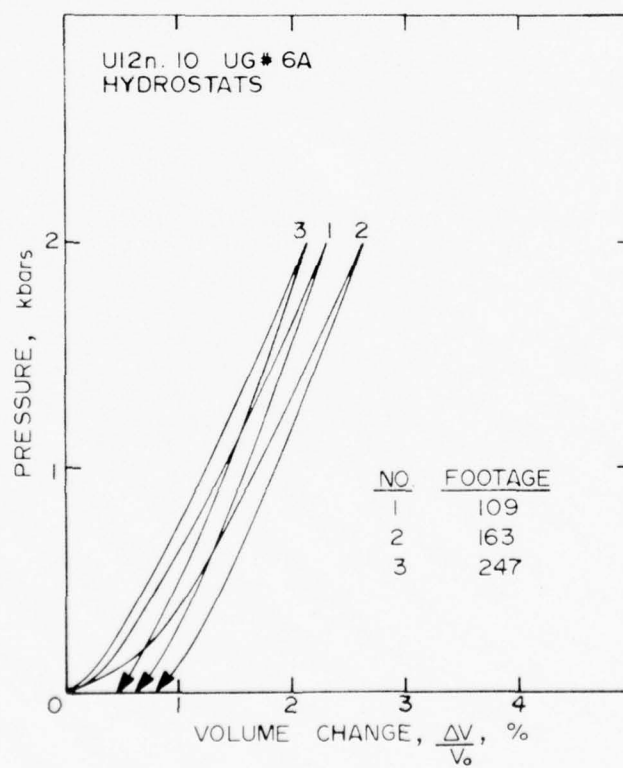
REFERENCES

1. Butters, S. W., Nielsen, R. N., Jones, A. H., Green, S. J., "Mechanical & Physical Properties of Nevada Test Site Tuffs and Grouts from Exploratory Drill Holes", Terra Tek Report TR 73-69, December, 1973.
2. Butters, S. W., Johnson, J. N., Green, S. J., "The Mechanical Behavior of NTS Grout", Terra Tek Report TR 74-40, August, 1974.

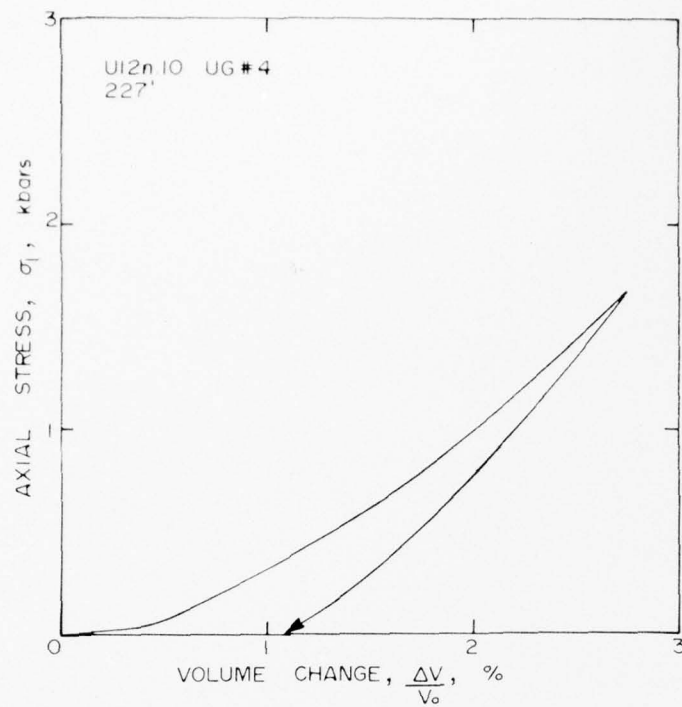
APPENDIX



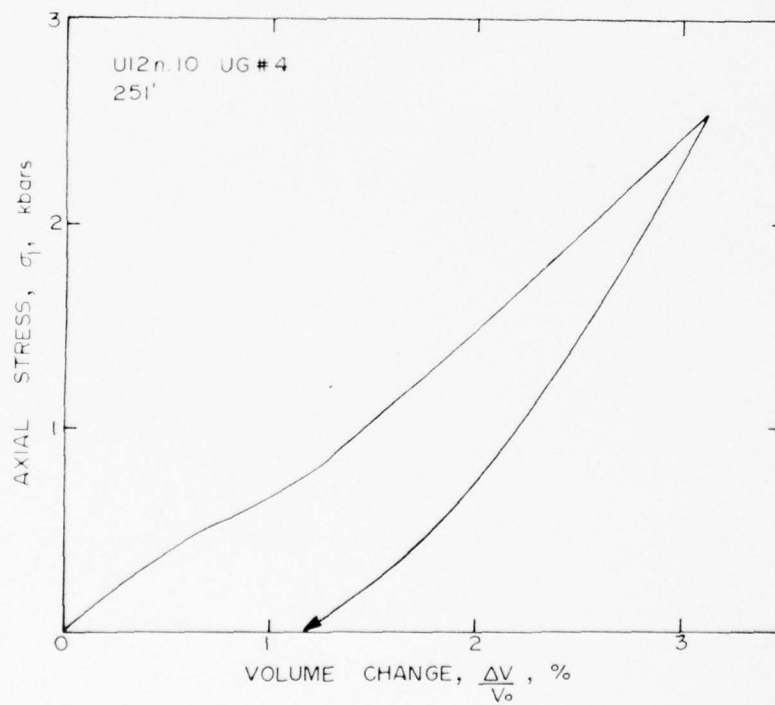
Hydrostatic Compression, UI2n.10 UG #4



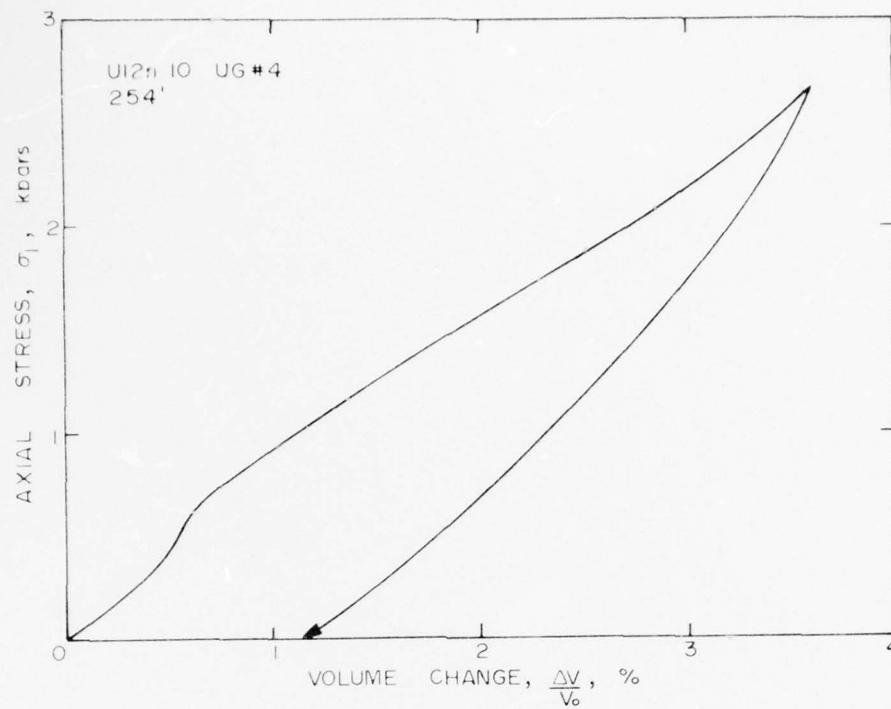
Hydrostatic Compression, UI2n.10 UG #6a



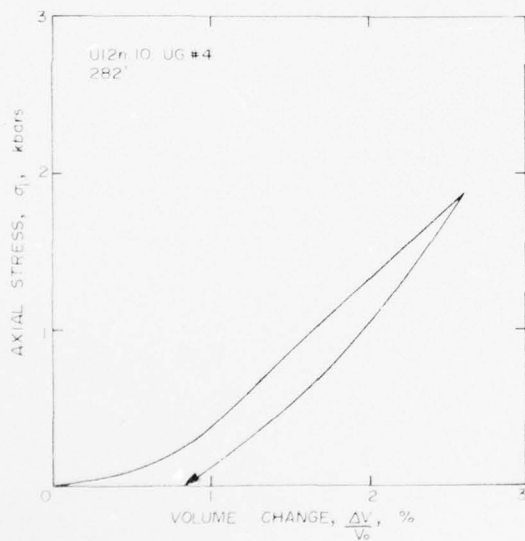
Uniaxial Strain, UI2n.10 UG #4



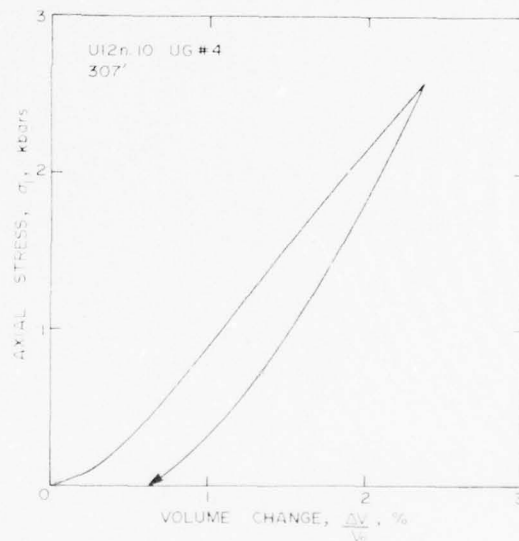
Uniaxial Strain, UI2n.10 UG #4



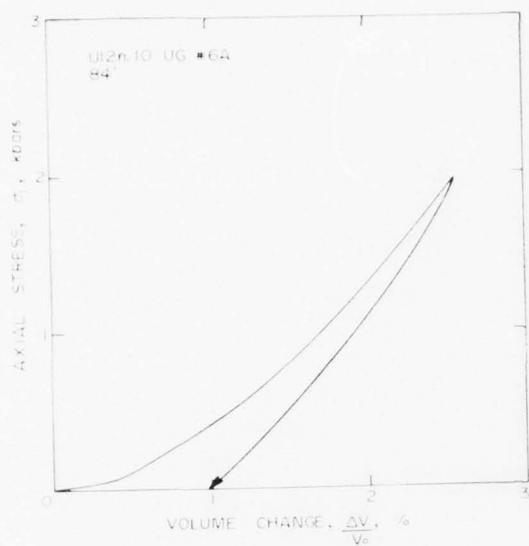
Uniaxial Strain, U12n.10 UG #4



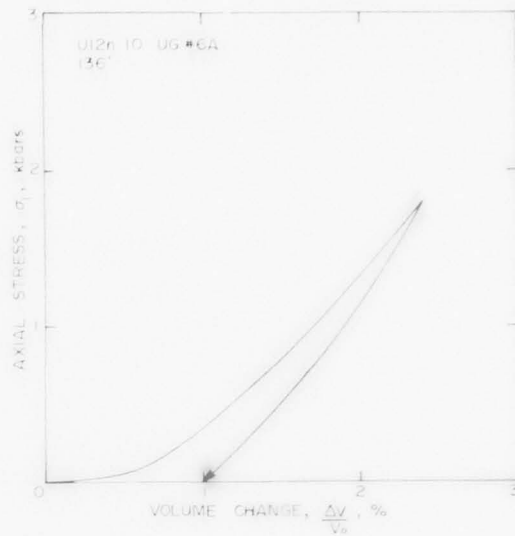
Uniaxial Strain, U12n.10 UG #4



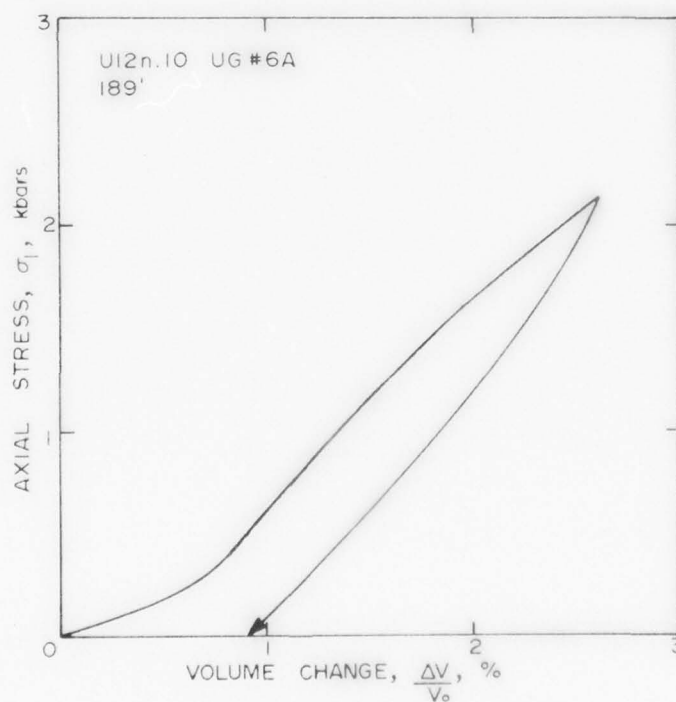
Uniaxial Strain, U12n.10 UG #4



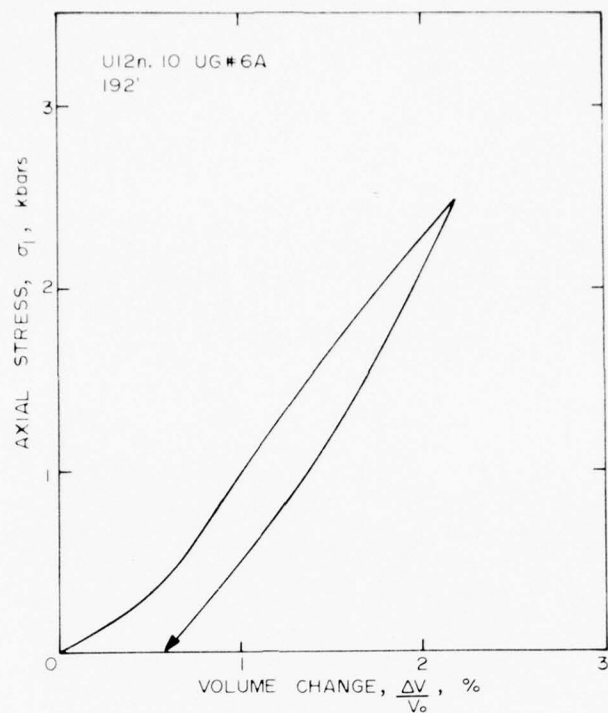
Uniaxial Strain, U12n.10 UG #6a



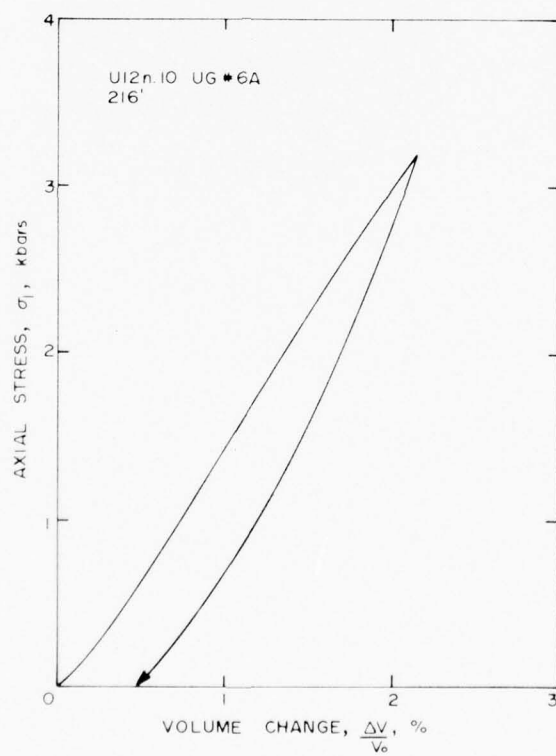
Uniaxial Strain, U12n.10 UG #6a



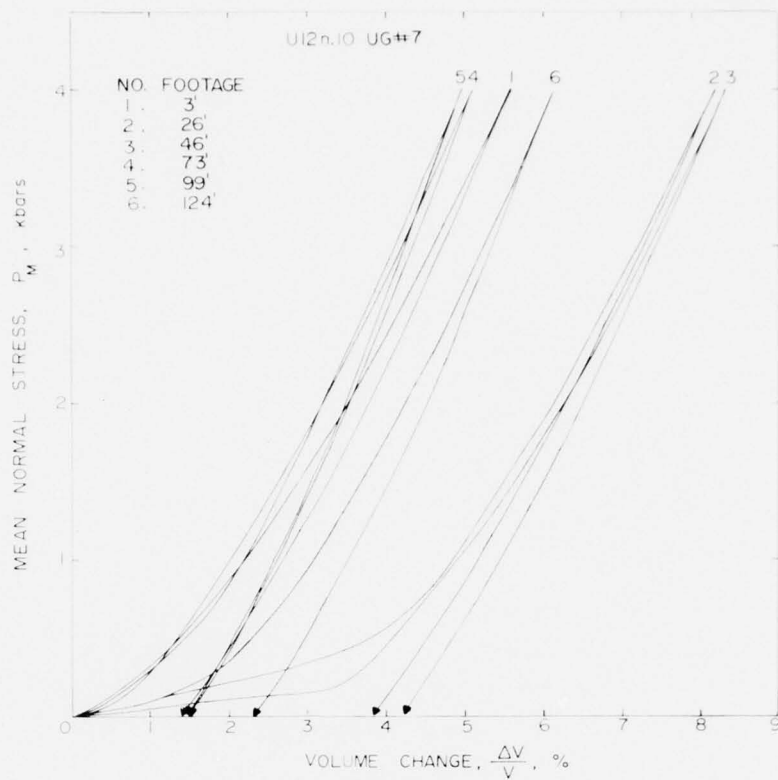
Uniaxial Strain, U12n.10 UG #6a



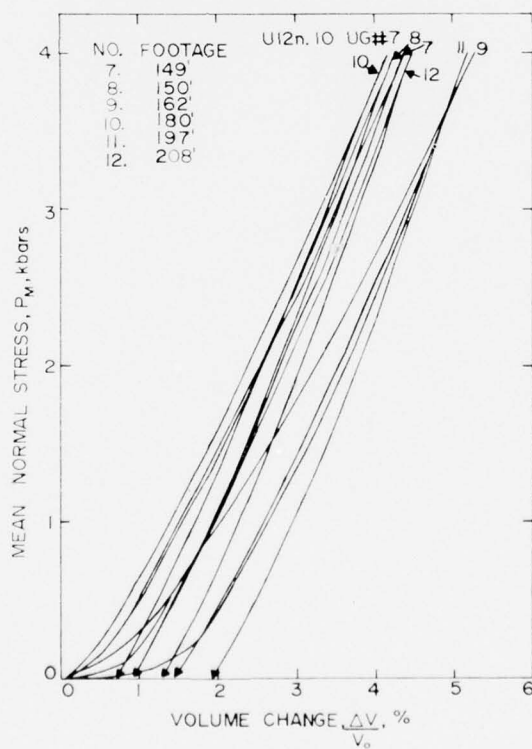
Uniaxial Strain, UI2n.10 UG #6a



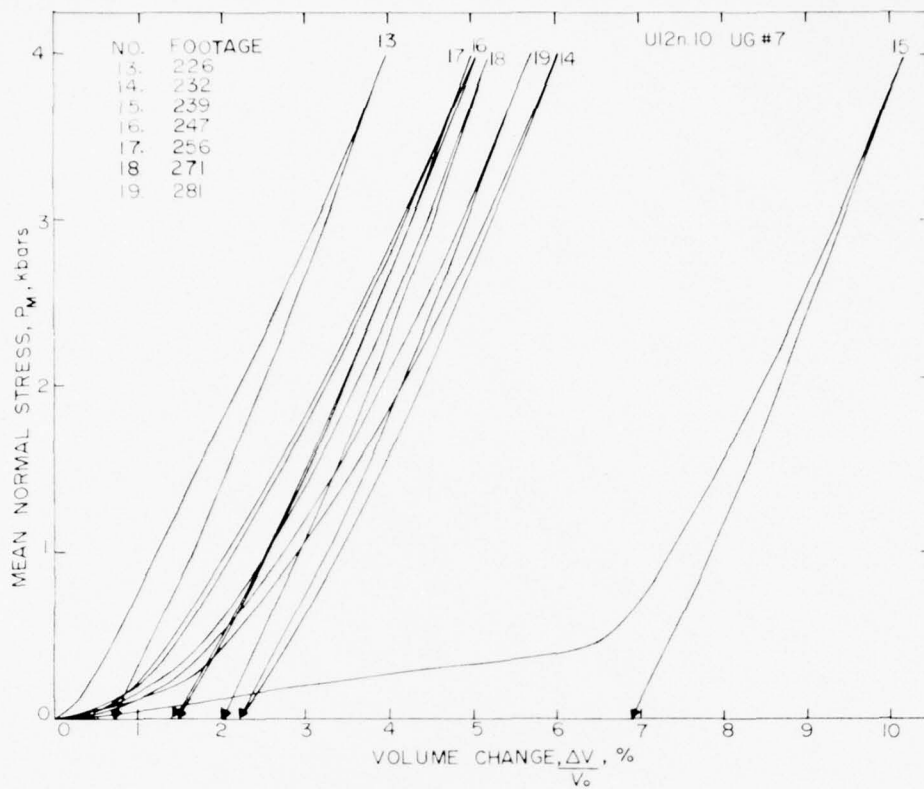
Uniaxial Strain, UI2n.10 UG #6a



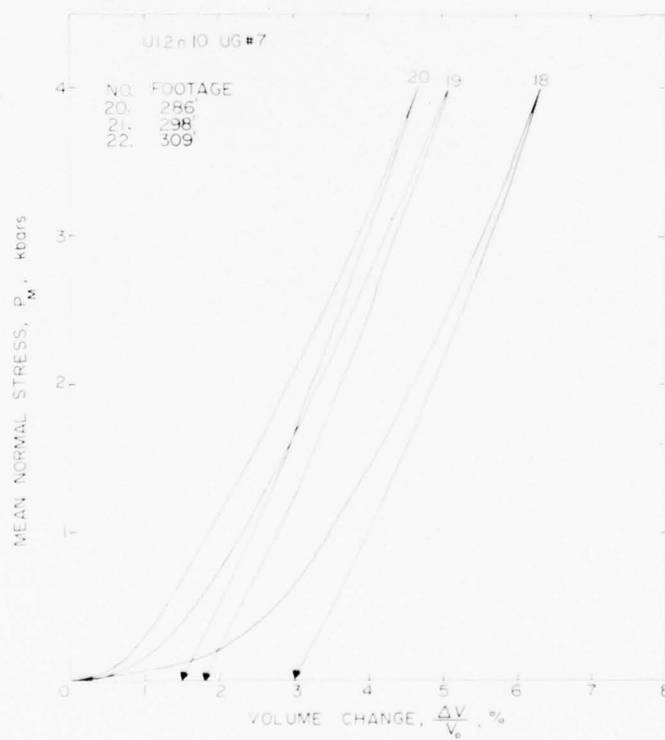
Uniaxial Strain, U12n.10 UG #7



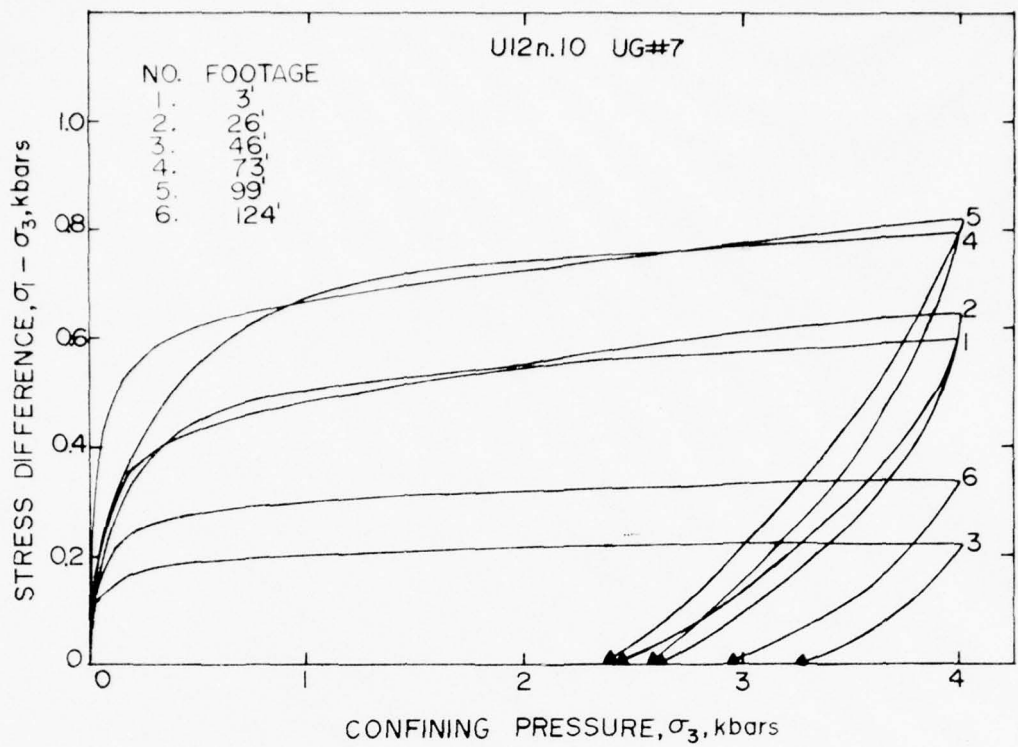
Uniaxial Strain, U12n.10 UG #7



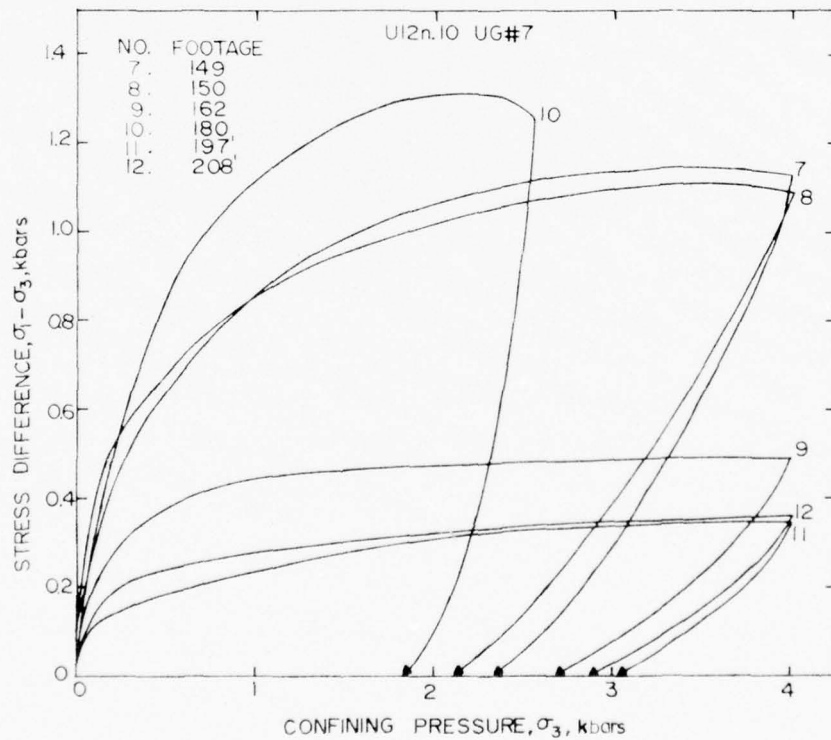
Uniaxial Strain, U12n.10 UG #7



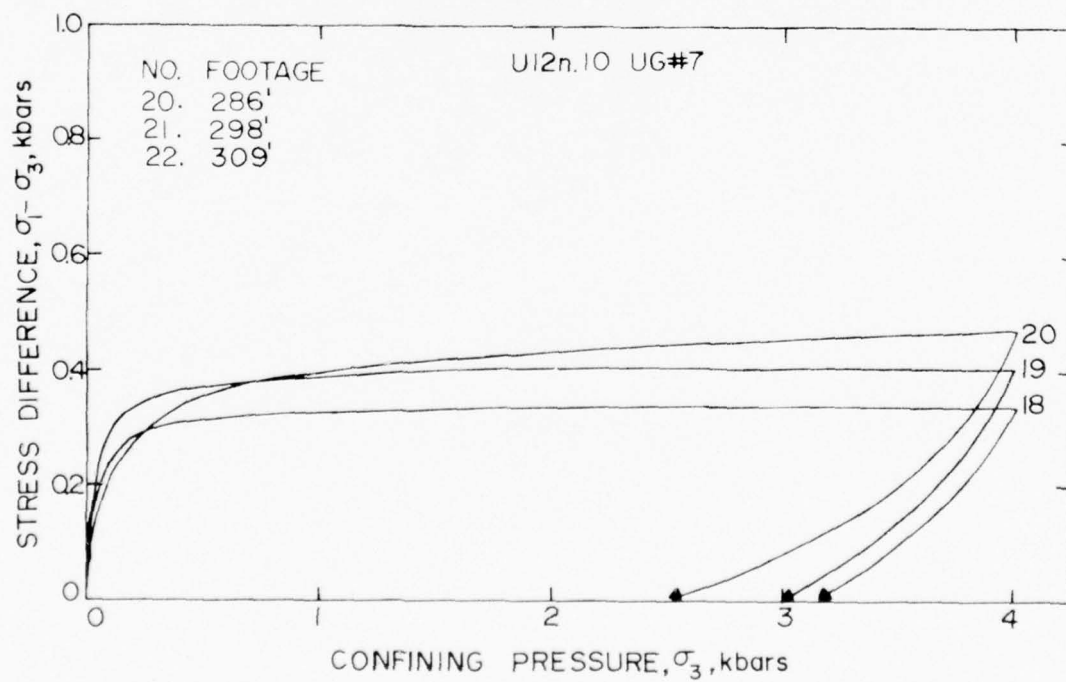
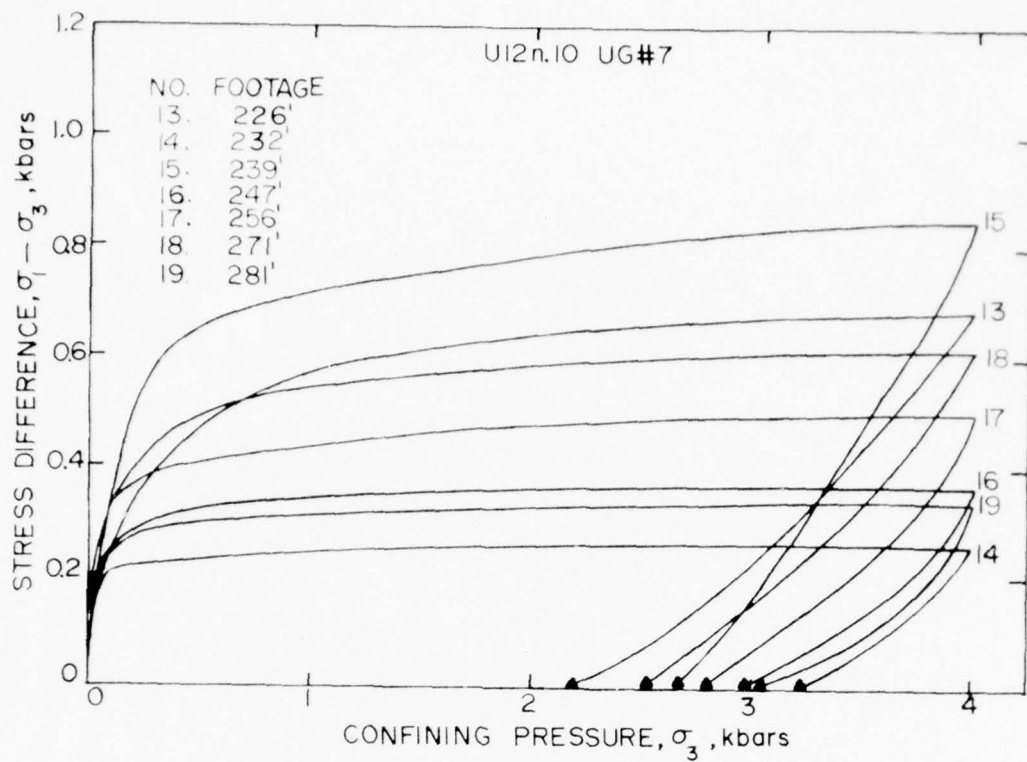
Uniaxial Strain, U12n.10 UG #7

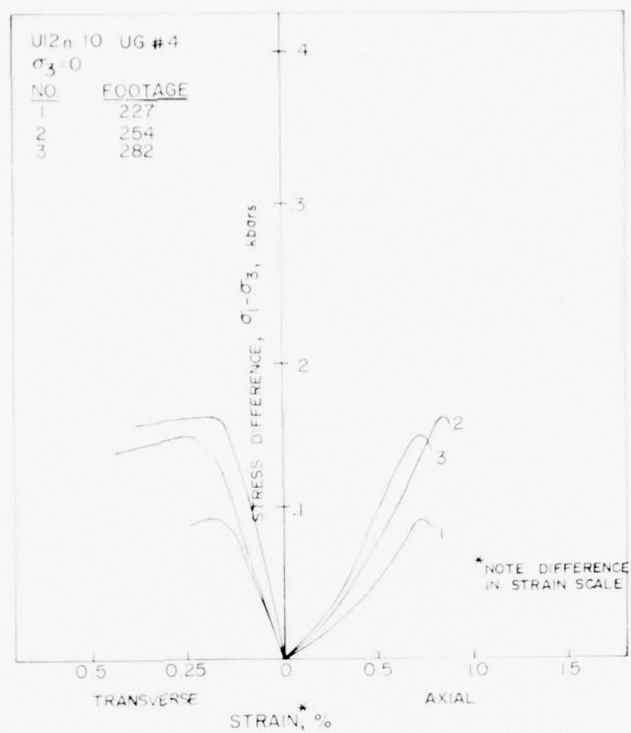


Uniaxial Strain, U12n.10 UG #7

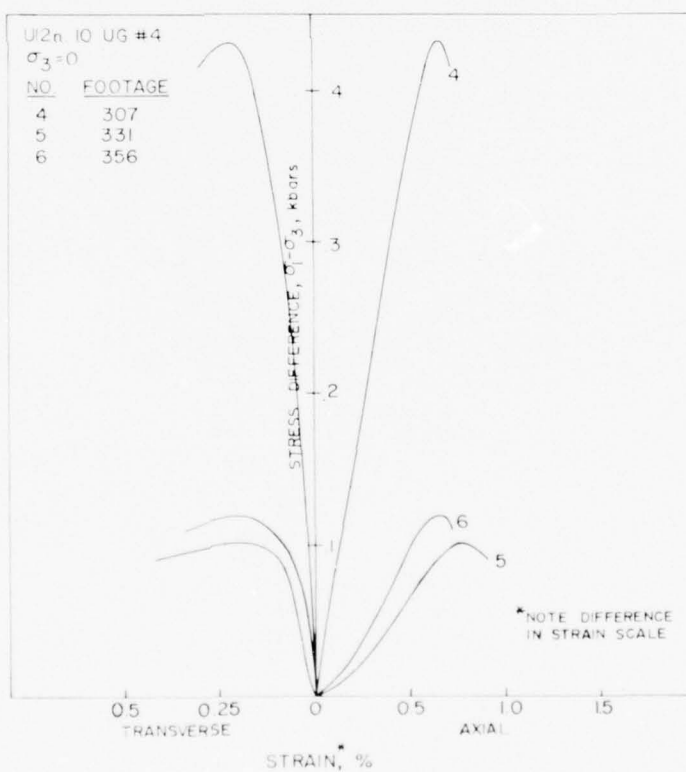


Uniaxial Strain, U12n.10 UG #7

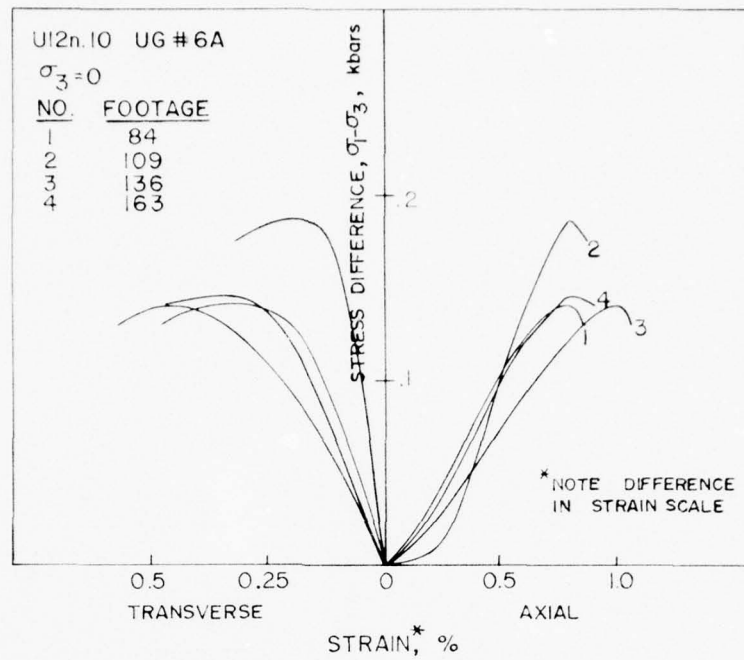




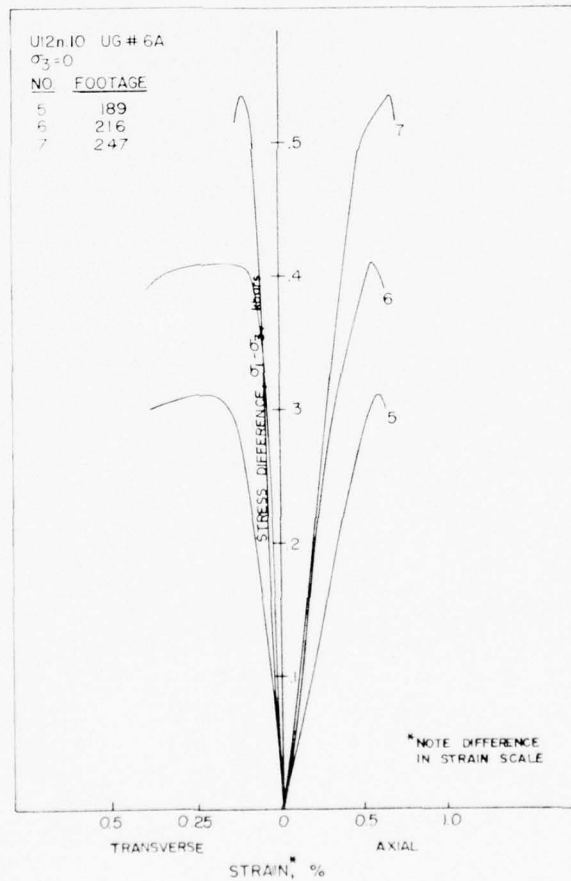
Unconfined Compression, U12n.10 UG #4



Unconfined Compression, U12n.10 UG #4



Unconfined Compression, U12n.10 UG #6a



Unconfined Compression, U12n.10 UG #6a

SOME MATERIAL PROPERTIES ON CORE SAMPLES
FROM SEVERAL DRILL HOLES RELATING TO THE MIGHTY EPIC EVENT

by

S. W. Butters
A. H. Jones
S. J. Green

Submitted to

Commander
Defense Nuclear Agency
Field Command
Mercury, NV 89023

Attn: J. W. LaComb

Submitted by

Terra Tek, Inc.
420 Wakara Way
University Research Park
Salt Lake City, UT 84108

TR 75-64

November 1975

BACKGROUND

In preparation for the Mighty Epic event at the Nevada Test Site, several studies have required material properties for the surrounding rock media (tuff) and several grout mixtures. The tuff material properties determined thus far have been from several drill holes¹ beginning with initial exploratory drill holes to more recent drill holes in the immediate vicinity of the working point and the structures studies. Material properties of several grout mixtures² have also been determined.

The material properties determined have been physical properties (as-received density, dry density, grain density, percentage water, porosity, saturation and air void content), mechanical properties (shear strength as a function of confining pressure), ultrasonic longitudinal and shear velocities and other properties such as the air void content estimated from the permanent compaction of the uniaxial strain load-unload tests.

The Mighty Epic related reports distributed to date are as follows:

1. Properties of Quartzite from Area 12 of the Nevada Test Site, TR 75-7, January, 1975.
2. Progress Report I - Material Properties for Mighty Epic Experiment, TR 75-36, June, 1975.
3. Determination of the Angle of Internal Friction, TR 75-38, July, 1975.
4. Progress Report II - Mighty Epic Material Properties, TR 75-42, August, 1975.
5. Physical and Mechanical Properties of Several Grout Mixtures, TR 75-45, August, 1975.
6. Progress Report III - Material Properties on Samples from Mighty Epic Drill Holes U12n.10 UG#4, U12n.10 UG#6a and U12n.10 UG#7, TR 75-50, September, 1975.

TABLE OF CONTENTS

Background	80
Table of Contents	81
List of Illustrations	82
List of Tables	84
Introduction	86
Test Program	88
Test Results	89
Discussion	112
References	116

LIST OF ILLUSTRATIONS

	<u>Page</u>
Figure 1: Plan view of the Mighty Epic area showing the drill holes from which core samples have been tested	87
Figure 2a: Uniaxial strain tests on UE12n#9 core samples -- mean normal stress versus volume change	91
Figure 2b: Uniaxial strain tests on UE12n#9 core samples -- stress difference versus confining pressure	91
Figure 3: Unconfined compression tests on UE12n#9 core samples -- stress difference versus individual strains.	92
Figure 4: Hydrostatic compression test on U12n.10 UG#7 core samples -- confining pressure versus volume change	92
Figure 5: Unconfined compression tests on U12n.10 UG#7 core samples -- stress difference versus individual strains	93
Figure 6: Triaxial compression tests at 0.5 kilobars confining pressure on U12n.10 UG#7 core samples -- stress difference versus individual strains.	93
Figure 7: Triaxial compression tests at 4.0 kilobars confining pressure on U12n.10 UG#7 core samples -- stress difference versus individual strains.	94
Figure 8: Failure envelope from triaxial compression tests on U12n.10 UG#7	94
Figure 9a: Uniaxial strain tests on U12n.10 ISS#1 core samples -- mean normal stress versus volume change.	95
Figure 9b: Uniaxial strain tests on U12n.10 ISS#1 core samples -- stress difference versus confining pressure	95
Figure 10: Hydrostatic compression tests on U12n.10 ISS#5 core samples -- confining pressure versus volume change	96
Figure 11: Unconfined compression tests on U12n.10 ISS#5 core samples -- stress difference versus individual strains	96
Figure 12: Triaxial compression tests at 0.5 kilobars confining pressure on U12n.10 ISS#5 core samples -- stress difference versus individual strains	97
Figure 13: Triaxial compression tests at 4.0 kilobars confining pressure on U12n.10 ISS#5 core samples -- stress difference versus individual strains	97

	<u>Page</u>
Figure 14: Failure envelope from triaxial compression tests on U12n.10 ISS#5.	98
Figure 15a: Uniaxial strain tests on U12n.10 HF#2 core samples -- mean normal stress versus volume change	99
Figure 15b: Uniaxial strain tests on U12n.10 HF#2 core samples -- stress difference versus confining pressure	99
Figure 16a: Uniaxial strain tests on U12n.10 HF#4 core samples -- mean normal stress versus volume change.	100
Figure 16b: Uniaxial strain tests on U12n.10 HF#4 core samples -- stress difference versus confining pressure	100
Figure 17a: Uniaxial strain tests on U12n.10 A Structures (31 feet), B Structures (25 feet) and C Structures (30 feet) core samples -- mean normal stress versus volume change	101
Figure 17b: Uniaxial strain tests on U12n.10 A Structures (31 feet), B Structures (25 feet) and C Structures (30 feet) core samples -- stress difference versus confining pressure	101
Figure 18a: Hydrostatic compression and uniaxial strain tests on ME801 grout samples -- mean normal stress versus volume change (14 day age).	104
Figure 18b: Uniaxial strain test on ME801 grout sample -- stress difference versus confining pressure (14 day age).	104
Figure 19a: Low stress-strain portion of the triaxial compression tests on ME801 grout samples -- stress difference versus individual strains (14 day age), see Figure 19b for entire test curves	105
Figure 19b: Triaxial compression tests on ME801 grout samples -- stress difference versus individual strains (14 day age), see Figure 19a for low stress-strain response.	105
Figure 20a: Hydrostatic compression and uniaxial strain tests on ME802 grout samples -- mean normal stress versus volume change (14 day age)	106
Figure 20b: Uniaxial strain test on ME802 grout sample -- stress difference versus confining pressure (14 day age).	106
Figure 21: Triaxial compression tests on ME802 grout sample -- stress difference versus individual strains (14 day age)	107
Figure 22: Unconfined compression test on ME804 grout sample -- stress difference versus individual strains (14 day age)	107

	<u>Page</u>
Figure 23: Hydrostatic compression test on ME805 grout sample -- confining pressure versus volume change (14 day age) . . .	108
Figure 24a: Low stress-strain portion of the triaxial compression tests on ME805 grout samples -- stress difference versus individual strains (14 day age), see Figure 24b for entire test curves	108
Figure 24b: Triaxial compression tests on ME805 grout samples -- stress difference versus individual strains (14 day age), see Figure 24a for low stress-strain response	109
Figure 25: Unconfined compression tests on ME806 grout sample -- stress difference versus individual strains (14 day age) .	109
Figure 26a: Uniaxial strain tests on ME8011 grout sample -- mean normal stress versus volume change (14 day age).	110
Figure 26b: Uniaxial strain tests on ME8011 grout sample -- stress difference versus confining pressure (14 day age).	110
Figure 27: Failure envelope based on the triaxial compression tests on ME801, ME802 and ME805 grout samples (14 day age). Also shown is the unconfined compression tests on ME804 and ME806	111
Figure 28: Estimated failure envelopes based on uniaxial strain test results on core samples from U12n.10 UG#4, UG#6a, ISS#5 and ISS#7 drill holes ³	114
Figure 29: Representative failure envelope for the tuff in the Structures area, based on uniaxial strain tests and triaxial compression test data from Terra Tek and WES ⁴	114
Figure 30: Combined structures tuff failure envelope and grout failure envelopes shown in Figure 29 and Figure 27, respectively	115

LIST OF TABLES

Table 1: Terra Tek Laboratory Test Program on Tuff and Grout Samples.	88
Table 2: Physical Properties, Uniaxial Strain Permanent Volume Compaction and Ultrasonic Wave Velocities on Individual Tuff Samples Tested	90
Table 3: Physical Properties, Hydrostatic Compression and Uniaxial Strain Permanent Volume Compaction and Ultrasonic Wave Velocities on Grout Samples	111

Table 4:	Average Structures Tuff Physical Properties, Permanent Compaction and Ultrasonic Wave Velocities. Also listed for comparison is the physical properties of the grout as reported in Table 3	115
----------	--	-----

INTRODUCTION

As a continuing effort to determine material properties for site evaluation and development of material models for subsequent use in ground motion calculations, tests have been conducted to determine physical and mechanical properties of tuff and grout relating to the Mighty Epic event at the Nevada Test Site. The purpose of the laboratory testing program has been several fold: 1) initial evaluation of the global material properties, 2) development of material models for purposes of predicting stemming and containment, 3) prediction of the response across a soft to hard interface, 4) determine if the material properties are a function of distance from the tunnel wall (this question is related to the seismic velocities obtained in the field) and 5) to insure a proper match between the tuff properties and the emplaced grout properties surrounding the structures experiments.

Core samples were tested from the following drill holes:

- UE12n#9
- U12n.10 UG#7
- U12n.10 ISS#1
- U12n.10 ISS#5
- U12n.10 HF#2
- U12n.10 HF#4
- U12n.10 A Structures
- U12n.10 B Structures
- U12n.10 C Structures

The locations of these drill holes are shown in Figure 1. Grout mixtures tested were designated:

- ME801
- ME802
- ME804
- ME805
- ME806
- ME8011

The tuff and grout data are reported in tabular and graphic form followed by a discussion which specifically addresses the question of the material properties of the tuff as compared to the properties of the grouts.

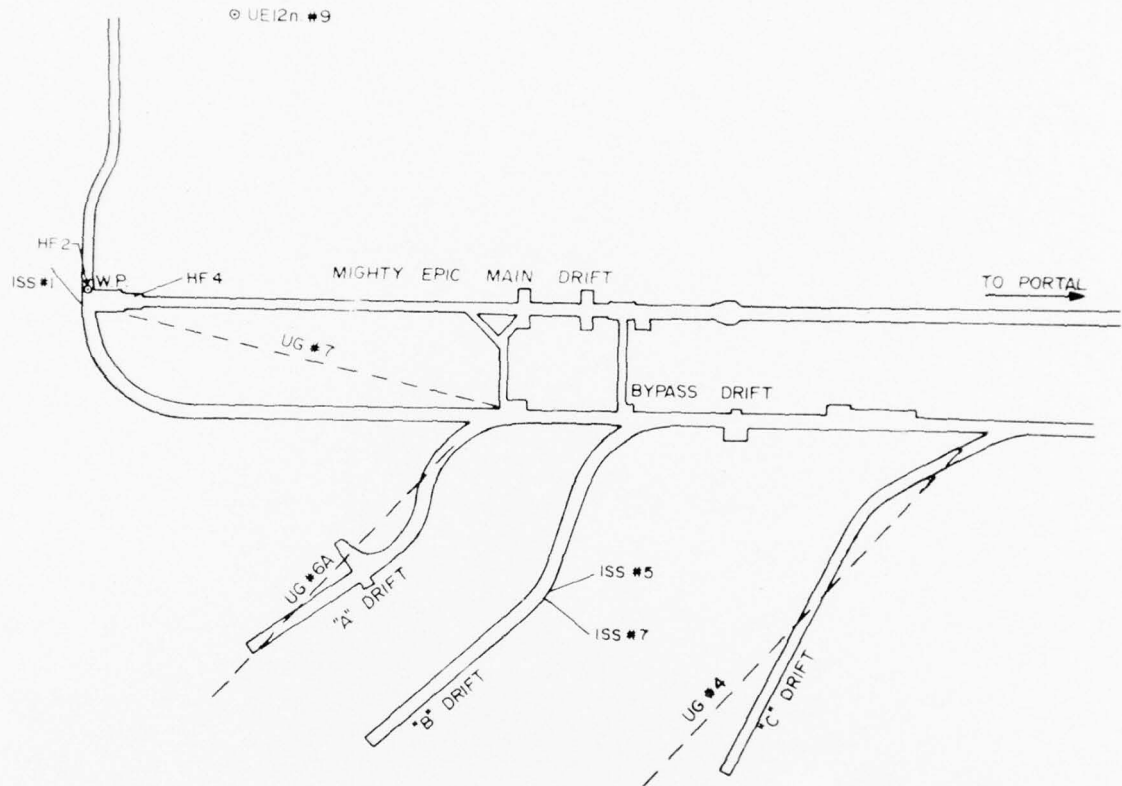


Figure 1: Plan view of the Mighty Epic area showing the drill holes from which core samples have been tested.

TEST PROGRAM

As discussed in the introduction, the purpose of the core sample testing was several fold. The types of tests, therefore, varied according to the purpose for which the data was intended. For example, the U12n.10 ISS#5 drill hole samples were subjected to triaxial compression tests since the shear strength of the material is important for the structural tests.

The types of tests conducted on the subject drill hole samples and the grout are listed in Table 1.

TABLE 1
Terra Tek Laboratory Test Program on Tuff and Grout Samples

DRILL HOLE	MECHANICAL TESTS				PHYSICAL PROPERTIES
TUFF	HYDROSTATIC COMPRESSION	TRIAXIAL COMPRESSION	UNIAXIAL STRAIN	ULTRASONIC VELOCITIES	AS REC, DRY AND GRAIN DENSITIES
U12n#9		$\sigma_3=0$	X	X	X
U12n.10 UG#7	X	$\sigma_3=0,0.5,4$ kb		X	X
U12n.10 ISS#1			X	X	X
U12n.10 ISS#5	X	$\sigma_3=0,0.5,4$ kb		X	X
U12n.10 HF#2			X	X	X
U12n.10 HF#4			X	X	X
U12n.10 A,B,C structures			X	X	X
<u>GROUT</u>					
ME801	X	$\sigma_3=0,0.1,0.25,0.5,4$ kb	X	X	X
ME802	X	$\sigma_3=0,0.5,4$ kb	X	X	X
ME804	X			X	X
ME805	X	$\sigma_3=0.05,0.1,0.5,1.0,4$ kb		X	X
ME806	X			X	X
ME8011			X	X	X

TEST RESULTS

TUFF

UE12n#9 Drill Hole Samples: The physical properties, uniaxial strain permanent volume compaction and ultrasonic longitudinal and shear wave velocities are listed in Table 2. The uniaxial strain test curves are shown in Figure 2 and the unconfined compression results in Figure 3.

U12n.10 UG#7 Drill Hole Samples: The hydrostatic pressure-volume strain response is shown in Figure 4. The stress difference versus individual strains for the triaxial compression at pressures of 0, 0.5 and 4 kilobars are shown in Figures 5, 6 and 7, respectively. The strength of the core samples at these three confining pressure states are replotted in Figure 8 and indicate the failure surface for these materials. The physical properties, hydrostatic compression permanent volume compaction and ultrasonic longitudinal and shear wave velocities are listed in Table 2.

U12n.10 ISS#1 Drill Hole Samples: The uniaxial strain test curves are shown in Figure 9. The physical properties, uniaxial strain permanent volume compaction and ultrasonic longitudinal and shear wave velocities are listed in Table 2.

U12n.10 ISS#5 Drill Hole Samples: The hydrostatic pressure--volume strain response is shown in Figure 10. The stress difference versus individual strains for constant confining pressures of 0, 0.5 and 4 kilobars are shown in Figures 11, 12 and 13, respectively. Again the maximum stress differences obtained at these confining pressures are replotted in Figure 14 to indicate the failure surface for the material. The physical properties, the hydrostatic compression permanent volume compaction and ultrasonic longitudinal and shear wave velocities are listed in Table 2.

U12n.10 HF#2 Drill Hole Samples: The uniaxial strain test curves are shown in Figure 15 and the physical properties, uniaxial strain permanent volume compaction and ultrasonic longitudinal and shear wave velocities are listed in Table 2.

U12n.10 HF#4 Drill Hole Samples: The uniaxial strain test curves are shown in Figure 16 and the physical properties, uniaxial strain permanent volume compaction and ultrasonic longitudinal and shear velocities are listed in Table 2.

U12n.10 A, B and C Structures Drill Hole Samples: The uniaxial strain test curves are shown in Figure 17 and the physical properties, uniaxial strain permanent volume compaction and ultrasonic longitudinal and shear wave velocities are listed in Table 2.

TABLE 2

Physical Properties, Uniaxial Strain Permanent Volume Compaction and Ultrasonic Wave Velocities on Individual Tuff Samples Tested

DRILL HOLE FOOTAGE	DENSITY gm/cc			% WATER BY WET WEIGHT	POROSITY %	SATURATION %	% CALC AIR VOIDS	% MEAS PERMANENT COMP.	VELOCITY ft/sec	
	AS- RECEIVED	DRY	GRAIN						LONG	SHEAR
U12n #9										
1130	1.77	1.37	2.39	22.6	43	93	2.9	2.8	9469	4226
1170	1.85	1.47	2.43	20.5	40	96	1.6	1.3	9459	4613
1224	1.82	1.42	2.44	22.0	42	95	2.0	2.2	10696	5794
1276	1.95	1.62	2.48	17.0	34	98	0.6	1.8	10217	4764
U12n.10 UG#7										
169	1.88	1.52	2.45	19.2	38	95	1.9		8668	4193
211	1.95	1.62	2.47	16.7	34	95	1.8		9482	4396
262	1.94	1.61	2.45	16.9	34	96	1.3		10003	4770
U12n.10 HF2										
9	2.04	1.77	2.44	13.1	27	97	0.8	0.6	12064	6483
16	2.08	1.83	2.48	12.4	22	97	0.7	0.8	10253	4587
29	1.91	1.58	2.43	17.4	35	95	1.8	1.2	10833	5371
U12n.10 HF4										
15	1.94	1.61	2.44	16.9	34	97	1.1	1.1	10249	4997
22	1.95	1.64	2.42	15.7	32	95	1.6	1.2	10308	5016
26	1.96	1.64	2.43	16.2	33	97	0.9	1.0	9980	4793
U12n.10 (SS#1)										
5	1.96	1.64	2.44	16.6	33	99	0.4	0.6	11923	6752
19	1.95	1.63	2.43	16.2	33	96	1.4	1.3	11204	5892
20	1.95	1.62	2.46	17.0	34	98	0.8	0.8	11394	5981
27	1.85	1.51	2.40	18.4	38	91	3.4	3.5	9446	4758
28	1.80	1.44	2.42	21.2	41	93	4.2	4.8	9829	4393
U12n.10 (SS#5)										
9	1.91	1.55	2.48	18.5	37	94	2.1		8960	4070
11	1.93	1.63	2.36	15.4	31	97	1.1		10760	4970
17	1.91	1.59	2.40	16.8	33	96	1.4		9380	4280
26	1.88	1.52	2.43	19.0	36	98	0.7		9390	4170
28	1.93	1.64	2.36	15.5	31	96	1.1		10190	4900
U12n.10										
A Structure										
31	1.92	1.61	2.39	16.7	33	94	1.9	0.9	11206	6162
B Structure										
25	1.95	1.66	2.46	10.6	26	97	0.9	0.8	9567	4512
C Structure										
30	1.84	1.48	2.46	22.8	41	95	0.9	0.6	10801	5382

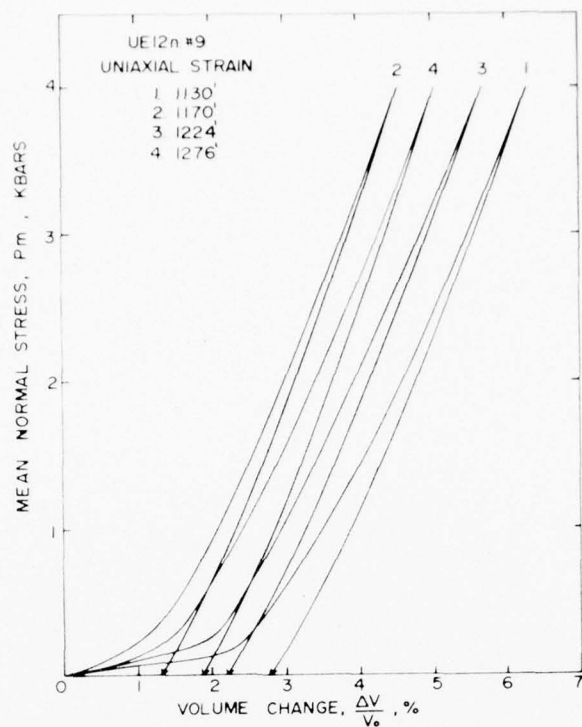


Figure 2a: Uniaxial strain tests on UE12n#9 core samples -- mean normal stress versus volume change.

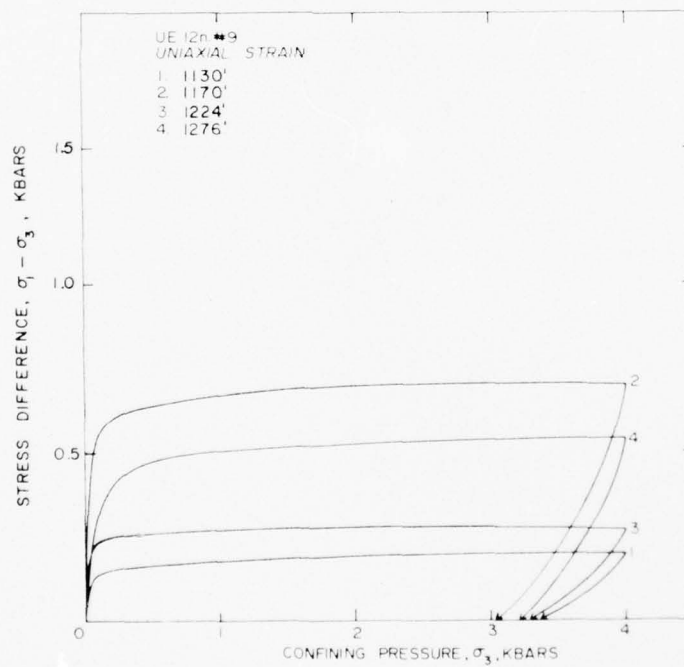


Figure 2b: Uniaxial strain tests on UE12n#9 core samples -- stress difference versus confining pressure.

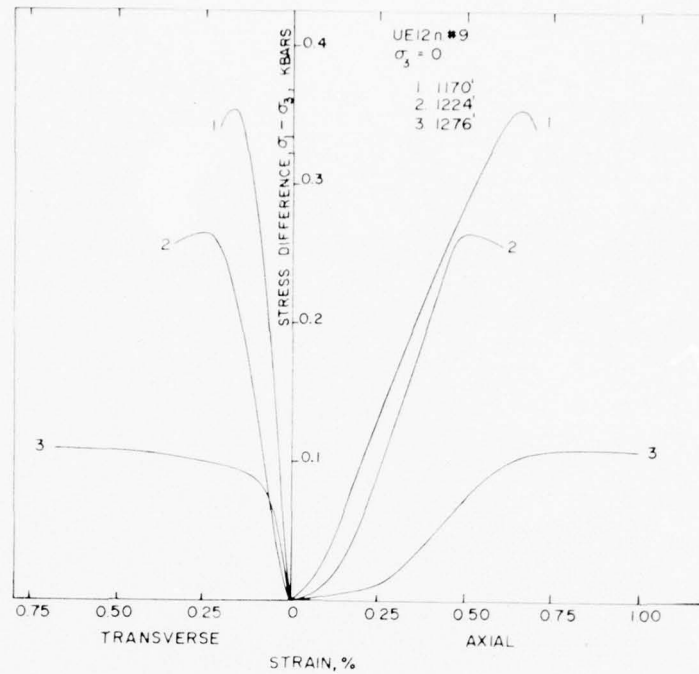


Figure 3: Unconfined compression tests on UE12n#9 core samples -- stress difference versus individual strains.

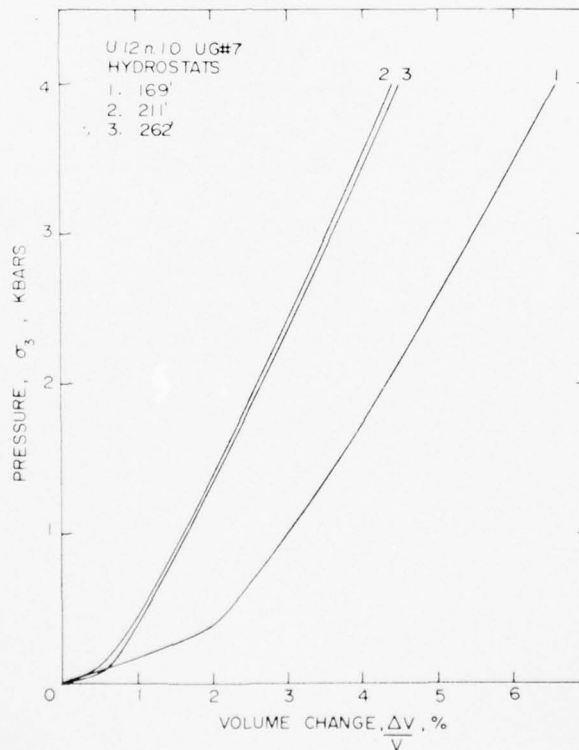


Figure 4: Hydrostatic compression test on U12n.10 UG#7 core samples -- confining pressure versus volume change.

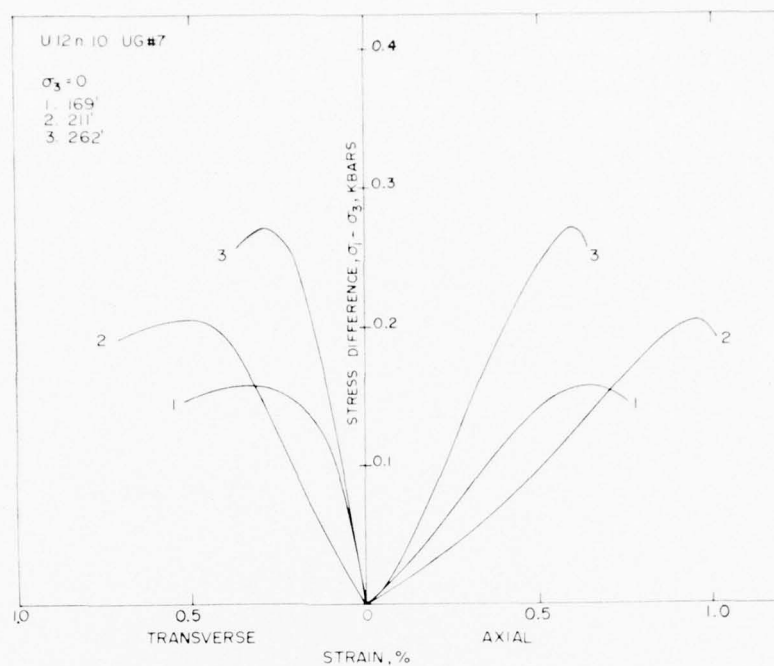


Figure 5: Unconfined compression tests on U12n.10 UG#7 core samples -- stress difference versus individual strains.

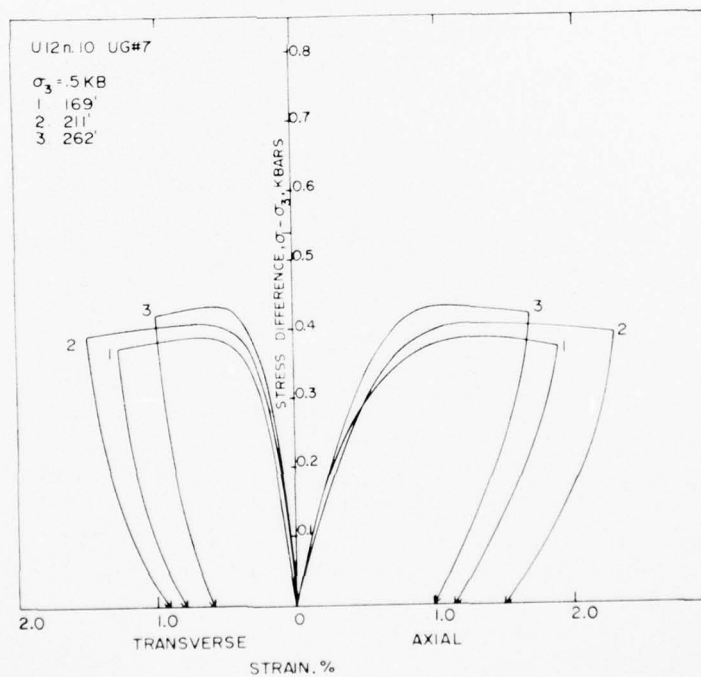


Figure 6: Triaxial compression tests at 0.5 kilobars confining pressure on U12n.10 UG#7 core samples -- stress difference versus individual strains.

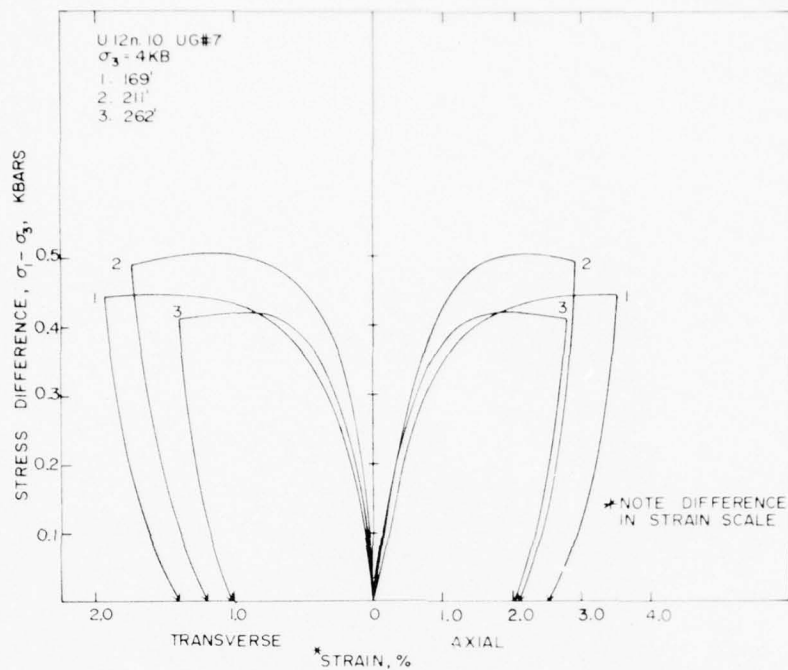


Figure 7: Triaxial compression tests at 4.0 kilobars confining pressure on U12n.10 UG#7 core samples -- stress difference versus individual strains.

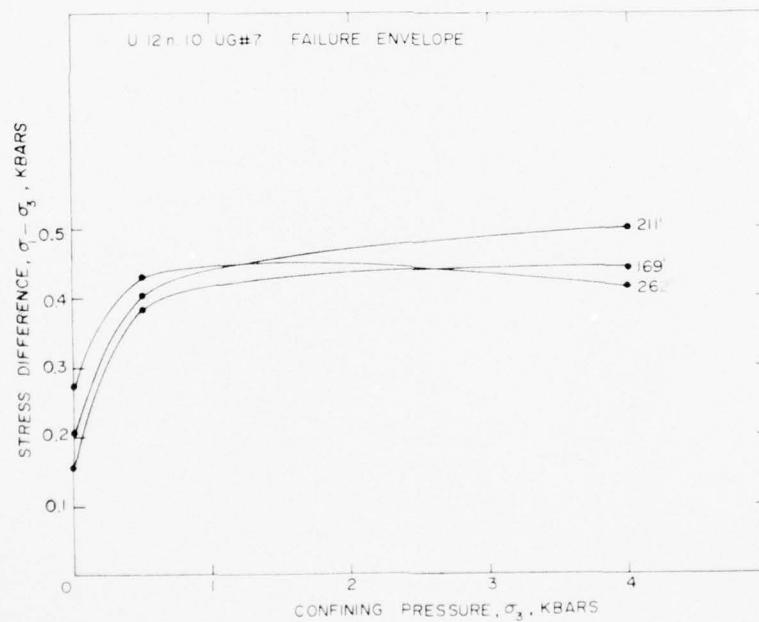


Figure 8: Failure envelope from triaxial compression tests on U12n.10 UG#7.

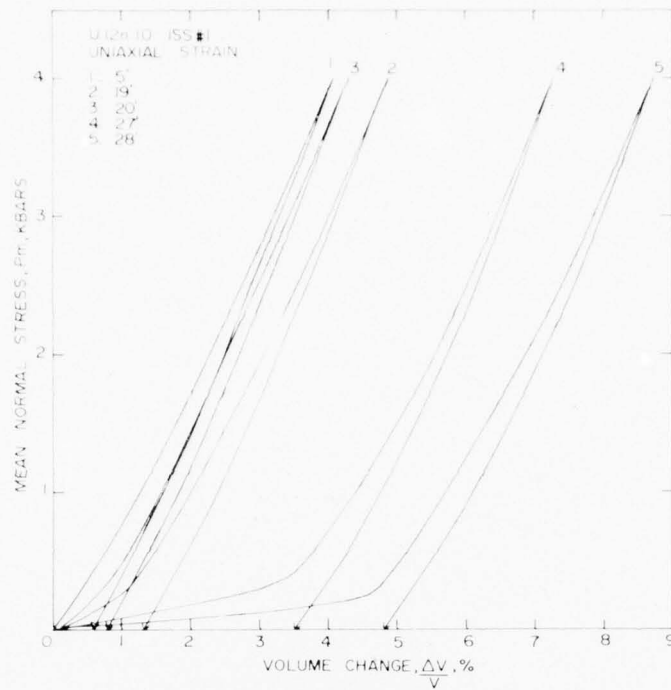


Figure 9a: Uniaxial strain tests on U12n.10 ISS#1 core samples -- mean normal stress versus volume change.

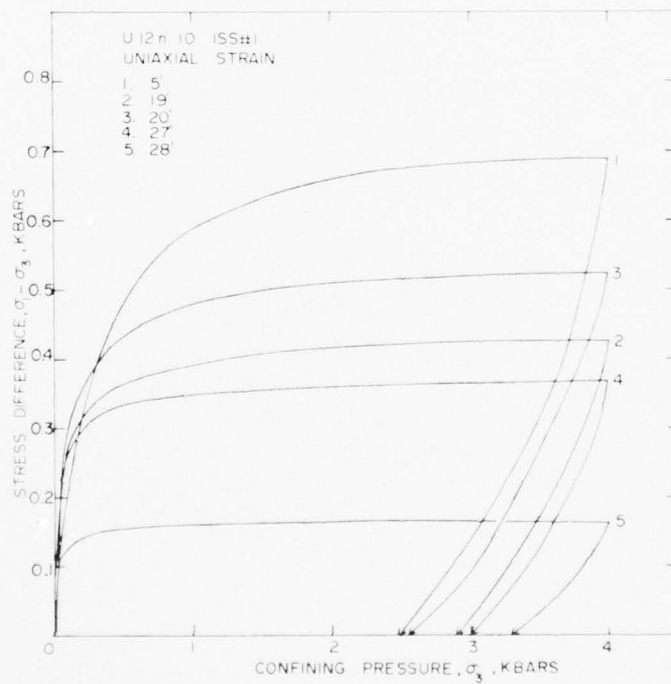


Figure 9b: Uniaxial strain tests on U12n.10 ISS#1 core samples -- stress difference versus confining pressure.

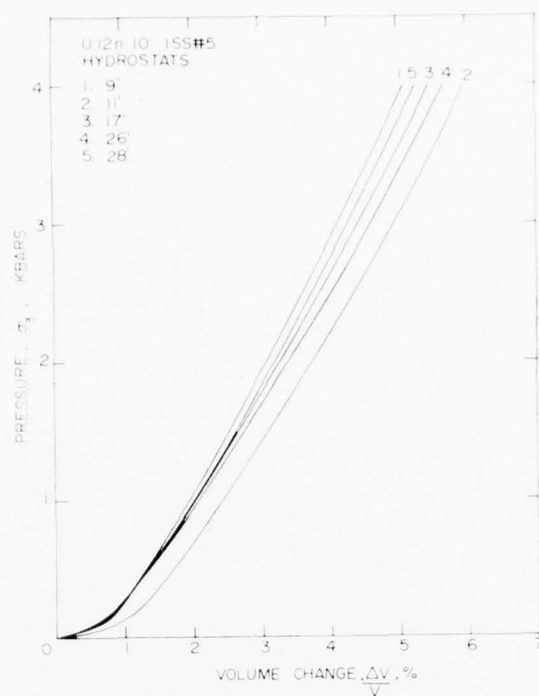


Figure 10: Hydrostatic compression tests on U12n.10 ISS#5 core samples
-- confining pressure versus volume change.

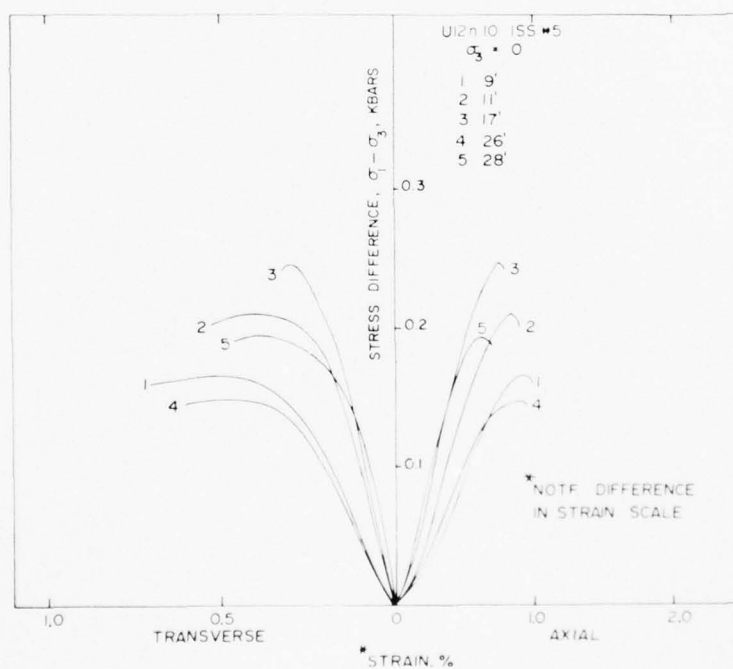


Figure 11: Unconfined compression tests on U12n.10 ISS#5 core samples
-- stress difference versus individual strains.

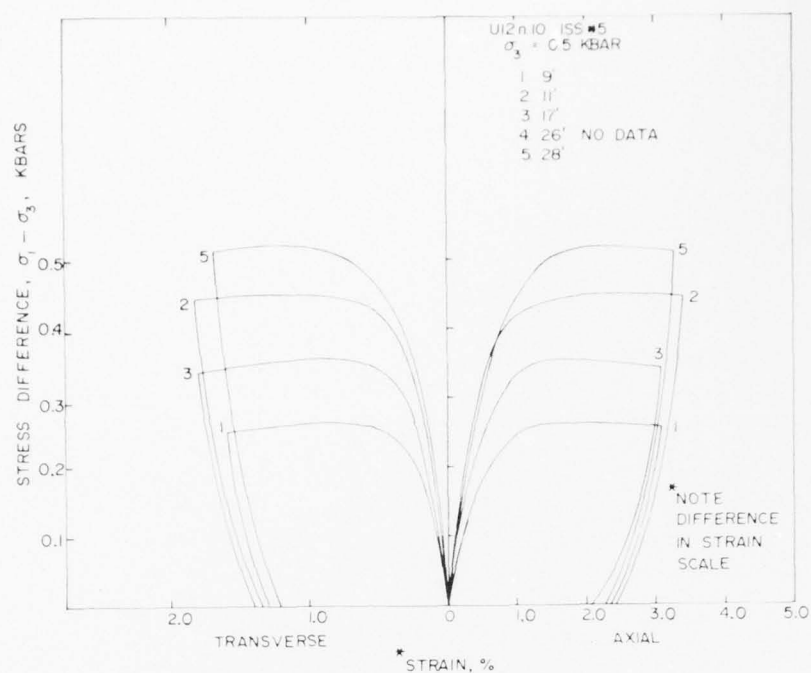


Figure 12: Triaxial compression tests at 0.5 kilobars confining pressure on U12n.10 ISS#5 core samples -- stress difference versus individual strains.

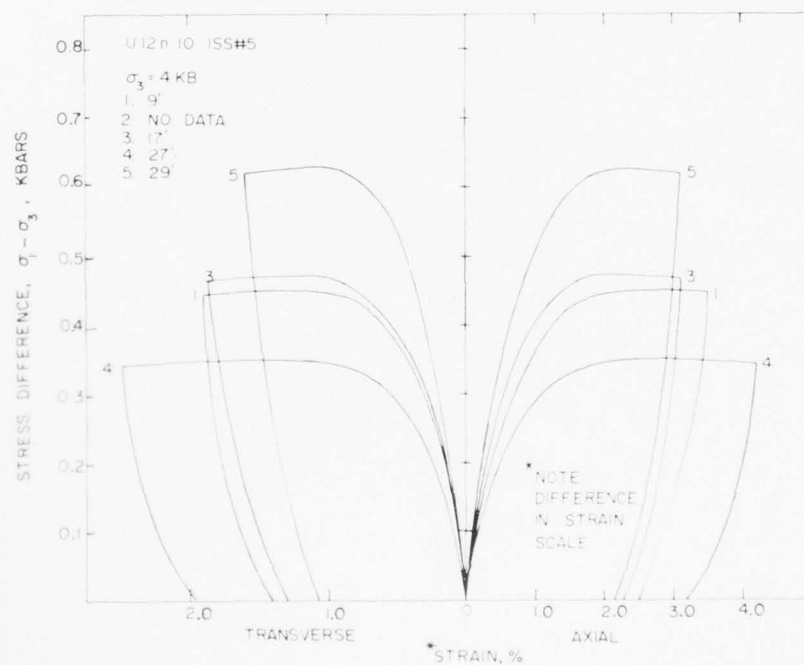


Figure 13: Triaxial compression tests at 4.0 kilobars confining pressure on U12n.10 ISS#5 core samples -- stress difference versus individual strains.

AD-A043 977

TERRA TEK INC SALT LAKE CITY UTAH

F/G 18/3

MATERIAL PROPERTIES OF NEVADA TEST SITE TUFF AND GROUT - WITH E--ETC(U)

NOV 76 S W BUTTERS, R K DROPEK, A H JONES

DNA001-75-C-0260

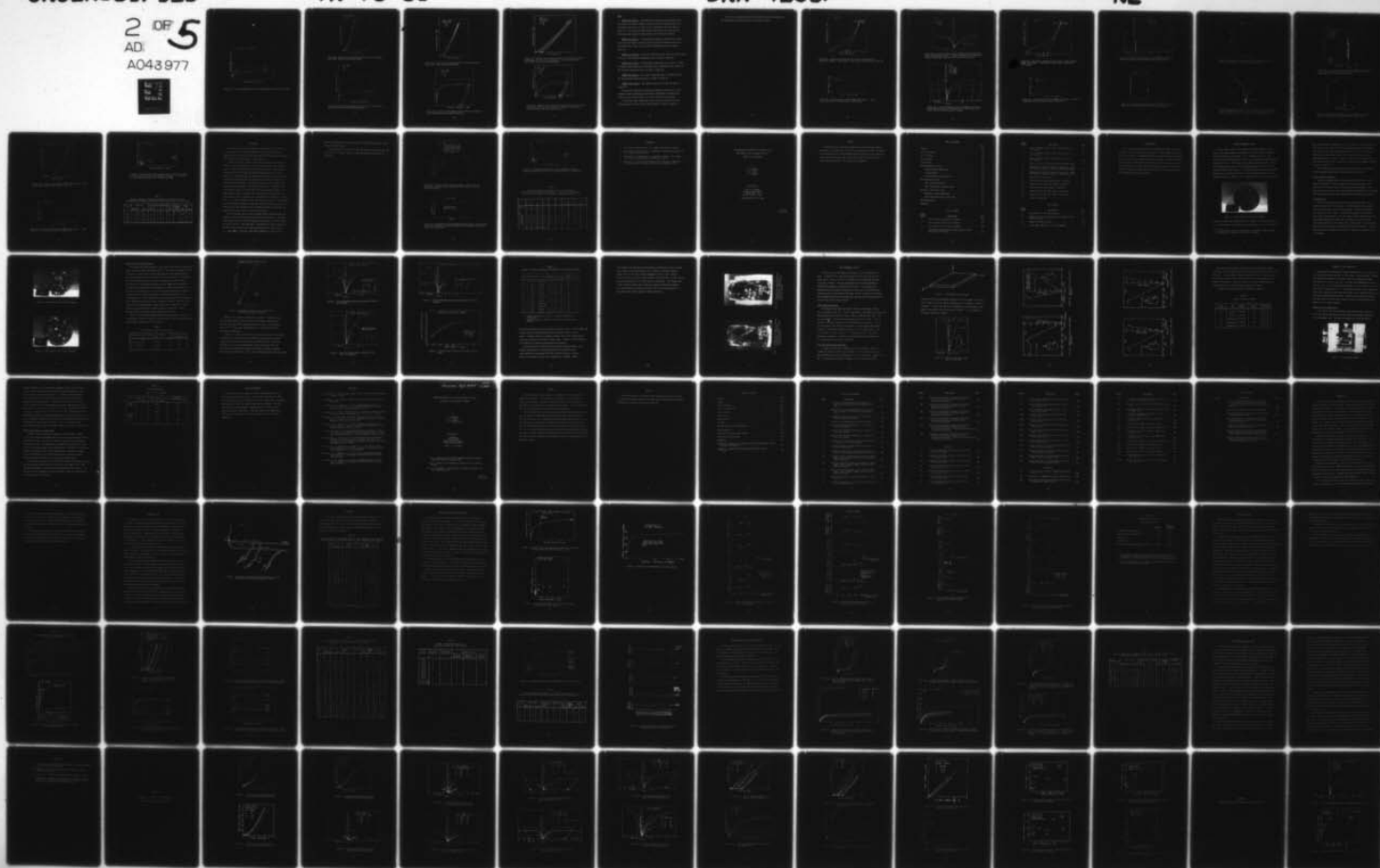
UNCLASSIFIED

TR-76-63

DNA-4235F

NL

2 OF 5
AD
A043 977



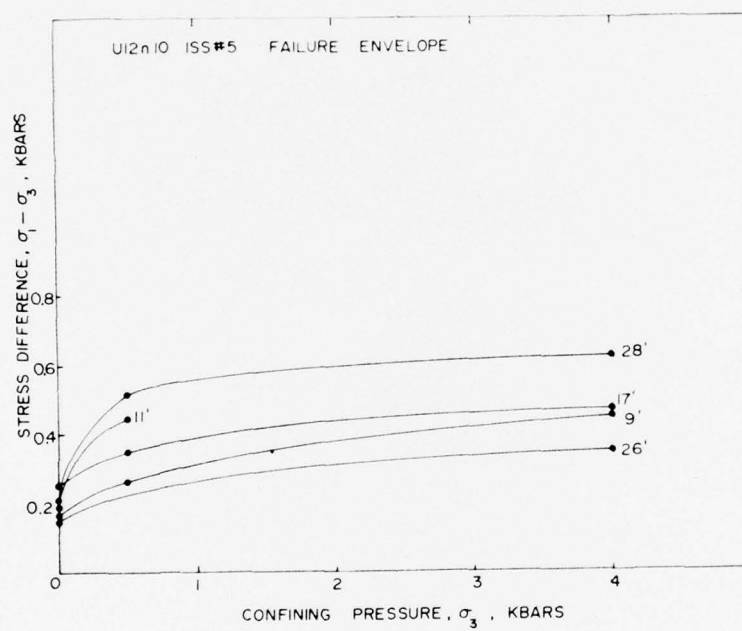


Figure 14. Failure envelope from triaxial compression tests on U12n.10 ISS#5.

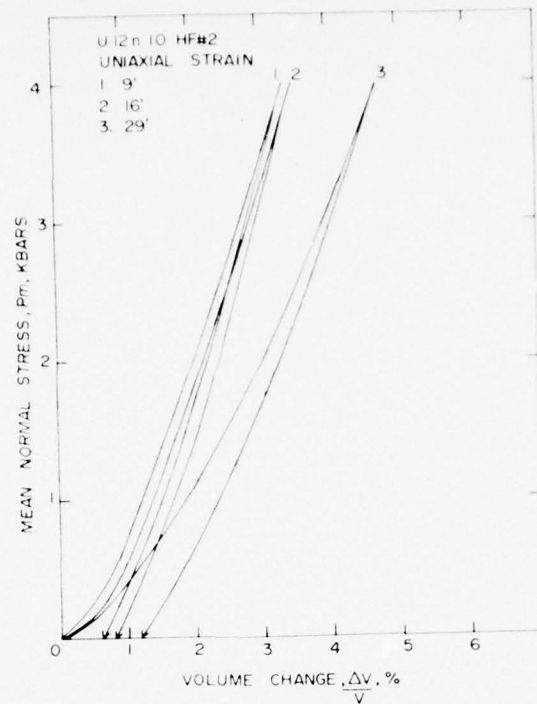


Figure 15a: Uniaxial strain tests on U12n.10 HF#2 core samples -- mean normal stress versus volume change.

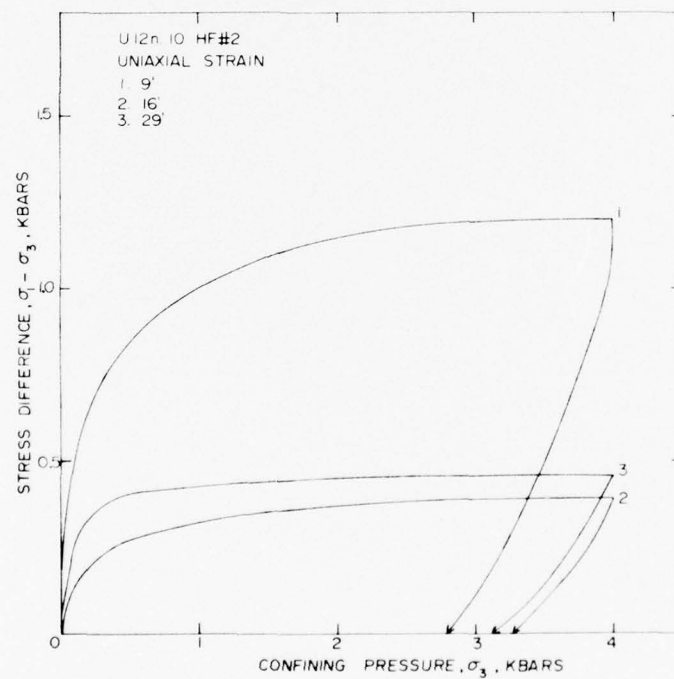


Figure 15b: Uniaxial strain tests on U12n.10 HF#2 core samples -- stress difference versus confining pressure.

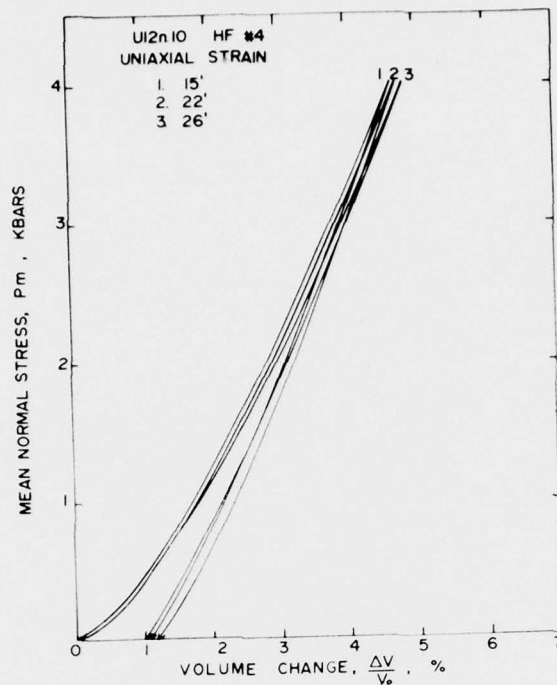


Figure 16a: Uniaxial strain tests on U12n.10 HF#4 core samples -- mean normal stress versus volume change.

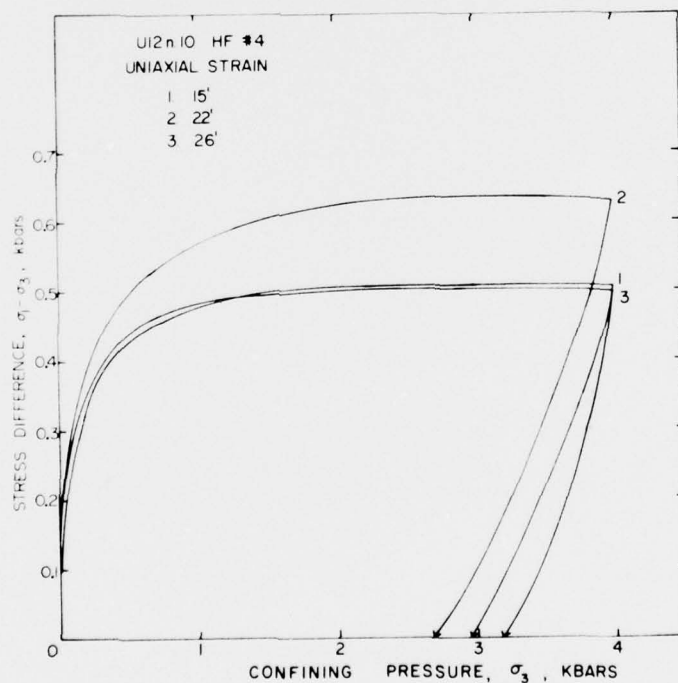


Figure 16b: Uniaxial strain tests on U12n.10 HF#4 core samples -- stress difference versus confining pressure.

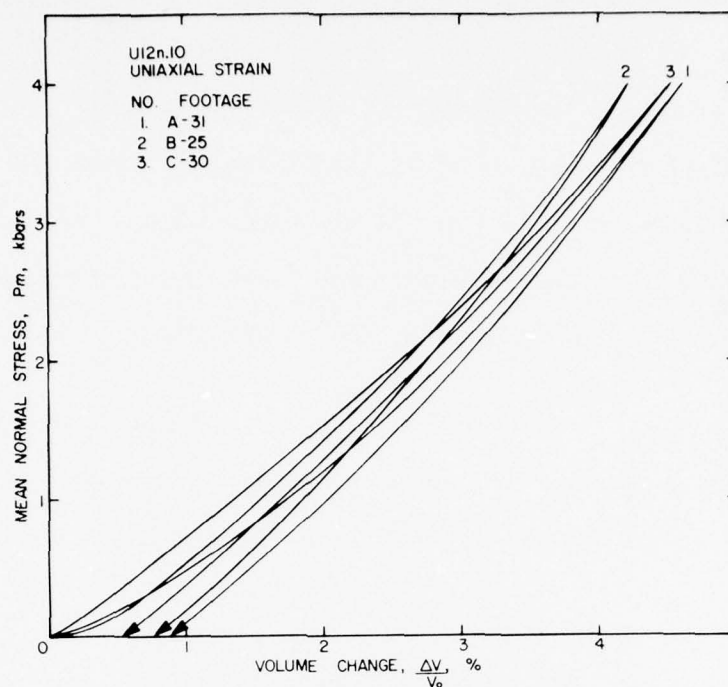


Figure 17a: Uniaxial strain tests on U12n.10 A Structures (31 feet), B Structures (25 feet) and C Structures (30 feet) core samples -- mean normal stress versus volume change.

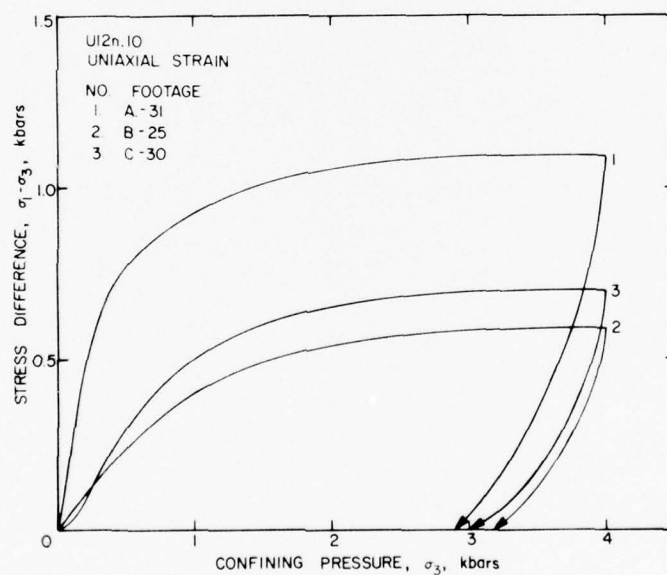


Figure 17b: Uniaxial strain tests on U12n.10 A Structures (31 feet), B Structures (25 feet) and C Structures (30 feet) core samples -- stress difference versus confining pressure.

GROUT

ME801 Grout Samples: The hydrostatic compression and uniaxial strain test curves are shown in Figure 18 while the stress difference versus the individual strain curves for the triaxial compression tests are shown in Figure 19. The failure surfaces based on the triaxial test data for the different grouts tested are shown at the end of this grout section.

ME802 Grout Samples: The hydrostatic compression and uniaxial strain test curves are shown in Figure 20 while the stress difference versus the individual strain curves for the triaxial compression tests are shown in Figure 21.

ME804 Grout Samples: The stress difference versus the axial and transverse strains for the unconfined compression test is shown in Figure 22.

ME805 Grout Samples: The hydrostatic compression test result is shown in Figure 23 while the stress difference versus individual strain curves for the triaxial compression tests are shown in Figure 24.

ME806 Grout Samples: The stress difference versus individual strains for the unconfined compression tests is shown in Figure 25.

ME8011 Grout Samples: The uniaxial strain test curves are shown in Figure 26.

The physical properties, hydrostatic compression and uniaxial strain permanent volume compactions and ultrasonic longitudinal and shear wave velocities are listed in Table 3 for all of the six grout mixtures.

The maximum stress difference (failure surface) during the triaxial compression tests on the various grout mixtures is shown in Figure 27.

As a note, the grout data shown was obtained from tests conducted at the fourteen day aging point of all of the grout mixtures.

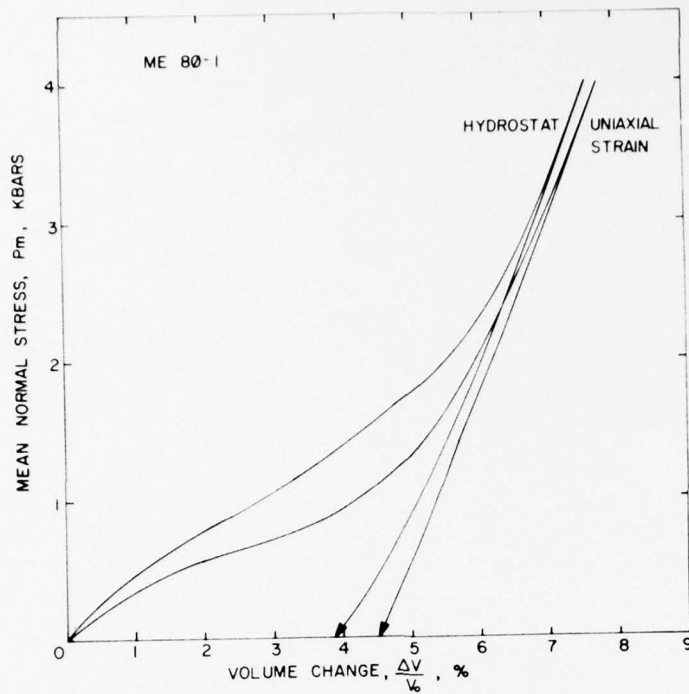


Figure 18a: Hydrostatic compression and uniaxial strain tests on ME801 grout samples -- mean normal stress versus volume change (14 day age).

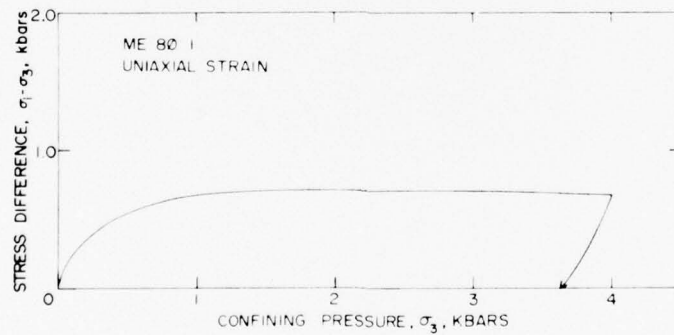


Figure 18b: Uniaxial strain test on ME801 grout sample -- stress difference versus confining pressure (14 day age).

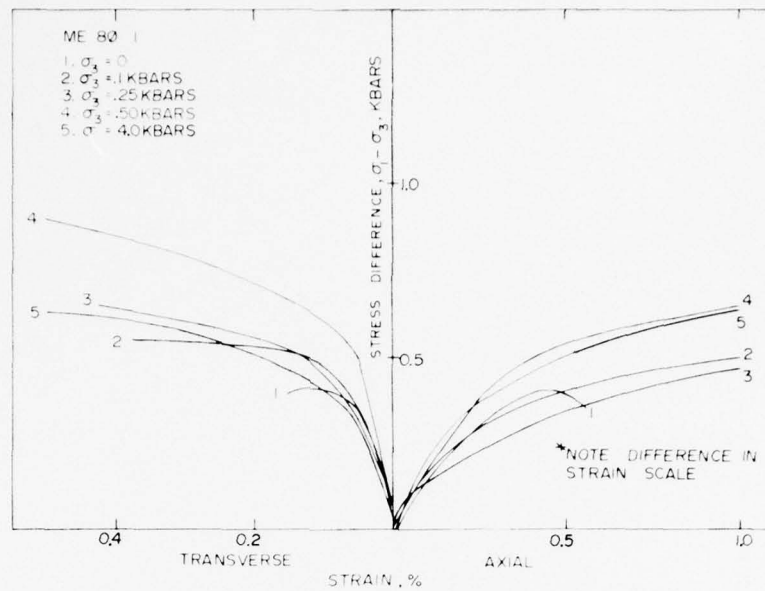


Figure 19a: Low stress-strain portion of the triaxial compression tests on ME801 grout samples -- stress difference versus individual strains (14 day age), see Figure 19b for entire test curves.

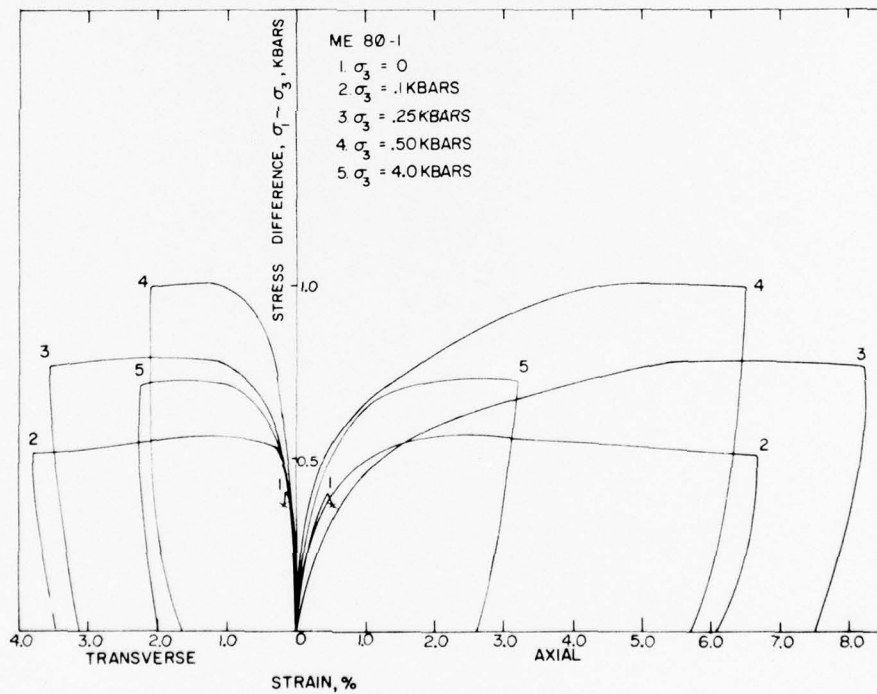


Figure 19b: Triaxial compression tests on ME801 grout samples -- stress difference versus individual strains (14 day age), see Figure 19a for low stress-strain response.

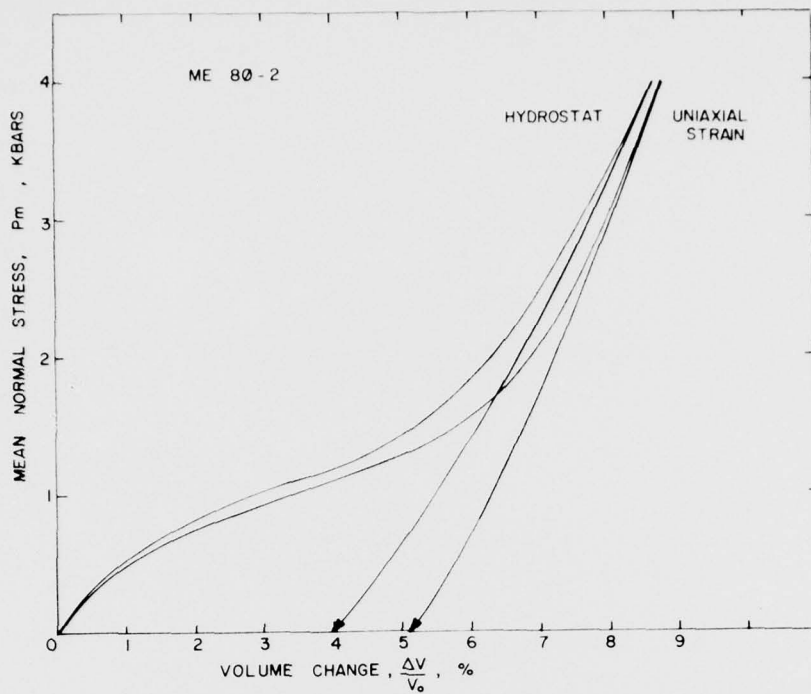


Figure 20a: Hydrostatic compression and uniaxial strain tests on ME802 grout samples -- mean normal stress versus volume change (14 day age).

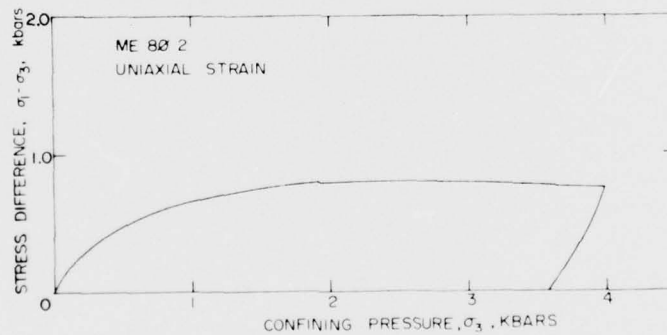


Figure 20b: Uniaxial strain test on ME802 grout sample -- stress difference versus confining pressure (14 day age).

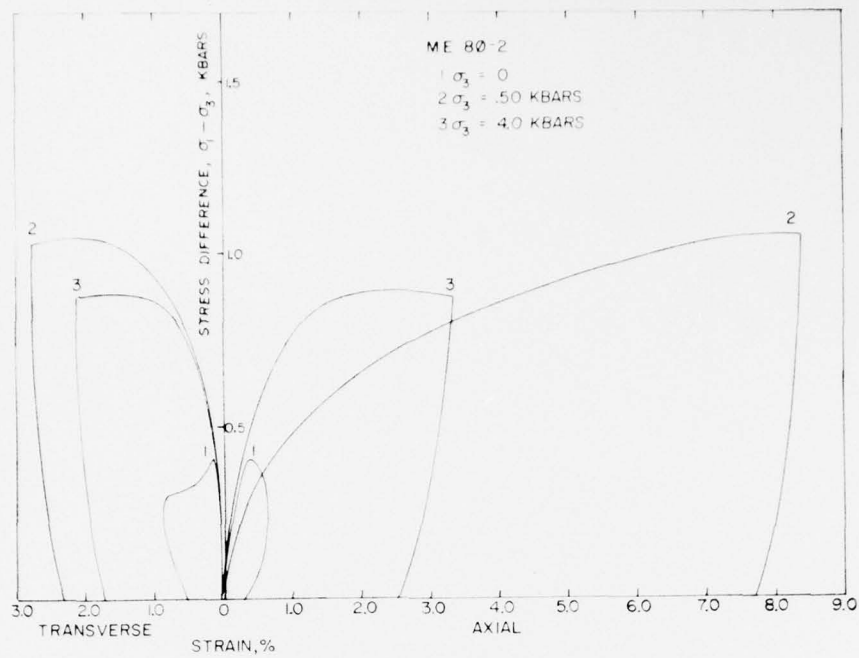


Figure 21: Triaxial compression tests on ME802 grout sample -- stress difference versus individual strains (14 day age).

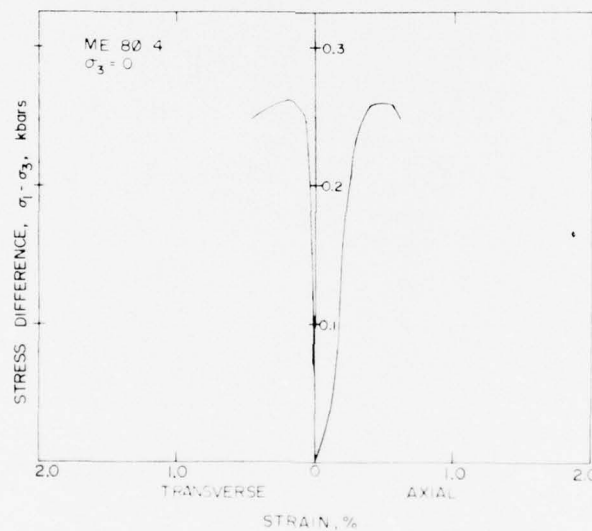


Figure 22: Unconfined compression test on ME804 grout sample -- stress difference versus individual strains (14 day age).



Figure 23: Hydrostatic compression test on ME805 grout sample -- confining pressure versus volume change (14 day age).

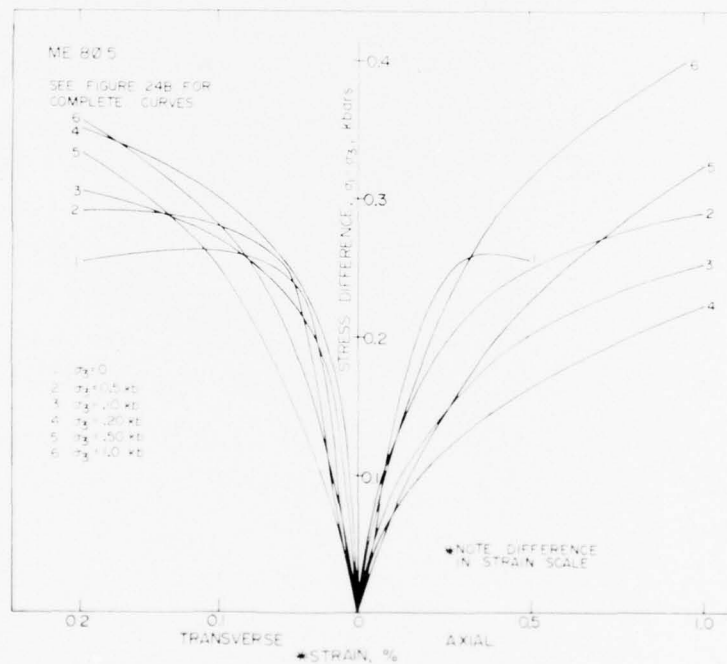


Figure 24a: Low stress-strain portion of the triaxial compression tests on ME805 grout samples -- stress difference versus individual strains (14 day age), see Figure 24b for entire test curves.

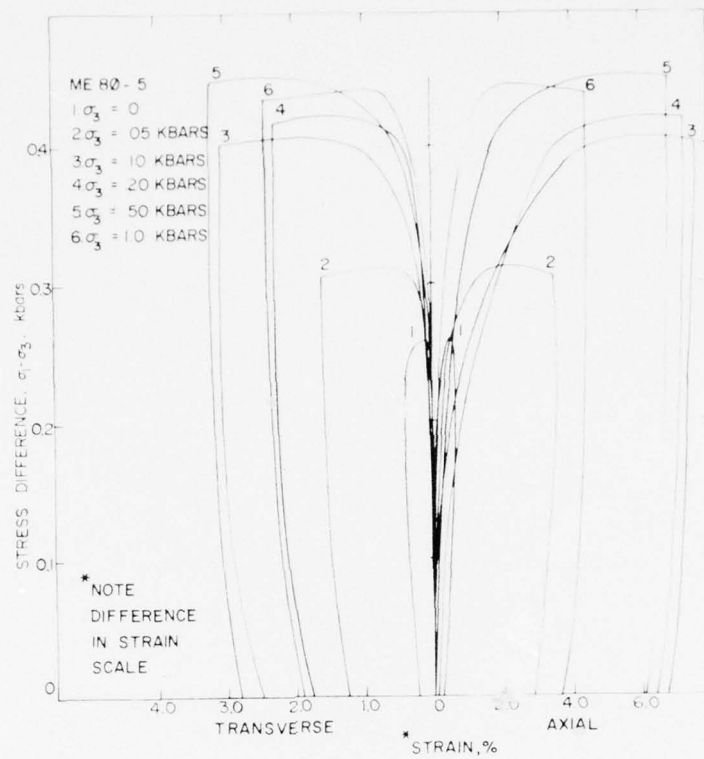


Figure 24b: Triaxial compression tests on ME805 grout samples -- stress difference versus individual strains (14 day age), see Figure 24a for low stress-strain response.

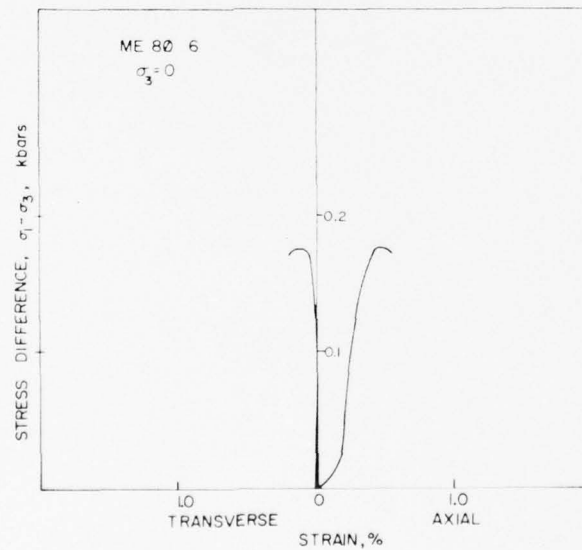


Figure 25: Unconfined compression tests on ME806 grout sample -- stress difference versus individual strains (14 day age).

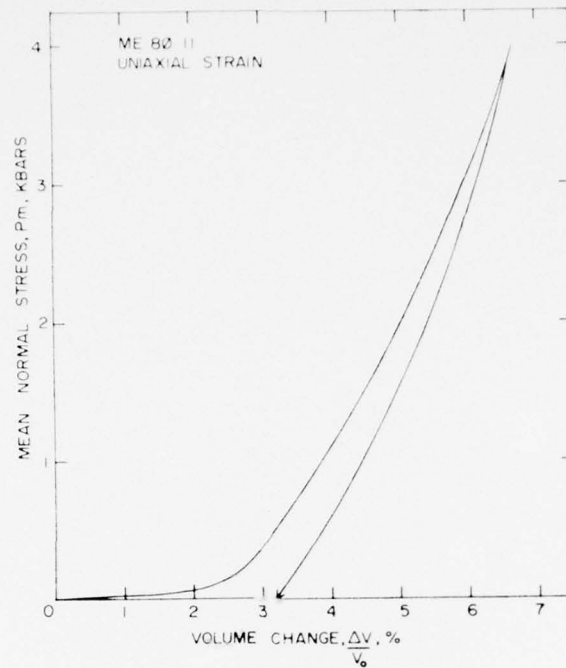


Figure 26a: Uniaxial strain tests on ME8011 grout sample -- mean normal stress versus volume change (14 day age).

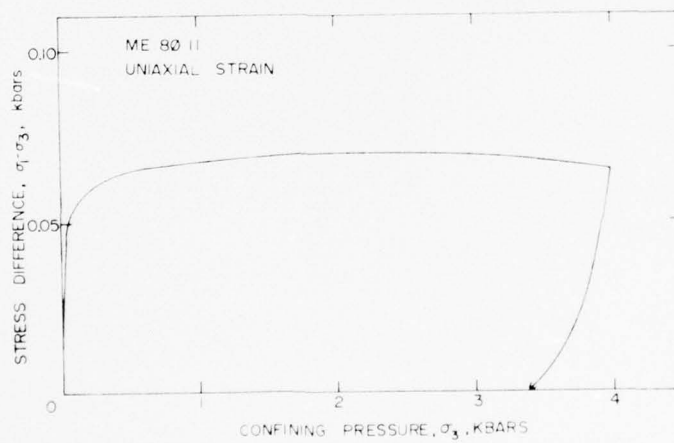


Figure 26b: Uniaxial strain tests on ME8011 grout sample -- stress difference versus confining pressure (14 day age).

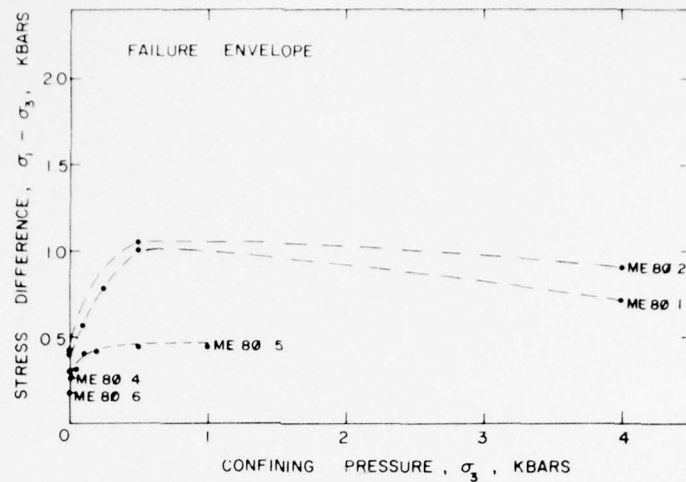


Figure 27: Failure envelope based on the triaxial compression tests on ME801, ME802 and ME805 grout samples (14 day age). Also shown is the unconfined compression tests on ME804 and ME806.

TABLE 3

Physical Properties, Hydrostatic Compression and Uniaxial Strain
Permanent Volume Compaction and Ultrasonic Wave Velocities on Grout Samples

DRILL HOLE FOOTAGE	DENSITY gm/cc			% WATER BY WET WEIGHT	POROSITY %	SATURATION %	% CALC. AIR VOIDS	% MEAS. PERMANENT CCMP.	VELOCITY ft/sec	
	AS- RECEIVED	DRY	GRAIN						LONG	SHEAR
ME801	1.95	1.61	2.57	17.4	38	90	3.7	Hyd. 1-D 3.9 4.5 4.0 5.1	12670	7402
ME802	1.89	1.57	2.54	17.0	38	84	6.1		12864	7188
ME804	1.91	1.56	2.52	18.5	38	92	2.9			
ME805	1.97	1.67	2.53	15.5	34	89	3.7		12700	7100
ME806	2.01	1.74	2.50	13.6	31	90	3.2			
ME8011	2.05	1.77	2.53	13.7	30	93	2.0	3.4	9420	4272

DISCUSSION

The matching of the grout properties to the properties of the tuff in the structural test area is essential to the structures program. A good match would eliminate many pre-shot and most likely post-shot questions about the effect of differences in the properties.

In order to achieve a match, it was first necessary to characterize the tuff in the structures area. Up to the time that the match question arose, a number of exploratory tests had been conducted. These tests included uniaxial strain, physical property measurements and ultrasonic velocities. From these data, one could obtain absolute values for most of the important properties with the exception of the shear strength of the material (failure envelope). The failure envelope may be estimated from the stress-strain response of the uniaxial strain test. Therefore, the stress-strain curves for forty uniaxial strain tests were averaged. From these averages, failure envelopes were estimated (from experience, the stress-strain curve is assumed to be a lower bound) as reported in a letter to Mr. J. W. LaComb, 29 August, 1975, and shown in Figure 28. The estimated failure envelopes, admittedly, do not give the exact shape and can vary in magnitude, but they provided an early strength estimate in order that the process of matching a grout to the tuff could begin.

Failure envelopes from triaxial compression tests have since been obtained for the tuff from the structures test area (Figure 14). With this recent data, the early strength estimates and comparative triaxial compression data on U12n-10 ISS#7 from WES⁴, a representative failure envelope of the tuff in the structures area was approximated by the author and Mr. R. L. Stowe (WES), Figure 29. This failure envelope is shown again in

Figure 30 along with the failure surfaces of some of the Mighty Epic grout mixtures tested to date.

Other properties of the tuff in the structures area have been averaged and the data is listed in Table 4, again with the grout properties for comparison.

ESTIMATED FAILURE ENVELOPES

CURVE	SOURCE
1	10 UNIAXIAL STRAIN TESTS ON CORE SAMPLES, (1176 THUR 1399) FROM U12n.10 UG#1
2	5 UNIAXIAL STRAIN TESTS ON CORE SAMPLES, (227 THUR 307) FROM U12n.10 UG#4
3	5 UNIAXIAL STRAIN TESTS ON CORE SAMPLES, (84 THUR 216) FROM U12n.10 UG#6A
4	20 UNIAXIAL STRAIN TESTS ON CORE SAMPLES, (3 THUR 309) FROM U12n.10 UG#7
5	AVERAGE OF ALL OF THE ABOVE

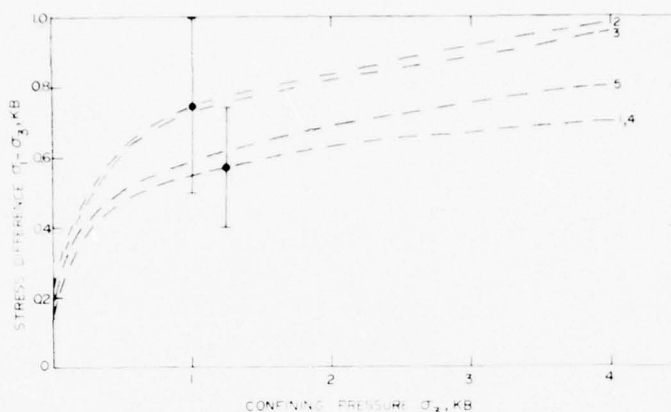


Figure 28: Estimated failure envelopes based on uniaxial strain test results on core samples from U12n.10 UG#4, UG#6a, ISS#5 and ISS#7 drill holes³.

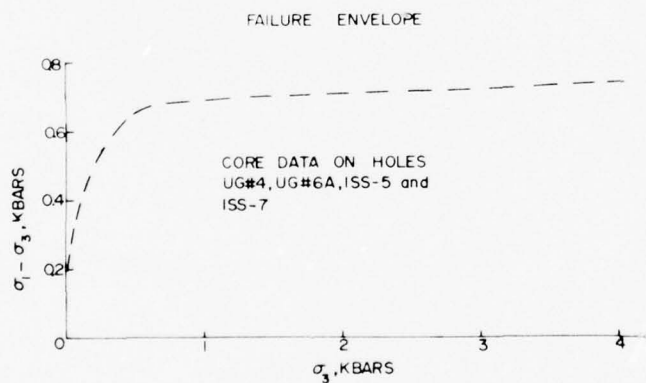


Figure 29: Representative failure envelope for the tuff in the Structures area, based on uniaxial strain tests and triaxial compression test data from Terra Tek and WES⁴.

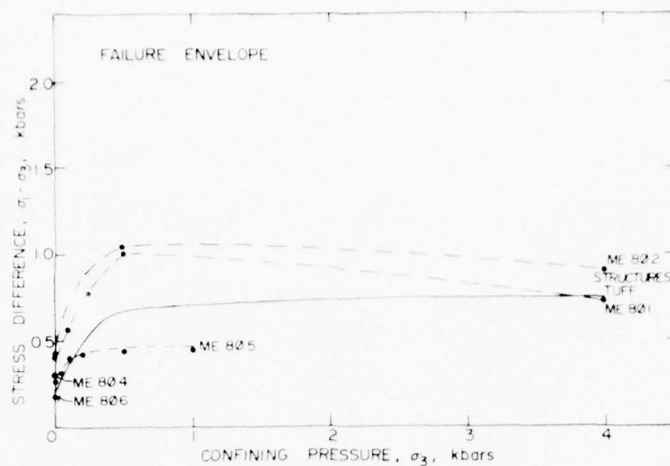


Figure 30: Combined structures tuff failure envelope and grout failure envelopes shown in Figure 29 and Figure 27, respectively.

TABLE 4

Average Structures Tuff Physical Properties, Permanent Compaction and Ultrasonic Wave Velocities. Also listed for comparison is the physical properties of the grout as reported in Table 3.

Drill Hole Footage	Density gm/cc			% Water By Wet Weight	Porosity %	Saturation %	Calc. Air Voids	Meas. Permanent Comp.		Velocity ft/sec	
	As- Received	Dry	Grain							Long	Shear
STRUCTURES TUFF	1.97 +0.04*	1.67 +0.08	2.40 +0.04	15 +2	29 +8	96 -2	1.2 +0.7	1.1 +0.3		10,400 +1100	5300 +1100
GROUT								Hyd. 1-D			
ME801	1.95	1.61	2.57	17.4	38	90	3.7	3.9 4.5		12670	7402
ME802	1.89	1.57	2.54	17.0	38	84	6.1	4.0 5.1		12864	7188
ME804	1.91	1.56	2.52	18.5	38	92	2.9				
ME805	1.97	1.67	2.53	15.5	34	89	3.7			12700	7100
ME806	2.01	1.74	2.50	13.6	31	90	3.2				
ME8011	2.05	1.77	2.53	13.7	30	93	2.0	3.2		9420	4272
* + values represent one standard deviation.											

REFERENCES

1. Core samples supplied by Mr. J. W. LaComb, DNA, Mercury, Nevada.
2. Grout samples supplied by Mr. R. Bendenelli, Waterways Experiment Station, Vicksburg, Mississippi.
3. Letter from S. W. Butters to J. W. LaComb, 29 August, 1975, subject -- "Estimated Failure Envelopes on Mighty Epic Tuff".
4. Stowe, R. L., "Triaxial Test Results of Tuff and Grout", Waterways Experiment Station, Vicksburg, Mississippi, September, 1975.

SOME MECHANICAL PROPERTIES OF CONCRETE, STEEL
AND CONCRETE-STEEL INTERFACES USED IN
MIGHTY EPIC STRUCTURES

by

R. K. Dropek
D. O. Enniss
R. S. Rosso
S. W. Butters

Submitted to

Mr. J. W. LaComb
Defense Nuclear Agency
Nevada Test Site
Mercury, Nevada 89023

Contract DNA 001-75-C-0260

TR 76-14
July 1976

PREFACE

Concrete and steel structure response was predicted and measured for the Mighty Epic nuclear test in Area 12 of the Nevada Test Site. In support of this analysis Terra Tek determined material properties of the steel and three types of concrete as well as the coefficient of friction for the steel-concrete interface. Test results are presented.

TABLE OF CONTENTS

	<u>Page</u>
Preface	118
Table of Contents	119
List of Figures	119
List of Tables	120
Introduction	121
Concrete Mechanical Tests	122
Concrete Sample Preparation	123
Instrumentation	123
Concrete Results and Conclusions	125
Steel Mechanical Tests	132
Steel Sample Preparation	132
Steel Test Results and Conclusions	132
Concrete - Steel Shear Tests	137
Apparatus and Instrumentation	137
Direct Shear Results and Conclusions	138
Concluding Remarks	140
References	141

LIST OF FIGURES

<u>Figure Number</u>	<u>Description</u>	<u>Page</u>
1	Cross section of LBC-5.5 ksi concrete	122
2	Cross section of LH-5.5 ksi concrete	124
3	Cross section of LH-7.2 ksi concrete	124
4	Hydrostatic pressure versus volume strain for the three types of concrete	126

<u>Figure Number</u>	<u>Description</u>	<u>Page</u>
5	Stress difference versus strain plots for LBC-5.5 ksi concrete	127
6	Stress difference versus strain plots for LH-5.5 ksi concrete	127
7	Stress difference versus strain plots for LH-7.2 ksi concrete	128
8	Ultimate stress surface for the three concrete types . . .	128
9	Photograph of sample 23 showing failure mode. Sample was triaxially tested at 212 bars confining pressure . . .	131
10	Photograph of sample 25 showing failure mode. Sample was triaxially tested at 552 bars confining pressure . . .	131
11	Orientation of steel plate	133
12	Tensile stress-strain steel sample, X direction	133
13	Compressive tests on steel sample, X direction	134
14	Tensile test on steel sample, Y direction	134
15	Compressive test on steel sample, Y direction	135
16	Compressive test on steel sample, Z direction	135
17	Direct shear machine	137

LIST OF TABLES

<u>Table Number</u>	<u>Description</u>	<u>Page</u>
I	Bulk Moduli for the Three Concretes	125
II	Summary of Triaxial Compression Test Results for the Three Concretes	129
III	Summary of Steel Test Data	136
IV	Direct Shear Data (LBC - 5.5 ksi concrete)	139

INTRODUCTION

One of the experiments planned for the Mighty Epic event in Area 12, Nevada Test Site was to evaluate the effects of shock loading on concrete and steel structures. Experimental analysis required mechanical properties for the concrete, steel and concrete-steel interfaces. Concrete properties were determined through uniaxial and triaxial compression tests at quasi-static loading rates. Steel samples were tested in uniaxial tension and compression while the coefficient of friction for the concrete interfaces were determined in direct shear tests.

CONCRETE MECHANICAL TESTS

Concrete samples used in this study were obtained from two sources. Lasker Boiler and Engineering Corporation of Chicago, Illinois supplied 30 standard cylindrical test samples 15.2 cm. diameter by 30.5 cm. long. This concrete was designated LBC-5.5 ksi (i.e., anticipated 28 day unconfined strength of 5.5 ksi). The average water-cement ratio was 0.36:1*; the mean coarse aggregate size was 1.9 cm. and comprised about 45 percent of the concrete by weight (see Figure 1).¹ The second concrete source was Lockheed Shipbuilding and Construction Company, Seattle, Washington from which 60 standard cylindrical samples, 15.2 cm. diameter by 30.5 cm. long were obtained.

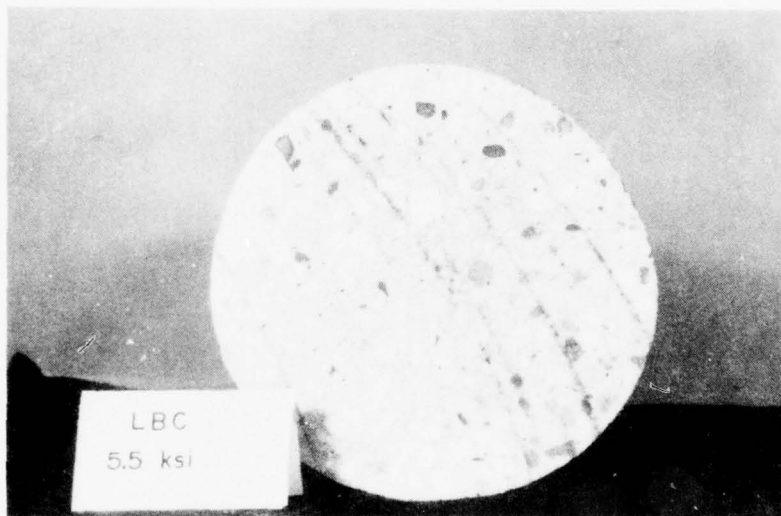


Figure 1. Cross section of LBC-5.5 ksi concrete.

These 60 cylinders were subdivided into two groups: 30 cylinders were a 5.5 ksi mix design while the remaining 30 cylinders were of a 7.2 ksi mix design.

* The water-cement ratio is here defined as the weight of water divided by the weight of cement per cubic yard of concrete.

These cylinders were designated as LH-5.5 ksi and LH-7.2 ksi, respectively, indicating a 5.5 ksi and 7.2 ksi 28 day unconfined compressive strength. Both concretes had a mean coarse aggregate size of 1.3 cm. The LH-5.5 ksi concrete had a water-cement ratio of 0.39:1 and was 56 percent coarse aggregate by weight as shown in Figure 2. The LH-7.2 ksi concrete had a water-cement ratio of 0.44:1 and was 14.5 percent coarse aggregate by weight as shown in Figure 3.²

The cylinders were shipped sealed to preserve moisture. Mechanical testing commenced approximately 2 months after the pour date.

Concrete Sample Preparation

Concrete test sample ends were ground parallel to within $\pm .005$ cm. Samples designated for triaxial compression testing were examined for subsurface cavities which might collapse during pressurization. These cavities were filled with a grout and subsequently jacketed with polyurethane. Steel endcaps were attached with rubber tape and stainless steel lockwire.

Instrumentation

Both axial and lateral stresses and strains were measured. Axial stress was measured to within 6 bars. A 350 ohm manganin wire pressure coil was used to obtain the confining pressure. Pressure coil readings were accurate to within 2 bars. Confining pressure was also monitored with a Heise pressure gauge. Axial and lateral strains were obtained using strain gauged cantilever systems and calibrated to be accurate within .006 percent strain and .003 percent strain, respectively. A more detailed description of the transducer systems may be found in Reference 3. During testing, data was recorded using a PDP Lab 11 computer in conjunction with x-y recorders.

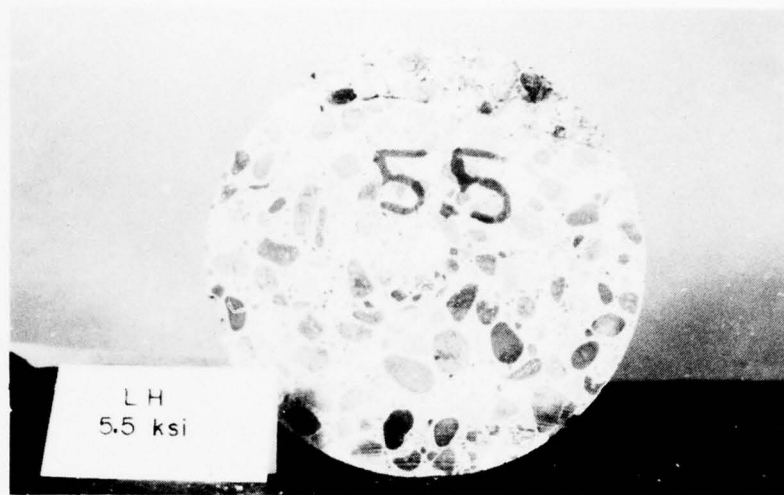


Figure 2. Cross section of LH-5.5 Ksi concrete.

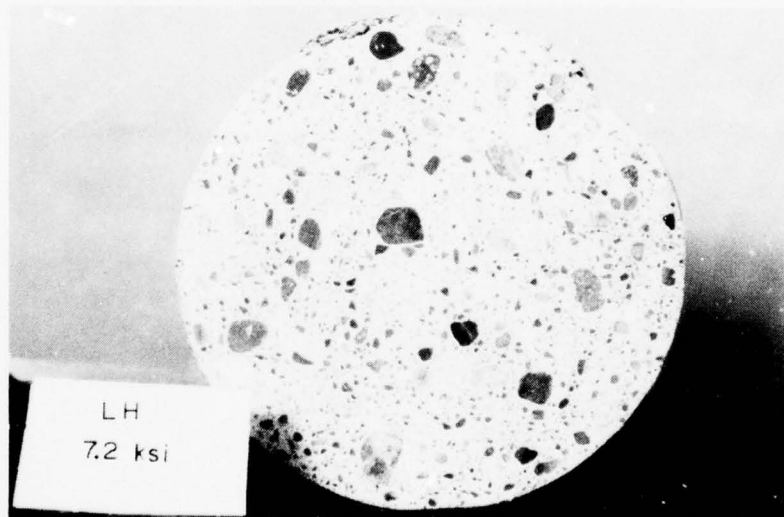


Figure 3. Cross section of LH-7.2 Ksi concrete.

Concrete Results and Conclusions

The general shape and character of the stress-strain triaxial compression curves agree with other published results.⁴⁻⁷ The initial non-linear portion of the stress-strain curves for both the hydrostatic and unconfined tests have been shown to occur if microcracks exist in the concrete.⁸ Microcracks may have resulted from excessive mortar shrinkage due to excess water or by separation of the aggregate and matrix due to temperature fluctuations. In addition, the handling and transportation of "green" concrete may have an effect on microcracking. This initial nonlinear portion was followed by a linear region up to about 50 percent of the failure strength for the unconfined tests. A third stage during unconfined testing was then observed which showed nonlinear stress-strain response to failure. After the initial nonlinear foot, the hydrostatic loading curves also showed fairly linear response up to about 500 bars confining pressure after which a second nonlinear confining pressure-volume strain region occurred.

Table I lists the bulk modulus determined from hydrostatic loading of the concrete as shown in Figure 4. The bulk moduli in Table I were determined using a secant slope from 0 to 0.55 kilobars.

TABLE I
Bulk Moduli for the Three Concretes

Concrete Type	Hydrostatic Stress Range, bars	Bulk Modulus, Kb (0 to 552 bars)
LBC - 5.5 ksi	0 to 552	110
LH - 5.5 ksi	0 to 552	138
LH - 7.2 ksi	0 to 552	96

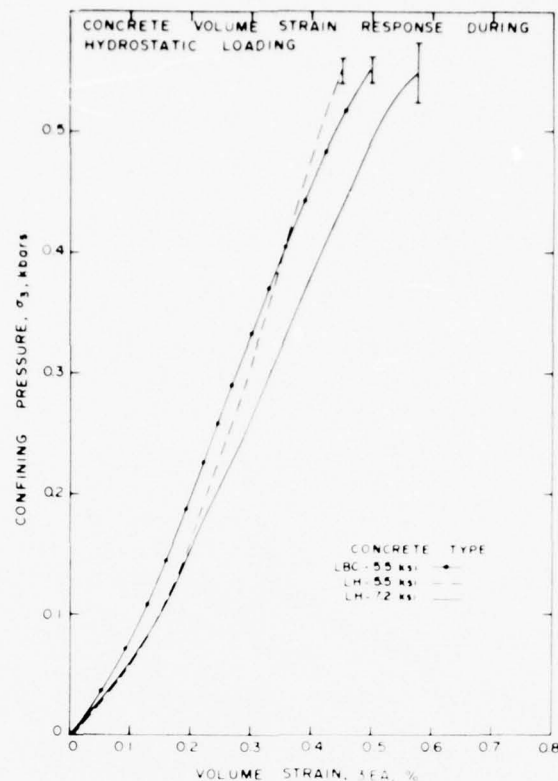


Figure 4. Hydrostatic pressure versus volume strain for the three types of concrete.

Table II lists triaxial compression test results. Published values for the Young's modulus range from 200 to 400 kilobars depending upon concrete mix design, while reported values for Poisson's ratio average about 0.2.^{9,10} The values reported herein are consistent with those previously reported data.

Figures 5, 6, and 7 show the triaxial stress-strain data for the three concrete types. The maximum stress difference attained during triaxial compression testing was interpreted as the ultimate stress. Obtaining reliable stress-strain data beyond the ultimate stress was often not possible due to catastrophic sample failure which resulted in exceeded data acquisition capabilities. Thus, the arrows indicate the direction taken

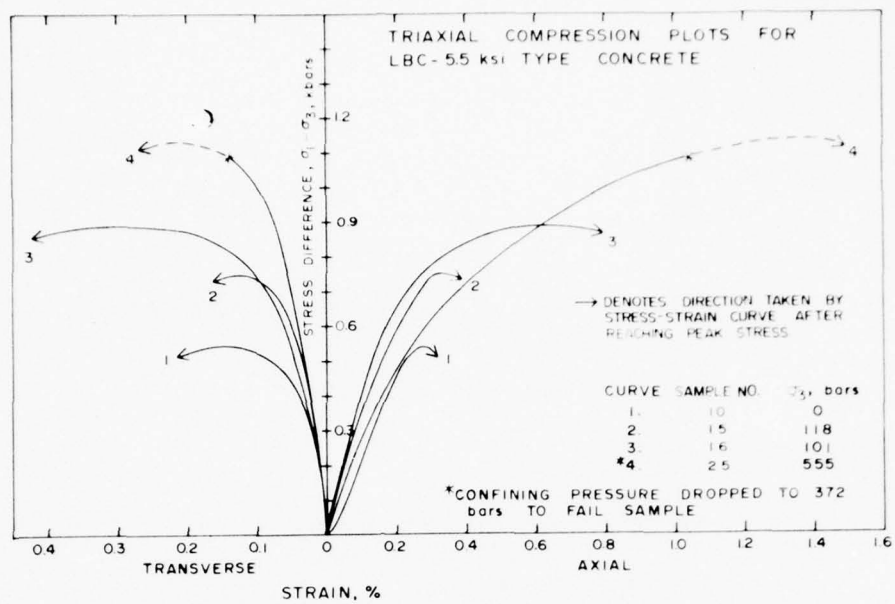


Figure 5. Stress difference versus strain plots for LBC-5.5 ksi concrete.

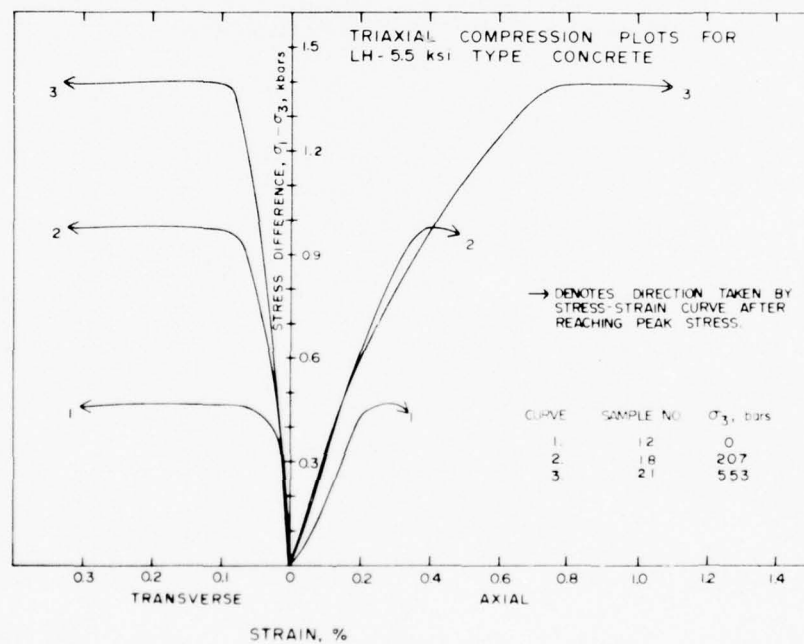


Figure 6. Stress difference versus strain plots for LH-5.5 ksi concrete.

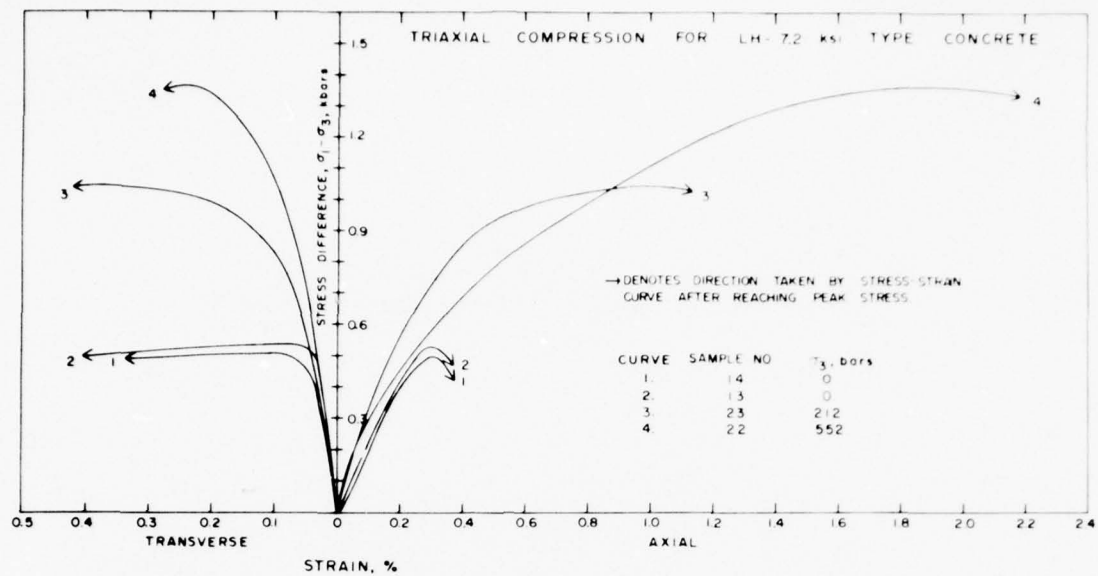


Figure 7. Stress difference versus strain plots for LH-7.2 ksi concrete.

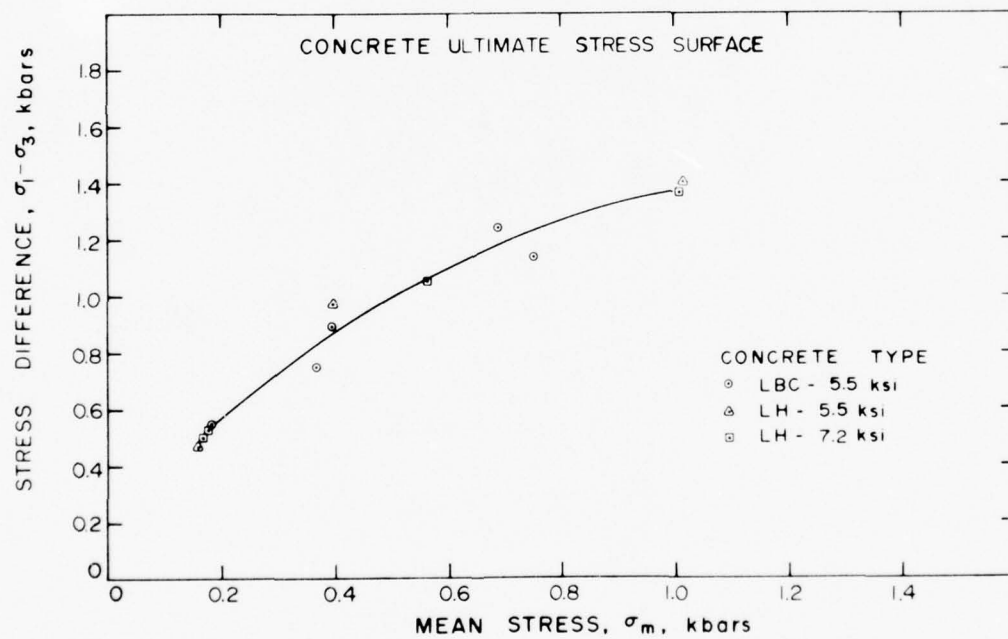


Figure 8. Ultimate stress surface for the three concrete types.

TABLE II
Summary of Triaxial Compression Test Results for the Three Concretes

Sample	Concrete Type	Test Type	Ultimate Stresses, bars			Young's Modulus, Kb	Poisson's Ratio
			σ_3	$\sigma_1 - \sigma_3$	σ_{mean}		
10	LBC-5.5	Unconfined	0	546	182	260*	0.12
16	LBC-5.5	Triaxial	101	888	397	445	0.33
15	LBC-5.5	Triaxial	118	750	368	400	0.20
17	LBC-5.5	Triaxial	276	1240	690	---	---
25	LBC-5.5	Triaxial	372	1138**	751	300	0.14
12	LH-5.5	Unconfined	0	470	157	260*	0.08
18	LH-5.5	Triaxial	207	976	395	320	0.13
21	LH-5.5	Triaxial	552	1395	1018	330	0.13
13	LH-7.2	Unconfined	0	528	176	210*	0.10
14	LH-7.2	Unconfined	0	500	167	230*	0.15
23	LH-7.2	Triaxial	212	1055	564	345	0.23
22	LH-7.2	Triaxial	552	1366	1007	345	0.20

* Scaled on linear portion of curve, (i.e., does not include the "foot on the curve).

** Confining pressure, σ_3 , lowered from 552 to 372 bars to achieve sample failure.

by the stress-strain curve after attaining ultimate stress. Figure 8 shows the ultimate stress surface determined from the ultimate stress for each sample. A general trend of increasing ultimate stress with increasing mean stress was observed for the three concrete types. However, little difference in ultimate stress between concrete types was observed.

The brittle-ductile transition for the three concretes appears to be between 100 and 500 bars confining pressure as exemplified by the large compressive strains above 500 bars confining pressure. Ductile behavior was defined as axial strain greater than 1 percent. Other

investigators have observed the brittle-ductile transition to occur at about 150 to 200 bars confining pressure for a concrete mix having a water to cement ratio of 0.6:1 and a maximum aggregate size of 1.0 cm. Figures 9 and 10 show the recovered samples (numbers 23 and 25) after triaxial testing at confining pressures of 212 and 552 bars, respectively. The figures show a more localized failure zone at 212 bars confining pressure as compared to a more generalized (diffuse) failure at 552 bars confining pressure. A more generalized failure suggests increased ductility.

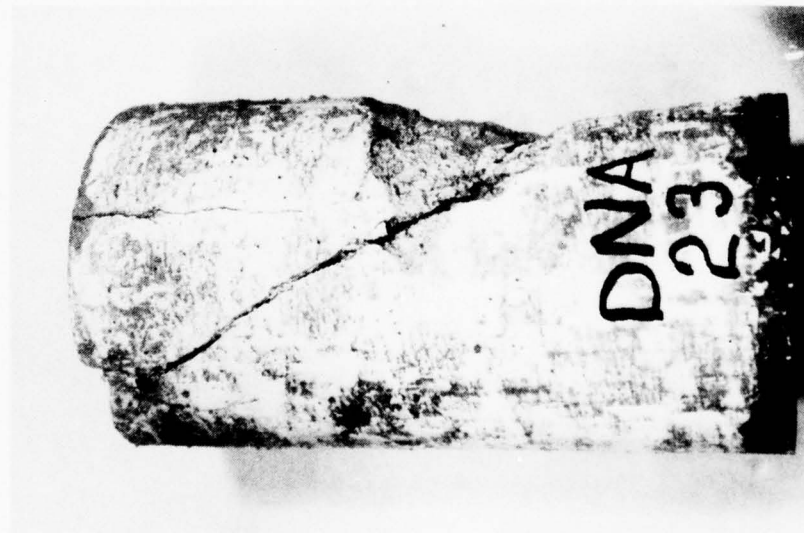


Figure 9. Photograph of sample 23 showing failure mode. Sample was triaxially tested at 212 bars confining pressure.



Figure 10. Photograph of sample 25 showing failure mode. Sample was triaxially tested at 552 bars confining pressure.

STEEL MECHANICAL TESTS¹¹

The steel used in the Mighty Epic structures was an ASTM A36 mild steel. A sample of this steel was supplied to Terra Tek in the form of a plate, 30 cm. x 30 cm. x 1.9 cm., by Lasker Boiler and Engineering Corp. of Chicago, Illinois. Tensile and compressive tests were performed to determine the mechanical properties of the steel. Test samples were obtained from two orthogonal directions in the plane of the plate and one direction normal to the plane of the plate in order to check for anisotropy. The orthogonal directions were arbitrarily selected since rolling directions were not specified by the contractor.

Steel Sample Preparation

The samples tested under the tensile load were cylindrical, $0.635 \pm .013$ cm. diameter, and $2.54 \pm .013$ cm. gage length. The samples for compressive testing were also cylindrical, $0.953 \pm .013$ cm. diameter, and $1.905 \pm .013$ cm. total length. Sample ends were prepared parallel to within $\pm .0003$ cm. Axiality of the test specimen with the loading piston was within $\pm .01$ cm. For both tensile and compression specimens, two strain gauges were bonded directly to the sample to monitor the axial and transverse strains. The strain gauges used were accurate to $\pm .005$ percent strain. All sample preparation was done in accordance with ASTM Standards E8-65T and E9-61. All loadings were applied quasi-statically.

Steel Test Results and Conclusions

In order to clarify the designation of the test samples, the plate orientation shown in Figure 11 was selected. Tensile and compressive tests were performed on samples from both the "x" and "y" directions. Samples from the "z" direction were tested in compression only since the 3/4 inch

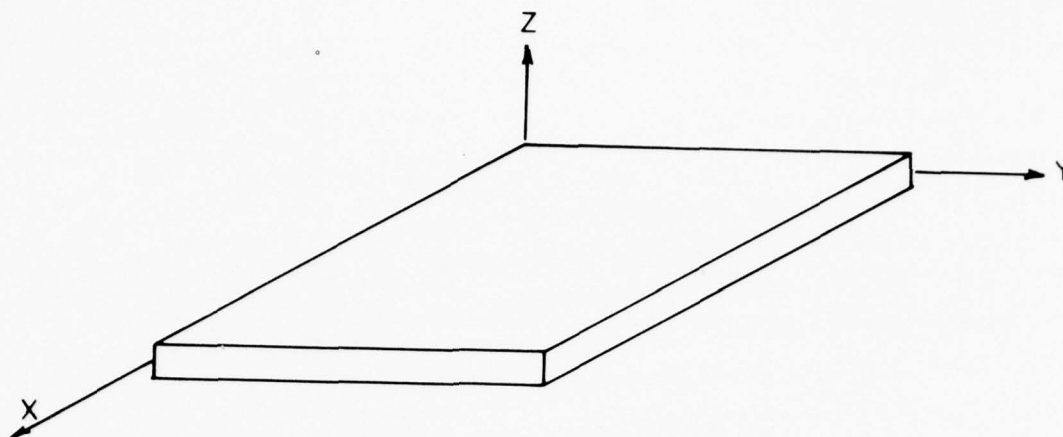


Figure 11. Orientation of steel plate.

thickness did not allow adequate length for a tensile sample. The stress-strain curves for various sample orientations are contained in Figures 12 through 16. In each case the test is designated by the direction of the samples longitudinal axis and the type of loading, i.e., XC indicates X direction, compressive loading.

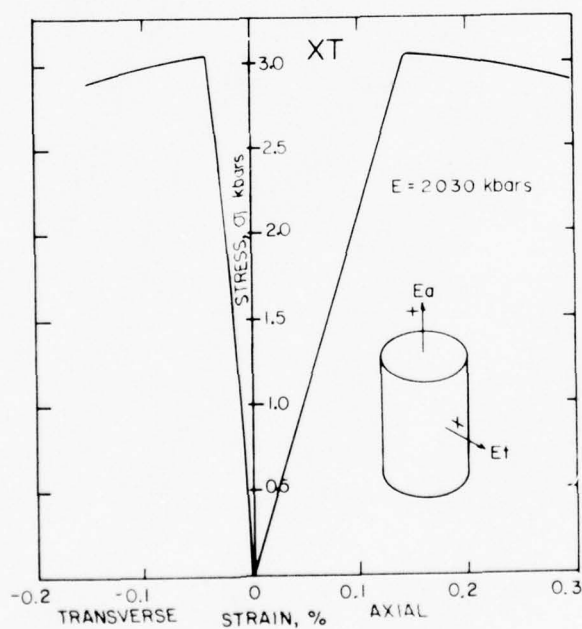


Figure 12. Tensile stress-strain steel sample, X direction.

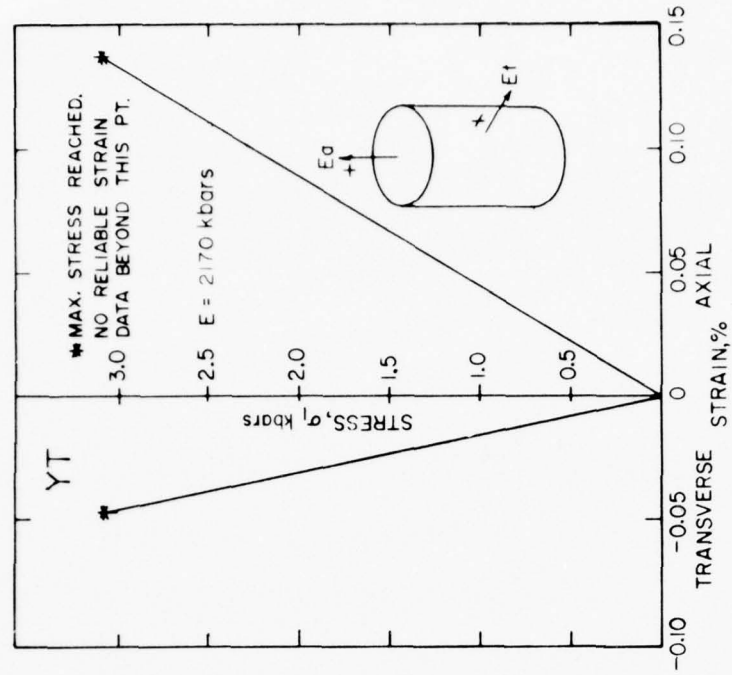


Figure 13. Compressive tests on steel sample, X direction.

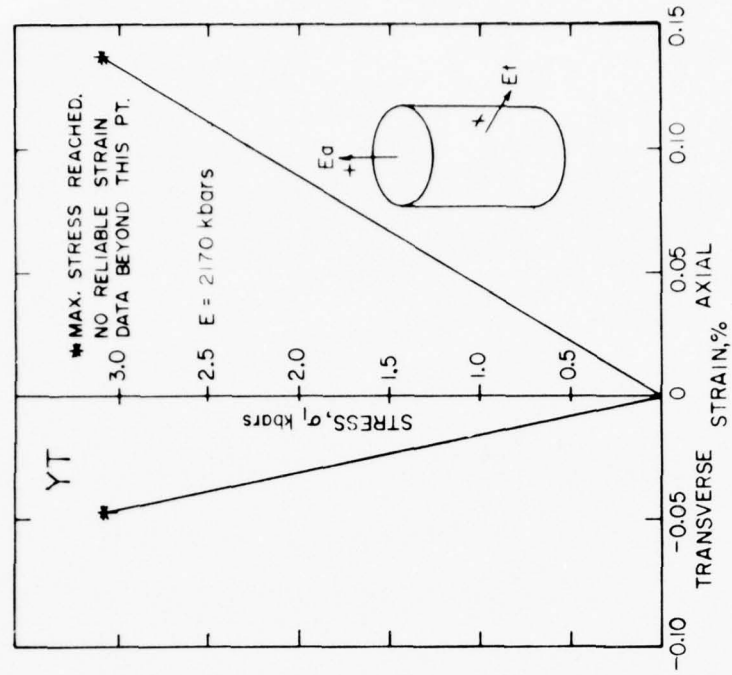


Figure 14. Tensile test on steel sample, Y direction.

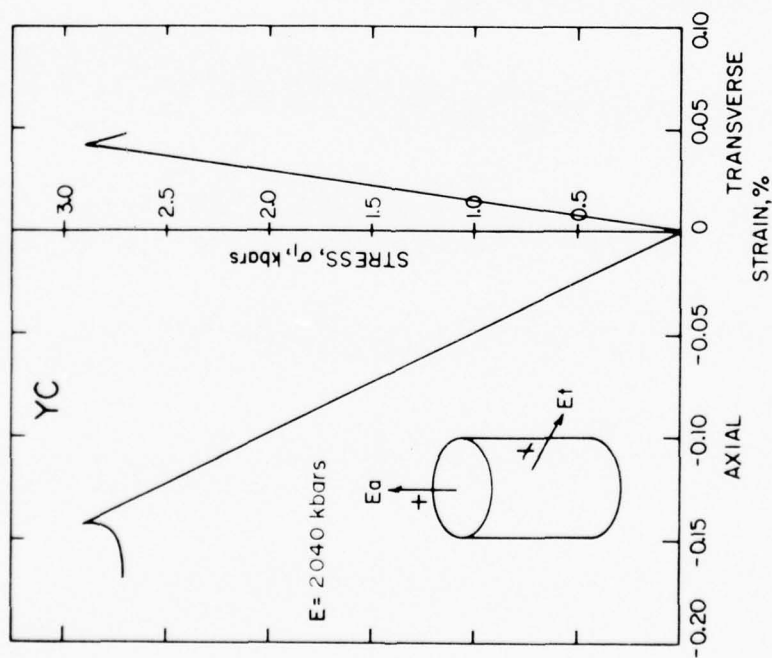


Figure 15. Compressive test on steel sample, Y direction.

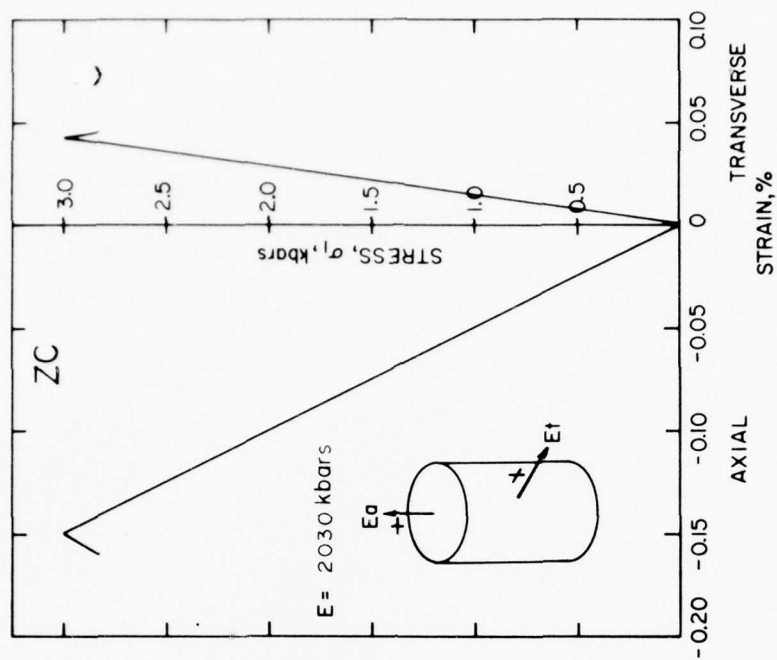


Figure 16. Compressive test on steel sample, Z direction.

All samples demonstrated a linear elastic region and a well defined yield point. The mean upper yield point observed during the loading was 2.96 ± 0.06 kbars. The mean Young's modulus measured was 2.090 ± 0.075 Mbars with a mean Poisson's ratio of 0.285 ± 0.015 . The variation in behavior for the different orientations is due most likely to the small sample population tested rather than to some anisotropic nature of the plate.

A summary of the steel behavior is contained in Table III.

TABLE III
Summary of Steel Test Data

Test Designation	Test Type	Young's Modulus	Poisson's Ratio	Upper Yield Strength
XT	Tensile	2030 Kb	0.27	2.96 Kb
YT	Tensile	2170 Kb	0.31	3.03 Kb
XC	Compressive	2170 Kb	0.29	2.88 Kb
YC	Compressive	2040 Kb	0.28	2.93 Kb
ZC	Compressive	2030 Kb	0.27	3.02 Kb

CONCRETE - STEEL SHEAR TESTS

Lasker Boiler and Construction Company supplied ten 10.2 cm. cubes for testing the frictional properties of the concrete - steel interface. Samples were designated according to structure in which the concrete and steel were used, i.e., C-Y-13, C-X-5, etc. The cubes were composed of a 10.2 cm. x 10.2 cm. x 5.1 cm. thick steel plate upon which a 10.2 cm. x 10.2 cm. x 5.1 cm. thick piece of concrete was cast. The concrete and steel used in making the direct shear cubes was of the same batch and/or type as concrete (LBC-5.5 ksi) and steel previously reported herein. The cubes were placed into a water bath upon arrival at Terra Tek in order to promote curing and approximate Nevada Test Site tunnel humidity.

Apparatus and Instrumentation

Direct shear tests were performed in the machine shown in Figure 17. The normal load was applied with a servo-controlled actuator operating in the load feedback mode. The shear was applied by a servo-controlled

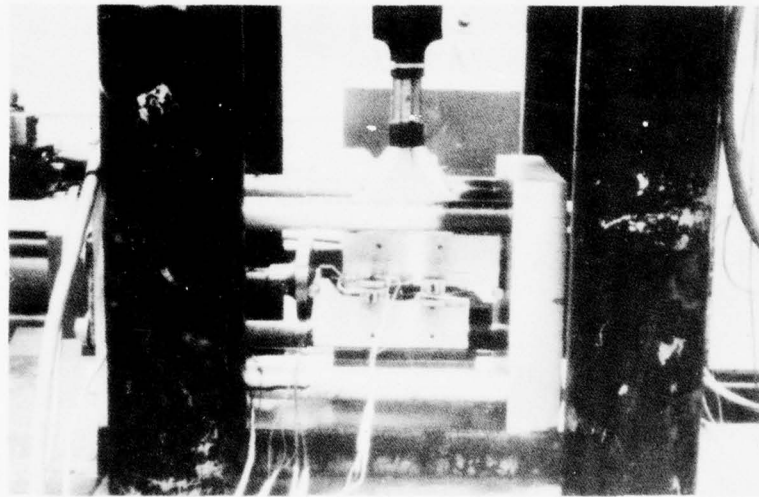


Figure 17. Direct shear machine.

actuator operating in the displacement feedback mode at a rate of 0.001 cm/sec. Both the normal and shear loads were measured directly by load cells placed in line with the actuators. Frictional load contribution due to the shear box was minimized by incorporating ball bearings and hardened steel bearing surfaces. Although the coefficient of friction for this bearing proved to be dependent upon normal load negligible errors were incurred. For a normal stress of 70 bars, the friction coefficient was .009 and at a normal stress of 700 bars it was .002. Through calibration, horizontal and vertical loads were determined to be accurate to within ± 0.25 bars. Transducers mounted on the shear boxes measured the relative horizontal displacement of the two boxes to within $\pm .015$ cm. The direct shear specimens were held in place in the shear boxes using a grout, Ultra-Cal 30.

Direct Shear Results and Conclusions

Table IV lists the direct shear data for the three cubes. Sample C-Y-13 "stub" showed no breakdown shear stress and gave an average friction coefficient of 0.53. Sample C-Y-13 "sphere" showed an initial breakdown shear stress of 28.1 bars dropping to a residual shear stress of 25.2 bars giving initial and residual friction coefficients of .80 and .73, respectively. Sample C-X-5 showed no significant breakdown stress and gave an average friction coefficient of 0.70. Note that the terms "stub" and "sphere" indicate the type of structure in which the concrete was used.

The coefficient range 0.69 to 0.73 listed in Table IV should be considered the representative coefficient of friction since the sample C-Y-13 "stub" had become unbonded at the concrete-steel interface prior to testing. The authors feel this unbonding could have affected the data via some mechanism such as drying of the surfaces.

TABLE IV
DIRECT SHEAR DATA
(LBC - 5.5 ksi concrete)

Sample	Shear Rate 10^{-3} cm/sec	Normal Stress, bars (to shear plane)	Residual Friction Coefficient μ
C-Y-13 "stub"	1	34.5	.53
	1	68.3	.52
	1	101.4	.53
C-Y-13 "sphere"	1	34.5	.73
C-X-5	1	34.5	.69
	1	71.0	.70

CONCLUDING REMARKS

The concrete and steel mechanical tests showed behavior consistent with previously published results. Young's modulus and Poisson's ratio for the concrete averaged 310 kilobars and 0.17, respectively. The average bulk modulus for the three concrete types was 115 kilobars. The steel samples gave an average Young's modulus and Poisson's ratio of 2090 kilobars and 0.28, respectively. The direct shear tests showed that a coefficient of friction of 0.70 best represented the concrete-steel interface.

REFERENCES

1. Brumfield, M., 1976, Personal Communication, Carol Construction Company, Chicago, Illinois.
2. Merwood, D., 1976, Personal Communication, Concrete Technology, Tacoma, Washington.
3. Johnson, J. N., Dropek, R. K., 1975, "Measurements and Analysis of Pore Pressure Effects in the Inelastic Deformation of Rocks," Terra Tek, Inc., Technical Report TR 75-29.
4. Gardner, N. J., 1969, "Triaxial Behavior of Concrete," American Concrete Institute Journal, Proceedings, Vol. 66, No. 2, pp. 136-146.
5. Hatano, T., 1969, "Theory of Failure of Concrete and Similar Brittle Solid on the Basis of Strain," International Journal of Fracture Mechanics, Vol. 5, No. 1, pp. 73-79.
6. Kupfer, H. B., Gerstle, K. H., 1973, "Behavior of Concrete Under Biaxial Stresses," Journal of the Engineering Mechanics Division, ASCE Proceedings, EM-4, pp. 853-866.
7. Ishai, O., 1965, "The Time-Dependent Deformational Behavior of Cement Paste, Mortar and Concrete," The Structure of Concrete, Cement and Concrete Association Proceedings, September 1965, pp. 345-364.
8. Glucklich, J., 1965, "The Effect of Microcracking on Time-Dependent Deformations and the Long Term Strength of Concrete," The Structure of Concrete, Cement and Concrete Association Proceedings, September 1965, pp. 176-189.
9. Liu, T. C. Y., Nielson, A. H., Slate, F. O., 1972, "Biaxial Stress Strain Relations for Concrete," Journal of Structural Division, ASCE Proceedings, ST. 5, pp. 1025-1034.
10. Green, S. J., Swanson, S. R., 1973, "Static Constitutive Relations for Concrete," Air Force Weapons Laboratory Technical Report AFWL-TR-72-244.
11. Enniss, D. O., Butters, S. W., 1976, "Mechanical Behavior of Steel Used for Mighty Epic Structures," Terra Tek, Inc., Technical Report TR 76-38.

NOT
Preceding Page BLANK - FILMED

CHARACTERIZATION OF TUFF AND DEVELOPMENT OF GROUTS
FOR MIGHTY EPIC STRUCTURES PROGRAM

by

S. W. Butters
R. L. Stowe*
J. W. LaComb**
R. A. Bendinelli***

Submitted to

Commander
Field Command
Defense Nuclear Agency
Albuquerque, New Mexico

Attn: J. W. LaComb

* R. L. Stowe, Concrete and Rock Properties Branch, Waterways
Experiment Station, Vicksburg, Miss.

** J. W. LaComb, Civil Engineering, Nevada Test Site, Mercury,
Nevada

*** R. A. Bendinelli, Grouting Branch, Waterways Experiment Sta-
tion, Vicksburg, Miss.

TR 76-21
April 1976

SUMMARY

A Defense Nuclear Agency program at the Nevada Test Site to study the effect of shock waves -- both magnitude and direction -- on structures of varying configurations and designs required a complete characterization of the material (tuff and grout) surrounding the structures. It was also desired that the grout properties be similar to the tuff properties.

Tuff surrounding the structures was characterized through mechanical and physical properties measurements performed at Waterways Experiment Station (WES) and Terra Tek, Inc. Subsequent grout development then performed at the Grouting Branch of the Concrete Laboratory at WES with mechanical testing by both the Rock Properties Branch of the Concrete Laboratory at WES and Terra Tek, Inc. As samples from each mixture were tested, new mixtures were designed. Approximately twenty mixtures were analyzed before final grout selection, ME8-11. This ME8-11 grout was implaced in the structures drifts in preparation for the Mighty Epic event.

PREFACE

The authors would like to express their appreciation for the excellent and expedient laboratory support by the Grouting and Rock Properties Branches of Waterways Experiment Station and by Terra Tek.

TABLE OF CONTENTS

Summary	144
Preface	145
Table of Contents	146
List of Illustrations	147
List of Tables	151
Introduction	152
Structures Tuff	154
Test Data	156
Average Structures Tuff Properties	157
Grout Properties	165
Verification of Grout Field Mixtures	174
Discussion and Conclusions	179
References	181
Appendix A - Mechanical Test Results on U12n.10 UG#4, UG#6a, ISS#5 and ISS#7 Core Samples	182
Appendix B - Mechanical Test Results on Mighty Epic Grout Mixtures	193

LIST OF ILLUSTRATIONS

<u>Figure</u>	<u>Description</u>	<u>Page</u>
1	Plan View of the Mighty Epic Area Showing A, B, and C Structures Drifts and the Related Drill Holes	155
2	Average Stress-Stress Response of Uniaxial Strain Tests on U12n.10 UG#4 and UG#6a Core Samples (TTI)	158
3	Combined Failure Data from U12n.10 UG#4, UG#6a, ISS#5 and ISS#7 Core Samples	158
4	Structures Tuff Representative Failure Envelope	159
5	U12n.10 UG#4 Selected Properties as a Function of Drill Hole Footage	160
6	U12n.10 UG#6a Selected Properties as a Function of Drill Hole Footage	161
7	U12n.10 ISS#5 Selected Properties as a Function of Drill Hole Footage	162
8	U12n.10 A, B, and C Structures Selected Properties as a Function of Drill Hole Footage	163
9	Failure Envelopes of Several Grout Mixtures and a Typical Ash Fall Tuff	167
10	Hydrostatic Compression and Uniaxial Response of Several Grout Mixtures and a Typical Ash Fall Tuff.	168
11a	14 Day Age Failure Envelope on Grout Mixtures HPRM-1, HPRM-2, HPRM-3, HPRM-4, HPRM-5, HPSL-16, HPNS-1, HPRM-3C and HPNS-2	168
11b	28 Day Age Failure Envelope on Grout Mixtures HPRM-1, HPRM-2, HPRM-3, HPRM-4, HPRM-5, HPSL-16, HPNS-1, HPRM-3C and HPNS-2	169
11c	56 Day Age Failure Envelope on Grout Mixtures HPRM-1, HPRM-2, HPRM-3, HPRM-4, HPRM-5, HPSL-16, HPNS-1, HPRM-3C and HPNS-2	169
12	Combined Failure Data on ME801 through ME8-11 Grout Samples	172
13	Selected Properties of all Grout Mixtures Tested During this Grout Development	173

<u>Figure</u>	<u>Description</u>	<u>Page</u>
14a	Uniaxial Strain Results on Samples from Several Mixtures of ME8-11(R) Field Mixes (TTI) -- Stress-Strain Response	175
14b	Uniaxial Strain Results on Samples from Several Mixtures of ME8-11(R) Field Mixes (TTI) -- Stress-Stress Response	175
15a	Uniaxial Strain Results on Samples from Several Mixtures of ME8-11(R) Field Mixes (WES) -- Stress-Strain Response	176
15b	Uniaxial Strain Results on Samples from Several Mixtures of ME8-11(R) Field Mixes (WES) -- Stress-Stress Response	176
16a	Uniaxial Strain Results on Samples from Several Mixtures of ME8-11(R) Field Mixes (TTI) -- Stress-Strain Response. Tests were conducted close to Mighty Epic Shot Day	177
16b	Uniaxial Strain Results on Samples from Several Mixtures of ME8-11(R) Field Mixes (TTI) -- Stress-Stress Response. Tests were conducted close to Mighty Epic Shot Day	177

APPENDIX A

A1	Hydrostatic Compression Results on U12n.10 UG#6a Core Samples (WES)	183
A2	Hydrostatic Compression Results on U12n.10 ISS#5 Core Samples (TTI)	183
A3	Hydrostatic Compression Results on U12n.10 ISS#7 Core Samples (WES)	184
A4	Unconfined Compression Results on U12n.10 UG#4 Core Samples (TTI)	184
A5	Unconfined Compression Results on U12n.10 UG#6a Core Samples (TTI)	185
A6	Triaxial Compression Results on U12n.10 UG#6a Core Samples (WES)	185
A7	Triaxial Compression Results on U12n.10 ISS#5 Core Samples (TTI)	186

<u>Figure</u>	<u>Description</u>	<u>Page</u>
A8	Triaxial Compression Results on U12n.10 ISS#5 Core Samples (TTI)	186
A9	Triaxial Compression Results on U12n.10 ISS#5 Core Samples (TTI)	187
A10	Triaxial Compression Results on U12n.10 ISS#7 Core Samples (WES)	187
A11a	Uniaxial Strain Results on U12n.10 UG#4 Core Samples (TTI)	188
A11b	Uniaxial Strain Results on U12n.10 UG#4 Core Samples (TTI)	188
A12a	Uniaxial Strain Results on U12n.10 UG#6a Core Samples (TTI)	189
A12b	Uniaxial Strain Results on U12n.10 UG#6a Core Samples (TTI)	189
A13a	Uniaxial Strain Results on U12n.10 A, B, and C Drift Samples (TTI)	190
A13b	Uniaxial Strain Results on U12n.10 A, B, and C Drift Samples (TTI)	190
A14	Failure Data from Triaxial Compression Tests on U12n.10 UG#4 Core Samples	191
A15	Failure Data from Triaxial Compression Tests on U12n.10 UG#6a Core Samples	191
A16	Failure Data from Triaxial Compression Tests on U12n.10 ISS#5 Core Samples (TTI)	192
A17	Failure Data from Triaxial Compression Tests on U12n.10 ISS#7 Core Samples (WES)	192

APPENDIX B

B1	Triaxial Compression Tests on ME801 Grout Samples (TTI)	194
B2	Failure Data on ME801 Grout Samples (WES and TTI) . .	194
B3a	Hydrostatic Compression and Uniaxial Strain Tests on ME801 Grout Samples (TTI)	195

<u>Figure</u>	<u>Description</u>	<u>Page</u>
B3b	Hydrostatic Compression and Uniaxial Strain Tests on ME801 Grout Samples (TTI)	195
B4	Triaxial Compression Results on ME802 Grout Samples (TTI)	196
B5a	Hydrostatic Compression and Uniaxial Strain Results on ME802 (TTI)	197
B5b	Hydrostatic Compression and Uniaxial Strain Results on ME802 (TTI)	197
B6	Unconfined Compression Tests on ME804 Grout Samples (TTI)	198
B7	Failure Data on ME804 Grout Samples (WES)	198
B8	Failure Data on ME805 Grout Samples (WES and TTI) . .	199
B9	Hydrostatic Compression Results on ME805 Grout Samples (TTI)	199
B10	Unconfined Compression Results on ME806 Grout Samples (TTI)	200
B11	Failure Data on ME806 Grout Samples (WES and TTI) . .	200
B12	Failure Data on ME807 Grout Samples (WES)	201
B13	Failure Data on ME808 Grout Samples (WES)	201
B14	Failure Data on ME8-11 Grout Samples (WES)	202
B15a	Uniaxial Strain Results on ME8-11 Grout Samples (WES and TTI)	203
B15b	Uniaxial Strain Results on ME8-11 Grout Samples (WES and TTI)	203

LIST OF TABLES

<u>Table</u>	<u>Description</u>	<u>Page</u>
1	Physical Properties, Ultrasonic Velocities and Permanent Volume Compaction on U12n.10 UG#4, UG#6a, ISS#5 and A, B, and C Structures Drift Samples	156
2	Some Average Properties of the Structures Tuff	164
3	Selected Properties of Super Lean, Rock Matching and High Strength Grouts	167
4	Physical Properties, Ultrasonic Velocities and Permanent Volume Compaction on Nine Initial Grout Test Mixtures	170
5	Summary of Measurements and Tests Conducted on Mighty Epic Grout Mixutures	171
6	Physical Properties, Ultrasonic Velocities and Permanent Volume Compaction on Grout Mixtures ME801, ME802, ME804, ME805, ME806 and ME8-11	172
7	Physical Properties, Ultrasonic Velocities and Measured Permanent Volume Compaction on Several Field Cast Batches of ME8-11 Grout	178

INTRODUCTION

Line of Site (LOS) pipe emplacement for nuclear test programs utilize substantial amounts of grout materials. Different functional roles require different grout mixtures. For example, grouts have been designed to attenuate energy via high gas-filled porosity, to protect structures via the shear strength, to flow via the ductility, etc. It has proved difficult to obtain a single mixture with a combination of select properties. For example, to strengthen grout, the water content is decreased, this would, if saturation remained constant, result in a higher density, higher sound speeds, and a less workable mixture. A more detailed description of the dependence of properties on each other is included in the text.

Stringent requirements for grout properties was necessary for the Mighty Epic structures program at the Nevada Test Site Area 12. The grout and tuff properties were required pre-test for 1) evaluating pre-test static design methods, 2) determination of active instrumentation response for the structures in the nuclear test and 3) providing a basis for interpreting the Mighty Epic test data. To meet these objectives it was necessary to characterize the grout material and to match the grout properties very closely with those of the parent material-tuff.

Matching grout properties to that of the tuff required, first of all, the properties of the tuff. Material properties of primary importance were the shear strength, the air void content, the as-received density and the longitudinal pulse velocity. Waterways Experiment Station¹ (WES) and Terra Tek, were responsible for determining these properties.

Once an adequate tuff description was available, progress began on developing a matching grout. This process involved varying the constituents

of the grout mixtures by WES² and NTS³ personnel. Each mixture was then tested by WES or Terra Tek to determine its' properties. Two major concerns during this process, in addition to matching the tuff properties, were maintaining a pumpable grout and insuring a low temperature rise during curing.

This report contains the test results from which the average properties of the tuff were obtained, a description of the grout constituents, the grout tests conducted, and the eventual verification of the grout mix properties actually implaced in the structures drifts.

STRUCTURES TUFF

The Mighty Epic program is planned for the "n" tunnel complex, Area 12. Material properties data were available from other events in the immediate vicinity, namely, Misty North and Ming Blade. The tuff that had been tested, however, was from a considerable number of different rock units ("tunnel beds"). Additionally, most of the tests previously conducted were primarily for siting purposes and the tuffs were incompletely characterized. It was, therefore, necessary to conduct select tests on cores specifically from the structures area.

The structures drifts relative to the Mighty Epic working point are shown in Figure 1. The structures are in the same horizontal plane of the working point, are designated "A", "B" and "C" and are contained within tunnel bed units 3BC, 3D, 4AB and 4CD.

Core holes U12n.10 UG#4 and UG#6a were drilled into the area prior to mining the drifts. The core samples from these holes were initially used for core testing to determine the suitability of the area for structures emplacement. This data provided a generalized overview of the nature of the tuff in the structures area -- air void contents, densities, sound speeds and estimates of the strength of the material. These early estimates, especially on the strength of the tuff, were necessary to initiate a matching grout mixture development.

After completion of mining the structures drifts, core samples were obtained from the ISS #5 and ISS #7 drill holes and the A, B and C Structures areas. Along with samples remaining from the UG#4 and UG#6A holes, a number of triaxial compression tests were conducted to define the tuff failure envelope (maximum stress difference at varying confining pressures).

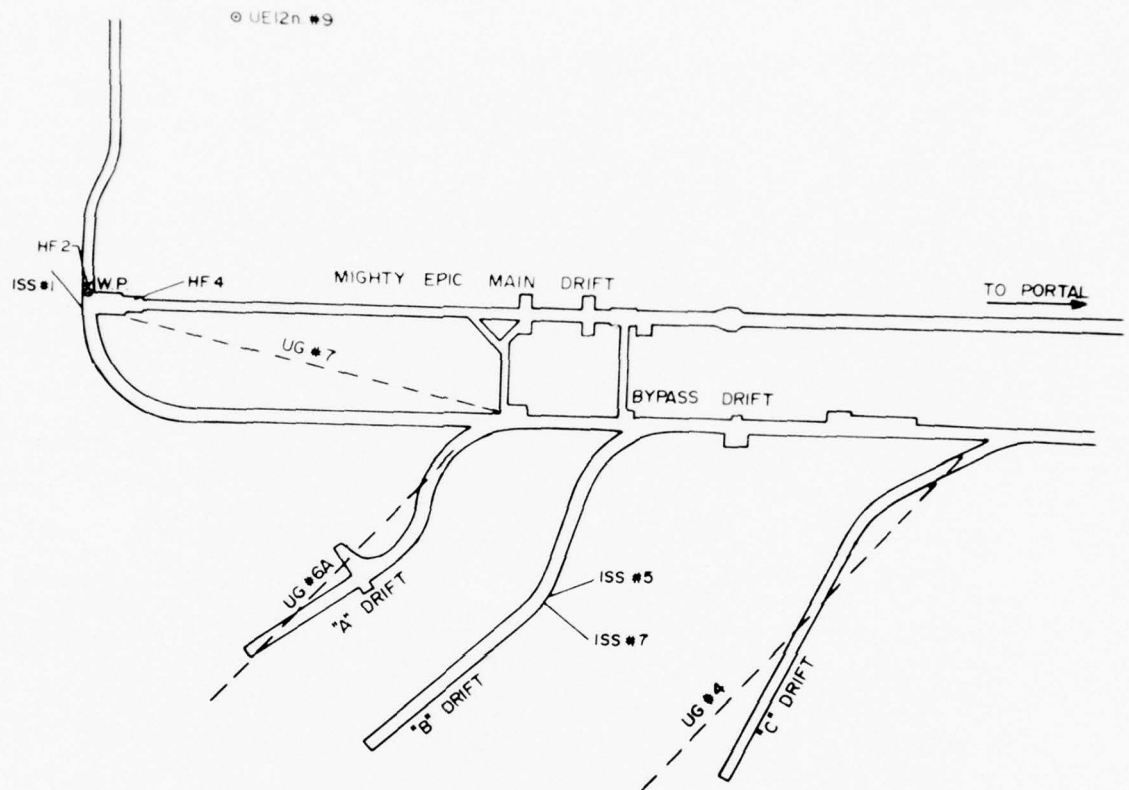


Figure 1. Plan View of the Mighty Epic Area Showing A, B, and C Structures Drifts and the Related Drill Holes.

TEST DATA

In many cases, the WES and Terra Tek data have been combined. This was done in order to use all data in establishing average properties. Selected properties are listed in Table 1 while the stress-strain response of the hydrostatic compression, triaxial compression and uniaxial strain tests are contained in Appendix A.

TABLE 1

PHYSICAL PROPERTIES, ULTRASONIC VELOCITIES AND PERMANENT VOLUME COMPACTION ON U12n.10 UG#4, UG#6a, ISS#5 AND A, B, AND C STRUCTURES DRIFT SAMPLES

DRILL HOLE FOOTAGE	DENSITY (gm/cc)			WATER BY WET WEIGHT (%)	POROSITY (%)	SATURATION (%)	CALC AIR VOIDS (%)	MEAS PERMANENT COMP (%)	VELOCITY (ft/sec)	
	AS- RECEIVED	DRY	GRAIN						LONG	SHEAR
U12n.10 UG#4								Hvd. 1-2		
227	1.86	1.52	2.44	18.6	38	91	3.2	1.4	9,469	4596
251	1.99	1.69	2.41	14.8	35	98	0.5	1.4	10,761	5261
254	1.95	1.65	2.39	15.4	31	96	1.3	1.8	10,099	5095
257	1.89	1.54	2.42	18.4	36	95	1.8			
263	1.97	1.65	2.50	16.2	34	94	1.9		8,694	4094
282	1.96	1.64	2.45	16.3	33	97	0.9	1.3	9,370	4704
307	2.01	1.73	2.41	14.0	28	99	0.2	0.9	9,557	4655
327	1.78	1.42	2.38	20.0	40	89	4.8		13,061	5154
331	1.74	1.37	2.36	21.0	42	88	5.2	3.2	10,548	4695
336	1.77	1.42	2.39	20.1	41	87	5.3	3.5	13,295	7523
339	1.77	1.38	2.38	22.1	42	93	2.7			
U12n.10 UG#6A										
84	1.99	1.69	2.43	14.8	30	97	0.8	1.1	10,200	4809
109	1.97	1.69	2.36	14.0	28	94	0.7	0.7	11,227	5675
113	1.93	1.59	2.41	17.4	34	99	0.4		9,226	4505
116	1.98	1.72	2.38	12.9	28	93	1.9			
136	1.93	1.60	2.42	17.1	34	97	1.0	1.0	9,827	4563
163	1.97	1.68	2.41	15.0	31	97	1.0	1.1	10,395	4737
189	1.94	1.65	2.38	14.9	31	95	1.6	1.1	9,947	4895
192	2.01	1.80	2.35	10.4	23	90	2.4	0.8	11,683	6046
216	2.03	1.82	2.34	10.2	22	95	1.1	0.6	12,342	7306
220	1.96	1.65	2.41	15.6	31	97	1.1		10,561	4859
231	2.01	1.75	2.41	13.0	27	96	1.1			
247	2.00	1.75	2.35	12.4	25	98	0.6	0.6	13,094	7549
U12n.10 ISS#5										
9	1.91	1.55	2.48	18.5	37	94	2.1		8,960	4070
11	1.93	1.63	2.36	15.4	31	97	1.1		10,760	4970
17	1.91	1.59	2.40	16.8	33	96	1.4		9,380	4280
26	1.88	1.52	2.40	19.0	36	98	0.7		9,390	4170
28	1.93	1.63	2.36	15.5	31	96	1.1		10,190	4900
U12n.10 A Structure										
31	1.92	1.61	2.39	16.2	33	94	1.9	0.9	11,206	6162
B Structure										
25	1.91	1.56	2.45	18.5	36	97	0.9	0.8	9,867	4612
C Structure										
30	1.84	1.44	2.46	22.0	41	98	0.9	0.6	10,801	5382

AVERAGE STRUCTURES TUFF PROPERTIES

As stated earlier, a preliminary estimate of the tuff strength was required for the grout development. To provide this estimate, the UG#4 and UG#6a uniaxial strain test stress-stress curves (Appendix A) were averaged, see Figure 2. These curves, from past experience, are known to be a lower bound to the failure envelope produced by the triaxial compression tests. It should be emphasized that these average uniaxial strain test stress-stress curves do not define the magnitude or shape of the failure envelope but will provide a lower bound. The uniaxial strain test data suggested that the shear strength for the tuff in the structures area was about twice as strong as that of the "average" area 12 tuff⁴. Subsequent triaxial compression tests produced the failure points shown in Figure 3. These limited data provided the necessary failure envelope detail, see Figure 4.

The other properties of the tuff determined from the testing are summarized in Figures 5 through 8 as a function of distance along the drill hole. The average and standard deviation for these properties are listed in Table 2.

The tuff in the structures area and, in general, the Mighty Epic area has higher shear strength, higher density and higher sound speeds than the typical 12 tuff. The water content is lower for the structures tuff while the air void content is approximately the same.

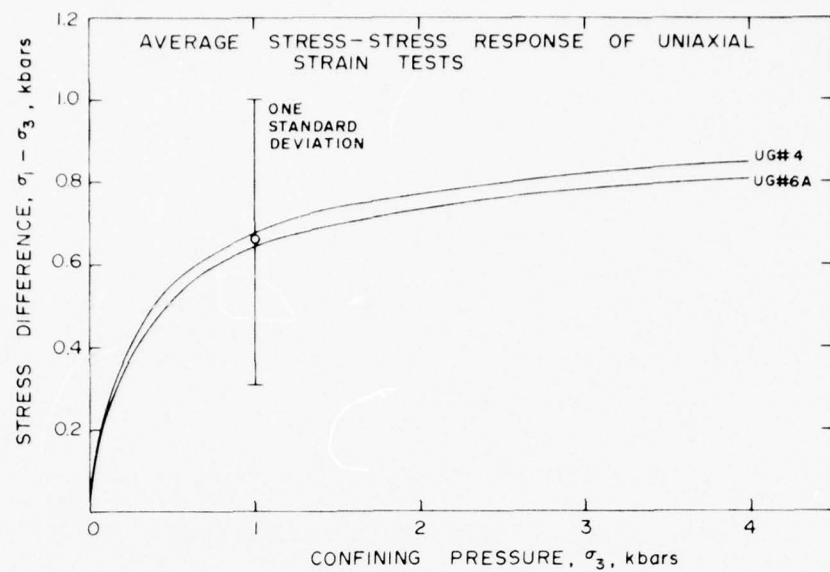


Figure 2. Average Stress-Stress Response of Uniaxial Strain Tests on U12n.10 UG#4 and UG#6a Core Samples (TTI).

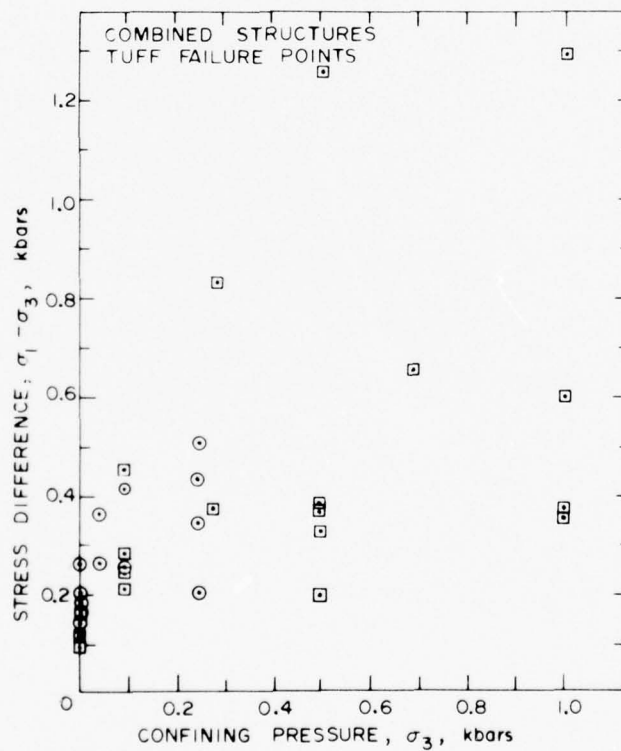


Figure 3. Combined Failure Data from U12n.10 UG#4, UG#6a, ISS#5 and ISS#7 Core Samples.

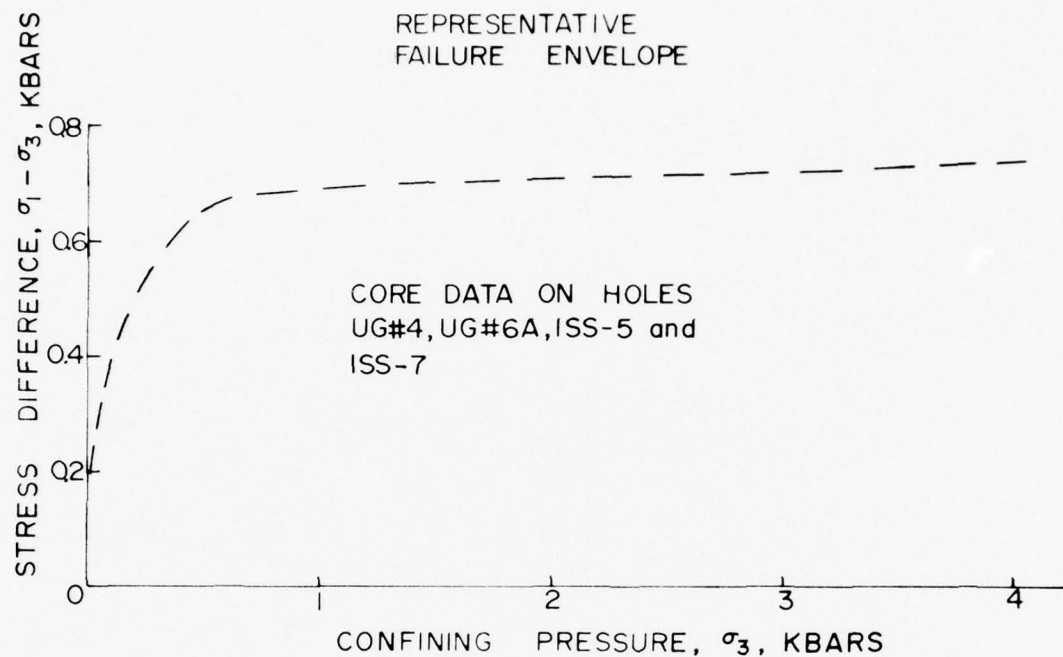


Figure 4. Structures Tuff Representative Failure Envelope.

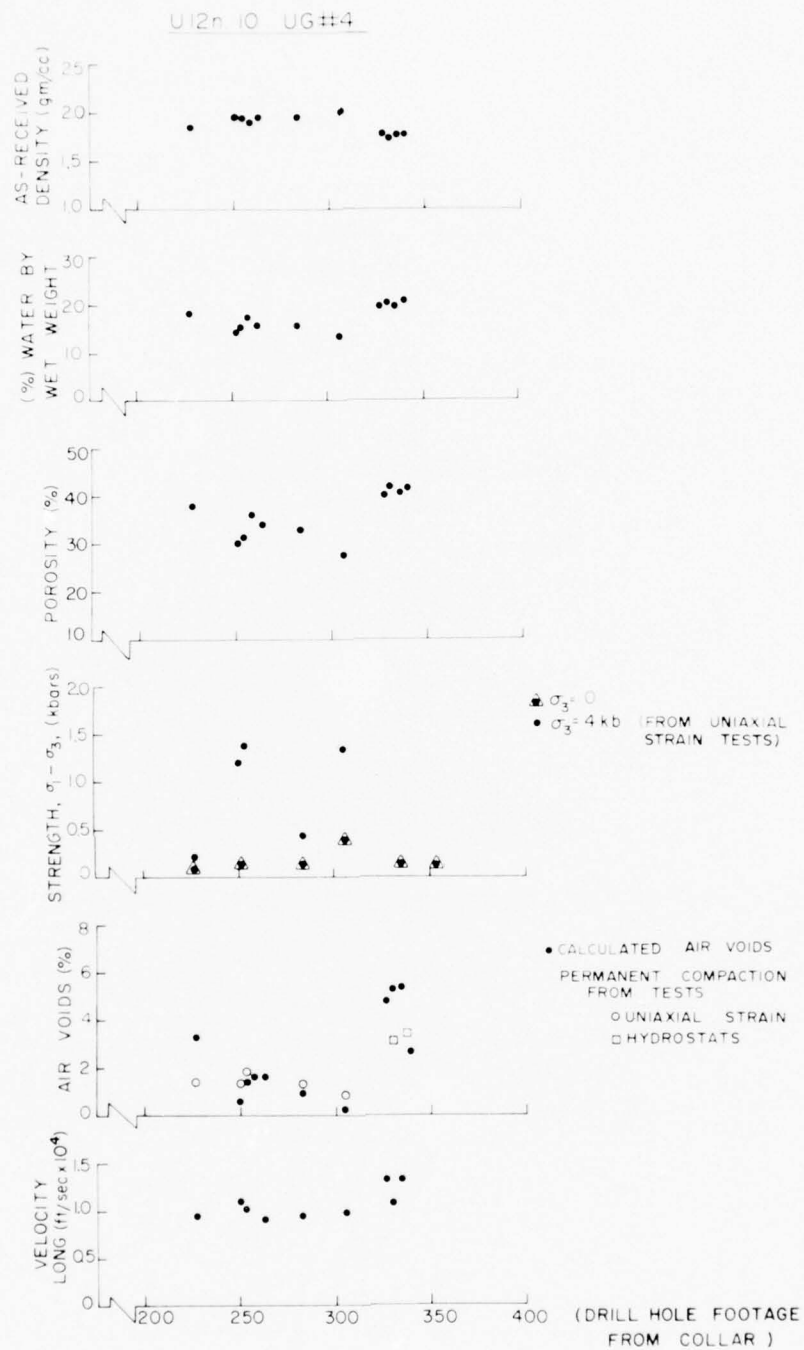


Figure 5. U12n.10 UG#4 Selected Properties as a Function of Drill Hole Footage.

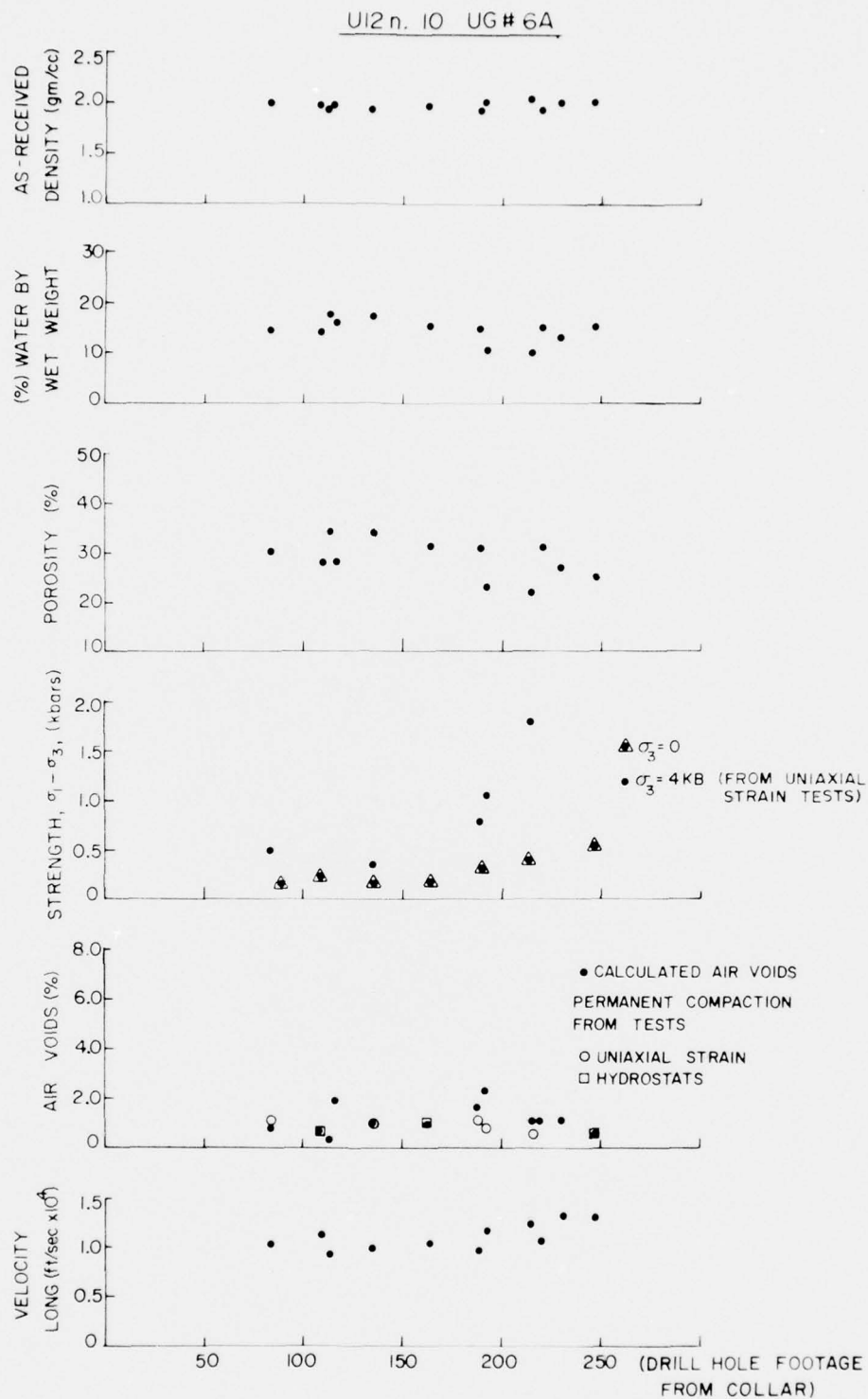


Figure 6. U12n.10 UG#6a Selected Properties as a Function of Drill Hole Footage.

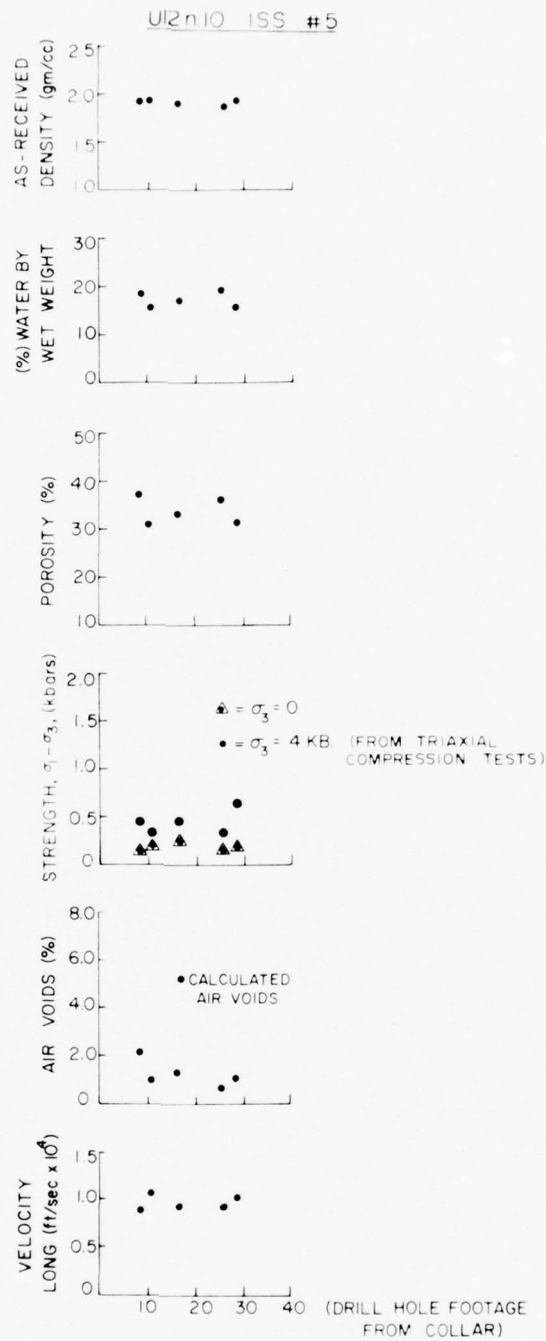


Figure 7. U12n.10 ISS#5 Selected Properties as a Function of Drill Hole Footage.

U12n.10, A, B, C STRUCTURE

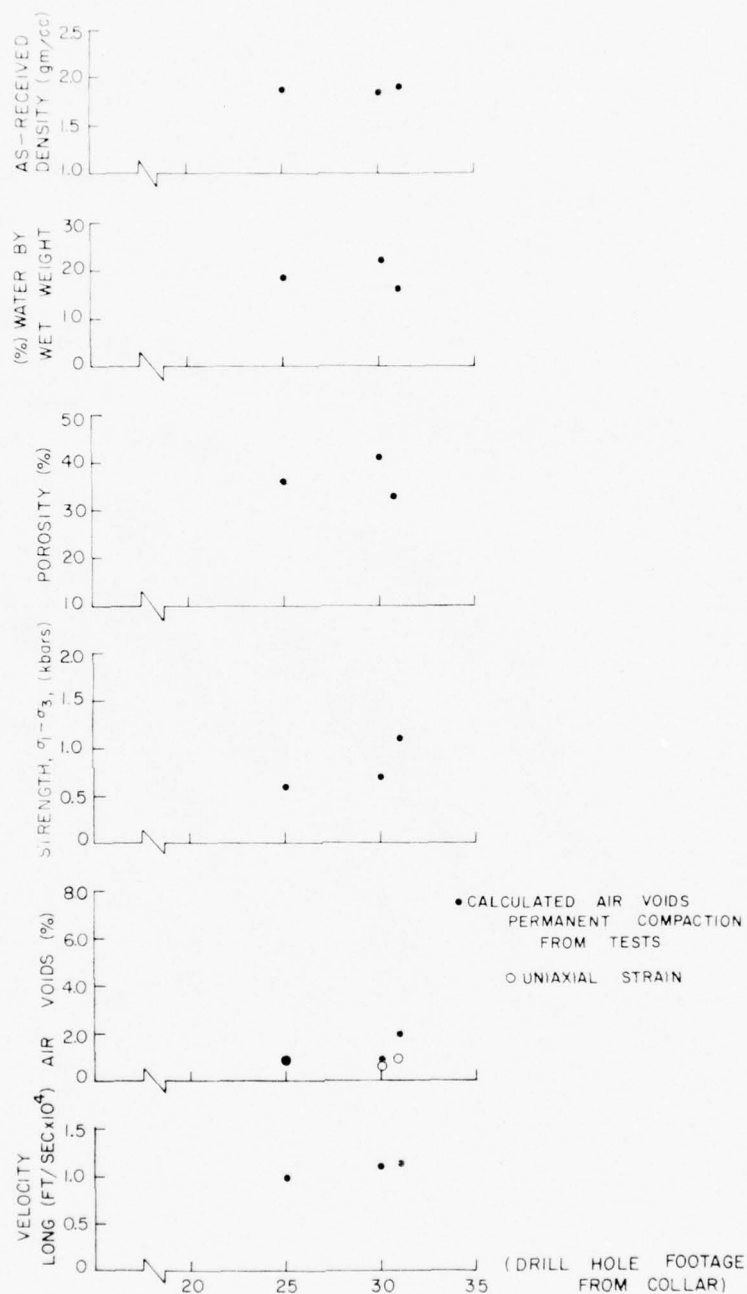


Figure 8. U12n.10 A, B, and C Structures Selected Properties as a Function of Drill Hole Footage.

TABLE 2
SOME AVERAGE PROPERTIES OF
THE STRUCTURES TUFF*

	<u>AVERAGE</u>	<u>STANDARD DEVIATION</u>
As Received Density (gm/cc)	1.95	0.05
Water Content by Wet Weight (%)	15.7	2.6
Porosity (%)	31	7
Air Voids (%)**	1.0	0.43
Ultrasonic Longitudinal Velocity (ft/sec)	10,300	1,000

* The averages includes all values (with the exception of the last 4 samples from U12n.10 UG#4 which were not considered as representative) on samples from U12n.10 UG#4, UG#6a, ISS#5 and ISS#7.

** The air void content is taken here as the permanent volume compaction from the uniaxial strain test.

GROUT PROPERTIES

Material properties have been determined on a number of grout types during the last several years of the Nevada Test Site program. Grout types were all variations of basic super lean, rock matching and high strength grouts. Table 3 and Figures 9 and 10 summarize selected properties of these basic types⁴.

Following the preliminary estimate of the structures tuff properties, nine different mixtures of grout, used mainly in stemming and containment systems of past events, were sent to Terra Tek for testing. The grout designations were HPRM-1, HPRM-2, HPRM-3, HPRM-4, HPRM-5, HPSL-16, HPNS-1, HPNS-2 and HPRM-3C. Hydrostatic compression tests, triaxial compression tests, uniaxial strain tests, physical property measurements and ultrasonic velocity measurements were conducted on these grout types at 14, 28 and 56 day ages. These data are listed in tabular form in Table 4 and as the triaxial compression derived failure envelopes in Figure 11. These data indicate variations in the shear strength from tens of bars to hundreds of bars, ultrasonic longitudinal velocities from 7,000 to 11,000 feet per second, air void contents from 1.5% to 4.5%, and as-received densities from 1.86 gm/cc to 2.10 gm/cc. Based on these grout properties, changes were made in mix constituents to "fine tune" the grout properties, (i.e., bring all of the properties of a single mix close to that of the tuff).

The subsequent grout mixtures were designated ME801 through ME8-11. In most cases, each grout mixture was reportioned in the developmental studies based on the properties of the previous mixture. The tests on these grout mixtures varied from unconfined compression tests to triaxial compression tests to verify the shear strength of the mixture. If other properties were also

needed, uniaxial strain tests, physical property measurements and ultrasonic longitudinal and shear wave velocities were conducted - Table 5 summarizes the measurements and tests.

The Mighty Epic grout failure envelopes, based on the triaxial compression tests, are shown in Figure 12 while the physical properties and ultrasonic velocities are tabulated in Table 6.

Selected properties of all grout mixtures (HPRM-1 through ME8-11) are summarized in Figure 13 with the average structures tuff shown for reference. This plot, along with the shear strength data (Figure 12), substantiate the evolution of the grout development for the Mighty Epic structures program.

TABLE 3
SELECTED PROPERTIES OF SUPER LEAN, ROCK MATCHING
AND HIGH STRENGTH GROUTS

Type	Density gm/cc			H ₂ O by Wet Wgt. %	Satur- ation %	Porosity Total %	Air Voids %	Meas. Perm. Comp. %	Velocity (Ft/Sec)	
	As Rec.	Dry	Grain						Long	Shear
<u>SLG</u>	Meas.	Calc.	Meas.	Meas.	Calc.	Calc.	Calc.	Meas.	Meas.	Meas.
14-45* Day Age	1.74 ±0.03	1.25 ±0.03	2.63 ±0.02	28 ±2.0	94	52	3	2-4	5600	2600
<u>RMG</u>										
14-45* Day Age	2.04 ±0.03	1.51 ±0.03	3.20 ±0.02	26 ±2.0	100	53	0	2-4	7400	3600
Full** Strength	2.02	1.62	3.20	20	82	49	7	7	8300	4500
<u>HSG</u>										
Full** Strength	1.95	1.68	2.70	14	56	38	11	10+	11500	6800

* Average of about 10 batches for physical properties and permanent compactions and one batch only for velocities.
** One batch only for all values. For the RMG, see RMG test data section for explanations of the change in physical properties with age.

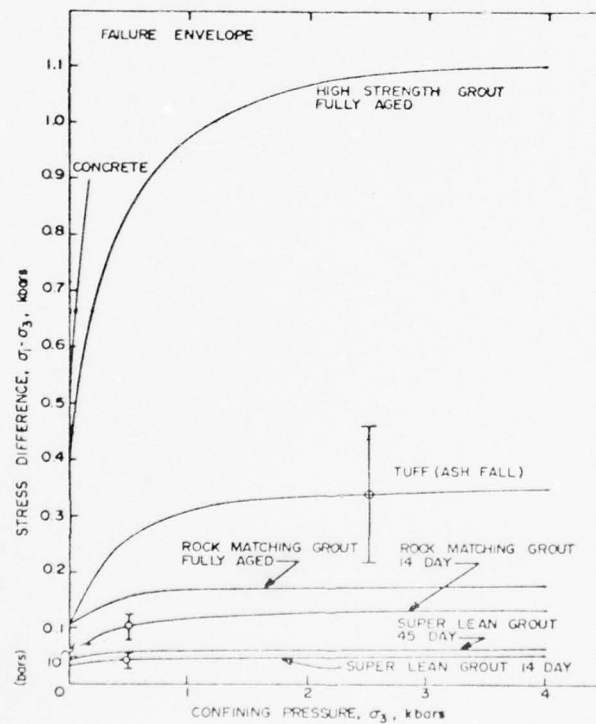


Figure 9. Failure Envelopes of Several Grout Mixtures and a Typical Ash Fall Tuff.

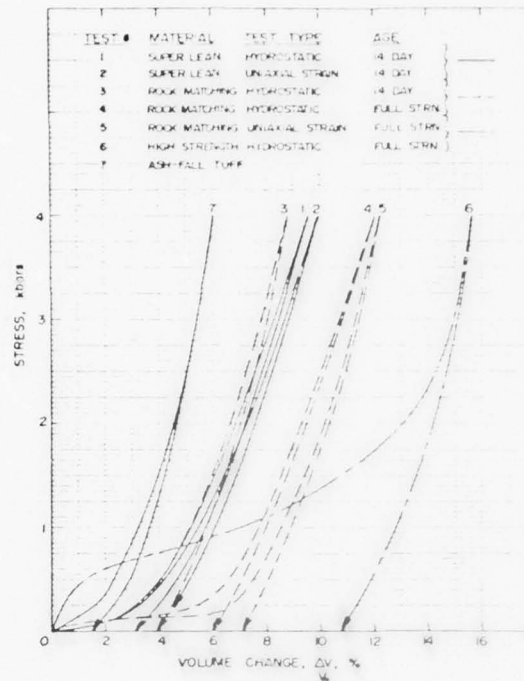


Figure 10. Hydrostatic Compression and Uniaxial Response of Several Grout Mixtures and a Typical Ash Fall Tuff.

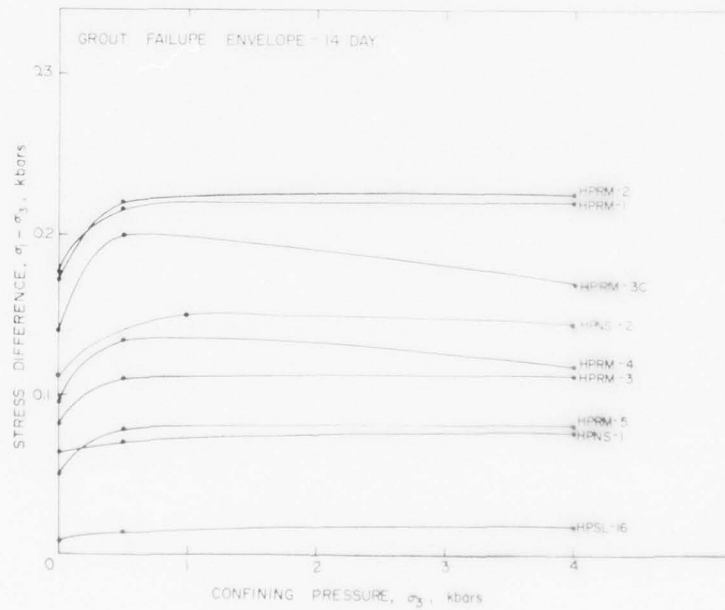


Figure 11a. 14 Day Age Failure Envelope on Grout Mixtures HPRM-1, HPRM-2, HPRM-3, HPRM-4, HPRM-5, HPSL-16, HPNS-1, HPRM-3C and HPNS-2.

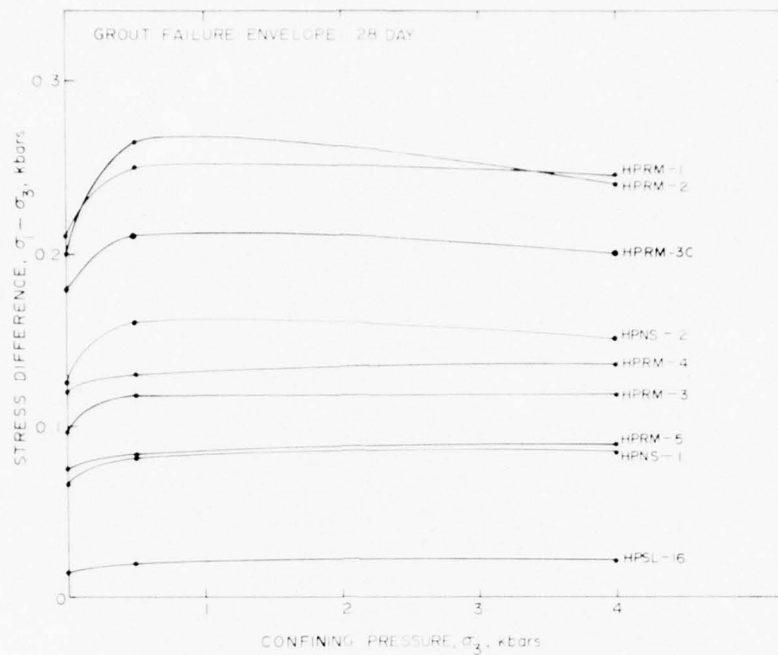


Figure 11b. 28 Day Age Failure Envelope on Grout Mixtures HPRM-1, HPRM-2, HPRM-3, HPRM-4, HPRM-5, HPSL-16, HPNS-1, HPRM-3C and HPNS-2.

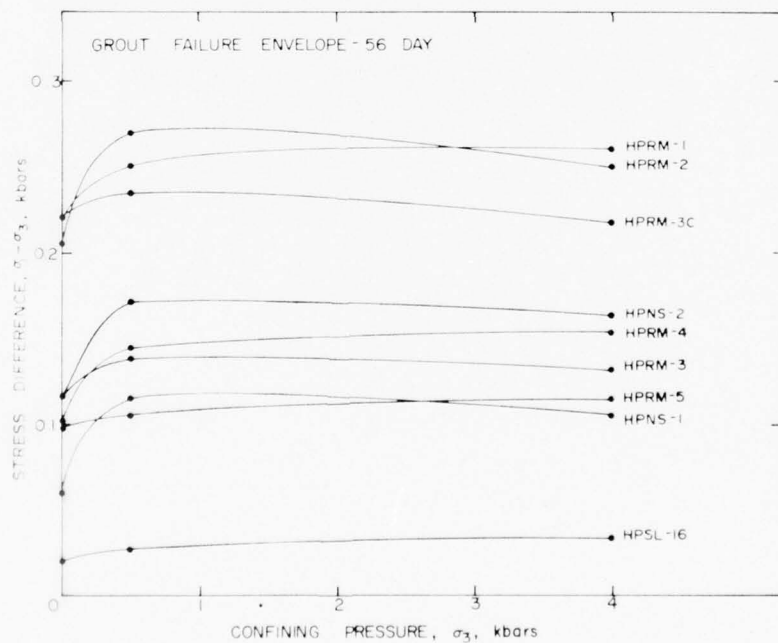


Figure 11c. 56 Day Age Failure Envelope on Grout Mixtures HPRM-1, HPRM-2, HPRM-3, HPRM-4, HPRM-5, HPSL-16, HPNS-1, HPRM-3C and HPNS-2.

TABLE 4

PHYSICAL PROPERTIES, ULTRASONIC VELOCITIES AND PERMANENT VOLUME
COMPACTION ON NINE INITIAL GROUT TEST MIXTURES

GROUT MIXTURES	DENSITY (gm/cc)			WATER BY WET WEIGHT (%)	POROSITY (%)	SATURATION (%)	CALC AIR VOIDS (%)	MEAS PERMANENT COMP. (%)	VELOCITY (ft/sec)	
	AS- RECEIVED	DRY	GRAIN						LONG	SHEAR
Grout 14 Day								hyd. 1-0		
HPRM-1	2.06	1.65	2.97	20.1	44	93	3.0	2.1 2.3	9478	5274
HPRM-2	2.04	1.64	3.01	19.8	46	89	5.1	2.2 2.2	9166	5022
HPRM-3	2.07	1.58	3.11	23.6	49	99	0.5	1.6 1.6	8366	4472
HPRM-4	2.01	1.55	3.06	22.9	49	94	3.2	3.1 3.5	9084	4640
HPRM-5	1.92	1.46	3.02	23.9	52	88	5.9	3.5 4.0	7910	3753
HPSL-16	1.86	1.37	2.94	26.5	54	92	4.3	2.4 2.5	6579	2459
HPNS-1	2.04	1.51	3.35	25.9	55	96	2.0	1.8 1.8	7213	3427
HPRM-3C	2.10	1.71	3.03	18.9	44	91	3.9	2.4 2.6	9850	5333
HPNS-2	1.92	1.40	3.21	27.1	56	92	4.3	3.7 4.9	8240	4240
Grout 28 Day										
HPRM-1	2.02	1.56	2.97	22.9	48	97	1.3	2.2 2.8	10259	5696
HPRM-2	2.04	1.61	3.01	21.0	46	93	3.3	1.7 2.7	11591	6363
HPRM-3	2.08	1.61	3.11	22.7	48	98	1.0	1.5 1.9	8871	4695
HPRM-4	1.98	1.53	3.06	22.9	50	91	4.5	3.5 3.9	9058	4678
HPRM-5	1.94	1.45	3.02	27.4	52	95	2.6	2.9 3.1	7707	3796
HPSL-16	1.86	1.36	2.94	27.0	54	93	3.7	2.4 2.7	6303	2717
HPNS-1	2.05	1.51	3.35	26.7	55	99	0.2	2.0 2.5	7519	3619
HPRM-3C	2.12	1.70	3.03	19.6	44	95	2.3	2.0 2.5	9786	5275
HPNS-2	1.94	1.41	3.21	27.4	56	95	2.9	3.2 3.4	8360	4265
Grout 56 Day										
HPRM-1	2.05	1.63	2.97	20.5	45	93	3.2	2.5 3.0	10269	5545
HPRM-2	2.02	1.57	3.01	22.4	48	94	2.7	1.5 2.9	11591	6368
HPRM-3	2.10	1.65	3.11	21.2	47	95	2.5	1.6 2.5	9672	5230
HPRM-4	1.96	1.49	3.06	24.1	51	92	4.3	4.3 4.4	8215	3976
HPRM-5	1.97	1.48	3.02	24.8	51	96	2.0	2.5 2.7	8064	4117
HPSL-16	1.85	1.34	2.94	27.4	54	93	3.6	2.3 3.0	8291	3819
HPNS-1	2.09	1.58	3.35	24.2	53	96	2.2	2.1 2.6	8015	4006
HPRM-3C	2.15	1.73	3.03	19.5	43	98	1.0	1.9	10780	5480
HPNS-2	1.88	1.34	3.21	28.7	58	93	4.3	2.4 5.7	8780	4560

TABLE 5
SUMMARY OF MEASUREMENTS AND TESTS
CONDUCTED ON MIGHTY EPIC GROUT MIXTURES

GROUT MIXTURES	PHYSICAL PROPERTIES	ULTRASONIC VELOCITIES	MECHANICAL TESTS		
			TRIAXIAL COMPRESSION	HYDROSTATIC COMPRESSION	UNIAXIAL STRAIN
ME801	X	X	X	X	X
ME802	X	X	X	X	X
ME804	X		X		
ME805	X	X	X	X	
ME806	X		X		
ME807			X		
ME808			X		
ME8-11	X	X	X		
ME8-11(R) (Field Cast)	X	X	X	X	X

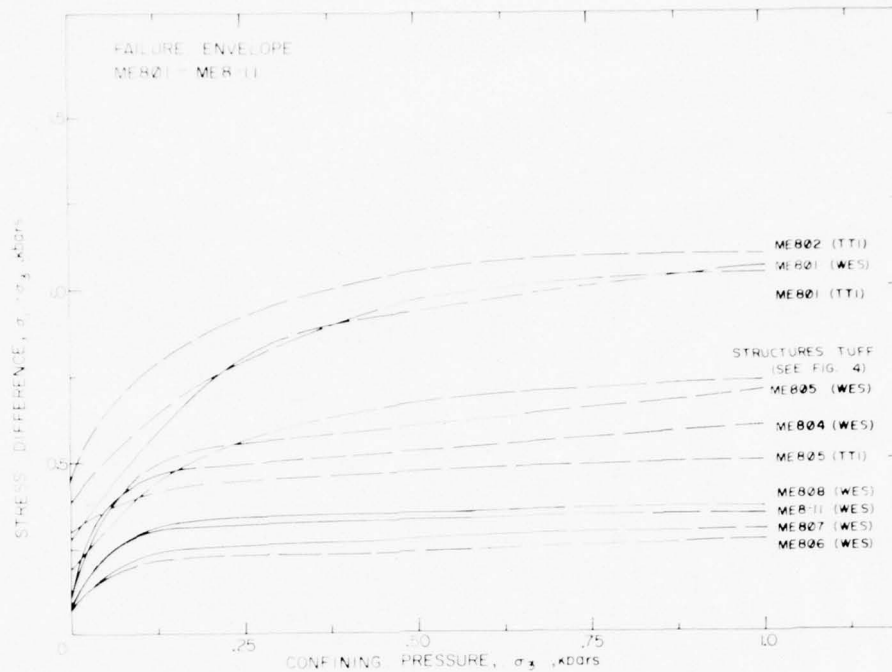


Figure 12. Combined Failure Data on ME801 through ME8-11 Grout Samples.

TABLE 6

PHYSICAL PROPERTIES, ULTRASONIC VELOCITIES AND PERMANENT VOLUME COMPACTION ON GROUT MIXTURES ME801, ME802, ME804, ME805, ME806 and ME8-11

GROUT MIXTURES	DENSITY (gm/cc)			WATER BY WET WEIGHT (%)	POROSITY (%)	SATURATION (%)	CALC. AIR VOIDS (%)	MEAS. PERMANENT COMP. (%)	VELOCITY (ft/sec)	
	AS-RECEIVED	DRY	GRAIN						LONG	SHEAR
ME801	1.95	1.61	2.57	17.4	38	90	3.7	Hyd. 1-D 3.9 4.5	12670	7402
ME802	1.89	1.57	2.54	17.0	38	84	6.1	4.0 5.1	12864	7188
ME804	1.91	1.56	2.52	18.5	38	92	2.9			
ME805	1.97	1.67	2.53	15.5	34	89	3.7		12700	7100
ME806	2.01	1.74	2.50	13.6	31	90	3.2			
ME8-11	2.05	1.77	2.53	13.7	30	93	2.0	3.4	9420	4272

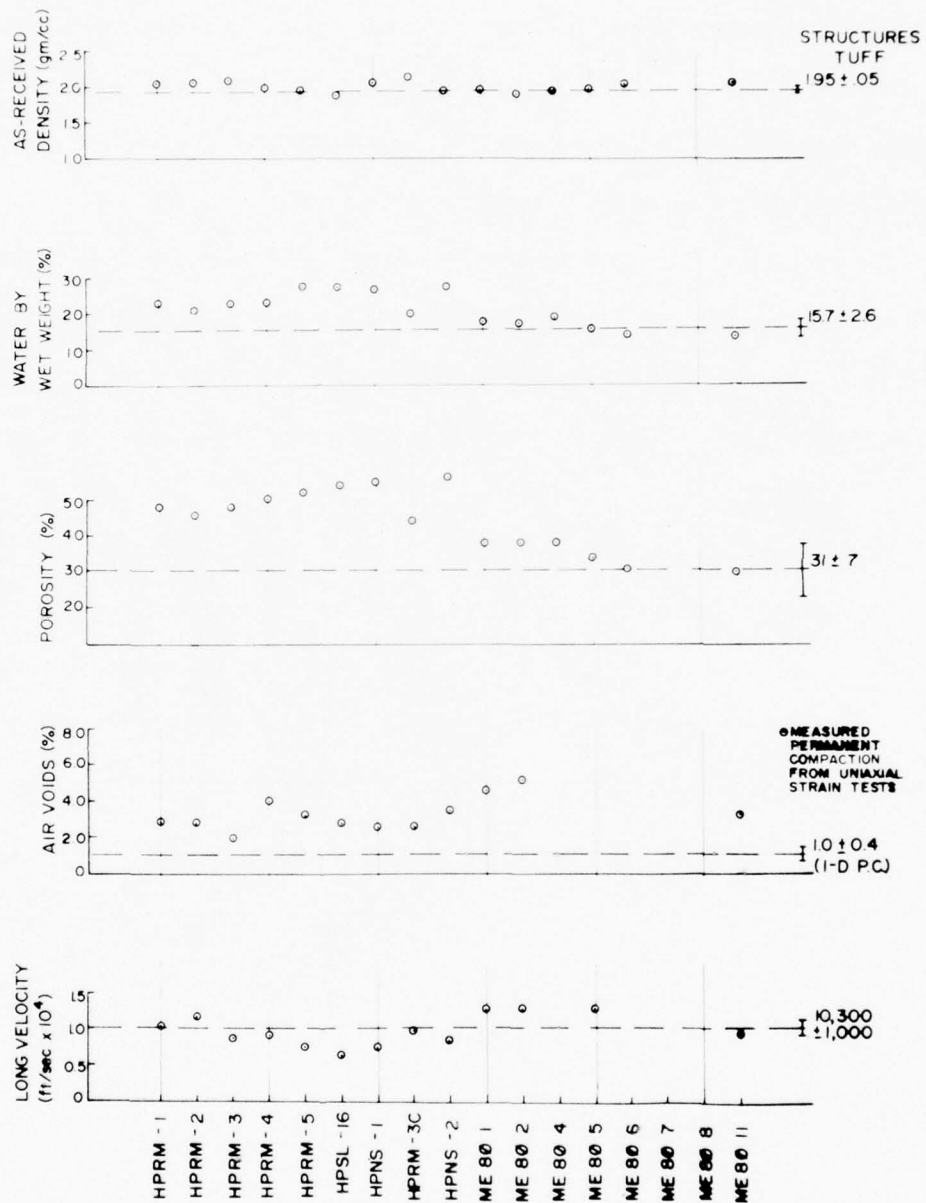


Figure 13. Selected Properties of all Grout Mixtures Tested During this Grout Development.

VERIFICATION OF FIELD GROUT MIXTURES

An added precaution, and one that has been standard procedure for past events, is periodic sampling of the grout mixes that are actually implaced in the tunnels. This was especially necessary for the structures grout where the properties were of utmost importance.

Selected samples obtained from batches of the field cast ME8-11 grout were tested by WES and TTI. The test results are shown in Figure 14 and 15 during the aging process and in Figure 16 for grout tests conducted close to shot day. Table 7 summarizes selected properties on these field cast mixtures.

The finalized mixture contained; Portland cement, expansive cement, flyash, Barite, Bentonite, pumice sand, fine silica sand, water reducing-retarder admixture and water. The water-cementitious ratio by weight was 1.4. The theoretical unit weight and theoretical cementitious content were 125.9 pounds per cubic feet and 5.0 bags per cubic yard, respectively.

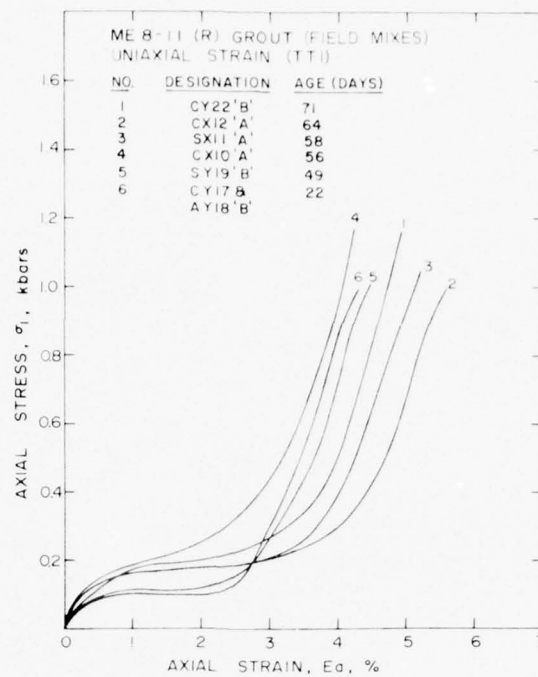


Figure 14a. Uniaxial Strain Results on Samples from Several Mixtures of ME8-11(R) Field Mixes (TTI) -- Stress-Strain Response.

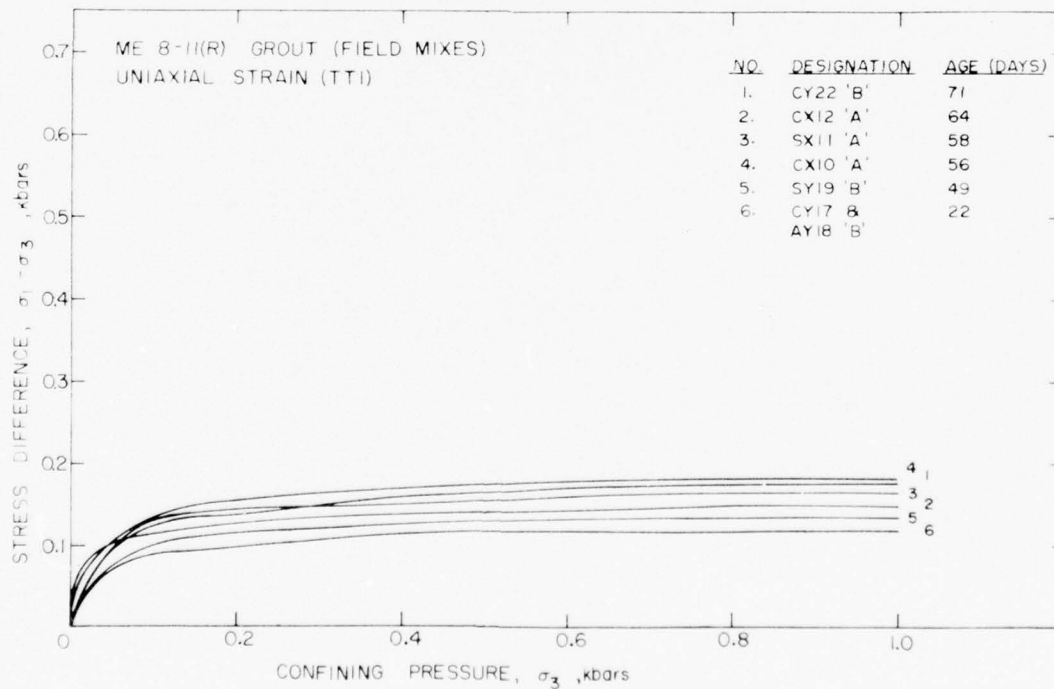


Figure 14b. Uniaxial Strain Results on Samples from Several Mixtures of ME8-11(R) Field Mixes (TTI) -- Stress-Stress Response.

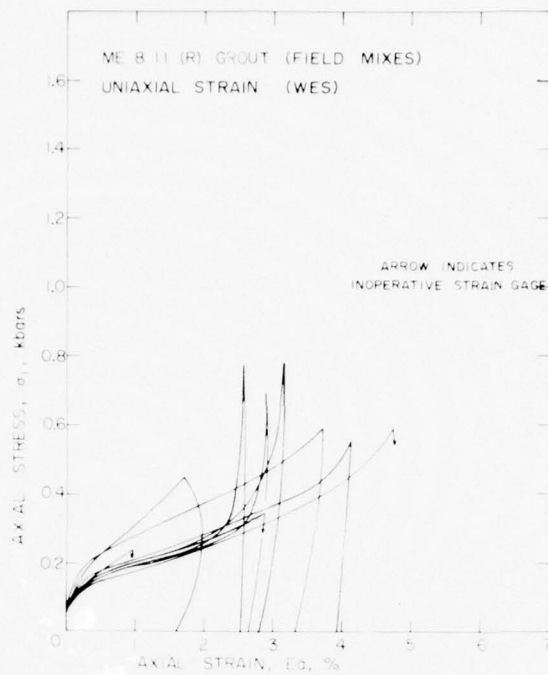


Figure 15a. Uniaxial Strain Results on Samples from Several Mixtures of ME8-11(R) Field Mixes (WES) -- Stress-Strain Response.

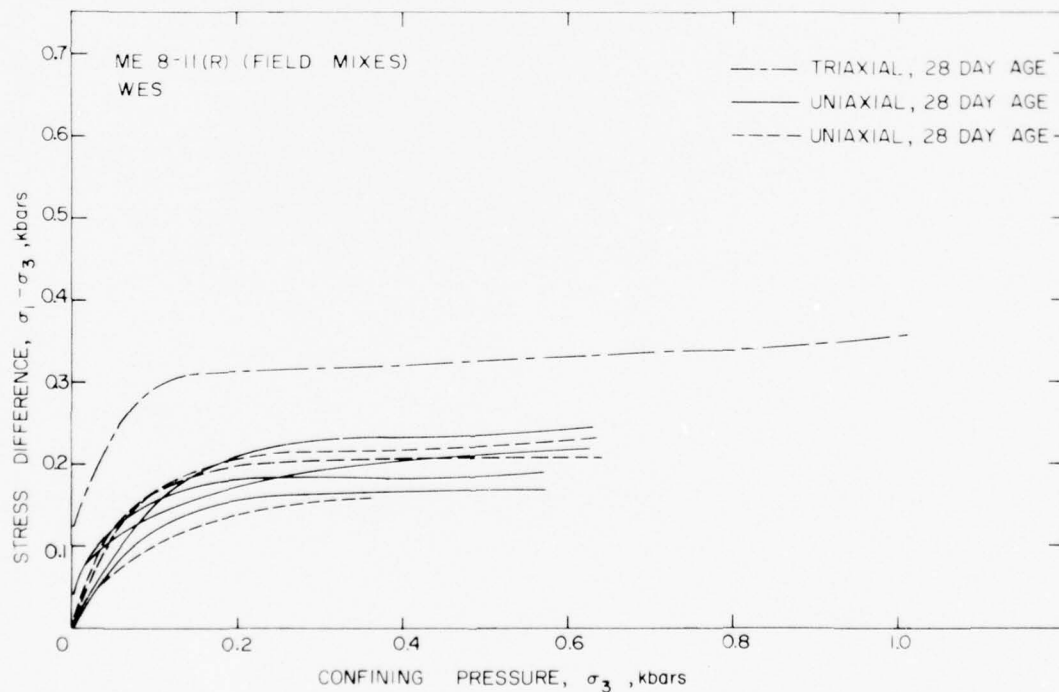


Figure 15b. Uniaxial Strain Results on Samples from Several Mixtures of ME8-11(R) Field Mixes (WES) -- Stress-Stress Response.

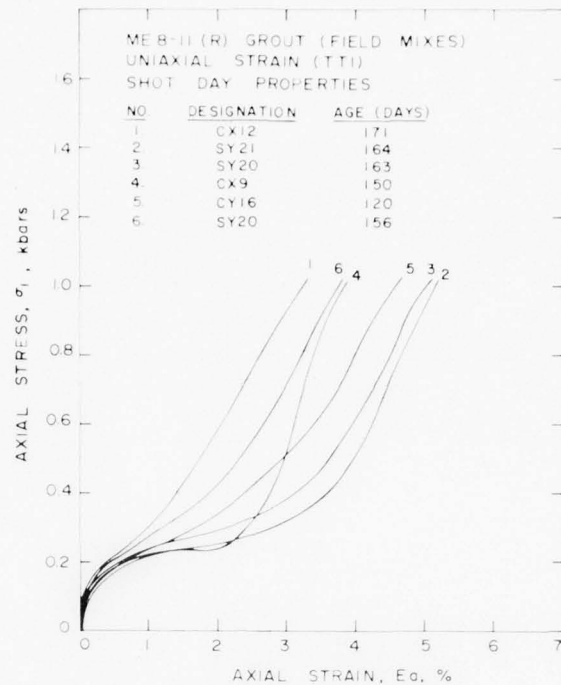


Figure 16a. Uniaxial Strain Results on Samples from Several Mixtures of ME8-11(R) Field Mixes (TTI) -- Stress-Strain Response. Tests were conducted close to Mighty Epic Shot Day.

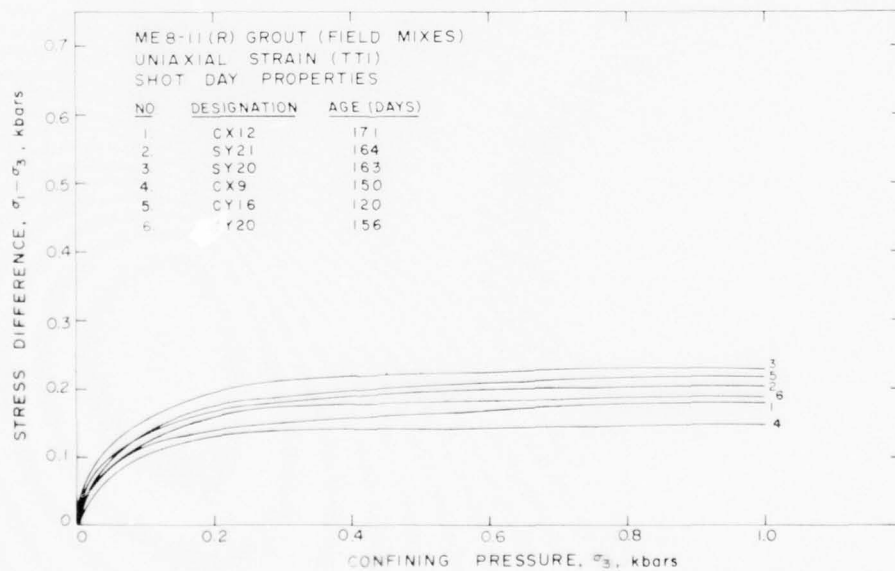


Figure 16b. Uniaxial Strain Results on Samples from Several Mixtures of ME8-11(R) Field Mixes (TTI) -- Stress-Stress Response. Tests were conducted close to Mighty Epic Shot Day.

TABLE 7

PHYSICAL PROPERTIES, ULTRASONIC VELOCITIES AND MEASURED PERMANENT VOLUME
COMPACTION ON SEVERAL FIELD CAST BATCHES OF MEB-11 GROUT

DESIGNATION	AGE (DAYS)	DENSITY (gm/cc)			WATER BY WET WEIGHT (%)	POROSITY (%)	SATURATION (%)	CALC. AIR VOIDS (%)	MEAS. PERMANENT COMP. (%)	ULTRASONIC VELOCITY (ft/sec)	
		AS- RECEIVED	DRY	GRAIN						LONG	SHEAR
CY22 'B'	71	2.12	1.75	3.01	17.7	42	90	4.3	4.0	10,240	5300
CX12 'A'	64	2.14	1.77	3.05	17.6	42	90	4.3	4.9	10,490	5300
SX11 'A'	58	2.09	1.73	2.94	17.5	41	88	5.1	4.7	11,260	5600
CX10 'A'	56	2.12	1.75	3.03	17.5	42	87	5.4	5.4	10,500	5540
SY19 'B'	49	2.12	1.73	3.00	18.1	42	91	3.9	4.0	11,150	5360
CY17 & AY18 'B'	22	2.11	1.73	2.96	17.8	42	90	4.1	3.9	9,700	4970
CX12(FFSH)	171	2.10	1.73	2.96	17.6	42	89	4.6		11,125	5789
SY21	164	2.09	1.73	3.00	17.5	43	86	6.0		10,614	5425
SY20(FFSH)	163	2.13	1.77	3.07	16.8	42	85	6.6		10,904	5450
SY20	156	2.17	1.79	3.03	17.5	41	93	2.9		10,564	5721
CX9	150	2.19	1.83	3.07	16.5	40	90	4.2		9,570	5179
CY16	120	2.12	1.75	3.03	17.3	42	87	5.6		10,287	5520

DISCUSSION AND CONCLUSIONS

The mechanical and physical properties of the tuff in the structures area are well documented. The structures tuff, as compared to the typical ash fall tuff in Area 12, has about twice the shear strength with densities and sound speeds 10 to 20 percent higher, porosities and water contents 10 to 20 percent lower and air void contents approximately the same. The scatter in the material properties is typical of tuff.

Once the tuff properties had been established, the development of a matching grout required several major considerations. The shear strength of the grout was of utmost importance, not only unconfined, but as a function of confining pressure (failure envelope). Grout mixtures with high porosity and saturation are much less pressure dependent than tuff. This behavior is primarily a function of the pore pressure and the resulting effective stress. The most obvious means to increase the pressure dependence of the grout shear strength was to decrease the water content of the grout. Lowering the water content and reportioning with various types of mixture constituents not only assisted in matching the shape of the tuff failure envelope but also in producing the overall increase in the shear strength needed. However, with this decrease in water and increase in shear strength, the pumpability of the grout was lowered. It should be obvious that with this dependence of properties on one another, the development required considerable effort and a number of changes in the grout constituents.

Aside from predicting what mixture changes were necessary to produce the desired results, the aging history of each test batch was important. Time, temperature and humidity all add an important factor to the grout

properties. Grout implaced in essentially a 100 percent humidity environment can develop a considerable temperature rise over a period of time. Also, the grout would be implaced weeks or months prior to test execution. Obviously, to have simulated these exact conditions on the development grouts would require a prohibitive test program time. Therefore, prior experience and knowledge of the aging characteristics were utilized to a considerable degree in this grout program. As an example, note the differences in the uniaxial strain test response of the ME8-11 grout as tested by WES and Terra Tek, Figure B15. The WES data was generated from samples which had been at elevated temperature and 100 percent humidity for 7 days. This aging history is approximately equivalent to 28 days of curing at room temperature while maintaining the water content constant. The Terra Tek tests were on 14 day age room temperature cured samples. The WES samples (7 day accelerated) produced about twice the shear strength and a much different stress-strain response than the Terra Tek samples (14 day room temperature).

In summary, the development of a grout to match select properties of the tuff was very successful. The ME8-11 grout mixture matches very closely the shape of the tuff failure surface, the as-received density, the sound speed, porosity and the water content. The air void content of the grout is slightly higher but will not be a problem because of the relatively thin layer of grout.

Concerning the absolute magnitude of the grout shear strength, it was the general consensus of the persons responsible for the structures experiments, that in consideration of the tuff material scatter, they would prefer to have the grout strength on the low side rather than the high side of the "representative" tuff strength. The ME8-11 grout mixture is therefore expected to peak out at a strength lower than the "representative" tuff strength.

REFERENCES

1. R. L. Stowe, Concrete and Rock Properties Branch, Waterways Experiment Station, Vicksburg, Mississippi.
2. Ralph Bendenelli, Grouting Branch, Waterways Experiment Station, Vicksburg, Mississippi.
3. J. W. LaComb, Civil Engineering, Nevada Test Site, Mercury, Nevada.
4. S. W. Butters, R. K. Dropek, S. J. Green and A. H. Jones, "Material Properties in Support of the Nevada Test Site Nuclear Test Program," Terra Tek Report TR 75-27, October 1975.

APPENDIX A

Mechanical Test Results on U12n.10 UG#4,
UG#6a, ISS#5 and ISS#7 Core Samples.

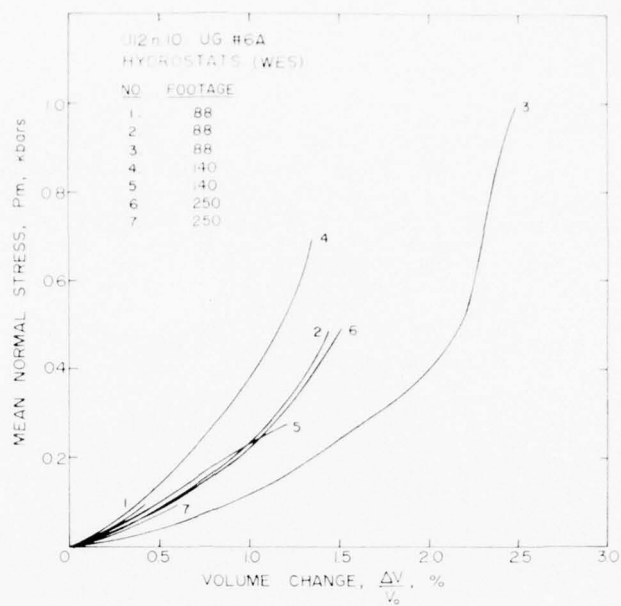


Figure A1. Hydrostatic Compression Results on U12n.10 UG#6a Core Samples (WES).

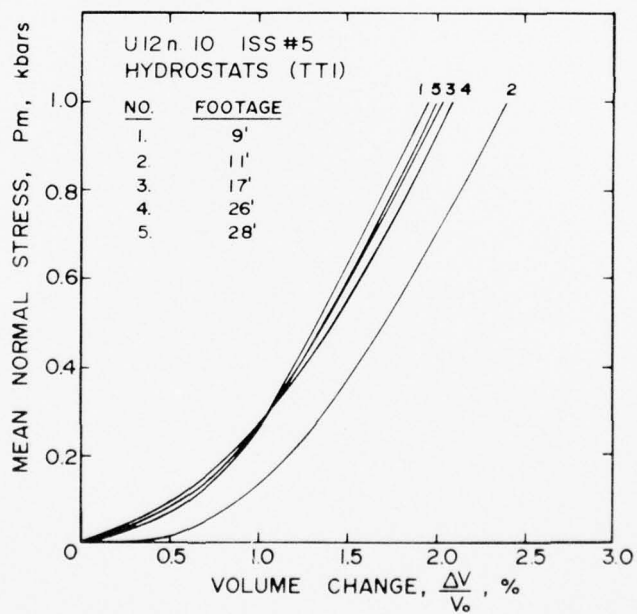


Figure A2. Hydrostatic Compression Results on U12n.10 ISS#5 Core Samples (TTI).

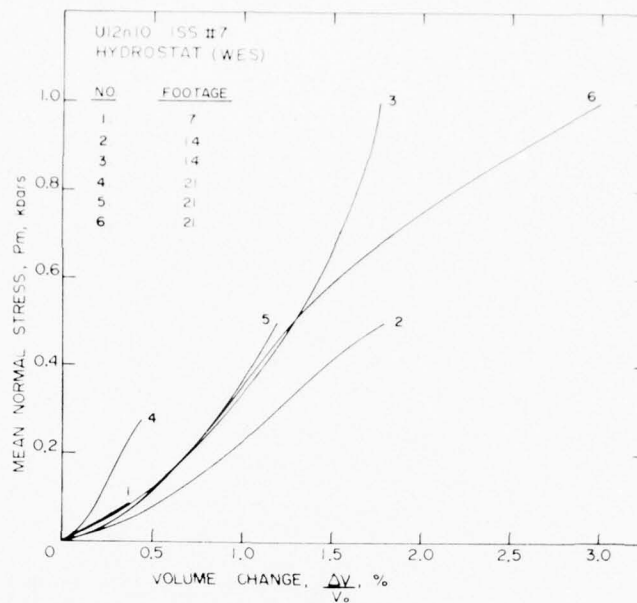


Figure A3. Hydrostatic Compression Results on U12n.10 ISS#7 Core Samples (WES).

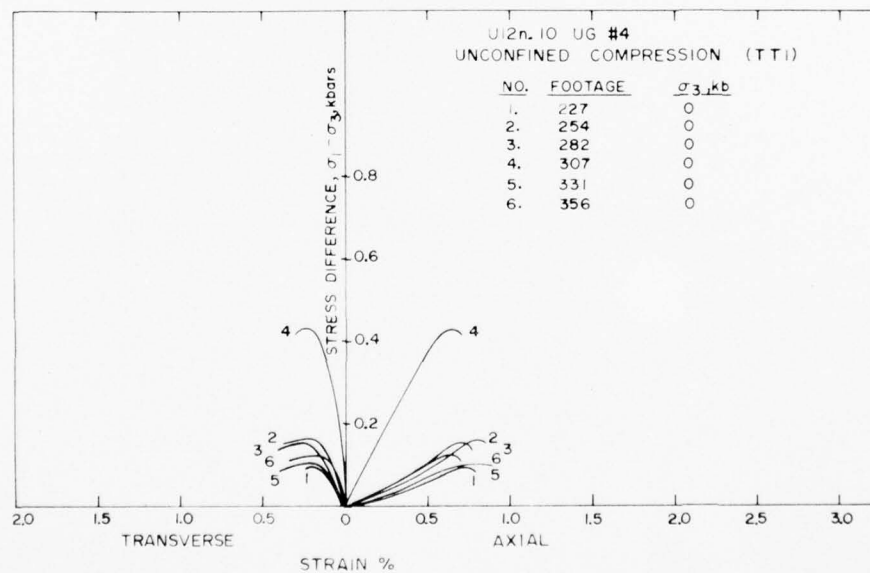


Figure A4. Unconfined Compression Results on U12n.10 UG#4 Core Samples (TTI).

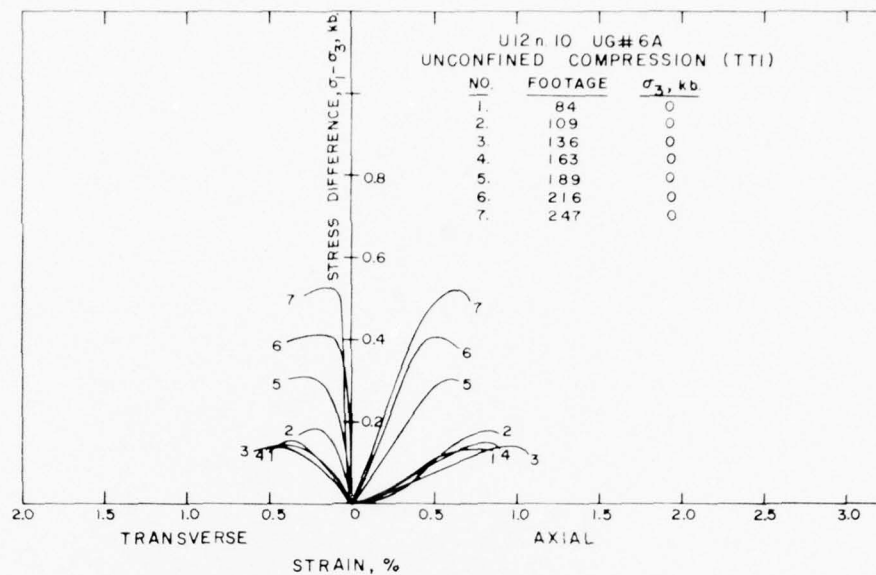


Figure A5. Unconfined Compression Results on U12n.10 UG#6a Core Samples (TTI).

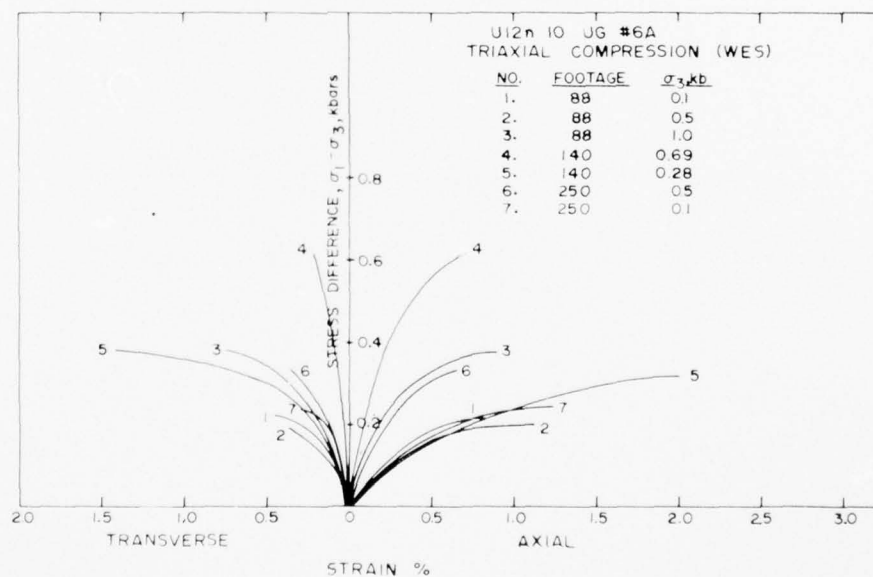


Figure A6. Triaxial Compression Results on U12n.10 UG#6a Core Samples (WES).

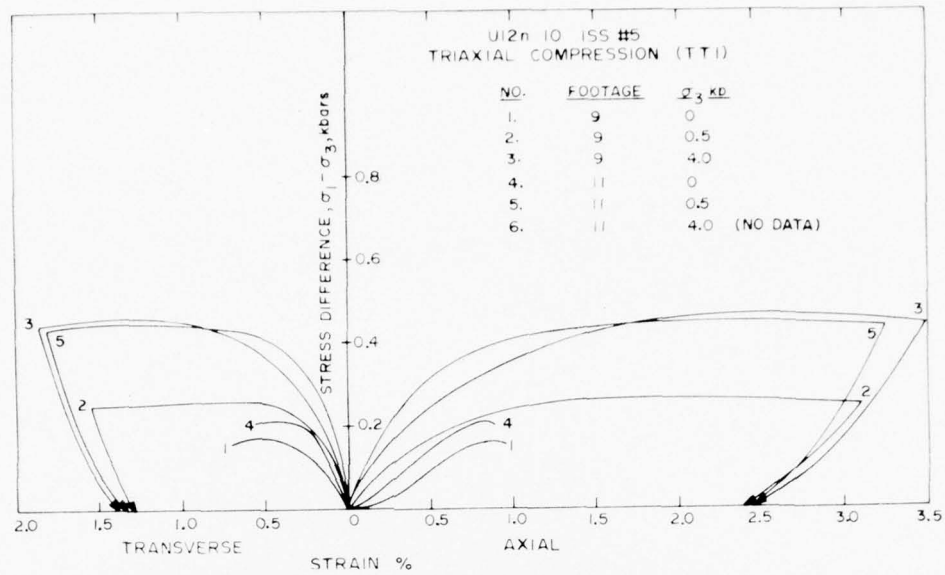


Figure A7. Triaxial Compression Results on U12n.10
ISS#5 Core Samples (TTI).

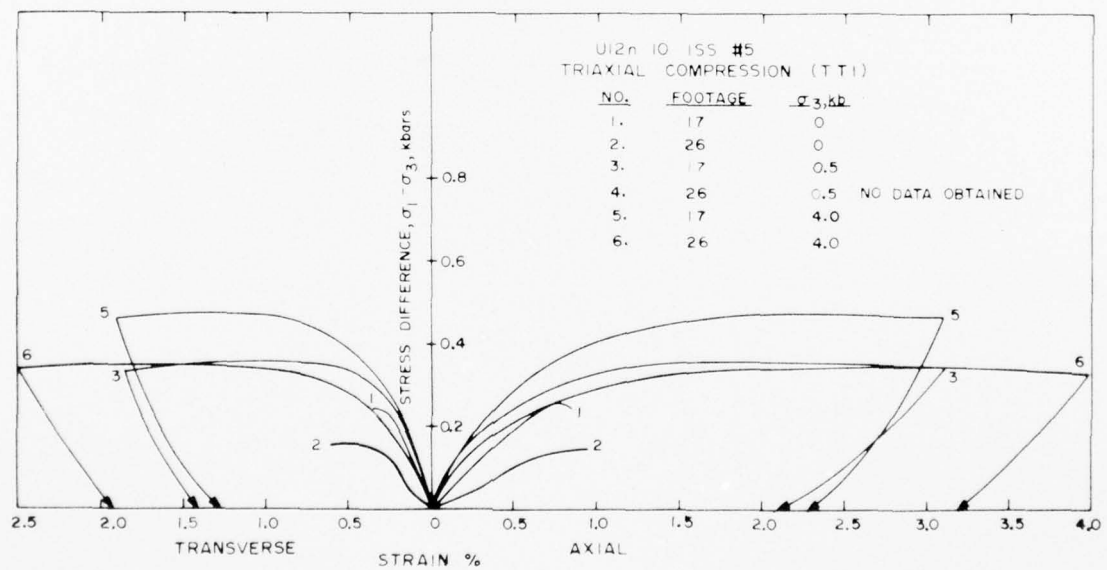


Figure A8. Triaxial Compression Results on U12n.10
ISS#5 Core Samples (TTI).

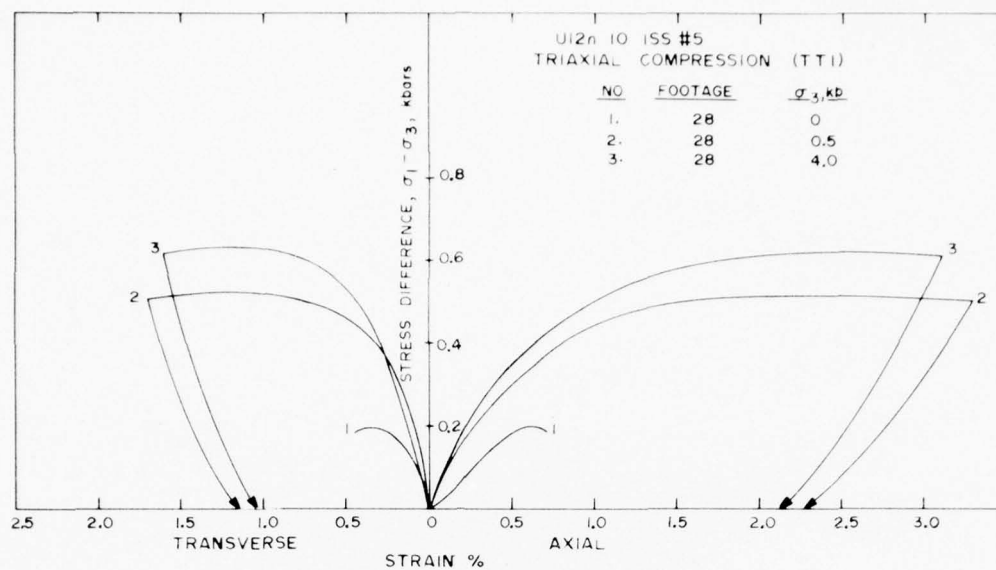


Figure A9. Triaxial Compression Results on U12n.10 ISS#5 Core Samples (TTI).

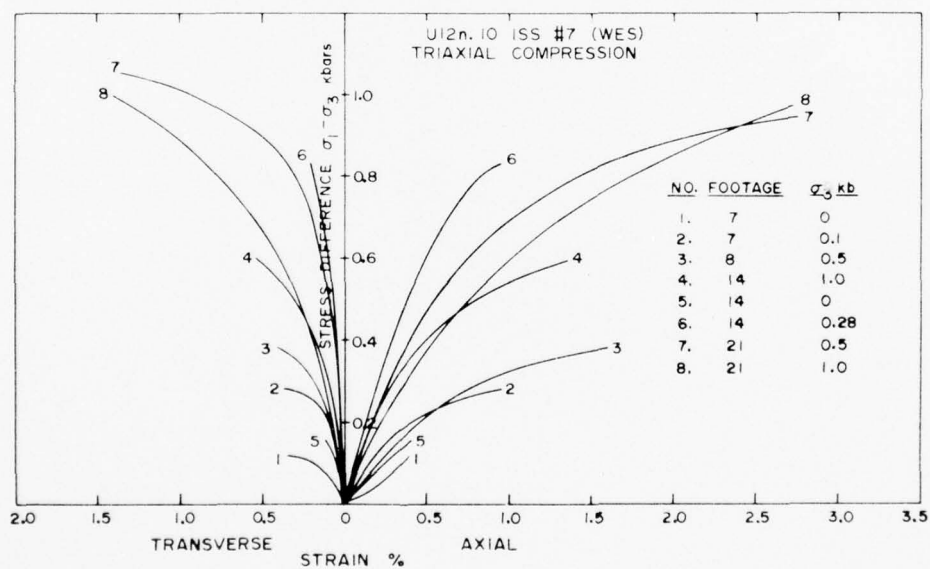


Figure A10. Triaxial Compression Results on U12n.10 ISS#7 Core Samples (WES).

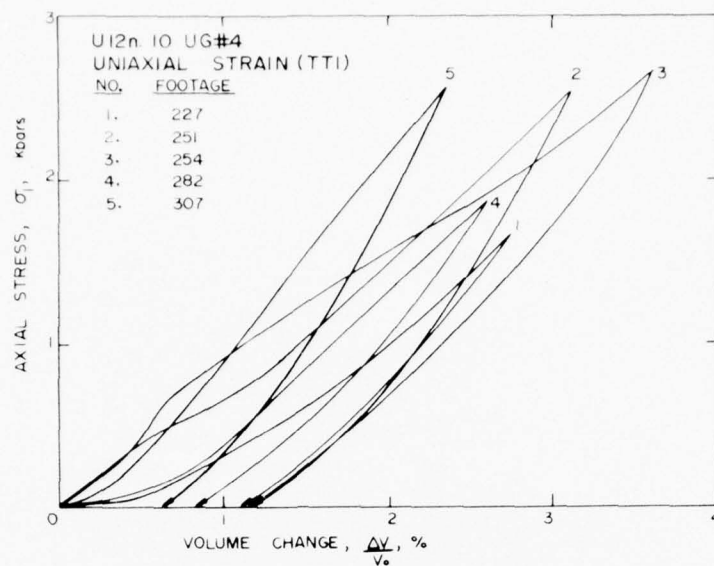


Figure A11a. Uniaxial Strain Results on U12n.10 UG#4 Core Samples (TTI).

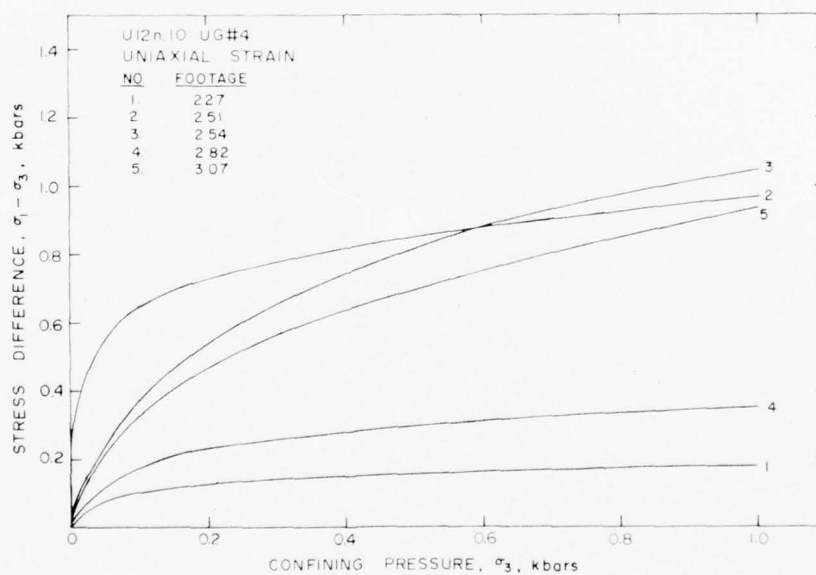


Figure A11b. Uniaxial Strain Results on U12n.10 UG#4 Core Samples (TTI).

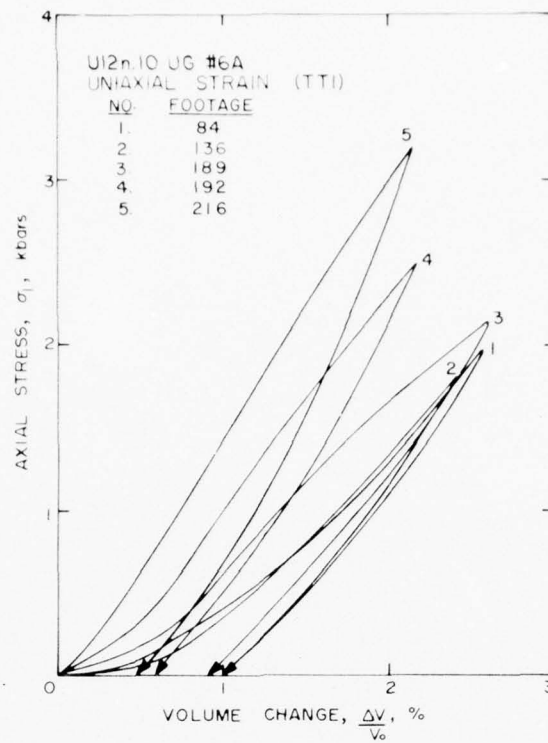


Figure A12a. Uniaxial Strain Results on U12n.10 UG#6a Core Samples (TTI).

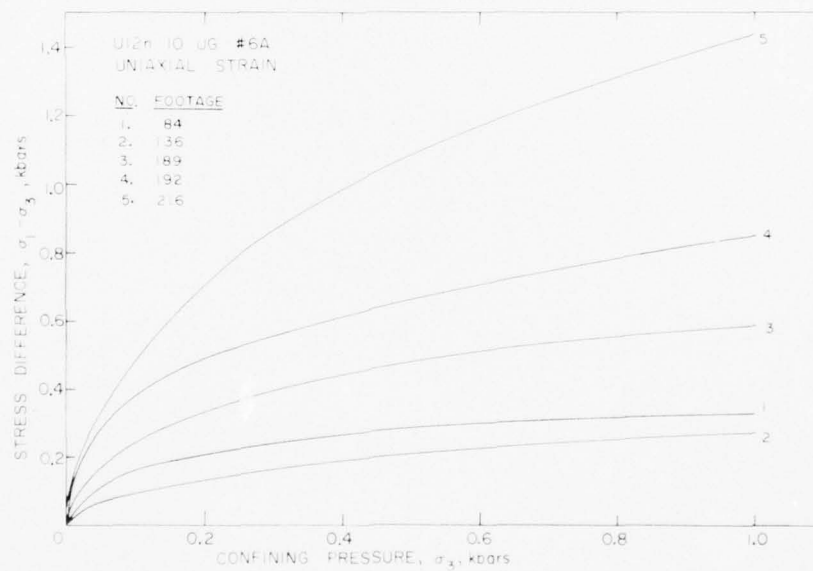


Figure A12b. Uniaxial Strain Results on U12n.10 UG#6a Core Samples (TTI).

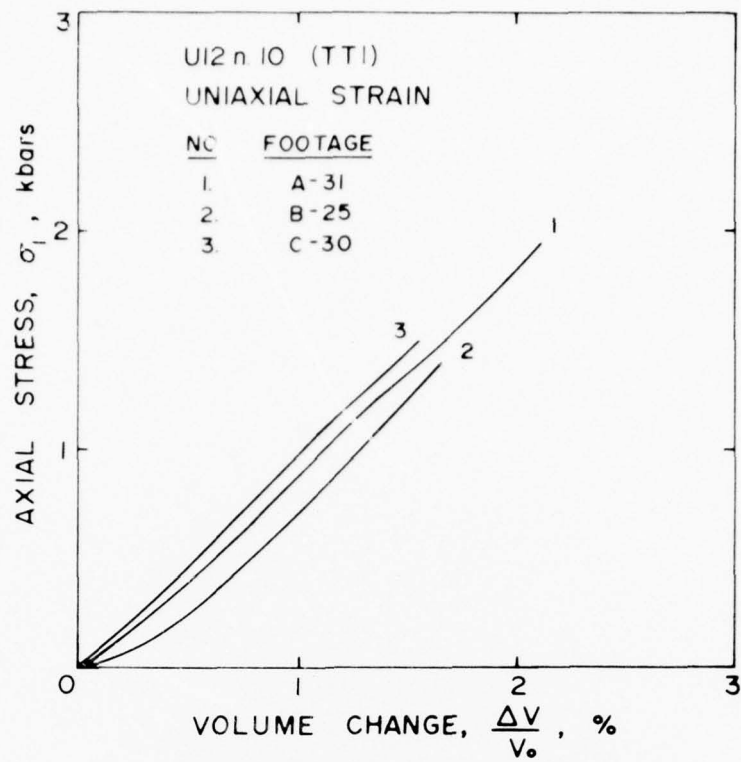


Figure A13a. Uniaxial Strain Results on U12n.10 A, B, and C Drift Samples (TTI).

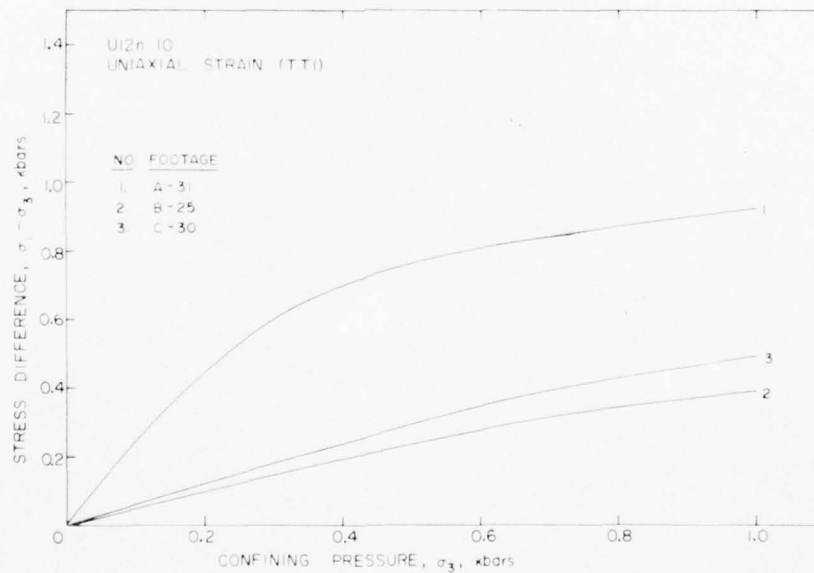


Figure A13b. Uniaxial Strain Results on U12n.10 A, B, and C Drift Samples (TTI).

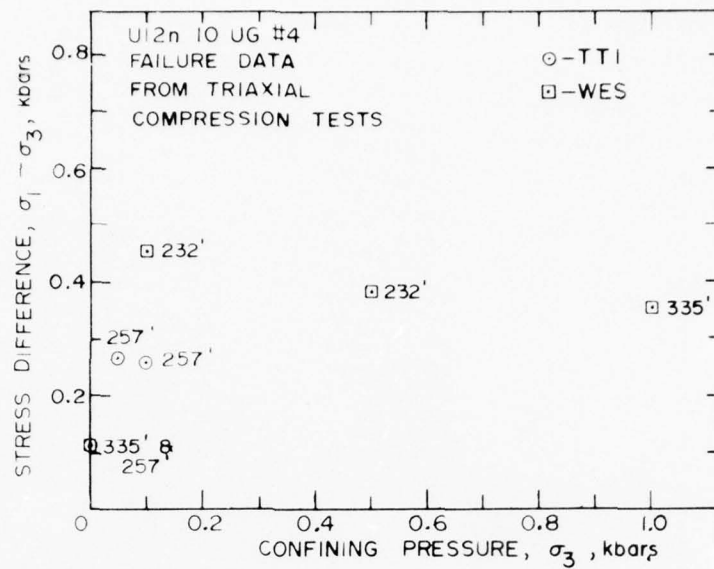


Figure A14. Failure Data from Triaxial Compression Tests on U12n.10 UG#4 Core Samples.

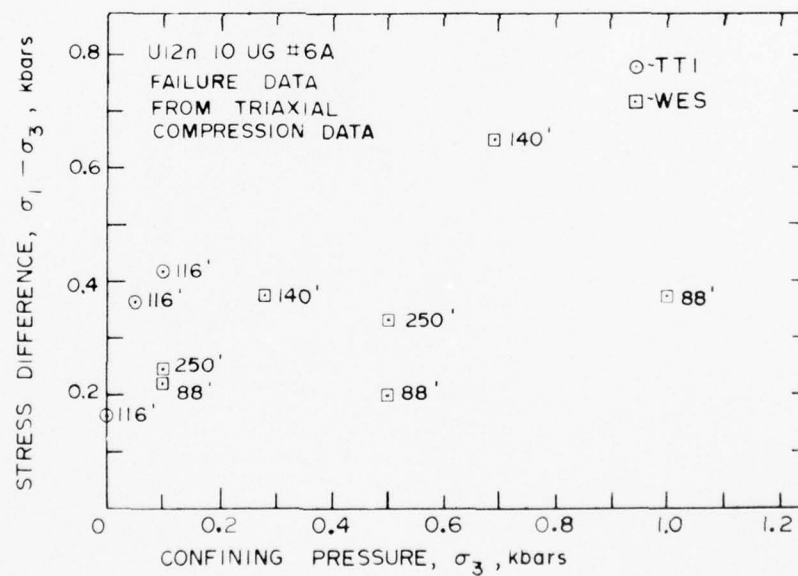


Figure A15. Failure Data from Triaxial Compression Tests on U12n.10 UG#6a Core Samples.

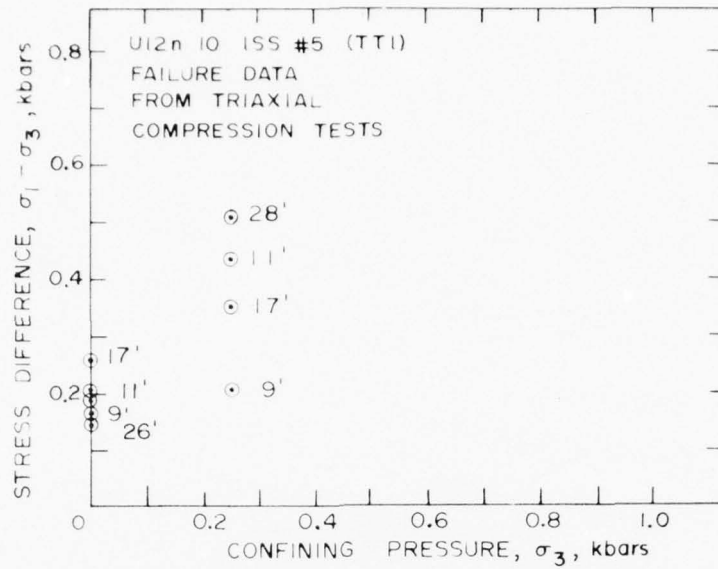


Figure A16. Failure Data from Triaxial Compression Tests on U12n.10 ISS#5 Core Samples (TTI).

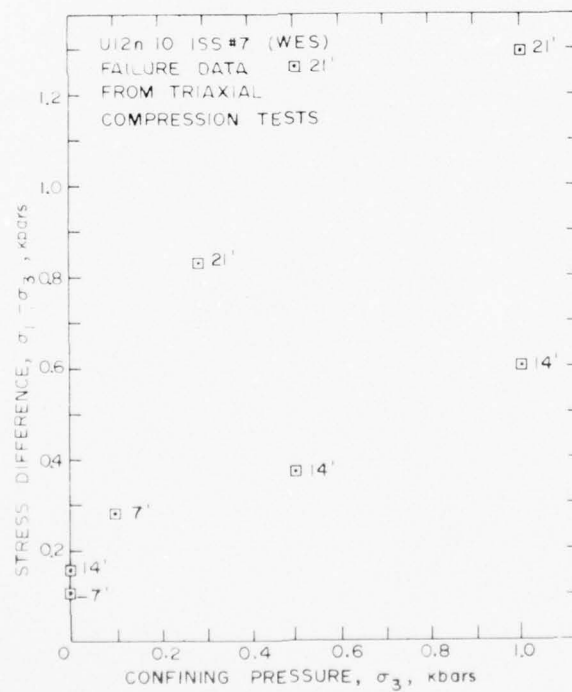


Figure A17. Failure Data from Triaxial Compression Tests on U12n.10 ISS#7 Core Samples (WES).

APPENDIX B

Mechanical Test Results on Mighty Epic Grout Mixtures

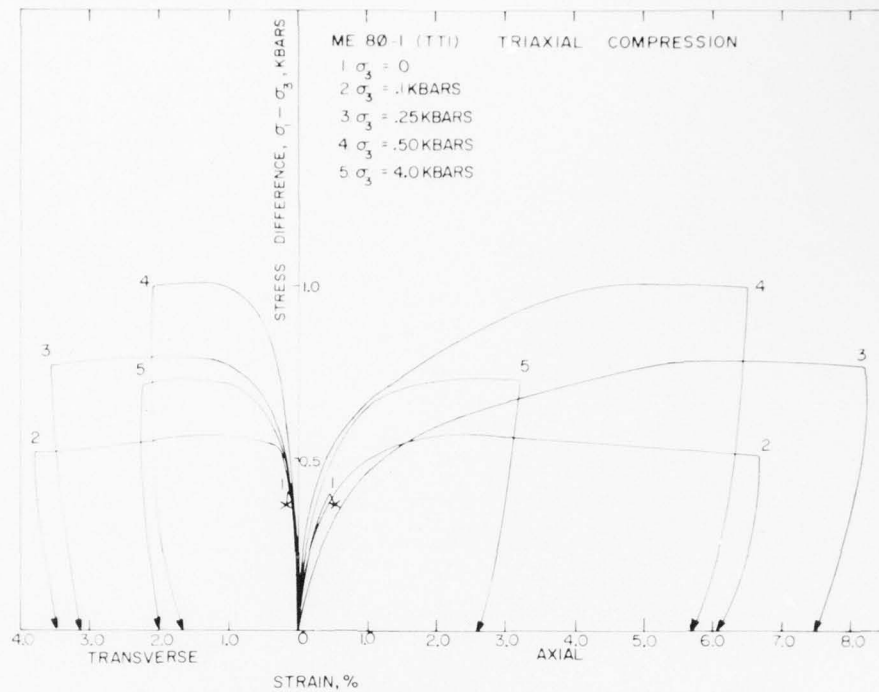


Figure B1. Triaxial Compression Tests on ME801 Grout Samples (TTI).

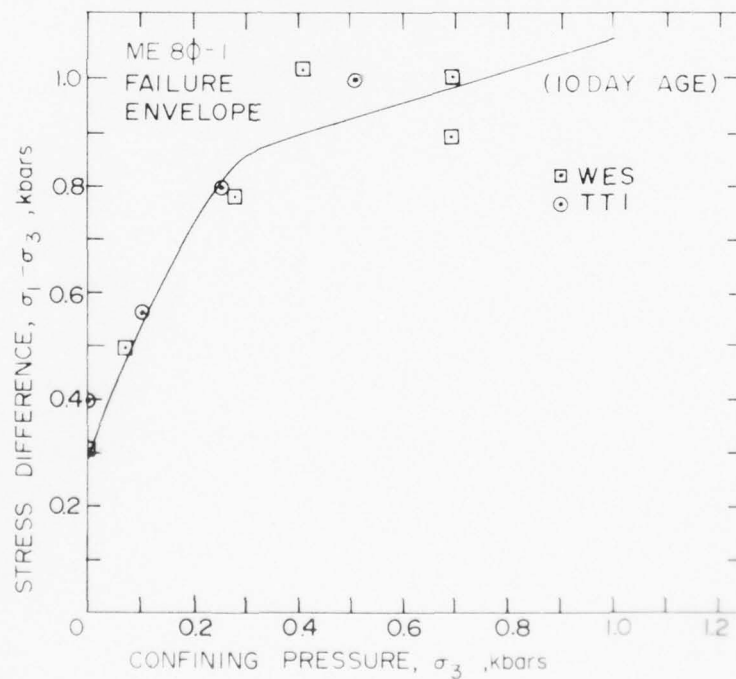


Figure B2. Failure Data on ME801 Grout Samples (WES and TTI).

AD-A043 977

TERRA TEK INC SALT LAKE CITY UTAH

F/G 18/3

MATERIAL PROPERTIES OF NEVADA TEST SITE TUFF AND GROUT - WITH E--ETC(U)

NOV 76 S W BUTTERS, R K DROPEK, A H JONES

DNA001-75-C-0260

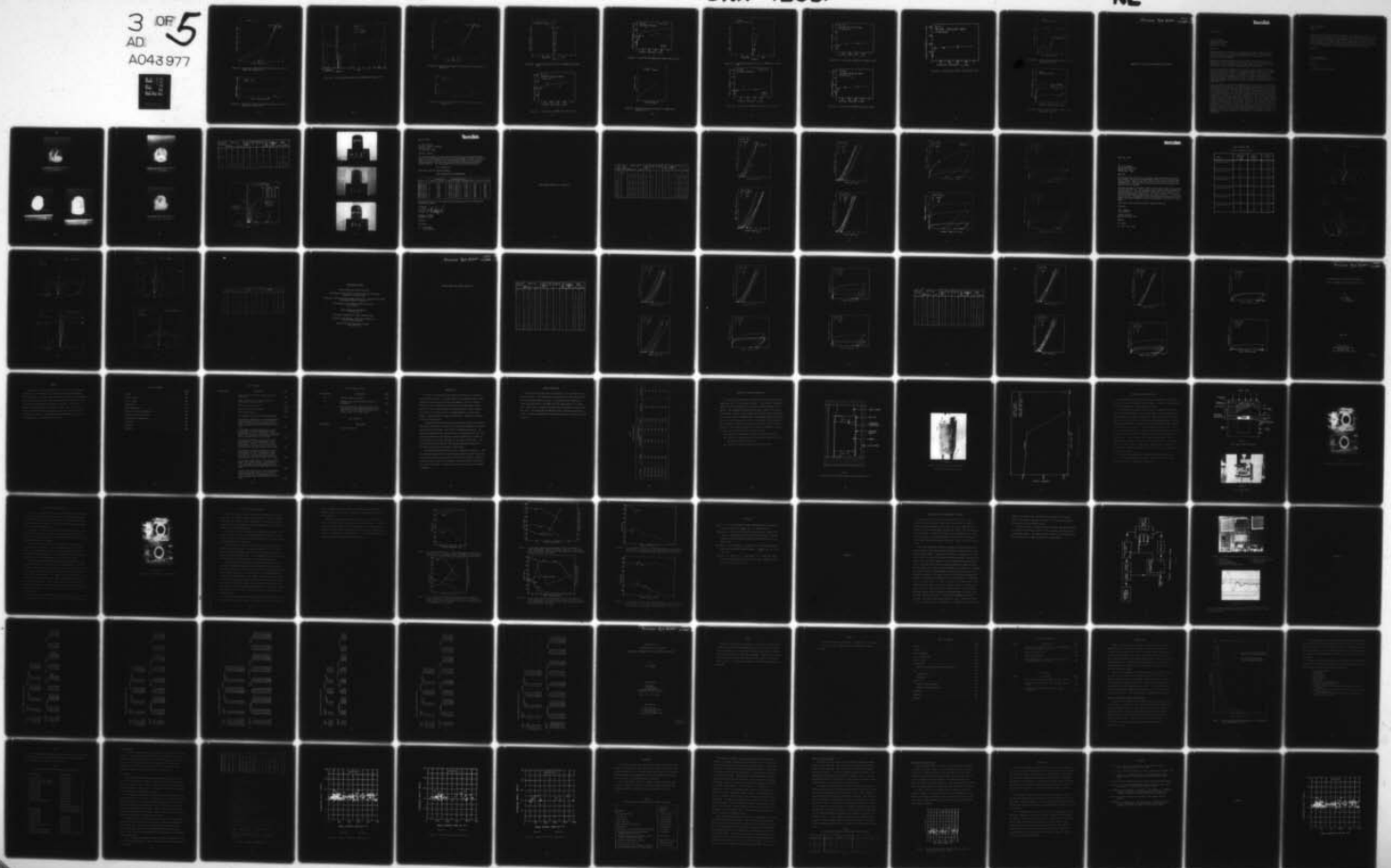
UNCLASSIFIED

TR-76-63

DNA-4235F

NL

3 OF 5
AD
A043977



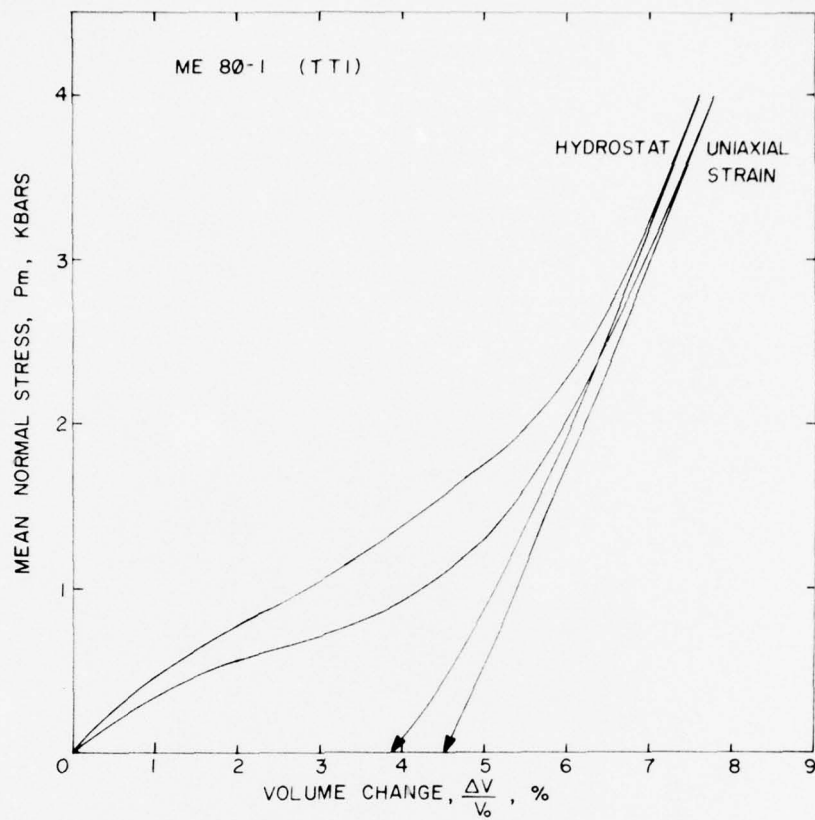


Figure B3a. Hydrostatic Compression and Uniaxial Strain Tests on ME801 Grout Samples (TTI).

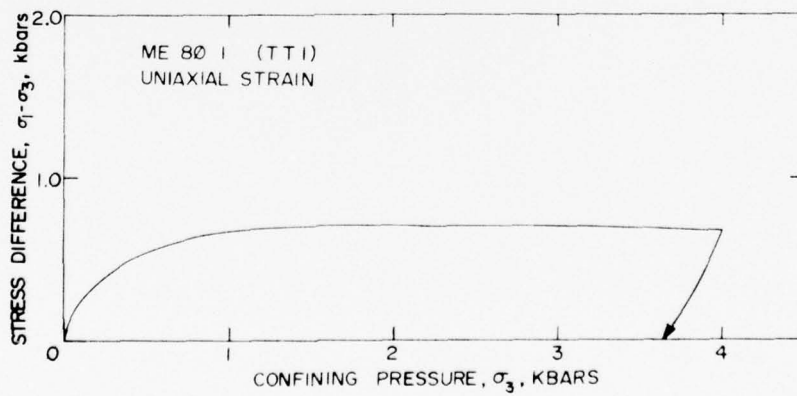


Figure B3b. Hydrostatic Compression and Uniaxial Strain Tests on ME801 Grout Samples (TTI).

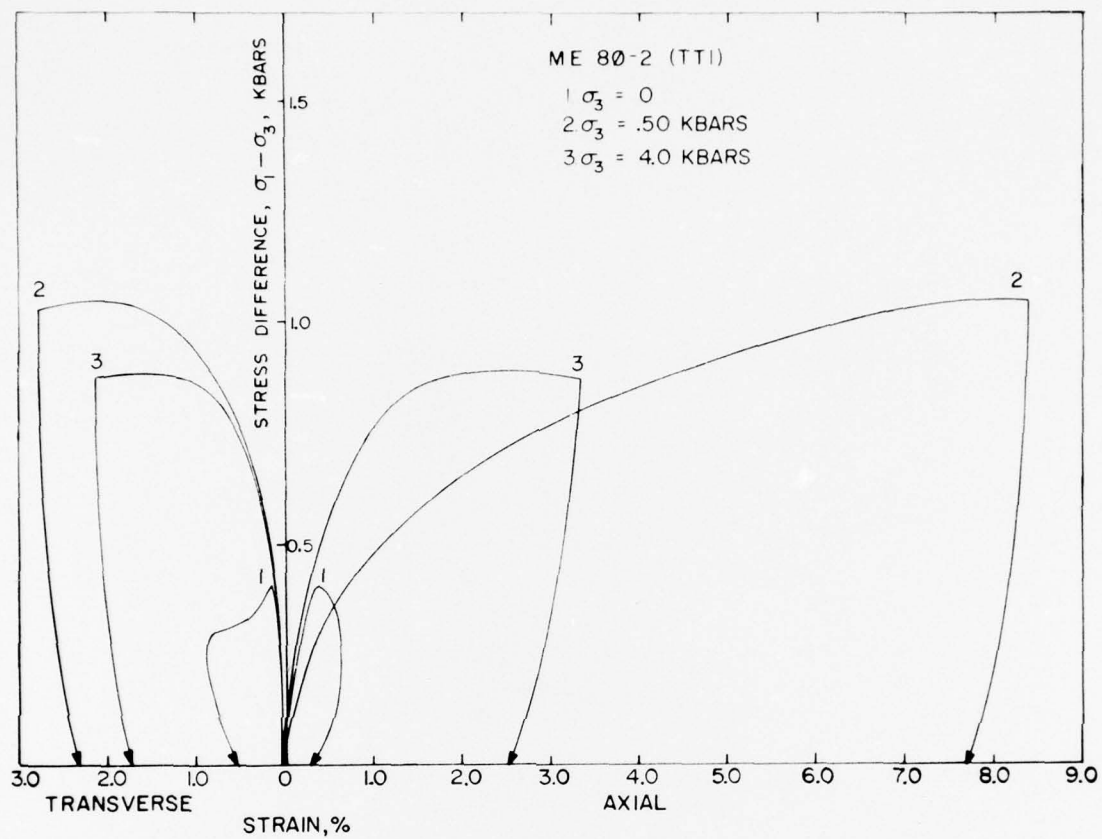


Figure B4. Triaxial Compression Results on ME802 Grout Samples (TTI).

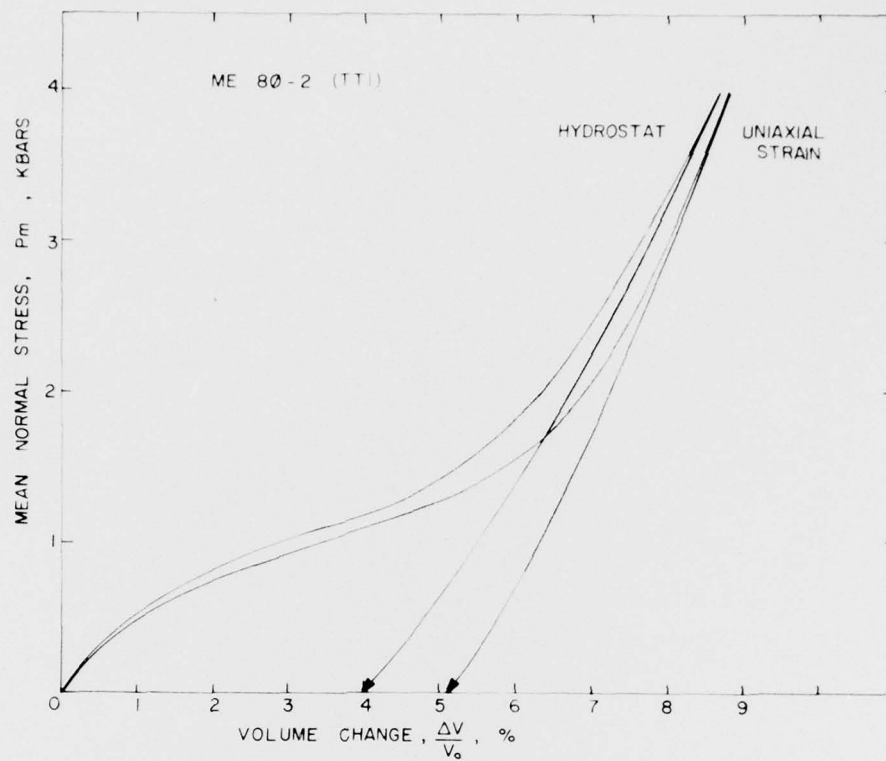


Figure B5a. Hydrostatic Compression and Uniaxial Strain Results on ME802 (TTI).

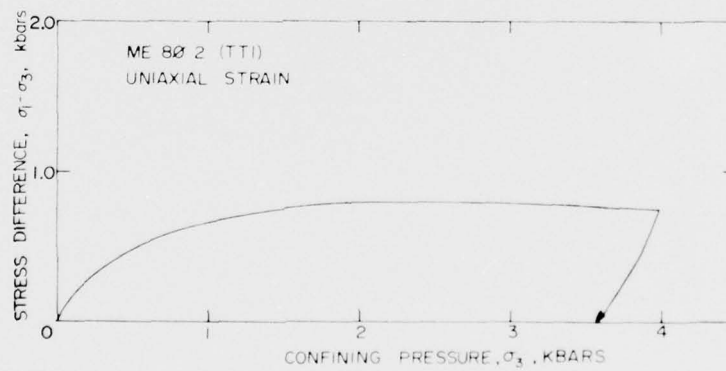


Figure B5b. Hydrostatic Compression and Uniaxial Strain Results on ME802 (TTI).

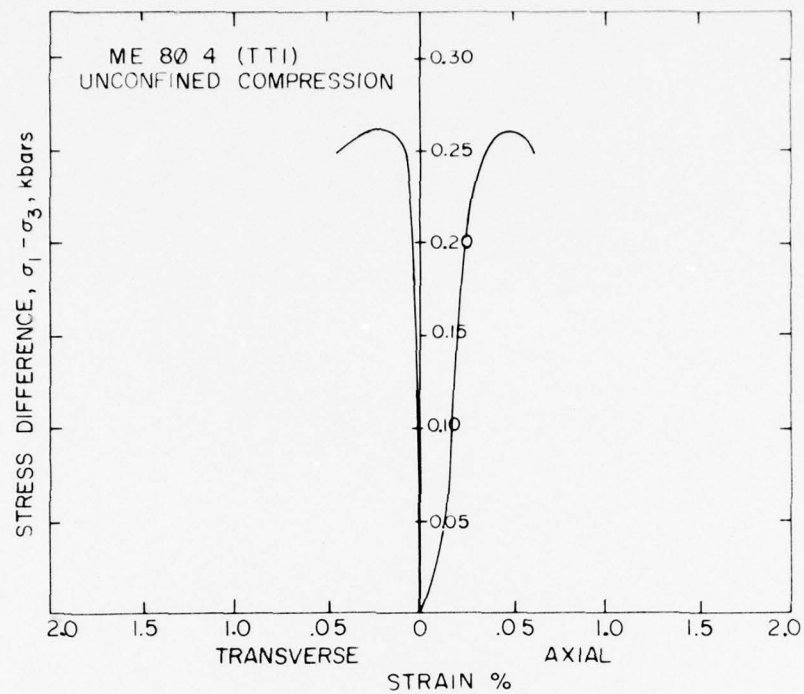


Figure B6. Unconfined Compression Tests on ME804 Grout Samples (TTI).

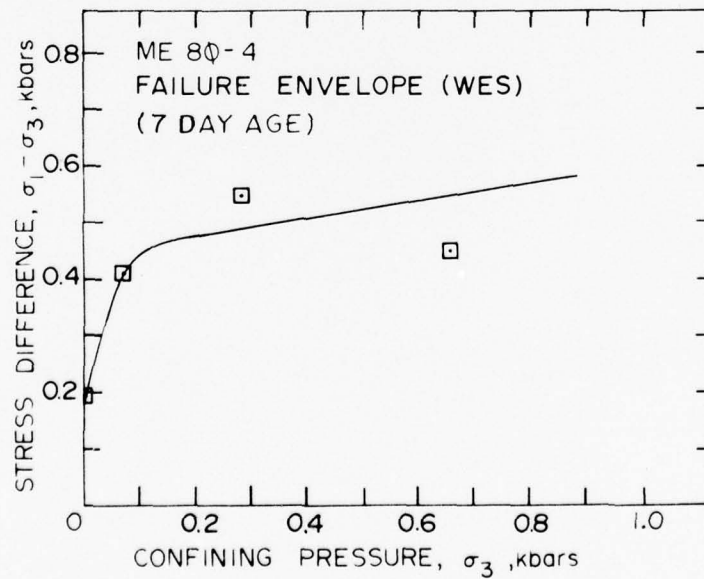


Figure B7. Failure Data on ME804 Grout Samples (WES).

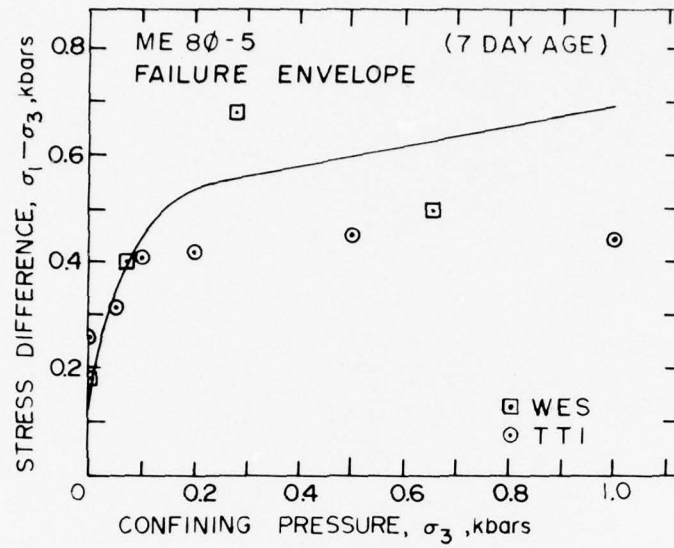


Figure B8. Failure Data on ME805 Grout Samples (WES and TTI).

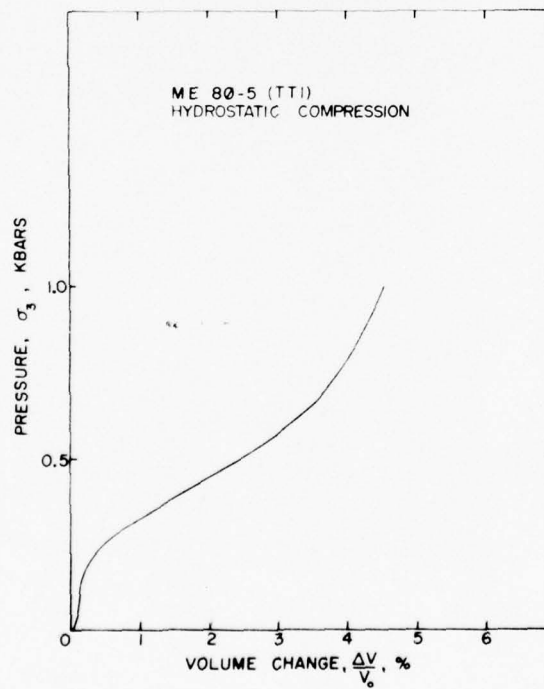


Figure B9. Hydrostatic Compression Results on ME805 Grout Samples (TTI).

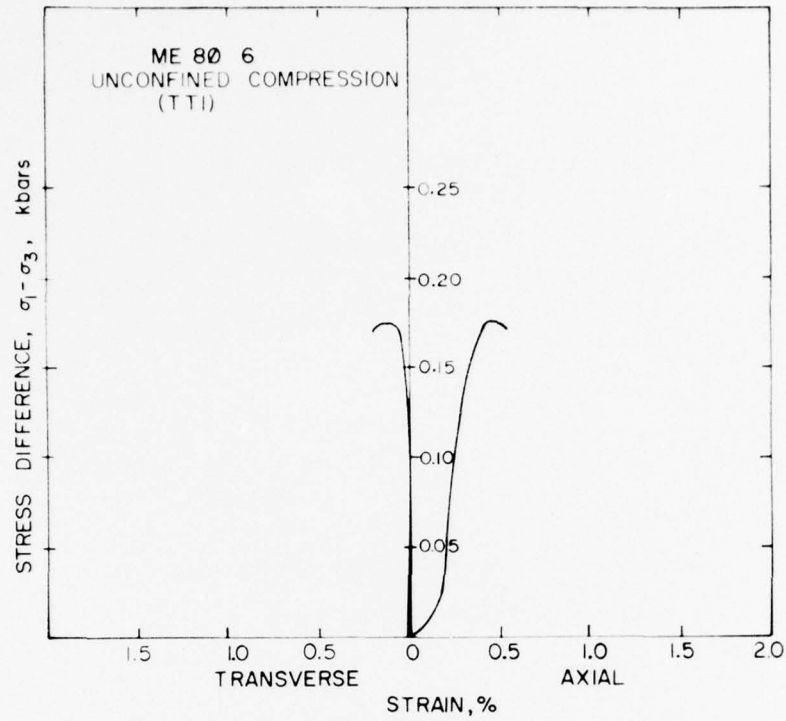


Figure B10. Unconfined Compression Results on ME806 Grout Samples (TTI).

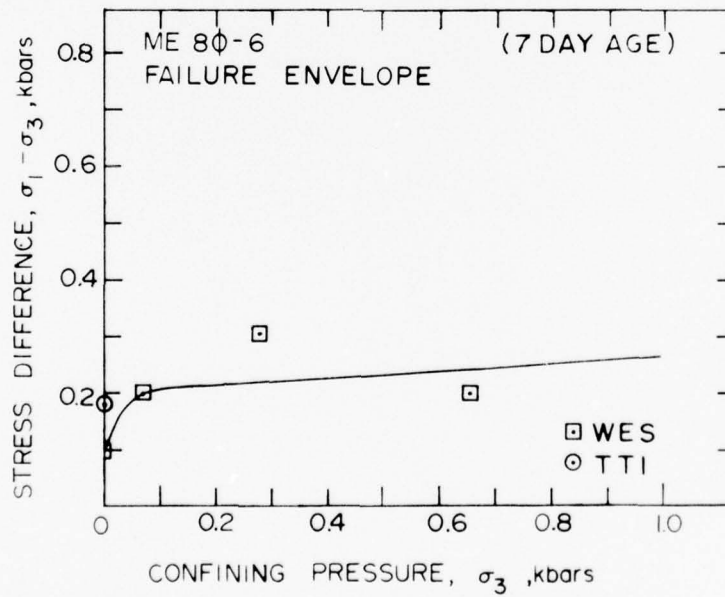


Figure B11. Failure Data on ME806 Grout Samples (WES and TTI).

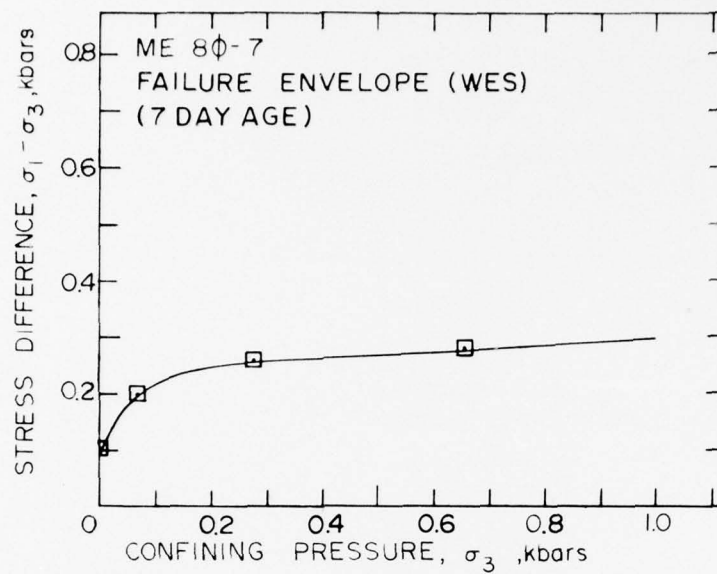


Figure B12. Failure Data on ME807 Grout Samples (WES).

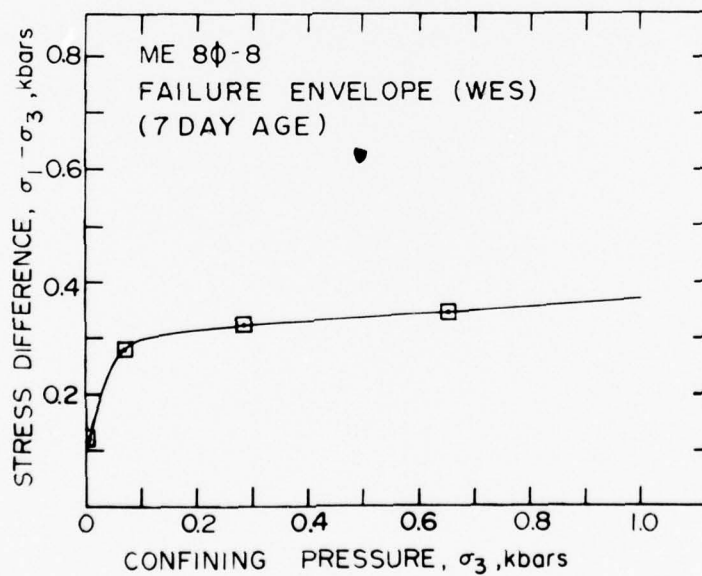


Figure B13. Failure Data on ME808 Grout Samples (WES).

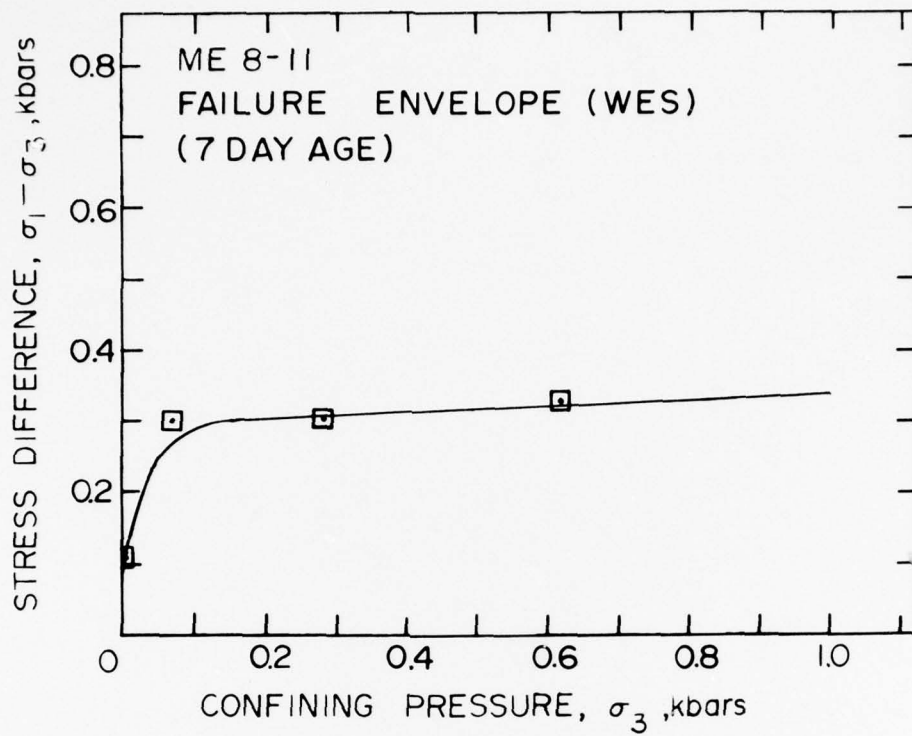


Figure B14. Failure Data on ME8-11 Grout Samples (WES).

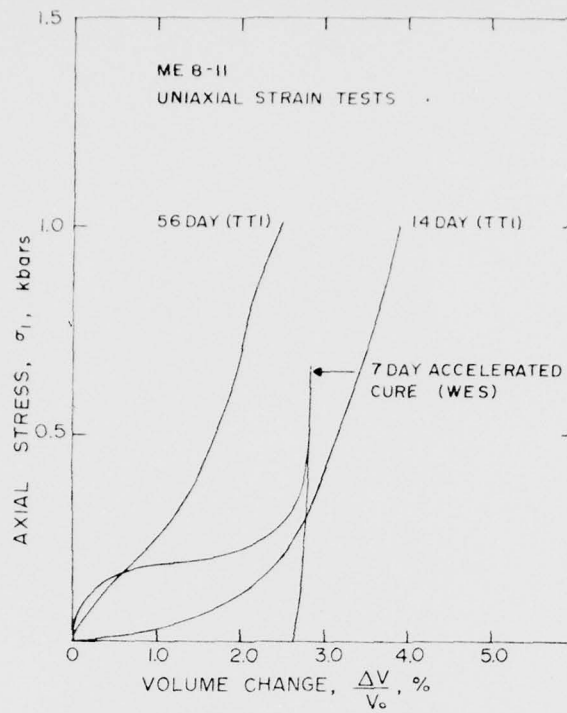


Figure B15a. Uniaxial Strain Results on ME8-11 Grout Samples (WES and TTI).

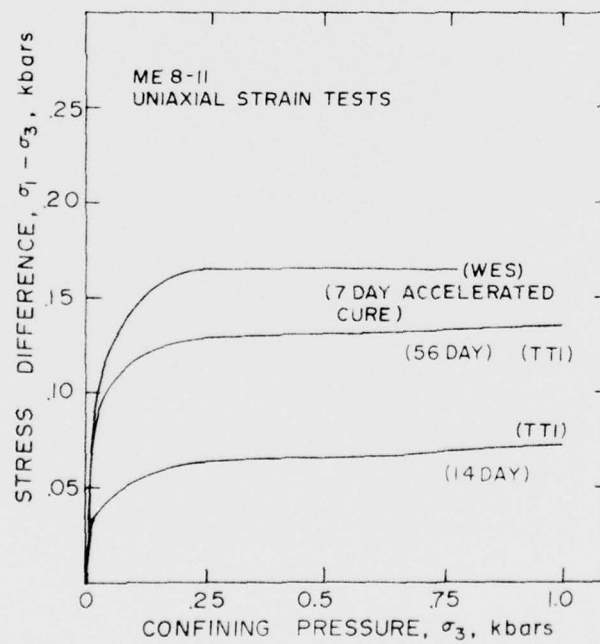


Figure B15b. Uniaxial Strain Results on ME8-11 Grout Samples (WES and TTI).

PRECEDING PAGE BLANK - ^{NOT} FILMED

PROPERTIES OF U12n.10 MH#2 AND MH#3 CORE SAMPLES

TerraTek

June 2, 1976

Mr. J. W. LaComb
Defense Nuclear Agency
Nevada Test Site
Mercury, NV 89023

Dear Joe:

Properties have been measured on core samples from U12n.10 MH#2 (90') and U12n.10 MH#3 (48', 51', 54', 57') interface drill holes. Physical properties and ultrasonic velocities were obtained on all samples while limited mechanical data was produced.

Attached are photographs showing the tuff sample from MH#3 at 48 feet, a combination tuff and rubble at 51 and 54 feet and a more competent paleozoic material at 57 feet. The MH#2 90 foot sample shown appears to be from the same region of the interface as the MH#3 51 and 54 foot samples.

The table following the photographs lists the physical properties and ultrasonic velocities of the samples. As noted by the data along a 2 inch length of the 90 foot sample, there is a considerable amount of variation in the interface region. The actual insitu physical properties would obviously require knowing the percentage of each type of material in the whole; although the material from 48' thru 57' does, in general, show higher densities, lower water contents and higher ultrasonic velocities than the Mighty Epic tunnel bed tuff.

Triaxial compression tests were conducted, with limited success, at confining pressures of 0.1 and 0.5 KB. The attached data indicates that the tuff sample (48') showed only slightly higher shear strength than the average tunnel bed tuff while the sample at 51 foot showed a shear strength within the lower bound of the tunnel bed tuff. Two tests were conducted on the 54 foot sample, both at a confining pressure of 0.5 kilobars, to determine the effect of the inhomogeneities in the material. One sample contained a number of rubble fragments on the order of 1 to 3 centimeters in diameter while the other sample contained fragments no greater than 1 centimeter in diameter. The former sample produced a maximum failure stress of 0.25 kilobars while the latter sample produced a maximum failure stress of 1.07 kilobars. This amount of variation is not at all unreasonable for the type of sample being tested. The 57 foot sample produced a maximum failure stress of 1.04 kilobars which would have, in all probability, been much higher had it not failed along the bedding plane shown in the earlier photograph. The 90 foot sample from MH#2 was noticeably weaker, but again, seemed to be a result of the size and orientation of the rubble fragments in the test sample.

Mr. J. W. LaComb
June 2, 1976
page 2

Preliminary direct shear test results on MH#2 - 84', MH#3 - 47' and MH#3 - 52' indicate shear strengths of 0.117 KB, 0.133 KB and .069 KB, respectively. The normal stress was constant at 0.069 kilobars. The coefficient of sliding friction was difficult to obtain as the initial fracture was not entirely in the shearing plane and continued fracturing occurred as the displacement increased. The data suggests, however, a coefficient of sliding friction on the order of 0.6 to 0.7. Photographs of the direct shear test samples are attached.

Sincerely,

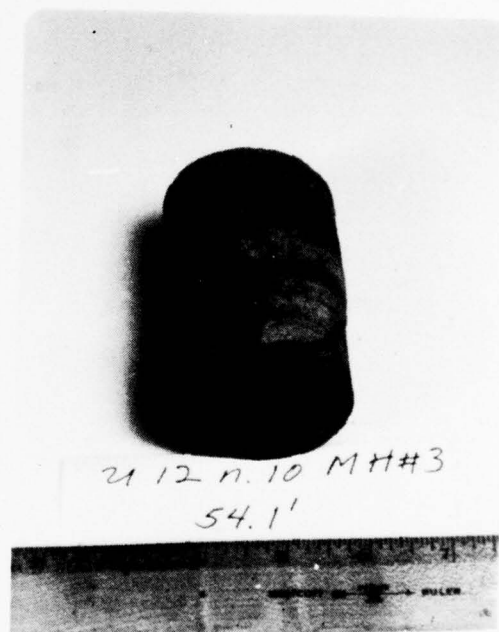


Scott W. Butters
Engineering Supervisor

SWB/jlg

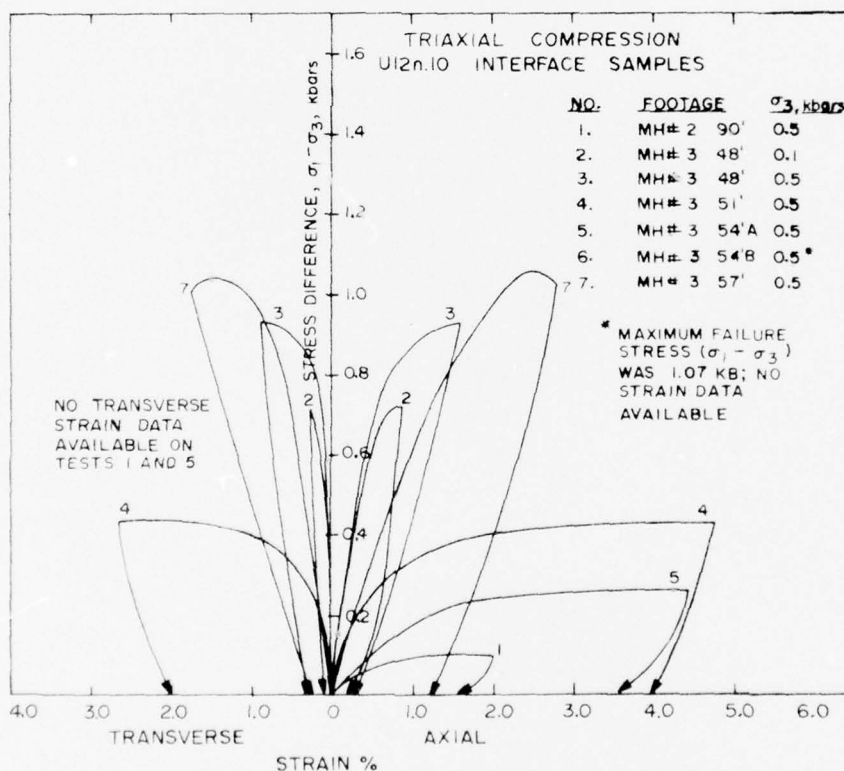
Enclosures

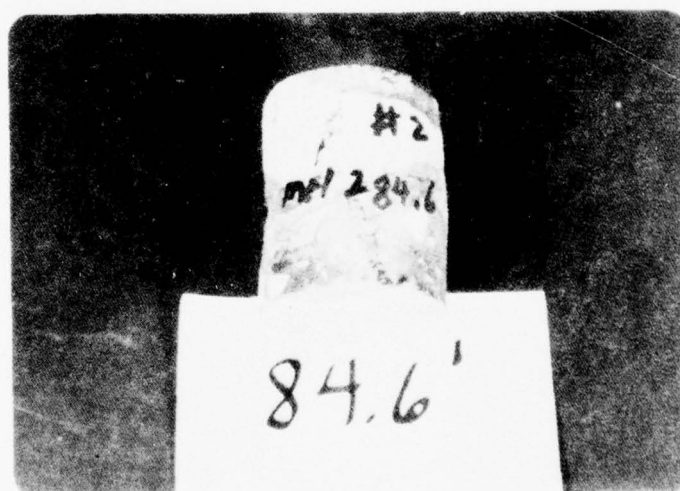
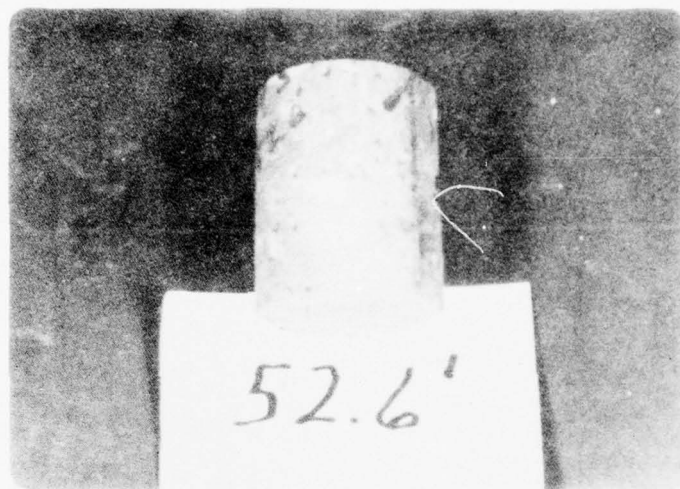
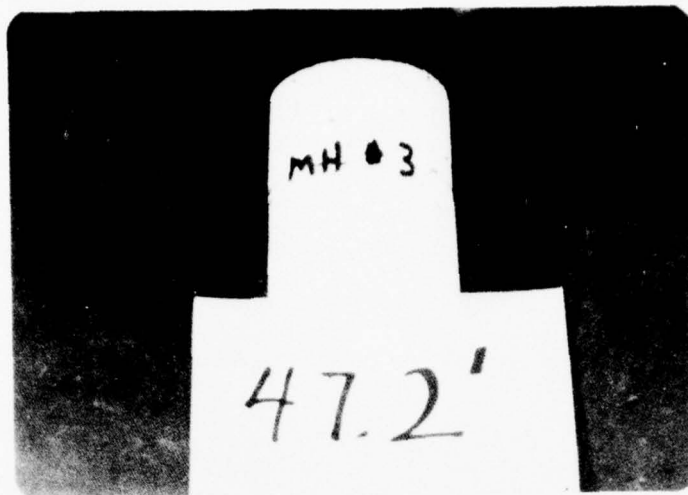
cc: Mighty Epic Distribution





DRILL HOLE FOOTAGE	DENSITY (gm/cc)			WATER BY WET WEIGHT (%)	POROSITY (%)	SATURATION (%)	CALC. AIR VOIDS (%)	MEAS. PERMANENT COMP. (%)	VELOCITY (ft/sec)	
	AS- RECEIVED	DRY	GRAIN						LONG	SHEAR
U12n.10 MH#2 90'										
Sample A	2.12	1.86	2.77	12.2	30	88	3.5	--	--	--
Sample B	2.23	1.97	2.81	11.9	33	78	7.2	--	--	--
Sample C	2.47	--	--	--	--	--	--	--	4710	2600
MH#3										
48'	2.15	1.91	2.56	11.0	25	93	1.9	--	12,420	6780
51'	2.65	2.48	3.05	6.7	19	95	0.9	--	12,840	6580
54'	2.44	2.26	2.86	7.3	21	86	3.0	--	9220	3840
57'	2.81	2.80	2.85	0.5	2	84	0.3	--	14,270	7540





TerraTek

May 17, 1976

Mr. Phil Coleman
Systems, Science & Software
P.O. Box 1620
La Jolla, CA 92037

Dear Mr. Coleman:

The following table lists the true susceptibilities as calculated from the apparent susceptibilities (Ka) for each of the footages from U12n.10 MH#2 and MH#3. The true susceptibilities were determined using Vc as the volume of powdered material, M as the mass of the material and Da as the calculated apparent density. The true susceptibility (Km) was then calculated as:

$$K_m = (D_m/D_a) \times K_a$$

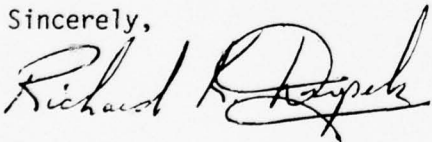
where Dm is the true material density.

TRUE SUSCEPTIBILITY DETERMINATION

Sample I.D.	As-Received Density, Dm,gm/cc	Powdered Material			Ka, 10 ⁻⁶ emu	Km, 10 ⁻⁶ emu
		Vc(cc)	M(gm)	Da,gm/cc		
MH#2 52.5'	1.61	93.0	97.9	1.05	285	437
MH#2 82.4'	2.11	90.5	111.5	1.23	576	988
MH#2 95.3'	2.65	90.0	143.6	1.60	412	682
MH#2 128.2'	2.64	92.0	144.0	1.57	605	1017
MH#3 42.2'	1.73	47.0	49.9	1.06	114	186
MH#3 56.4'	2.16	92.5	127.9	1.38	343	537
MH#3 65.55'	2.80	87.0	125.3	1.44	106	206
MH#3 80.0'	2.82	93.0	130.3	1.40	166	334

Enclosed are copies of the susceptibility procedures and the susceptibility machine description.

Sincerely,



Richard K. Dropek
Research Engineer

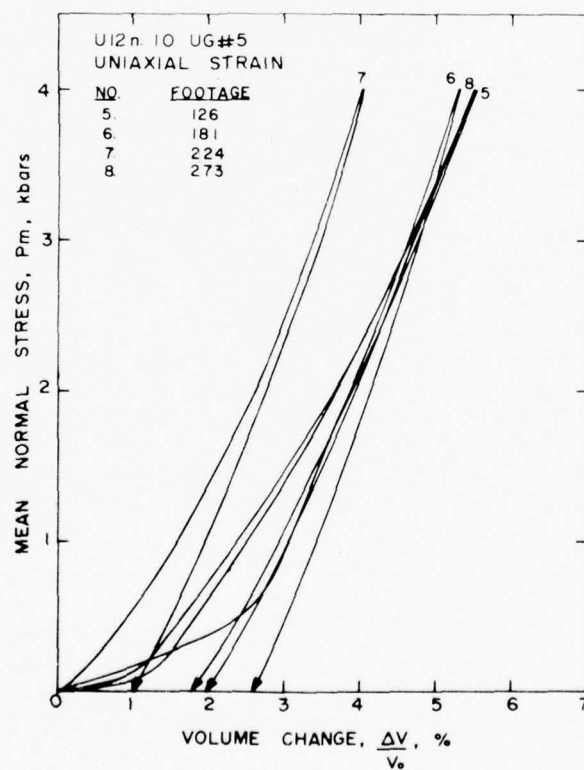
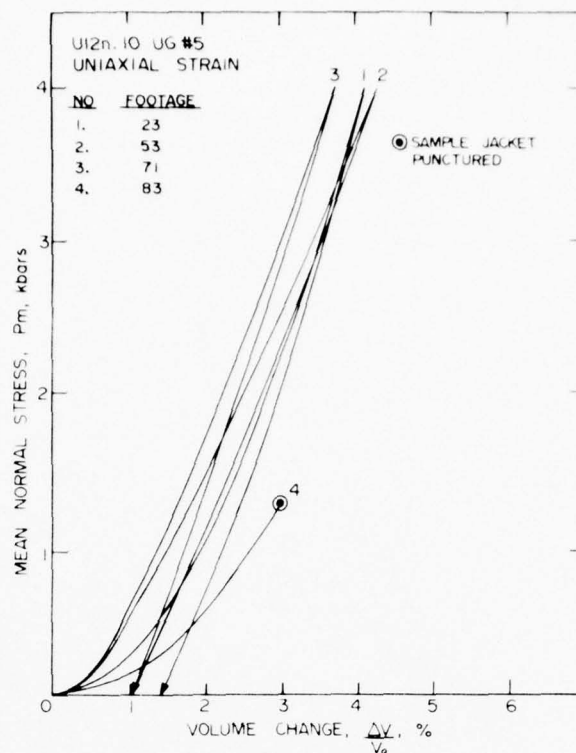
RDK/jlg

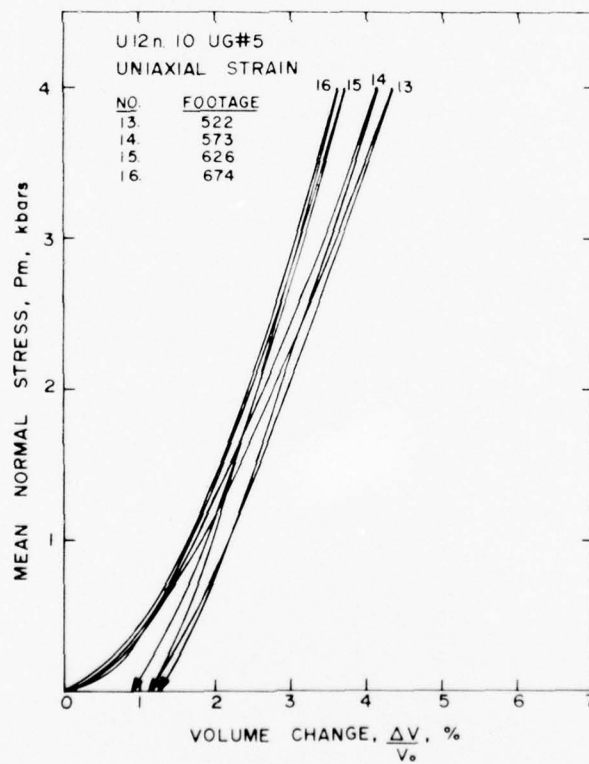
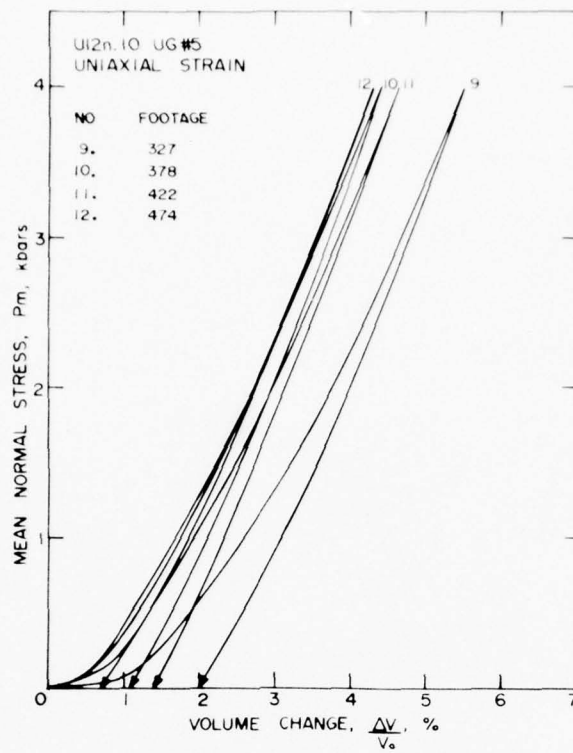
Enclosures

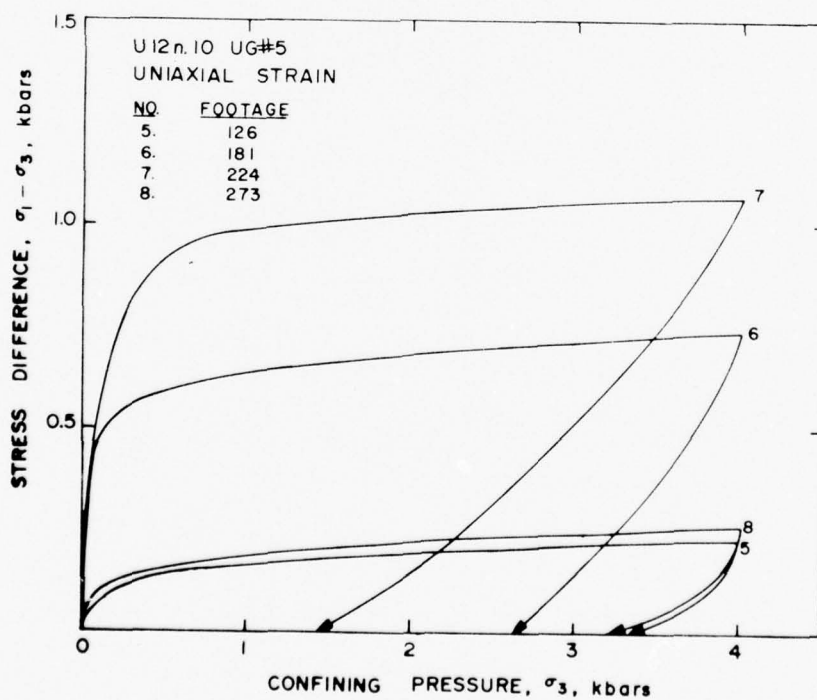
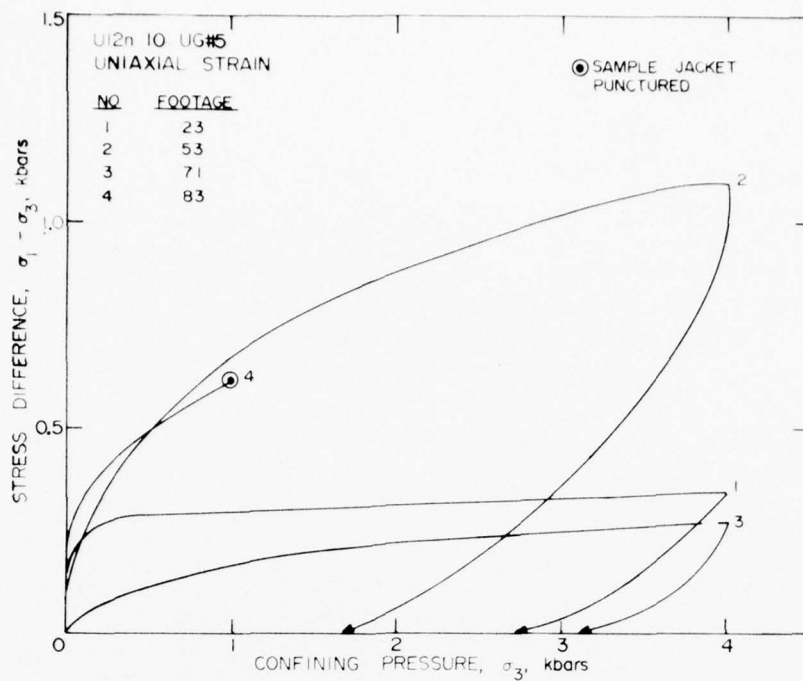
cc: Joe LaComb
Scott Butters

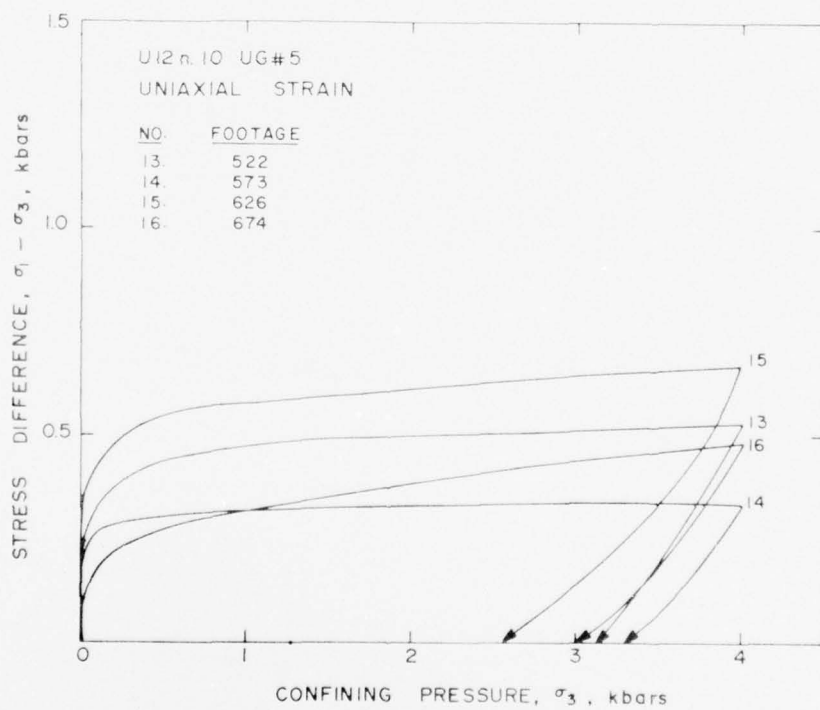
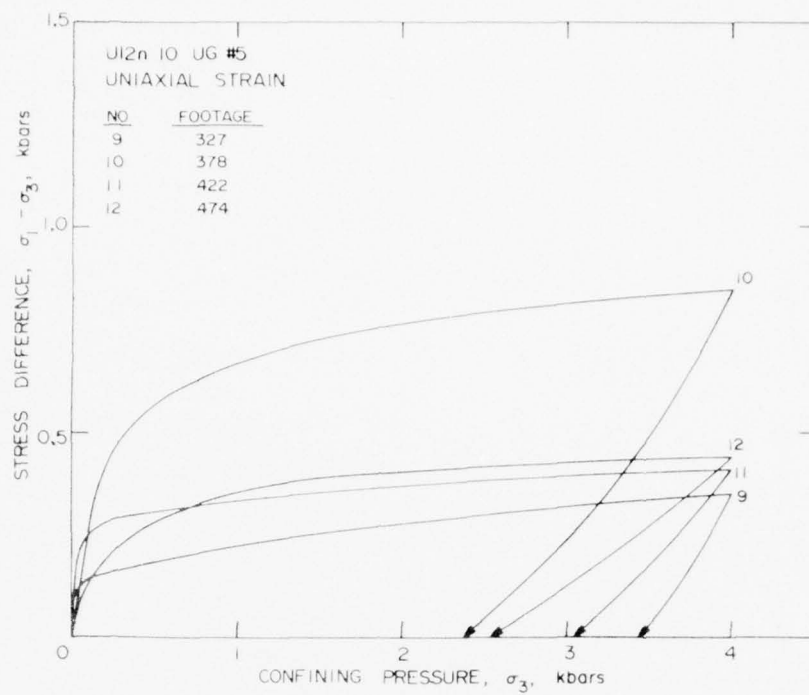
MISCELLANEOUS MIGHTY EPIC PROPERTIES

DRILL DIST. FROM COLLAR	HOLE DIST. FROM W.P.	DENSITY (gm/cc)			WATER BY WET WEIGHT (%)	POROSITY (%)	SATURATION (%)	CALC. AIR VOIDS (%)	MEAS. PERMANENT COMP. (%)	VELOCITY (ft/sec)	
		AS- RECEIVED	DRY	GRAIN						LONG	SHEAR
U12n 10	UG#5										
23'		1.86	1.53	2.42	17.6	37	89	3.9	1.4	9,440	4,450
53'		1.92	1.59	2.40	17.4	34	98	0.4	1.0	10,240	5,010
71'		1.94	1.62	2.48	16.7	35	94	2.1	1.0	10,830	5,550
83'		1.91	1.63	2.40	15.0	32	89	3.6		10,030	4,980
126'		1.95	1.66	2.41	14.8	31	93	2.2	1.8	8,740	3,380
181'		2.04	1.80	2.42	11.4	26	91	2.3	2.6	12,550	6,270
224'		1.82	1.52	2.26	16.6	33	93	2.4	1.0	11,800	5,850
273'		1.95	1.65	2.41	15.1	32	93	2.2	2.0	8,380	4,050
327'		1.88	1.52	2.43	19.3	37	97	1.2	2.0	9,740	5,020
378'		1.93	1.61	2.40	16.5	33	97	1.1	1.1	10,540	5,780
422'		1.94	1.61	2.51	17.4	36	94	2.1	1.4	10,020	4,650
474'		1.95	1.63	2.46	16.6	34	96	1.4	0.7	9,350	4,610
522'		2.00	1.69	2.50	15.9	33	97	0.8	1.1	10,430	5,360
573'		1.98	1.66	2.59	15.9	35	91	3.1	1.3	11,000	5,490
626'		1.98	1.67	2.55	15.6	34	90	3.5	1.1	12,600	6,380
674'		2.137	1.87	2.59	12.8	28	97	0.8	0.9	10,780	5,050









March 30, 1976

Mr. J. W. LaComb
Defense Nuclear Agency
Nevada Test Site
Mercury, NV 89023

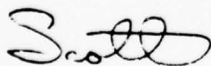
Dear Joe:

We have completed the triaxial compression tests on the U12n.10 ISS drill hole samples. The apparent Young's Moduli and Poisson's ratios have been scaled from the slopes of the stress-strain curves and are listed in the attached table. The individual stress-strain curves and the physical properties are also attached.

The data indicates a consistent increase in the Young's Moduli with increasing confining pressure. The Poisson's ratios listed for the unconfined compression tests ($\sigma_3 = 0$) were obtained by using the "linear portion" of the stress difference-axial strain curve. The "foot" that was not scaled on these curves would have produced much lower Poisson's ratios -- on the order of 0.05 to 0.10. The Poisson's ratios at the two confining pressure levels appear consistently between 0.20 and 0.25 regardless of the value of Young's Moduli.

Please call if you have any questions concerning the data.

Sincerely,



Scott W. Butters
Engineering Supervisor

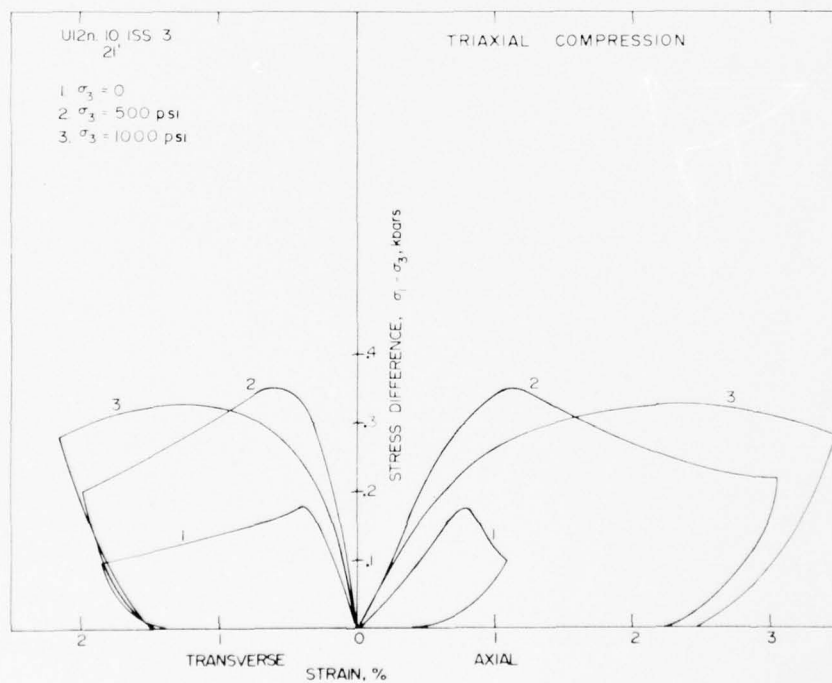
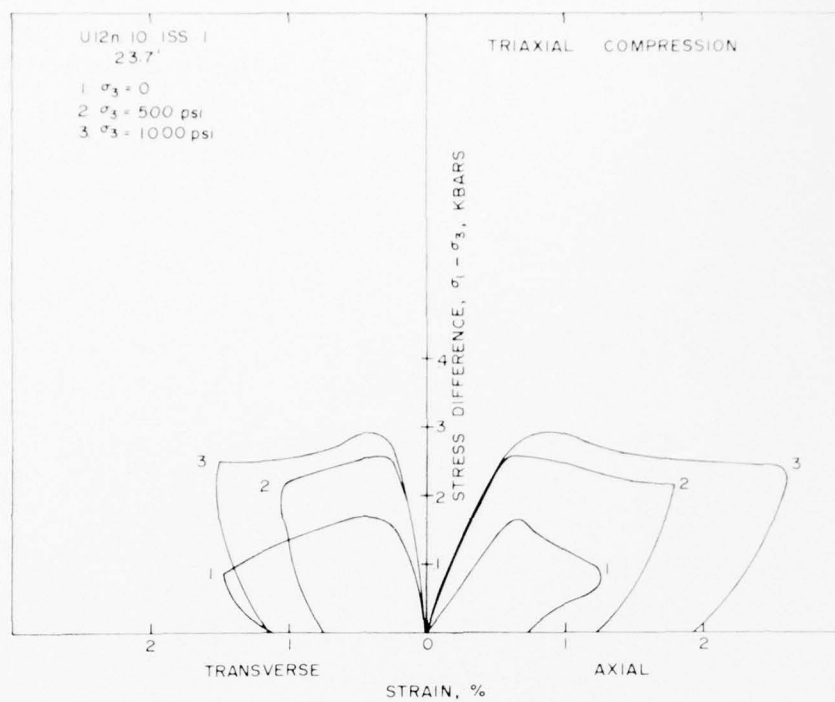
SWB/jlg

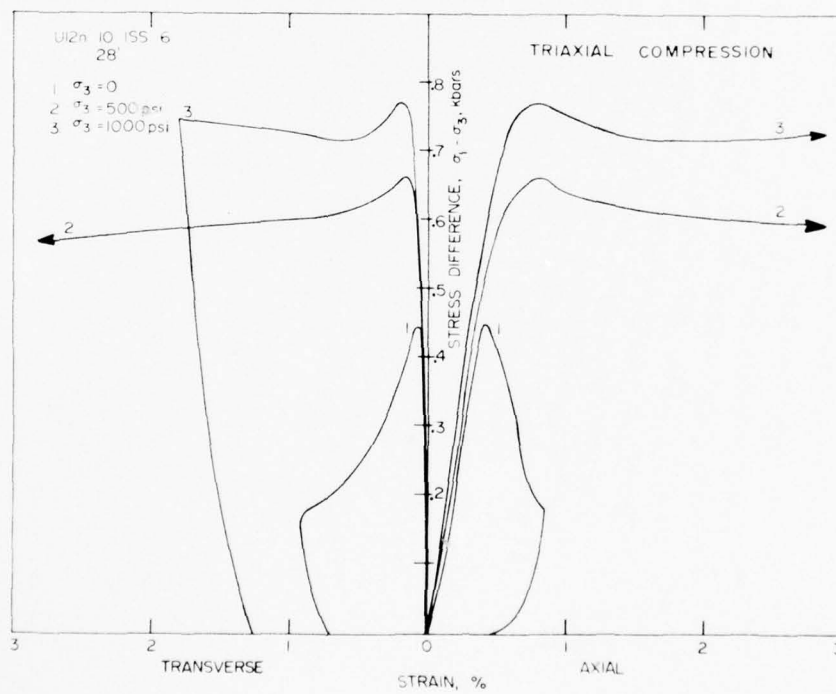
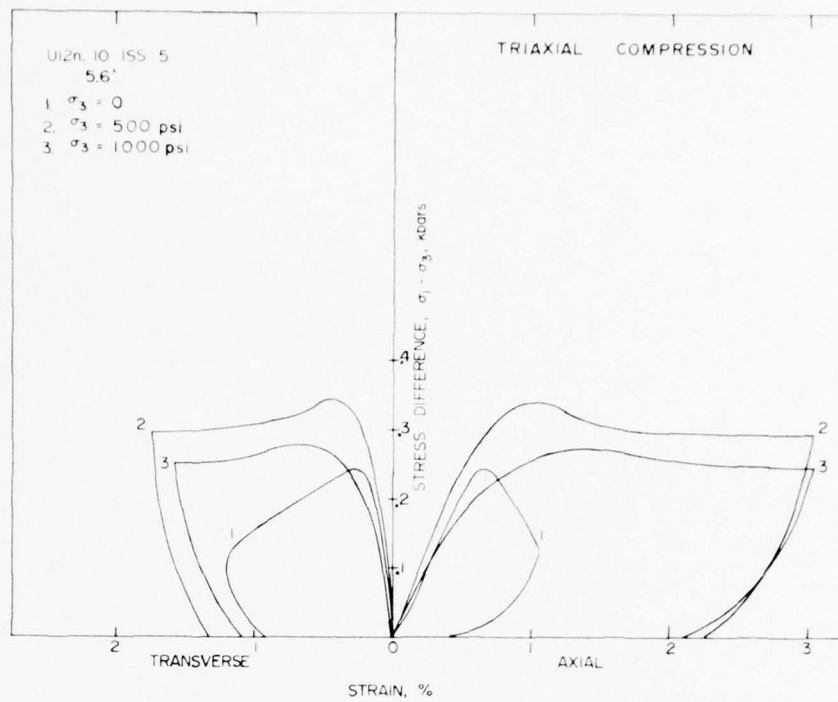
Enclosures

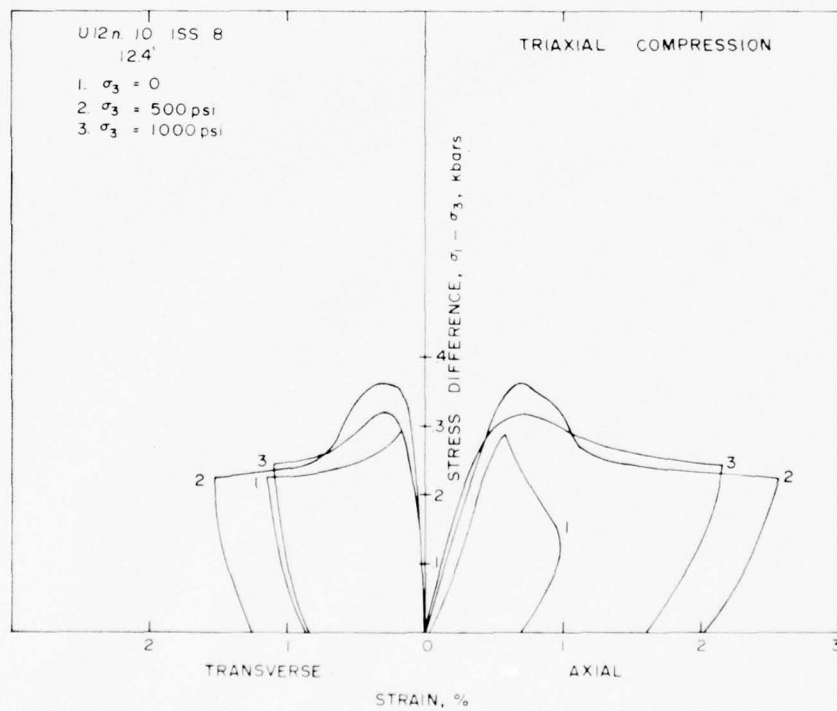
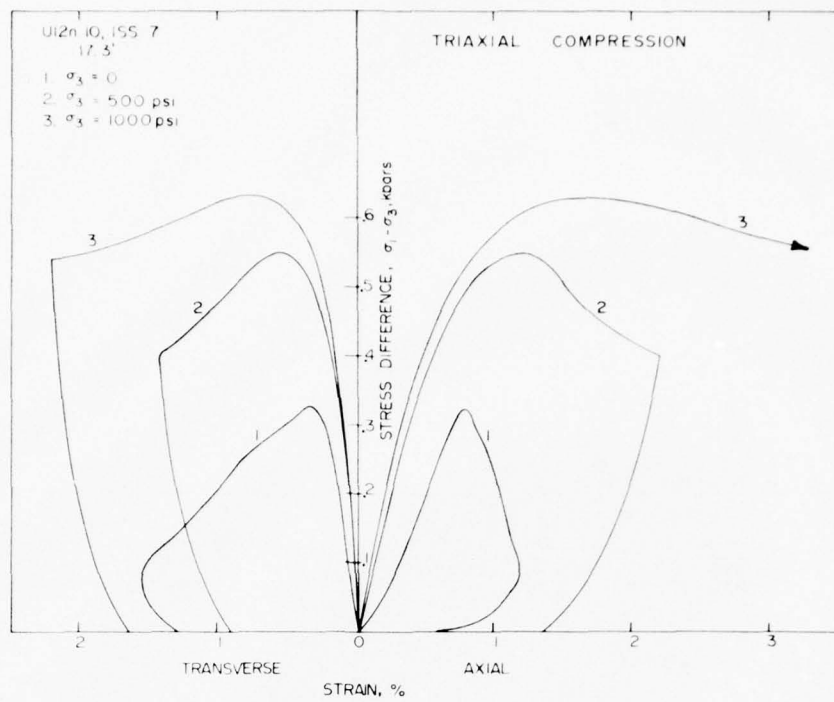
cc: Bill Ellis, USGS

ELASTIC MODULI FROM
TRIAXIAL COMPRESSION TESTS

SAMPLE	CONFINING PRESSURE σ_3 , BARS	YOUNG'S MODULUS E, KB	POISSON'S RATIO ν
U12n.10 ISS#1 23'	0	28	0.32
	34	48	0.24
	69	49	0.24
U12n.10 ISS#3 21'	0	27	0.40
	34	44	0.27
	69	37	0.23
U12n.10 ISS#5 5'	0	47	0.26
	34	54	0.22
	69	42	0.25
U12n.10 ISS#6 28'	0	130	0.25
	34	150	0.23
	69	160	0.23
U12n.10 ISS#7 17'	0	54	0.32
	34	75	0.22
	69	95	0.23
U12n.10 ISS#8 12'	0	64	0.15
	34	70	0.20
	69	80	0.23







DRILL DIST FROM COLLAR	HOLE DIST FROM W.P.	DENSITY (gm/cc)			WATER BY WET WEIGHT (%)	POROSITY (%)	SATURATION (%)	CALC AIR VOIDS (%)	MEAS PERMANENT COMP (%)	VELOCITY (ft/sec)	
		AS RECEIVED	DRY	GRAIN						LONG	SHEAR
U12n, 10											
ISS#1 23.7'		1.89	1.53	2.41	18.8	37	97	1.0		10,460	5,290
ISS#3 27.0'		2.00	1.70	2.45	14.7	30	96	1.0		10,800	5,140
ISS#5 5.6'		1.95	1.65	2.37	15.2	30	98	0.3		10,540	5,180
ISS#6 28.4'		1.88	1.50	2.42	20.2	38	99	0.1		10,040	4,980
ISS#7 17.3'		2.01	1.72	2.51	14.7	32	94	2.1		9,590	4,330
ISS#8 12.4'		1.95	1.63	2.49	16.6	35	93	2.6		9,680	4,710

MING BLADE EVENT

Miscellaneous Core Sample Properties

Investigation of the Effect of Fracturing on the Ultrasonic
Velocities in Ash-Fall Tuff

Nevada Test Site "Two-In-One Concept" Evaluation: Comparison of Preshot
and Postshot Material Properties

Determination of the Angle-of-Internal Friction
for NTS Tuffs

Water Extraction from Nevada
Test Site Tuffs

Hydrostatic Response of a Water Saturated Sand

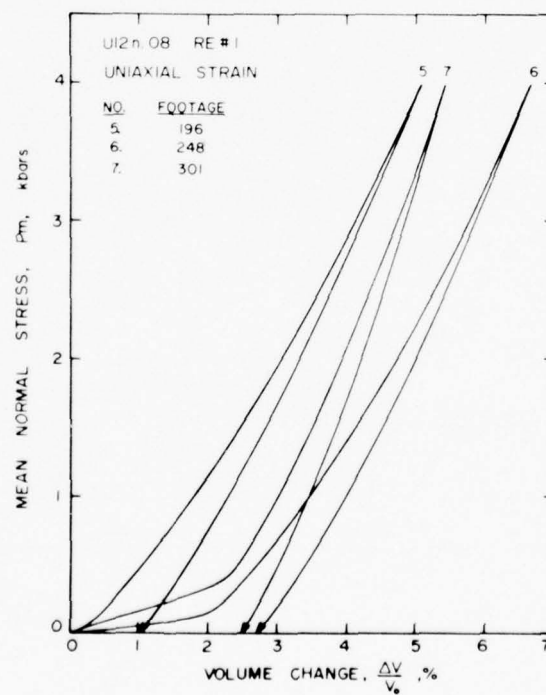
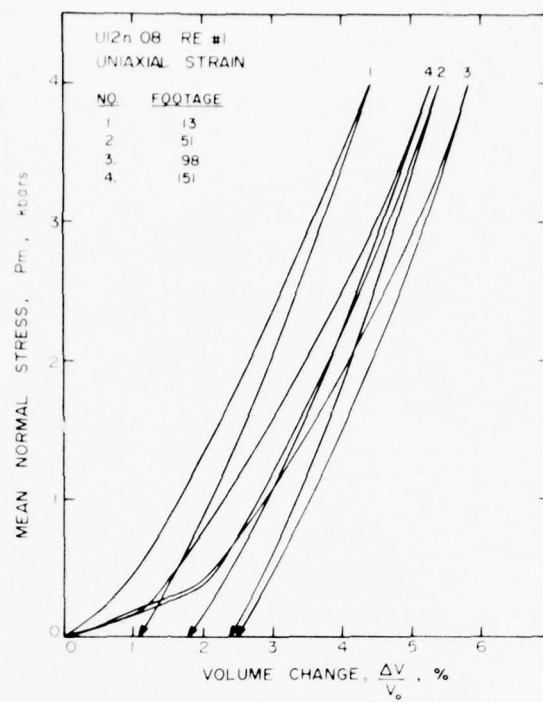
Laboratory Determination of the Elastic Modulus of
Stress-Relief Overcores

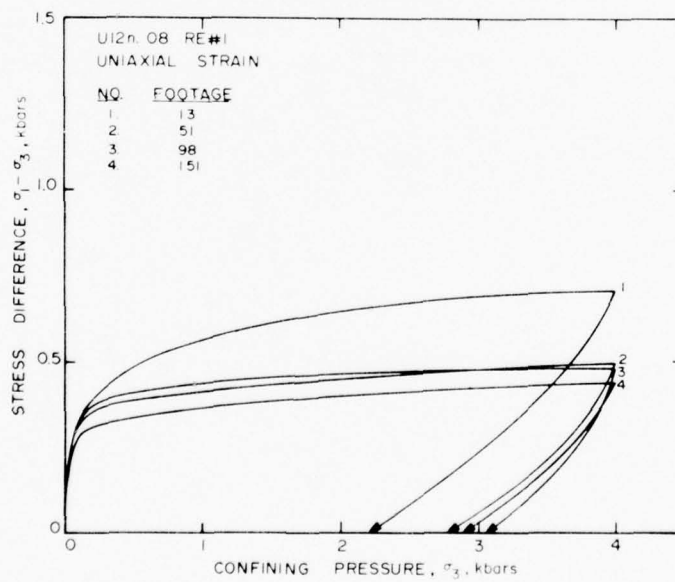
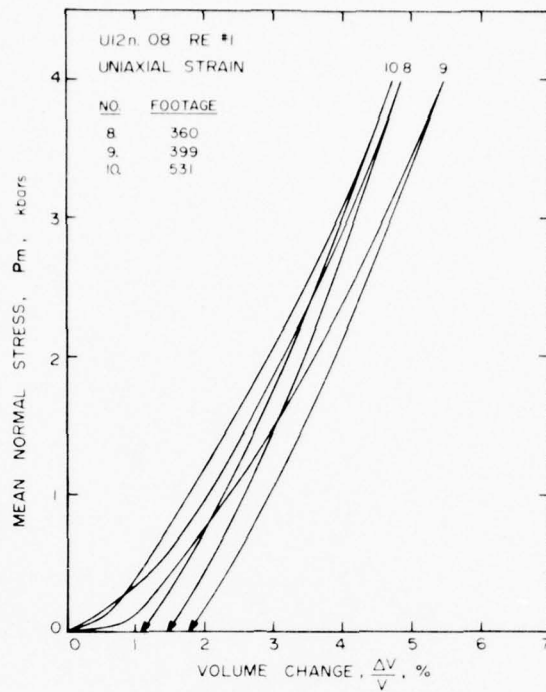
Specific Moisture Retention of Nevada
Test Site Tuffs

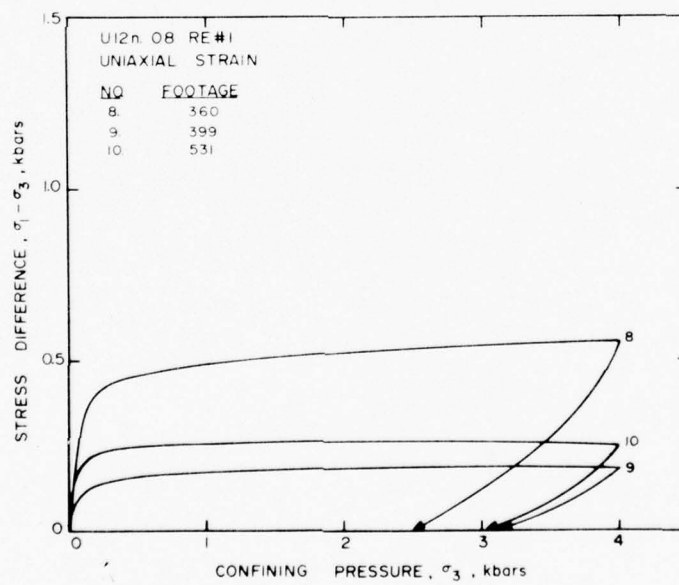
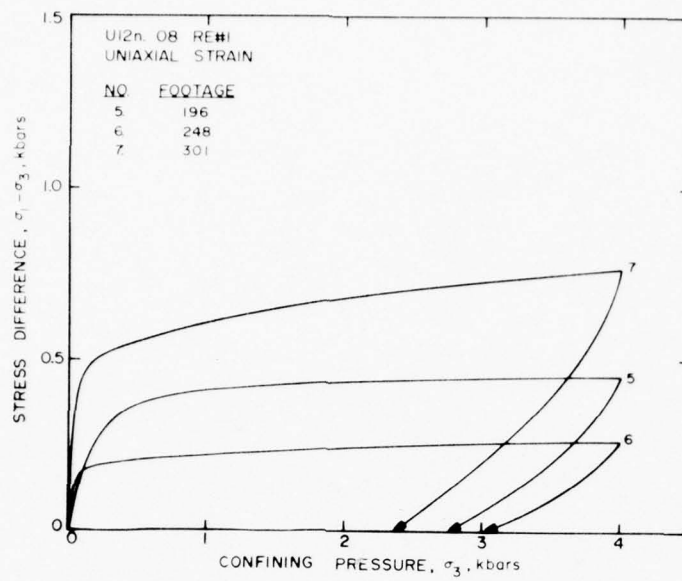
NOT
Preceding Page BLANK - FILMED

MISCELLANEOUS CORE SAMPLE PROPERTIES

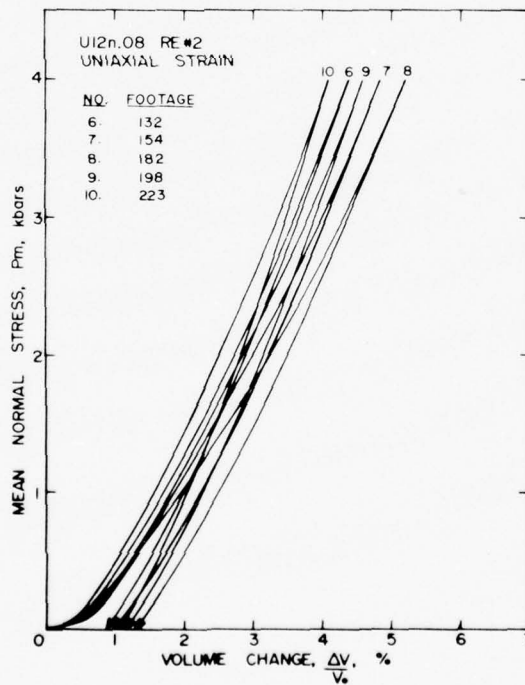
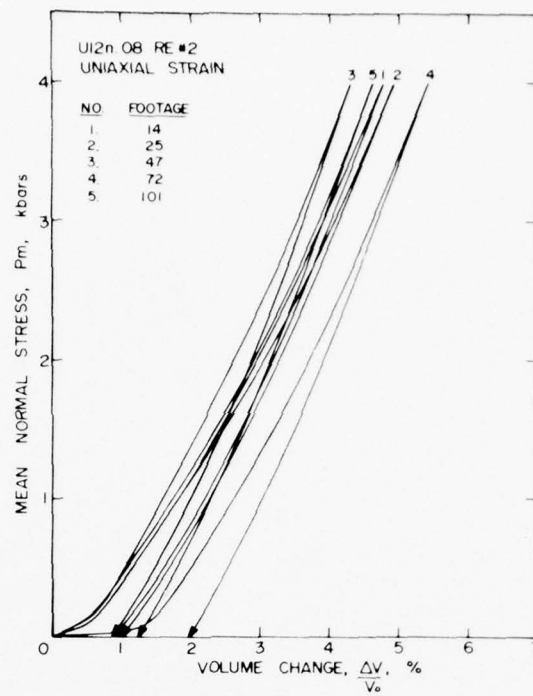
DRILL HOLE FOOTAGE	DENSITY (gm/cc)			WATER BY WET WEIGHT (%)	POROSITY (%)	SATURATION (%)	CALC. AIR VOIDS (%)	MEAS. PERMANENT COMP. (%)	VELOCITY (ft/sec)	
	AS- RECEIVED	DRY	GRAIN						LONG	SHEAR
U12n.08 RE #1										
13	1.90	1.57	2.40	17.1	34	95	1.8	1.1	12106	6696
27	1.80	1.41	2.40	21.8	41	95	2.2		8711	3681
51	1.96	1.65	2.47	16.1	33	95	1.8	2.4	10646	4993
75	1.85	1.46	2.44	21.1	40	97	1.1		9665	4829
98	1.85	1.46	2.46	21.2	41	96	1.5	2.5	9259	4541
123	1.71	1.27	2.36	25.9	46	96	2.1		9636	4288
151	1.90	1.51	2.48	20.4	39	99	0.4	1.8	9698	4403
174	1.82	1.43	2.50	21.3	43	91	3.4		8786	3760
196	1.79	1.36	2.43	24.2	44	99	0.5	1.0	8990	4420
223	1.86	1.50	2.44	19.8	39	95	1.8		10338	5292
248	1.77	1.37	2.39	22.6	42	94	2.5	2.7	9160	3976
272	1.75	1.36	2.47	22.6	45	87	5.6		7208	2930
301	1.88	1.50	2.46	20.3	39	98	0.8	2.5	12536	6969
326	1.82	1.46	2.44	19.5	40	89	4.4		7956	3179
360	1.94	1.63	2.40	16.3	32	98	0.7	1.5	10633	5433
378	2.05	1.84	2.37	10.3	23	94	1.4		12595	6975
399	1.90	1.49	2.52	21.4	41	99	0.4	1.8	8304	3481
414	2.05	1.83	2.38	11.0	23	96	1.2		11880	7011
531	1.90	1.54	2.48	18.9	38	95	1.9	1.1	9715	4679

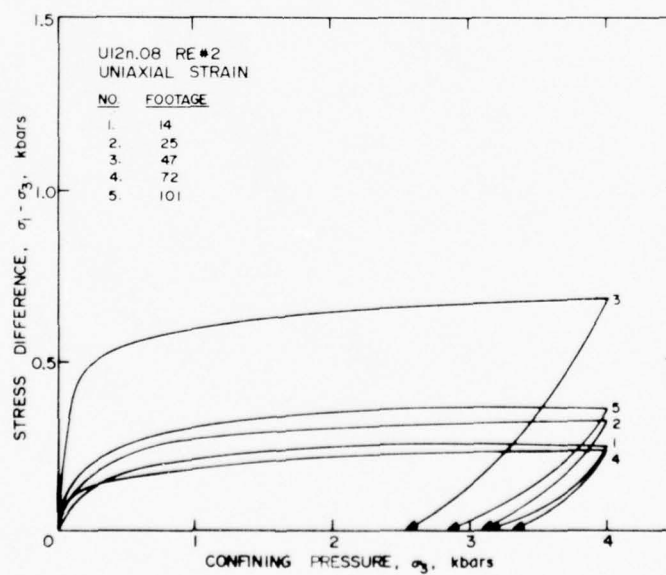
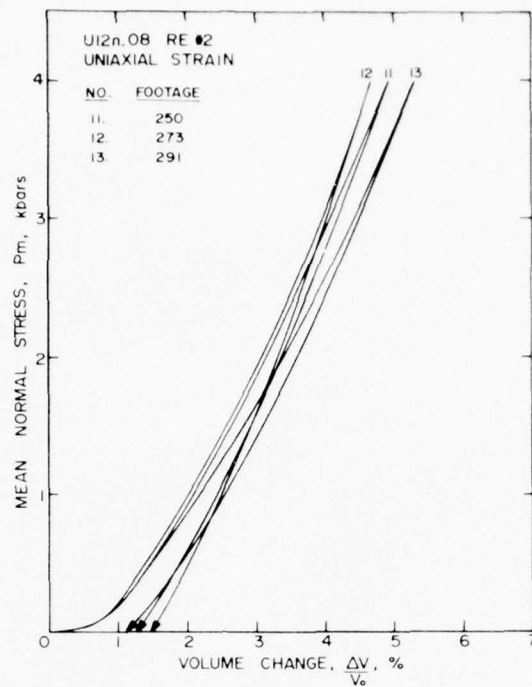


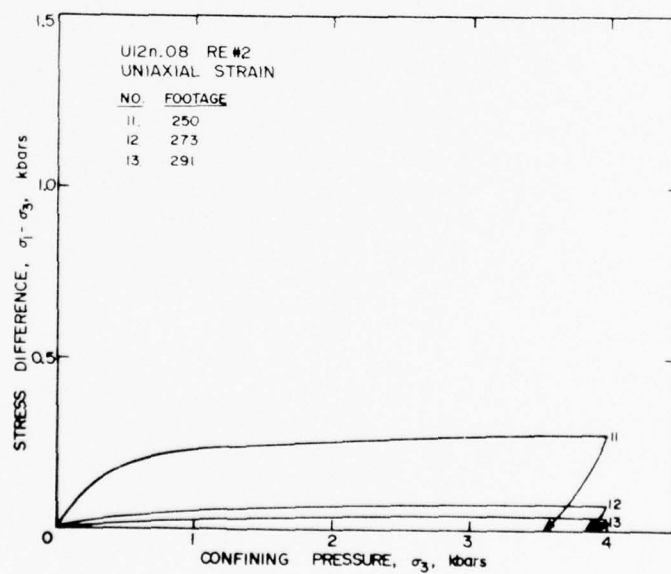
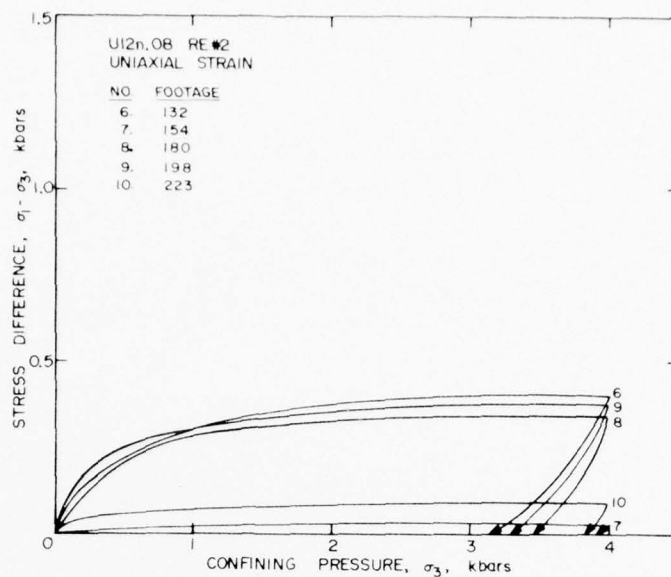




DRILL HOLE FOOTAGE	DENSITY (gm/cc)			WATER BY WET WEIGHT (%)	POROSITY (%)	SATURATION (%)	CALC. AIR VOIDS (%)	MEAS. PERMANENT COMP. (%)	VELOCITY (ft/sec)	
	AS- RECEIVED	DRY	GRAIN						LONG	SHEAR
U12n.08 RE #2										
14	1.88	1.52	2.43	19.4	38	97	1.3	0.9	8123	3130
25	1.92	1.57	2.42	18.1	35	99	0.4	1.0	9406	3760
47	1.96	1.66	2.43	15.7	32	97	0.9	0.9	10476	5233
72	1.92	1.57	2.47	18.3	37	96	1.3	2.0	8734	5610
101	1.96	1.61	2.55	17.6	37	94	2.2	1.3	8445	3201
132	1.95	1.62	2.46	16.9	34	96	1.1	0.9	8422	3520
154	1.83	1.44	2.49	21.3	42	93	3.0	1.0		
180	1.86	1.48	2.44	20.2	39	96	1.6	1.3	7861	2920
198	1.88	1.48	2.54	21.6	42	97	1.2	1.2	8694	5748
223	1.92	1.56	2.45	18.9	36	99	0.3	1.1	8189	4688
250	1.87	1.51	2.45	19.0	38	92	2.9	1.3	7713	4206
273	1.85	1.47	2.44	20.8	40	97	1.4	1.5	3717	1841
291	1.87	1.52	2.46	18.8	38	92	2.9	1.1	6529	3688







NOT
Preceding Page BLANK - FILMED

INVESTIGATION OF THE EFFECT OF FRACTURING
ON THE ULTRASONIC VELOCITIES IN ASH-FALL TUFF

by

R. Lingle
R. S. Rosso
L. M. Buchholdt

May 1975

Terra Tek, Inc.
University Research Park
420 Wakara Way
Salt Lake City, Utah 84108

TR 75-20

SUMMARY

The effect of fracturing on ultrasonic velocities in rock have been investigated. The material was an ash-fall tuff taken from the Nevada Test Site, Area 12. Fractures were generated in uniaxial load (compression) tests and direct shear tests. Both test techniques are described, as well as the means of determining the ultrasonic velocities. The results, in general, show the same trend as reported in other types of rock; i.e., a decrease in both the P-wave (longitudinal) and S-wave (shear) velocities resulting from fracture. The maximum change observed for the P-wave was ~ 25 percent, and ~ 10 percent for the S-wave.

TABLE OF CONTENTS

	<u>Page</u>
Summary	238
List of Figures	240
List of Tables	241
Introduction	242
Sample Preparation	243
Fracture by Uniaxial Compression	245
Fracture by Direct Shear Load	249
Test Results and Conclusions	252
References	257
Appendix A	258
Appendix B	263

LIST OF FIGURES

<u>Figure Number</u>	<u>Description</u>	<u>Page</u>
1	Technique Used to Fracture Sample by Uniaxial Compression	246
2	Sample U12t.03, 924 ft, fractured by the application of an axial load	247
3	Velocity versus Axial Load	248
4	Direct Shear Loading Technique	250
5	Direct Shear Machine	250
6	Tuff Sample in Shear Box After Being Sheared	251
7	P- and S-wave velocities vs. shear displacement, sample U12n.10 UG#1, 593 ft., $\rho=2.10 \text{ gm/cm}^3$, axial load=1000 psi (circled points are velocities measured before the application of axial load).	254
8	P- and S-wave velocities and vertical (axial) displacement vs. shear displacement, sample U12n.10 UG#1, 824 ft., $\rho=2.08 \text{ gm/cm}^3$, axial load=500 psi (circled points are velocities measured before the application of axial load).	254
9	P- and S-wave velocities and vertical (axial) displacement vs. shear displacement, sample U12n.10 UG#1, 1149 ft., $\rho=1.92 \text{ gm/cm}^3$, axial load=1000 psi (circled points are velocities measured before the application of axial load).	255
10	P- and S-wave velocities and vertical (axial) displacement vs. shear displacement, sample U12n.10 UG#1, 1276 ft., $\rho=1.85 \text{ gm/cm}^3$, axial load=1000 psi (circled points are velocities measured before the application of axial load).	255
11	P- and S-wave velocities vs. shear displacement, sample U12t.03 UG#3, 958 ft., $\rho=1.86 \text{ gm/cm}^3$, axial load=1000 psi (circled points are velocities measured before the application of axial load).	256
12	P- and S-wave velocities vs. shear displacement, sample U12t.03 UG#3, 1067 ft., $\rho=1.77 \text{ gm/cm}^3$, axial load=1000 psi (circled points are velocities measured before the application of axial load).	256

LIST OF FIGURES (CONT'D)

<u>Figure Number</u>	<u>Description</u>	<u>Page</u>
A1	Through Transmission System	261
A2	Equipment Used to Make Ultrasonic Velocity Measurements	262
A3	Oscilloscope display showing the comparison wave and the signal through a specimen in the lower trace and the comparison wave and the initial signal in the upper trace.	262

LIST OF TABLES

<u>Table Number</u>	<u>Description</u>	
I	Physical Properties	244

INTRODUCTION

The effect of fractures on the ultrasonic velocities in a variety of rocks has been studied. For example, Gupta (1973) performed P-wave (longitudinal) and S-wave (shear) velocity measurements on Indiana limestone; Matsushima (1960) measured the P-wave velocity on Kitashirakawa biotite granite as it was being fractured; and Peselnick, et al. (1975) reported the change in the P-wave velocity in powdered granite as it was being sheared. These results all showed the same trend: a decrease in velocity in the fractured material.

The objective of this study was to determine the effects of fracture on the acoustic velocities in ash-fall tuff to explain the reduction in seismic velocities with time noted in the pillars at underground locations. The samples were obtained from cores from Area 12 at the Nevada Test Site. Fractures were generated in the samples by uniaxial (compression) loading and direct shearing. Both test techniques are discussed in this report. The results obtained on the ash-fall tuff show the same general decrease in velocities with fracture as reported in other rocks.

The method of measuring the velocities is presented in Appendix A. Both the P-wave and S-wave velocities were measured during the direct shear test; only the P-wave velocity was obtained in the uniaxial load test. When both P-wave and S-wave velocities are obtained, the elastic moduli and Poisson's ratio can be calculated. A computer print-out of these moduli is included in Appendix B.

SAMPLE PREPARATION

The ash-fall tuff samples were all nominally 1 7/8 inch diameter cores taken from Area 12. They were saw-cut to length and the ends ground parallel to within two-thousandths of an inch. The compression test sample was 4 inches long; those used in the shear test were approximately 2 1/4 inches long. Samples with a variety of bulk densities were selected for the direct shear test. All samples were maintained in the as-received saturated condition. The physical properties of the material used in all tests are listed in Table I.

TABLE I
PHYSICAL PROPERTIES

Drill Hole	Footage	Density (gm/cc)			Porosity %	Saturation %
		As-Received	Dry	Grain		
U12n-10 UG #1	598	2.10	1.64	2.52	35	94
U12n-10 UG #1	824	2.08	1.78	2.57	31	99
U12n-10 UG #1	1149	1.95	1.65	2.45	33	96
U12n-10 UG #1	1276	1.85	1.44	2.48	42	98
U12t.03 UG #3	924	1.84	1.48	2.42	39	94
U12t.03 UG #3	958	1.86	1.48	2.38	38	99
U12t.03 UG #3	1067	1.77	1.44	2.39	40	97

FRACTURE BY UNIAXIAL COMPRESSION

The technique for determining ultrasonic velocities during uniaxial compression tests is illustrated in Figure 1. The ultrasonic transducers (500 KHz, PZT-5) are recessed in the end caps through which the load is applied. The propagation direction of the wave is parallel to the loading direction. Figure 2 shows a sample fractured by uniaxial compression. It is obvious from this photograph that the propagation path of the ultrasonic wave crosses the fracture plane at a high angle. Even though this one test showed a change in the P-wave velocity greater than 20 percent (Figure 3), this method of producing a fracture was abandoned in favor of the direct shear technique for the following reasons:

- Inability to independently control load normal to fracture.
- Inability to measure normal and shear displacements without prior knowledge of the fracture plane.
- Inability to predict azimuth of the fracture plane.

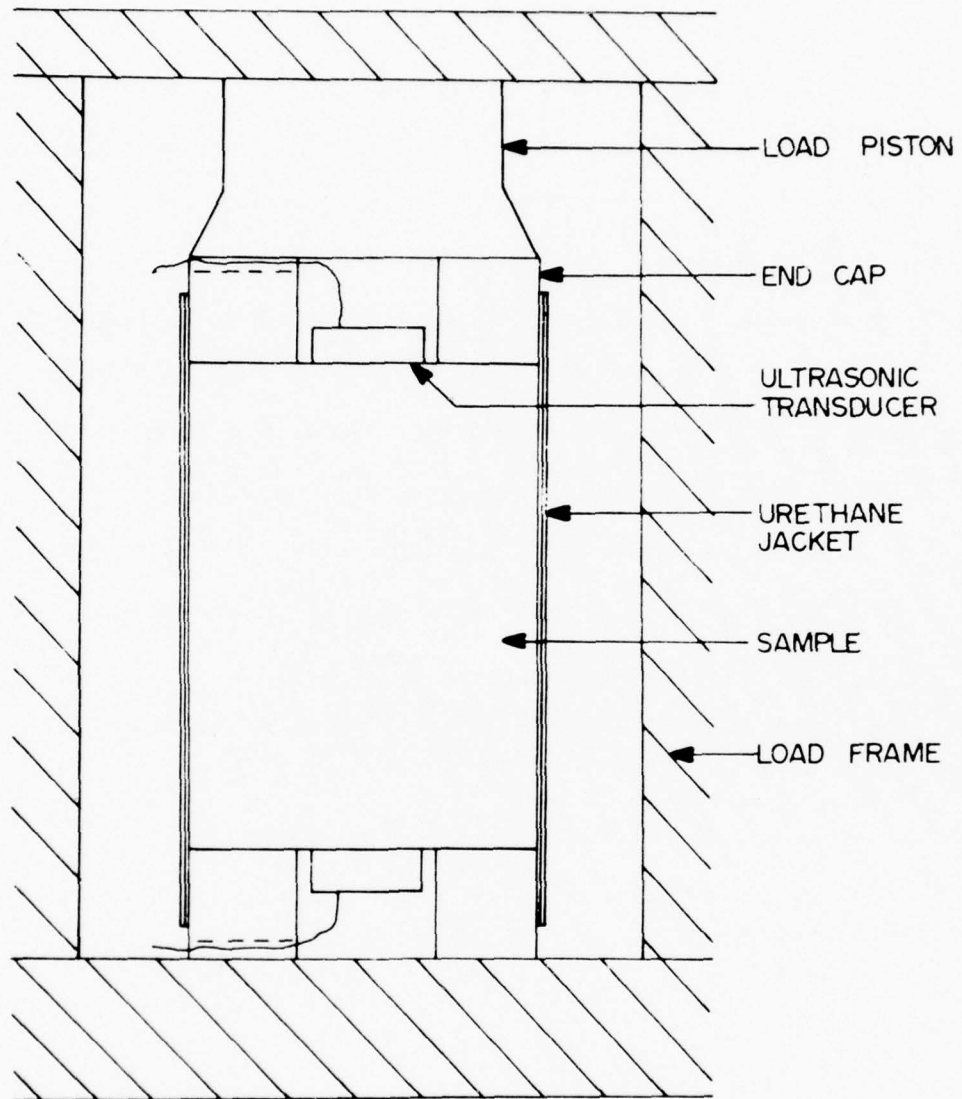


Figure 1
Technique Used to Fracture Sample by Uniaxial Compression



Figure 2

Sample U12t.03 UG #3, 924 ft, fractured by
the application of an axial load

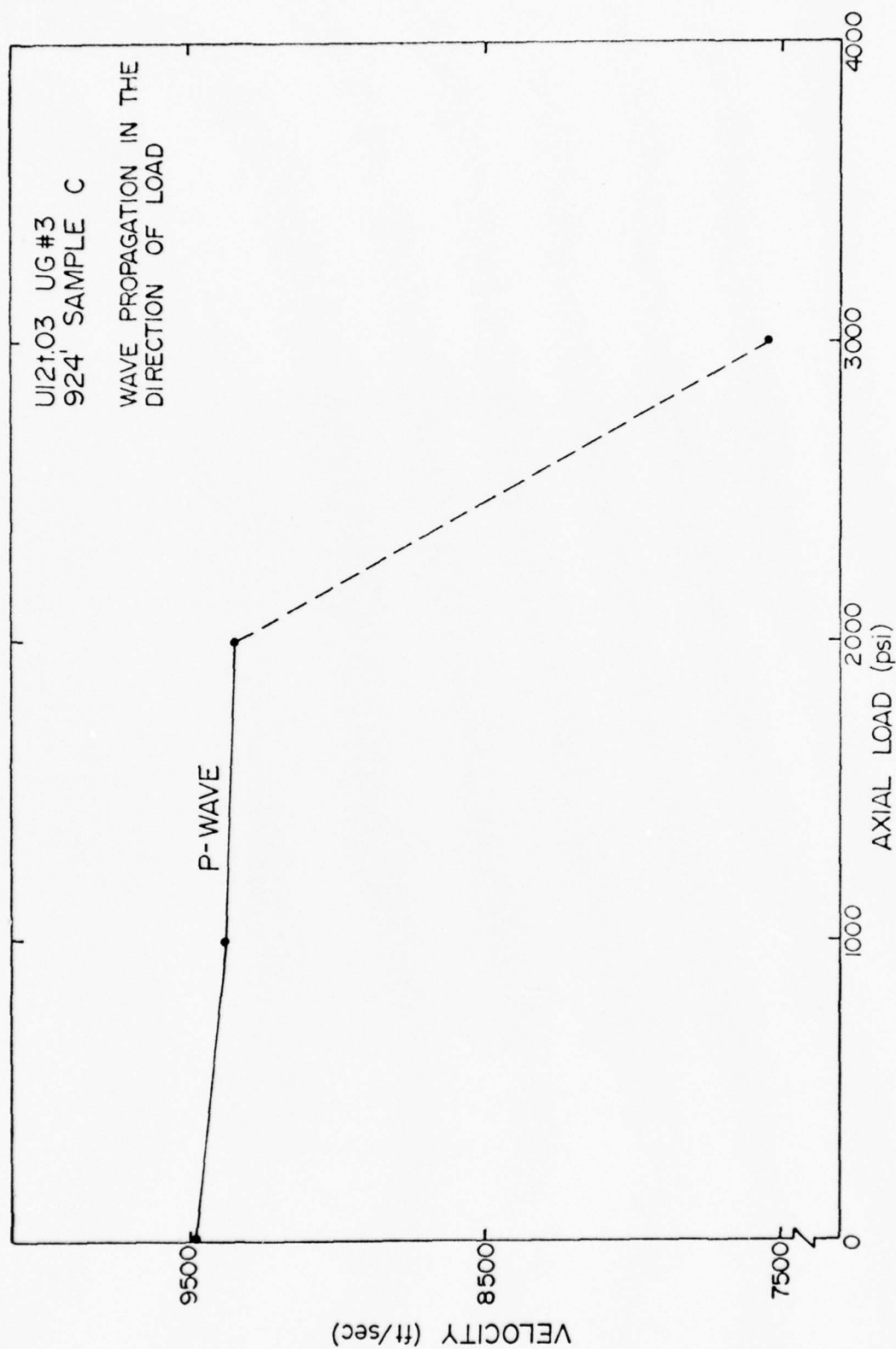


Figure 3. Velocity versus Axial Load

FRACTURE BY DIRECT SHEAR LOAD

The technique used to fracture samples by the application of a direct shear load is shown in schematic form in Figure 4. Figure 5 is a photograph of the test machine with a sample mounted in place.

The ultrasonic transducers (500 KHz, PZT-5) are bonded to the sample, one set for the P-wave and one set for the S-wave. The displacement transducer mounting rings, shown in Figure 6, are secured to the rock with epoxy glue. The sample is held in the shear boxes with hydrostone grout. The true horizontal displacement is obtained by taking the difference in the displacement of the average response for the two transducers mounted to the rings on either side of the sample. To help insure that fracture occurs in the zone between the rings, the sample is notched by a shallow saw cut around the circumference. Figure 6 shows a sample that has been sheared. The test machine shown in Figure 5 is capable of applying a normal force of 120,000 pounds and a shear force of 20,000 pounds. Both actuators are servocontrolled, with displacement feedback for the shear load and load feedback for the normal load.

All loads and displacements are recorded and stored digitally in a PDP-11 multi-user data acquisition system. Computer programs have been written to correct for transducer nonlinearities.

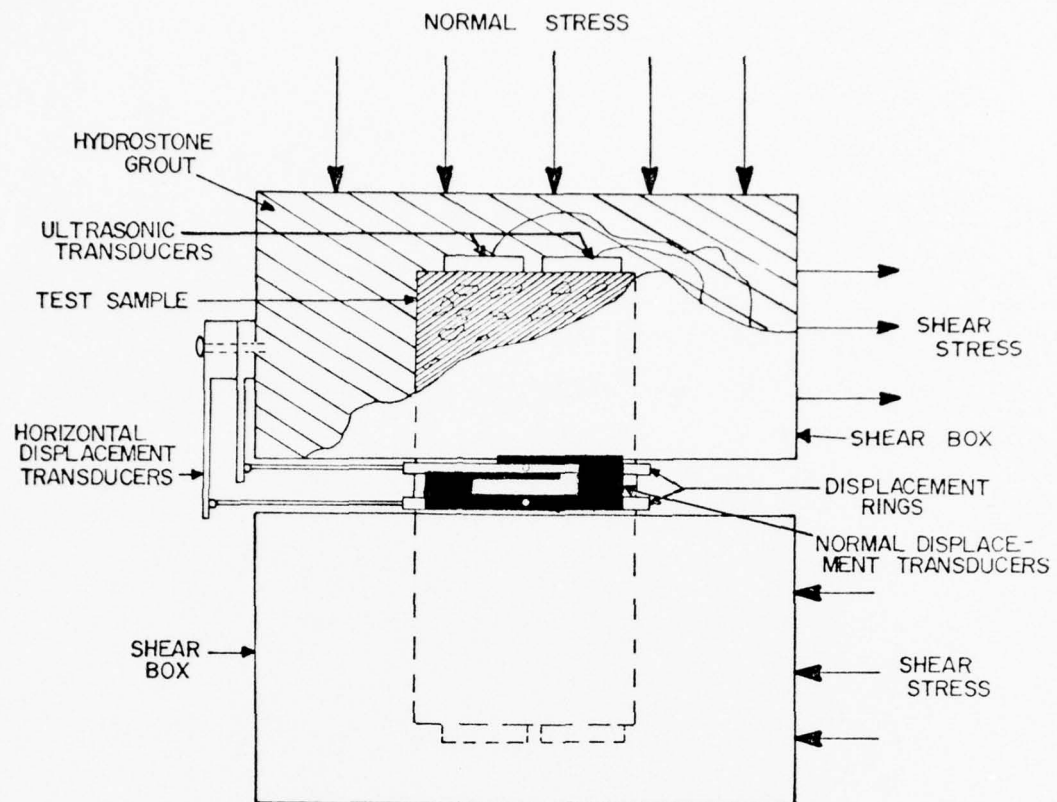


Figure 4
Direct Shear Loading Technique

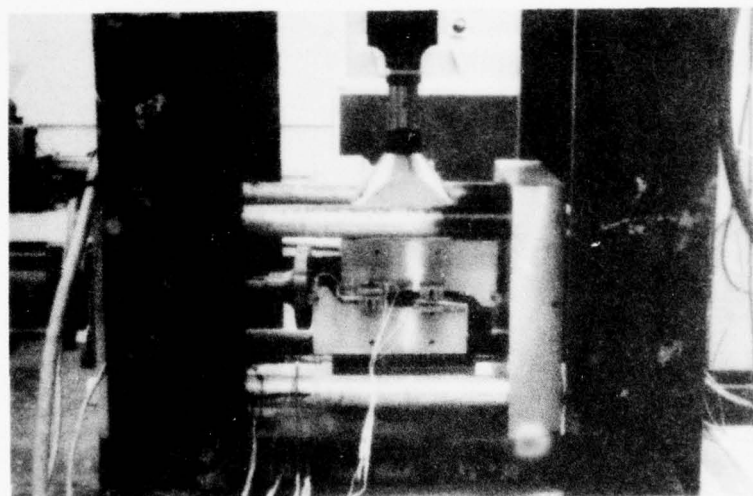


Figure 5
Direct Shear Machine
250

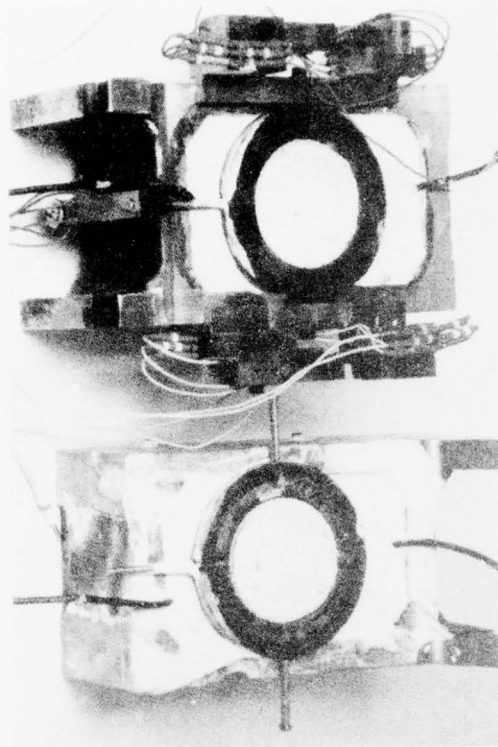


Figure 6.
Tuff Sample in Shear Box After Being Sheared

TEST RESULTS AND CONCLUSIONS

A total of six samples were fractured by the application of a direct shear load. The P-wave and S-wave velocities versus in plane horizontal displacement are shown in Figures 7 through 12. All tests were run with a normal (axial) load of 1000 psi, with the exception of the test shown in Figure 8 where the load was 500 psi.

In Figures 8, 9 and 10 the vertical displacement (displacement in the plane of the axial stress) is plotted along with the velocities. These results clearly show the opening up of the fracture zone (dilation) and the corresponding decrease in velocities.

In two of the tests, Figures 7 and 11, the P-wave signals were lost before the samples fractured. This was attributed to the loss of transducer to sample bond because of the shear stress applied directly to the transducer through the hydrostone. In all subsequent tests the transducers were isolated from the hydrostone by a thin layer of soft rubber.

In all tests, where the ultrasonic signal was maintained, the P-wave and S-wave both showed a decrease in velocity upon the onset of fracture. The overall change in the P-wave velocity, in most cases, exceeded the change in the S-wave; the maximum drop was 25 percent for the P-wave compared to 10 percent for the shear wave. This suggests that a measure of the change in P-wave velocity would be the most sensitive indication of fracture. However, some of the data also suggests that a measure of the change in the S-wave velocity might be a better early indicator of fracture, because several tests show a decline in S-wave velocities in advance of the change in the P-wave velocities.

The test on the sample with the lowest bulk density (Figure 12) showed very little change in velocities as it was sheared. This implies that the

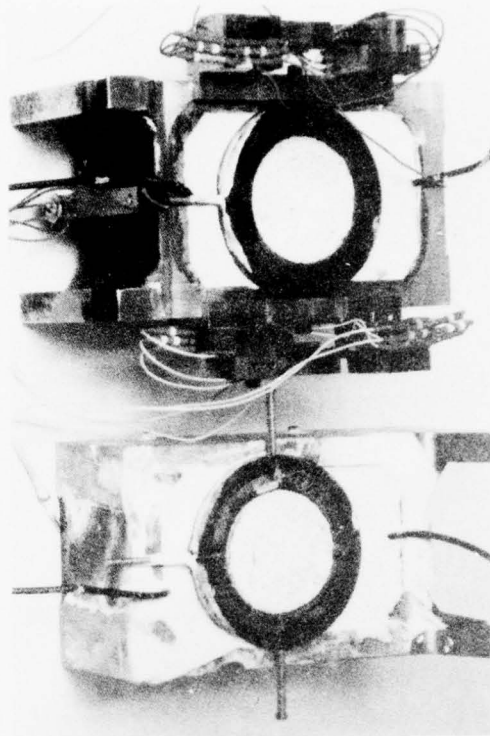


Figure 6.

Tuff Sample in Shear Box After Being Sheared

TEST RESULTS AND CONCLUSIONS

A total of six samples were fractured by the application of a direct shear load. The P-wave and S-wave velocities versus in plane horizontal displacement are shown in Figures 7 through 12. All tests were run with a normal (axial) load of 1000 psi, with the exception of the test shown in Figure 8 where the load was 500 psi.

In Figures 8, 9 and 10 the vertical displacement (displacement in the plane of the axial stress) is plotted along with the velocities. These results clearly show the opening up of the fracture zone (dilation) and the corresponding decrease in velocities.

In two of the tests, Figures 7 and 11, the P-wave signals were lost before the samples fractured. This was attributed to the loss of transducer to sample bond because of the shear stress applied directly to the transducer through the hydrostone. In all subsequent tests the transducers were isolated from the hydrostone by a thin layer of soft rubber.

In all tests, where the ultrasonic signal was maintained, the P-wave and S-wave both showed a decrease in velocity upon the onset of fracture. The overall change in the P-wave velocity, in most cases, exceeded the change in the S-wave; the maximum drop was 25 percent for the P-wave compared to 10 percent for the shear wave. This suggests that a measure of the change in P-wave velocity would be the most sensitive indication of fracture. However, some of the data also suggests that a measure of the change in the S-wave velocity might be a better early indicator of fracture, because several tests show a decline in S-wave velocities in advance of the change in the P-wave velocities.

The test on the sample with the lowest bulk density (Figure 12) showed very little change in velocities as it was sheared. This implies that the

use of ultrasonics as a tool to detect an increase in fracture density might be limited to those zones in the ash-fall tuff where the material is fairly competent.

Another point that should be made is the usual increase in the velocities of the material with the application of the axial load. In the case of the low density sample (Figure 12) the change in the P-wave velocity on application of normal load is greater than 9 percent due to pronounced compaction. This indicates a need to simulate *in situ* pressures during laboratory measurement on extremely low density material.

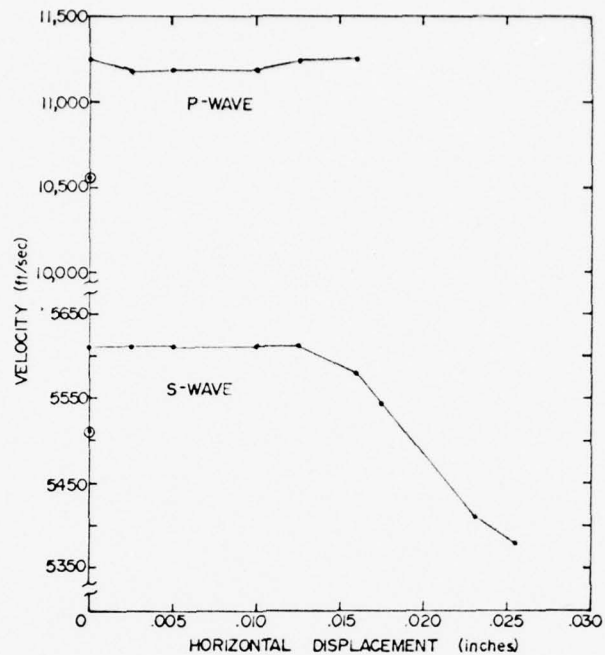


Figure 7. P- and S-wave velocities vs. shear displacement, sample U12n.10 UG#1, 593 ft., $\rho=2.10 \text{ gm/cm}^3$, axial load=1000 psi (circled points are velocities measured before the application of axial load).

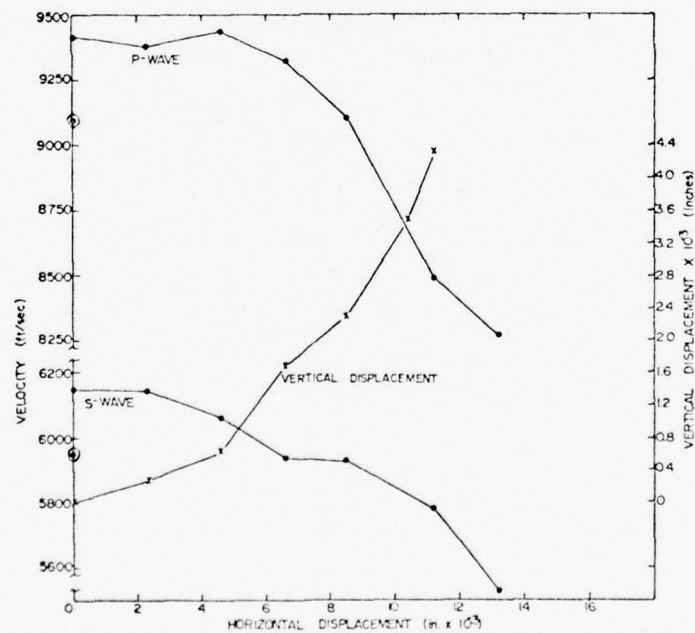


Figure 8. P- and S-wave velocities and vertical (axial) displacement vs. shear displacement, sample U12n.10 UG#1, 824 ft., $\rho=2.08 \text{ gm/cm}^3$ axial load=500 psi (circled points are velocities measured before the application of axial load).

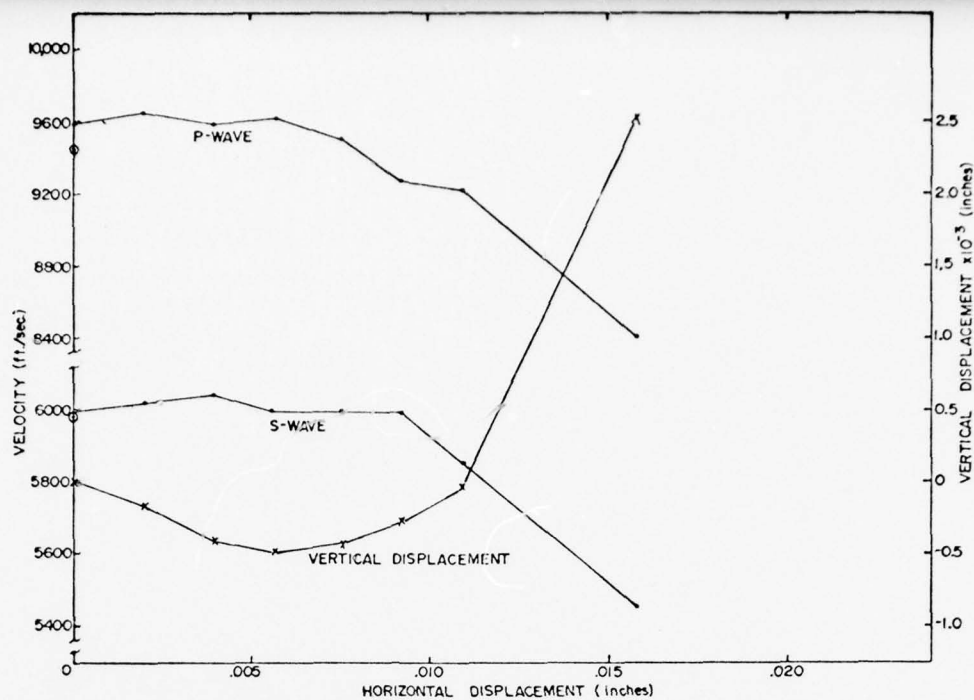


Figure 9. P- and S-wave velocities and vertical (axial) displacement vs. shear displacement, sample U12n.10 UG#1, 1149 ft., $\rho=1.92 \text{ gm/cm}^3$, axial load=1000 psi (circled points are velocities measured before the application of axial load).

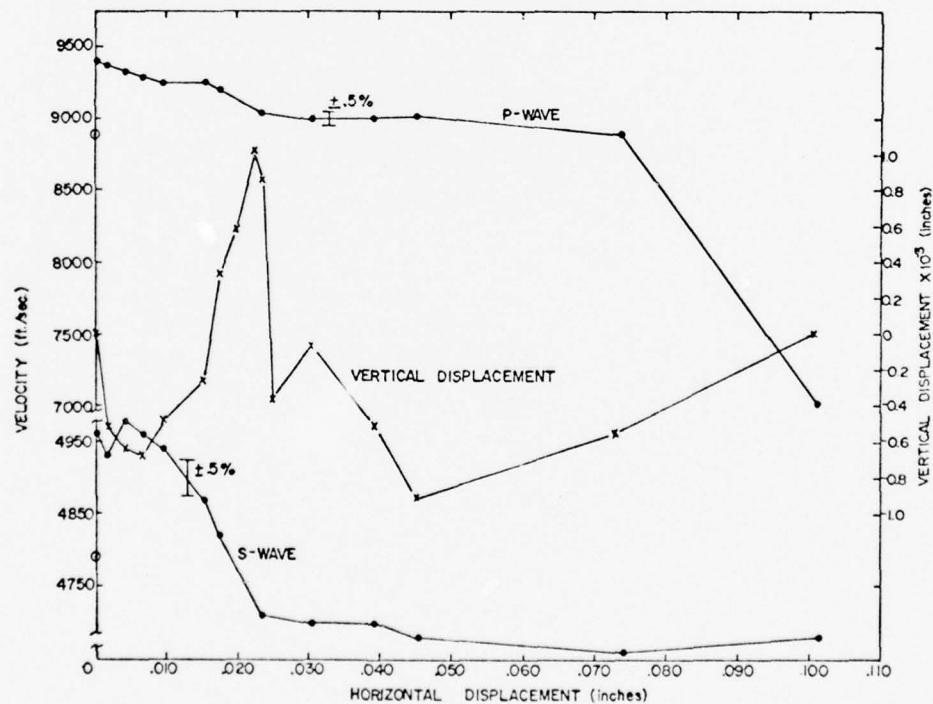


Figure 10. P- and S-wave velocities and vertical (axial) displacement vs. shear displacement, sample U12n.10 UG#1, 1276 ft., $\rho=1.85 \text{ gm/cm}^3$, axial load=1000 psi (circled points are velocities measured before the application of axial load).

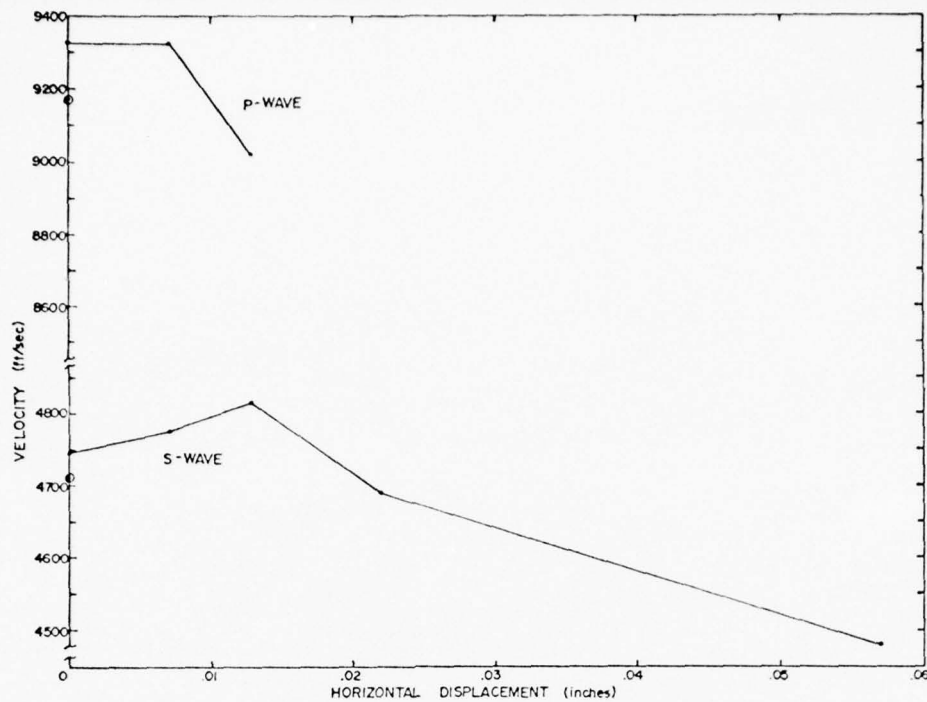


Figure 11. P- and S-wave velocities vs. shear displacement, sample U12t.03 UG#3, 958 ft., $\rho=1.86 \text{ gm/cm}^3$, axial load=1000 psi (circled points are velocities measured before the application of axial load).

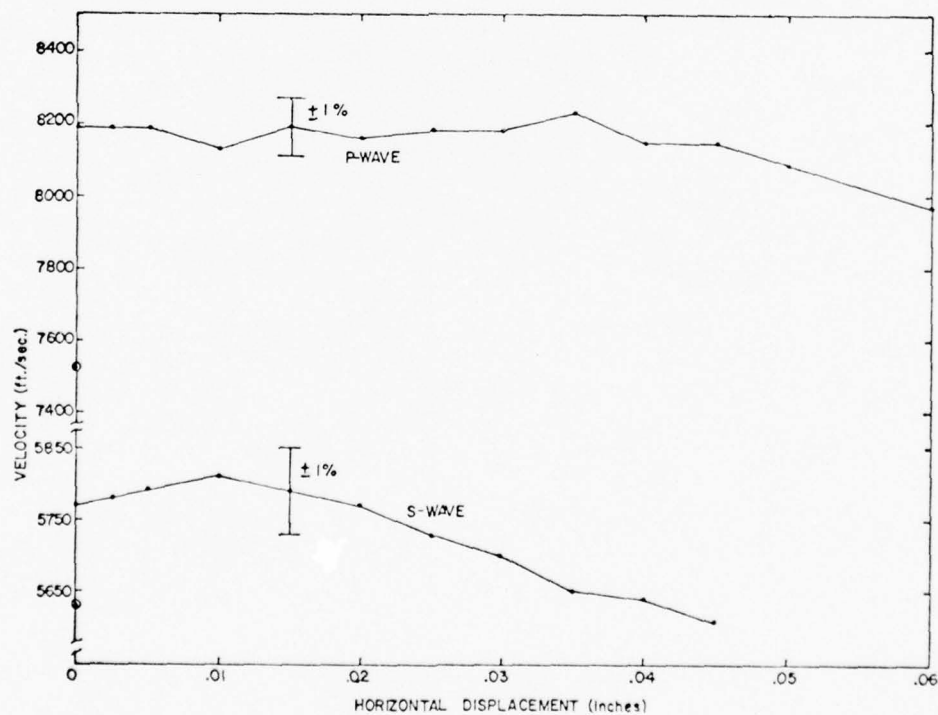


Figure 12. P- and S-wave velocities vs. shear displacement, sample U12t.03 UG#3, 1067 ft., $\rho=1.77 \text{ gm/cm}^3$, axial load=1000 psi (circled points are velocities measured before the application of axial load).

REFERENCES

- Gupta, I. N., Seismic Velocities in Rock Subjected to Axial Loading Up to Shear Fracture, J. Geophys. Res., 78, 6936-6942, 1973.
- Matsushima, S., Variation of the Elastic Wave Velocities of Rock in the Process of Deformation and Fracture Under High Pressure, Disaster Prevention Research Institute, Kyoto University Bulletin, No. 32, March, 1960.
- Mattaboni, P., and Schreiber, E., Method of Pulse Transmission Measurements for Determining Sound Velocities, J. Geophys. Res., 72, 5160-5163, 1967.
- Peselnick, L., Dieterich, J. H., and Stewart, R. M., Laboratory Experiments Duplicate Conditions in the Earth's Crust, Earthquake Information Bulletin, Vol. 6, 1974.

APPENDIX A

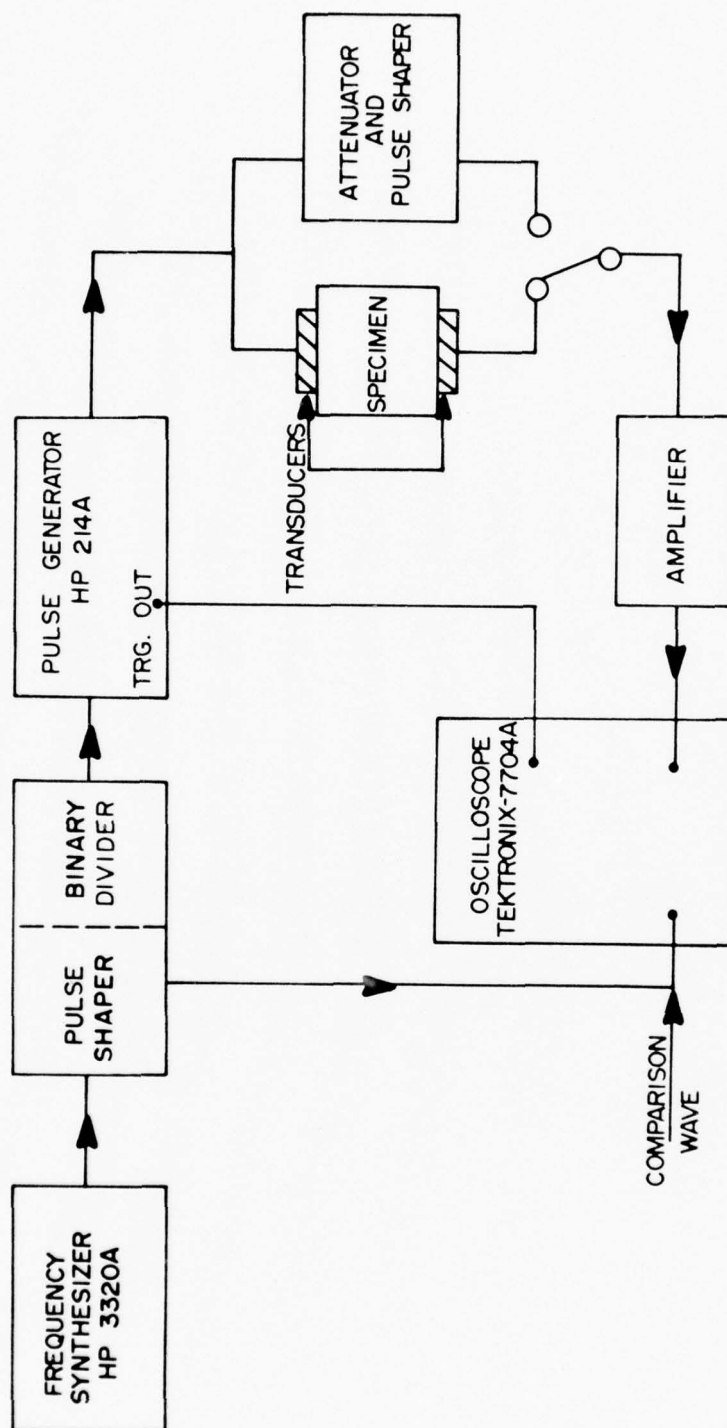
ULTRASONIC VELOCITY MEASUREMENT TECHNIQUE

The technique used to measure the ultrasonic velocities is the "Through Transmission System" shown in block diagram form in Figure A1. Figure A2 shows the equipment that is used. This is an adaptation of the technique introduced by Mattaboni and Schreiber [1965]. The main advantage of this technique is the ability to measure small elapsed times to a high degree of accuracy. The time measurement is derived from the frequency of a very stable frequency synthesizer (stability ± 1 part in 10^7 /mo, accuracy $\pm .001\%$).

The signal through the specimen is viewed on the oscilloscope, alternately with the signal from the variable frequency synthesizer after it has passed through a shaper. The shape of the latter is adjusted for an exact match of the first arrival of the wave through the specimen. The pulse that excites the transmitting transducer is next viewed and its shape matched to that of the shaped signal from the frequency synthesizer (comparison wave). Once the shapes are all the same, the frequency of the synthesizer is adjusted for an exact number of cycles between the transmitted signal and the signal through the specimen. The transit time of the ultrasonic wave through the material is obtained by dividing the cycles by the frequency. A photograph of an oscilloscope display is shown in Figure A3. The lower trace is the comparison wave matched to the signal through a specimen. The upper trace shows the initial signal matched to the comparison wave. In this example there were twelve cycles of comparison wave between the initial signal and the signal through the specimen. The frequency synthesizer setting was .3542 MHz, the elapsed time was therefore 33.879 μ sec. To obtain the velocity of the acoustic wave in the specimen it is necessary to divide the path

length by the elapsed time. Because of the difference in the inherent delay in the electrical and acoustic paths, it is necessary to determine the correction using a reference sample.

The binary divider is required in order to operate the pulse generator at a repetition rate that allows all of the ultrasonic wave energy to dissipate between pulses. This requires the oscilloscope to be triggered from the pulse generator in order to maintain the proper display.



THROUGH TRANSMISSION SYSTEM

Figure A1.

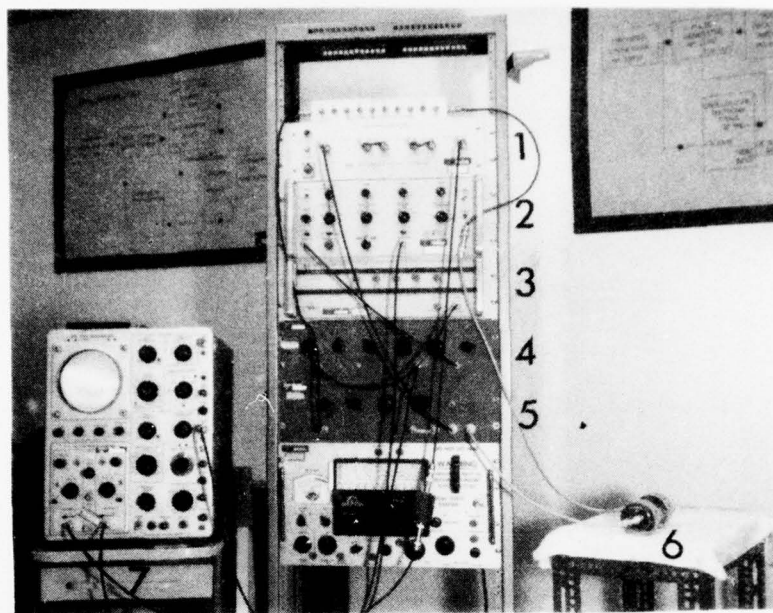


Figure A2. Equipment Used to Make Ultrasonic Velocity Measurements.

- | | |
|-----------------------------------|-------------------------------|
| 1 - Amplifier | 5 - Attenuator & Pulse Shaper |
| 2 - Pulse Generator | 6 - Specimen Holder |
| 3 - Frequency Synthesizer | 7 - Oscilloscope |
| 4 - Pulse Shaper & Binary Divider | |

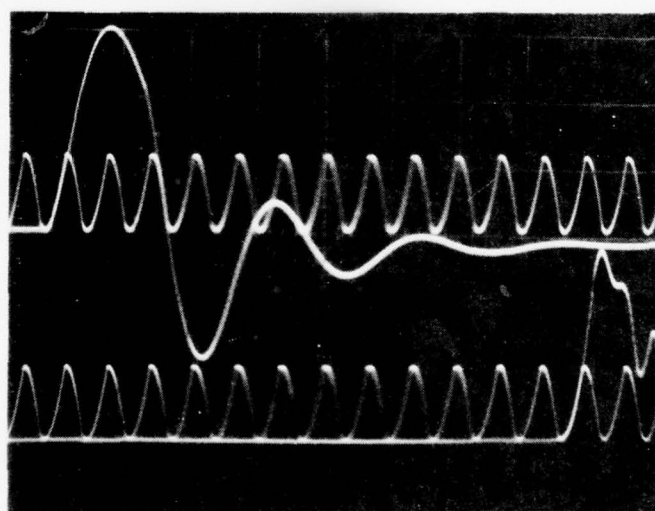


Figure A3.

Oscilloscope display showing the comparison wave and the signal through a specimen in the lower trace and the comparison wave and the initial signal in the upper trace.

APPENDIX B

DIRECT SHEAR TEST U12N10-UG#1 824FT

SAMPLE IDENT	DENSITY GM/CC	VELOCITIES			
		--- P-WAVE ---		--- S-WAVE ---	
		KM/SEC	FT/SEC	KM/SEC	FT/SEC
V L0=0	2.08	2.77	9087.93	1.81	5938.32
V L0=500	2.08	2.87	9415.01	1.87	6135.17
DISP=2.3	2.08	2.86	9383.2	1.87	6135.17
DISP=4.6	2.08	2.88	9448.82	1.85	6069.55
DISP=6.6	2.08	2.84	9317.59	1.81	5938.32
DISP=8.5	2.08	2.78	9120.73	1.81	5938.32
DISP=11.2	2.08	2.59	8497.38	1.76	5774.28
DISP=13.2	2.08	2.52	8267.72	1.69	5544.62

POISSONS RATIO	CONSTRAINED		SHEAR		BULK		YOUNG'S
	KBAR	PSI	KBAR	PSI	KBAR	PSI	
127445	159.596	231415E 7	68.1429	988072	68.7391	996718	152.655
131129	171.328	248425E 7	72.7355	105466E 7	74.3488	107801E 7	164.546
126615	170.136	246597E 7	72.7355	105466E 7	73.155	106075E 7	163.89
148751	172.524	250159E 7	71.189	102223E 7	72.6052	112529E 7	163.555
157991	167.764	243258E 7	68.1429	988072	76.9073	111516E 7	157.818
122039	160.751	233089E 7	68.1429	988072	69.8955	101346E 7	154.288
710289E-1	139.528	202316E 7	64.4301	934236	53.6217	777515	138.013
913202E-1	132.088	191328E 7	59.4069	861400	52.8791	766747	129.664

DIRECT SHEAR TEST U12N10 UG#1 1149FT

SAMPLE IDENT	DENSITY GR/CC	VELOCITIES			
		--- P-WAVE ---		--- S-WAVE ---	
		KN/SEC	FT/SEC	KN/SEC	FT/SEC
V LD=0	1.95	2.88	9448.82	1.82	5971.13
V LD=1000	1.95	2.92	9580.05	1.83	6003.94
DISP=2	1.95	2.94	9645.67	1.83	6003.94
DISP=3.9	1.95	2.92	9580.05	1.84	6036.75
DISP=5.7	1.95	2.93	9612.86	1.83	6003.94
DISP=7.6	1.95	2.89	9481.63	1.83	6003.94
DISP=9.2	1.95	2.82	9251.97	1.82	5971.13
DISP=10.9	1.95	2.81	9219.16	1.78	5539.9
DISP=15.8	1.95	2.56	8398.95	1.66	5446.19

POISSONS RATIO	CONSTRAINED				MODULI			
	KBAR	PSI	KEAR	SHEAR	PSI	KEAR	BULK	YOUNGS
167563	161.741	234524E 7	64.5918	93581	109647E 7	150.83	FEAR	FSI
17591	166.265	241064E 7	65.3035	945901	11483E 7	153.671		
18375	168.55	244398E 7	65.3035	945901	118144E 7	154.606		
170713	165.265	241064E 7	66.0192	952278	113447E 7	154.579		
160204	167.406	242738E 7	65.3035	945901	116485E 7	154.143		
163124	162.866	236196E 7	65.3035	945901	109902E 7	152.2		
14306	155.072	224854E 7	64.5918	93581	999766	147.665		
164911	153.974	223262E 7	61.7838	895865	103814E 7	143.945		
13723	127.795	185303E 7	53.7342	773146	814169	122.216		

DIRECT SHEAR TEST U12N10 UG#1 1276FT

SAMPLE IDENT	DENSITY GM/CC	VELOCITIES			
		P-WAVE		S-WAVE	
		KM/SEC	FT/SEC	KM/SEC	FT/SEC
V LD=0	1.85	2.71	8891.08	1.46	4790.03
V LD=1000	1.85	2.87	9416.01	1.51	4954.07
DISP=1.8	1.85	2.85	9350.39	1.5	4921.26
DISP=4.3	1.85	2.85	9350.39	1.52	4986.88
DISP=6.6	1.85	2.83	9284.78	1.51	4954.07
DISP=9.8	1.85	2.82	9251.97	1.51	4954.07
DISP=15.3	1.85	2.82	9251.97	1.48	4895.64
DISP=17.5	1.85	2.81	9219.16	1.47	4822.83
DISP=23.6	1.85	2.76	9055.12	1.44	4724.41
DISP=30.6	1.85	2.74	8989.5	1.43	4691.6
DISP=39.2	1.85	2.75	9022.31	1.43	4691.6
DISP=45.4	1.85	2.75	9022.31	1.43	4691.6
DISP=73.9	1.85	2.71	8891.08	1.42	4658.79
DISP=101.4	1.85	2.14	7021	1.43	4691.6

POISSONS
RATIO

POISSONS RATIO	CONSTRAINED		SHEAR		BULK		YOUNGS	
	KBAR	PSI	KBAR	PSI	KBAR	PSI	KBAR	PSI
29553	135.866	197005E 7	39.4346	571802	83.2864	120765E 7	102.177	148157E 7
308614	152.383	220955E 7	42.1818	611637	96.1402	139403E 7	110.399	160079E 7
308429	150.266	217888E 7	41.625	603562	94.7662	137411E 7	108.927	157944E 7
301242	150.266	217888E 7	42.7424	619765	93.2764	135251E 7	111.236	161293E 7
300937	148.165	214839E 7	42.1818	611637	91.9222	133687E 7	109.757	159147E 7
299015	147.119	213323E 7	42.1818	611637	90.8769	131772E 7	109.59	158905E 7
309927	147.119	213323E 7	40.5224	587575	93.0895	13498E 7	106.163	153958E 7
311611	146.078	211813E 7	39.9766	579661	92.7757	134255E 7	104.868	152058E 7
312987	140.926	204343E 7	38.3616	556243	89.7768	130176E 7	100.737	146068E 7
312831	138.891	201391E 7	37.8306	548544	88.4497	128253E 7	99.3305	144029E 7
314693	139.906	202864E 7	37.8306	548544	89.4654	129725E 7	99.4714	144231E 7
310763	135.866	197005E 7	37.3034	540599	86.128	124886E 7	97.7918	141798E 7
966189E-1	84.7226	122848E 7	37.8306	548544	34.2817	497085	82.9716	120309E 7

DIRECT SHEAR TEST U12T03 UG#3 958FT

SAMPLE IDENT	DENSITY GM/CC	VELOCITIES			
		--- P-WAVE ---		--- S-WAVE ---	
		KM/SEC	FT/SEC	KM/SEC	FT/SEC
V LD=0	1.86	2.8	9186.35	1.44	4724.41
V LD=1000	1.86	2.84	9317.59	1.45	4757.22
DISP=7.4	1.86	2.84	9317.59	1.46	4790.83
DISP=12.7	1.86	2.75	9022.31	1.47	4822.83

POISSONS
RATIO

-----MODULI-----

CONSTRAINED

SHEAR

BULK

YOUNGS

	KEAR	PSI	KEAR	PSI	KEAR	PSI	KEAR	PSI
3202	145.824	211445E 7	38.569	559250	94.3937	136878E 7	101.837	147664E 7
323707	150.82	217529E 7	39.1865	567044	97.8782	141923E 7	103.531	15012E 7
320391	150.82	217529E 7	39.6478	574892	97.1565	140877E 7	104.701	151817E 7
299976	140.663	203961E 7	40.1927	582795	87.0722	126255E 7	104.499	151524E 7

DIRECT SHEAR TEST U12N10 UG#1 598FT

SAMPLE IDENT	DENSITY GM/CC	VELOCITIES			
		P-WAVE		S-WAVE	
		FT/SEC	KM/SEC	FT/SEC	KM/SEC
VL0=0	2.1	10564.3	1.68	5511.81	
VL0=1000	2.1	11253.3	1.71	5610.24	
DISP=2.5	2.1	11154.9	1.71	5610.24	
DISP=5	2.1	11187.7	1.71	5610.24	
DISP=10	2.1	11187.7	1.71	5610.24	
DISP=12.5	2.1	11187.7	1.71	5610.24	
DISP=16	2.1	11154.9	1.7	5577.43	
DISP=17.5	2.1	11154.9	1.69	5544.62	

POISSONS RATIO	CONSTRAINED				SHEAR				BULK				YOUNGS			
	KEAR	PSI	KEAR	PSI	KEAR	PSI	KEAR	PSI	KEAR	PSI	KEAR	PSI	KEAR	PSI	KEAR	PSI
312987	217.736	315718E 7	59.2704	859421	138.709	201128E 7	155.643	201128E 7	155.643	201128E 7	155.643	201128E 7	155.643	201128E 7	155.643	201128E 7
334625	247.053	358241E 7	61.4061	890388	165.188	239521E 7	162.908	239521E 7	162.908	239521E 7	162.908	239521E 7	162.908	239521E 7	162.908	239521E 7
330701	242.76	352002E 7	61.4061	890388	160.895	233284E 7	163.426	233284E 7	163.426	233284E 7	163.426	233284E 7	163.426	233284E 7	163.426	233284E 7
332025	244.19	354076E 7	61.4061	890388	162.315	235357E 7	163.589	235357E 7	163.589	235357E 7	163.589	235357E 7	163.589	235357E 7	163.589	235357E 7
332025	244.19	354076E 7	61.4061	890388	162.315	235357E 7	163.589	235357E 7	163.589	235357E 7	163.589	235357E 7	163.589	235357E 7	163.589	235357E 7
332025	244.19	354076E 7	61.4061	890388	162.315	235357E 7	163.589	235357E 7	163.589	235357E 7	163.589	235357E 7	163.589	235357E 7	163.589	235357E 7
333333	242.76	352002E 7	60.69	880005	161.84	234668E 7	161.84	234668E 7	161.84	234668E 7	161.84	234668E 7	161.84	234668E 7	161.84	234668E 7
33593	242.76	352002E 7	59.9781	869682	162.789	236044E 7	160.253	236044E 7	160.253	236044E 7	160.253	236044E 7	160.253	236044E 7	160.253	236044E 7

DIRECT SHEAR TEST U12T03 UG#3 1067FT

SAMPLE IDENT	DENSITY GM/CC	VELOCITIES			
		P-WAVE		S-WAVE	
		FT/SEC	KM/SEC	FT/SEC	KM/SEC
V LD=0	1.77	7513.12	1.72	5643.04	1.72
V LD=1000	1.77	8202.1	1.76	5774.28	1.76
DISP=2.5	1.77	8202.1	1.76	5774.28	1.76
DISP=5	1.77	8202.1	1.76	5774.28	1.76
DISP=10	1.77	8136.43	1.77	5807.09	1.77
DISP=15	1.77	8202.1	1.77	5807.09	1.77
DISP=20	1.77	8169.29	1.76	5774.28	1.76
DISP=25	1.77	8169.29	1.75	5741.47	1.75
DISP=30	1.77	8169.29	1.74	5708.66	1.74
DISP=35	1.77	8234.91	1.72	5643.04	1.72
DISP=40	1.77	8169.29	1.72	5643.04	1.72
DISP=45	1.77	8169.29	1.71	5610.24	1.71

POISSONS RATIO	CONSTRAINED			SHEAR			BULK			YOUNGS		
	KEAR	PSI	KEAR	PSI	KEAR	PSI	KEAR	PSI	KEAR	PSI	KEAR	PSI
147154	92.8206	13459E 7	52.3637	759273	23.0023	332504	89.3163	129500E 7	110.608	160192E 7	110.608	160192E 7
89189E-2	110.625	160406E 7	54.8275	794999	37.5216	544064	110.608	160192E 7	110.608	160192E 7	110.608	160192E 7
89189E-2	110.625	160406E 7	54.8275	794999	37.5216	544064	110.608	160192E 7	110.608	160192E 7	110.608	160192E 7
89189E-2	110.625	160406E 7	54.8275	794999	37.5216	544064	110.608	160192E 7	110.608	160192E 7	110.608	160192E 7
191218E-1	108.862	15785E 7	55.4523	804059	34.9256	506422	108.784	157737E 7	108.784	157737E 7	108.784	157737E 7
25343E-2	110.625	160406E 7	55.4523	804059	36.6886	531984	110.624	160404E 7	110.624	160404E 7	110.624	160404E 7
789764E-3	103.742	159126E 7	54.8275	794999	36.6884	531257	103.742	159125E 7	103.742	159125E 7	103.742	159125E 7
119677E-1	109.742	159126E 7	54.2063	789991	37.4668	543268	109.71	159079E 7	109.71	159079E 7	109.71	159079E 7
228289E-1	103.742	159126E 7	53.5885	777034	38.2904	555211	109.625	158956E 7	109.625	158956E 7	109.625	158956E 7
573511E-1	111.512	161692E 7	52.3637	759273	41.6935	604556	110.734	160564E 7	110.734	160564E 7	110.734	160564E 7
436964E-1	109.742	159126E 7	52.3637	759273	39.9235	578891	109.394	15849E 7	109.394	15849E 7	109.394	15849E 7
537039E-1	109.742	159126E 7	51.7566	750470	40.733	590629	109.073	158155E 7	109.073	158155E 7	109.073	158155E 7

NEVADA TEST SITE
"TWO-IN-ONE CONCEPT" EVALUATION:
COMPARISON OF PRESHOT AND POSTSHOT MATERIAL PROPERTIES

by

S. W. Butters
C. N. Snow

Submitted to:

Commander
Field Command
Defense Nuclear Agency
Albuquerque, New Mexico 87117

Attn: Mr. J. W. LaComb

Submitted by:

Terra Tek, Inc.
University Research Park
420 Wakara Way
Salt Lake City, Utah 84108

TR 76-61
December 1976

SUMMARY

Material properties were evaluated for tuff cores retrieved both prior and after nuclear events at the Nevada Test Site. Core locations ranged for radial distances of 0 to 500 feet from the working points. Some permanent material properties changes were suggested. These changes, however, were insufficient to change site evaluation with respect to containment. Based on the *limited* data, further analysis of the "two-in-one-concept" is warranted.

PREFACE

The authors would like to thank E. R. Simonson, R. S. Rosso and D. O. Enniss for their support in writing the necessary computer programs.

TABLE OF CONTENTS

	Page
Summary	272
Preface	273
Table of Contents	274
List of Illustrations	275
List of Tables	275
Introduction	276
Media Properties Near Previous Nuclear Events	276
Data	276
Categorization	279
Comparisons	280
Discussion	280
Physical Property Changes	285
Mechanical Property Changes	287
Conclusions	288
References	289
Appendix	291

LIST OF ILLUSTRATIONS

<u>Figure</u>	<u>Description</u>	<u>Page</u>
1	Upper and lower bounds of peak stress from underground nuclear explosions in tuff	277
2	Example of computer data	281
3	Example of data plots	282
4	Stress difference at 4 kilobars confining pressure during uniaxial strain testing	288

LIST OF TABLES

<u>Table</u>	<u>Description</u>	<u>Page</u>
1	Drill Holes From Which Core Sample Data Was Retrieved . .	279
2	Expected Low and High Values for Tough Media Properties	285
3	Selected Preshot and Postshot Material Property Averages	287

INTRODUCTION

There is continual need for reducing underground nuclear test costs. Among the major cost reductions proposed is a concept of using common line-of-site pipe equipment for two or more nuclear events (referred to as the "two-in-one-concept"). The chosen configuration would insure containment of both events and optimize common equipment usage such as cable alcoves, gas seal doors, etc. The most logical tunnel layout is one in which the second nuclear event is placed several hundred feet in the portal direction from the first nuclear event.

Since nuclear containment is a major consideration in the Rainier Mesa, the first step in evaluating this "two-in-one-concept" is to insure, in the early stages of planning, containment of the second event. Previous site evaluaters have asked the question¹ -- "What are the media properties and conditions near the proposed working point?" It is now necessary to ask "What are the media properties and conditions near the site of a previously executed event?" This latter question prompted the present work.

Media Properties Near Previous Nuclear Events:

A review of past nuclear stress histories, Figure 1, (note: the "range" axis in Figure 1 is not meters -- peak stress is only obtainable knowing the kiloton magnitude of the event) indicated that 150 meters (500 feet) was the maximum distance that any relevant media changes could be expected. Imaginary 150 meter radius spheres were therefore placed around each of four past working points -- U12n.05, U12e.14, U12n.07 and U12n.08 -- and all preshot and postshot core sample data within these spheres were gathered for analysis.

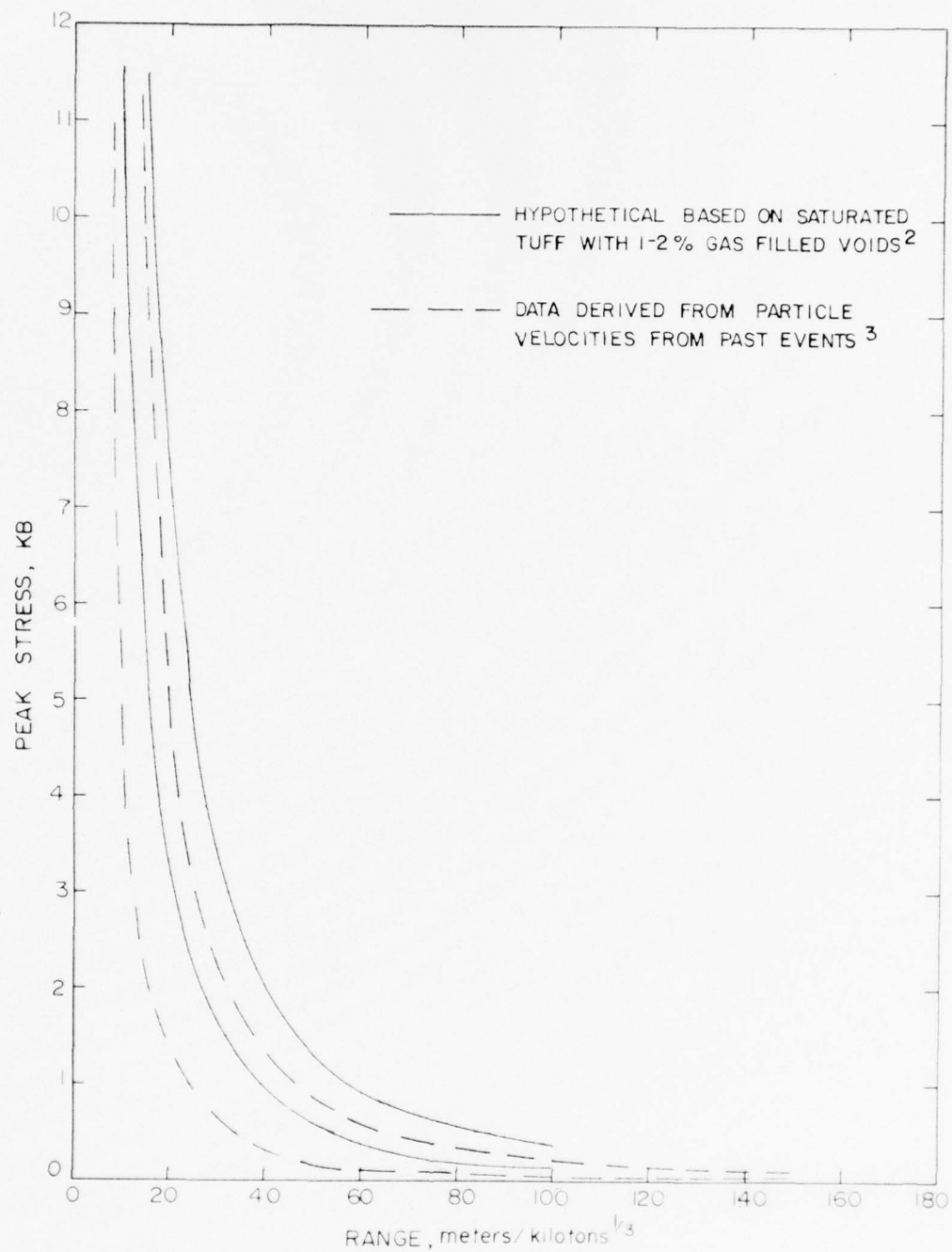


Figure 1. Upper and lower bounds of peak stress from underground nuclear explosions in tuff^{2,3}.

Material properties for the four events were determined primarily by Terra Tek with some properties obtained by Holmes and Narver, United States Geological Survey (Special Projects Branch, Denver, Colorado) and Nevada Testing Laboratories. Mr. Cliff Snow⁴ accumulated all of the preshot data from previous containment packages; postshot data was available in Terra Tek reports.

Selection of the material properties to be included in the comparisons was based on past containment evaluation. Experience indicated a combination of material properties was required, these being:

- as-received density
- dry density
- grain density
- total porosity
- water content
- saturation
- calculated air void content
- ultrasonic longitudinal velocity
- ultrasonic shear velocity
- permanent compaction from hydrostatic compression tests to 4 kilobars
- permanent compaction from uniaxial strain tests to 4 kilobars confining pressure
- stress difference at 4 kilobars confining pressure during uniaxial strain loading

DATA

Data, both preshot and postshot, were obtained on cores from horizontal and vertical drill holes in areas U12n.05, U12e.14, U12n.08 and U12n.07.

Table 1 contains a full listing of the drill holes.

TABLE 1

Drill Holes From Which Core Sample Data Was Retrieved

<u>U12n.05 Area</u>	<u>U12e.14 Area</u>
U12n.05 UG #1a	U12e.14 UG#1a
U12n.05 Pipe Drift Samples	U12e.14 UG#2
U12n.05 Bypass Drift Samples	U12e.14 UG#2a
U12n.05 UG#1	U12e.14 UG#3
U12n.05 UG#2	U12e.14 UG#4
U12n.05 UG#4	U12e.14 UG#5
U12n.05 UG#5	U12e.14 UG#6
U12n.05 UG#6	U12e.14 UG#7
U12n.05 UG#7	U12e.14 UG#8
U12n.10 UG#1 (postshot)	U12e.14 UG#9
	U12e.14 UG#11
	U12e.14 RE#1 (postshot)
	U12e.14 RE#2 (postshot)
	U12e.14 RE#4 (postshot)
<u>U12n.08 Area</u>	<u>U12n.07 Area</u>
U12n.05 UG#8	U12n.07 UG#1
U12n.08 UG#9	U12n.07 UG#2
U12n.08 UG#9a	U12n.07 UG#3
U12n.08 UG#10	U12n.07 UG#8
U12n.08 UG#11	U12n.07 UG#9
U12n.08 Gauge hole Y-2	U12n.07 UG#12 (postshot)
UE12n #2	
U12n.08 RE#1 (postshot)	
U12n.08 RE#2 (postshot)	

Categorization:

Cores were initially categorized by straight-line distance to the working point. They were further grouped according to geologic layers, designated by units and sub-units such as 3A, 3BC, 4AB, 4CDE, 4J, etc. Three basic "rock types", namely ash-fall tuff, reworked tuff and tuffaceous sandstone exist within these units and sub-units. Each individual core sample was, therefore, assigned a "rock unit" and "rock type".

Comparisons:

The core sample designations, working point distances, material properties, lithology and test laboratory codes were stored in the Terra Tek Digital PDP LAB-11 computer. Figure 2 shows a portion of the computer data with explanations for each column. The entire list of data is not included in this report but is available upon request.

Once the data was categorized, computer programs were written to screen and output the data. In this way, individual plots could be made for selected material properties (i.e., as-received density, water content, etc.) versus the radial distance from the working point, with distinction between pre-shot (diamonds) and postshot (crosses). Radial intervals could be varied in order to review the plots in detail. Further subdivision to reflect the various rock units and rock types was also possible.

An example of these data plots is shown in Figure 3. The as-received density has been plotted as a function of radial distance from the working point (0-500 feet). The rock units (4AB, 4CD, etc.) have been combined. In the three plots, the data has been subdivided into three rock types -- ash-fall tuff (Figure 3a), reworked ash-fall tuff (Figure 3b) and tuffaceous sandstone (Figure 3c).

All of the material properties listed in Figure 2 are plotted in Figure 3 and in the appended figures. Only a portion of the total plots generated are included.

	2	3	4	5	6	7	8	9	10	11	12	13	14	15	16	17	18	19	20
1	HOLE	01274	08	06#10	0-110														
	558	13	34	14	1	184	148	247	400	200	91	0	0	0	0	4720	0	1	0
	559	14	35	14	1	185	151	244	380	180	90	0	0	0	0	5250	0	1	0
	560	24	45	14	1	199	167	257	350	160	92	29	0	24	8730	4230	0	1	25
	561	37	58	14	1	190	152	247	380	200	99	5	0	9	9450	4820	0	1	40
	562	50	71	14	1	0	0	0	0	0	0	0	0	0	0	5020	0	1	0
	563	55	76	14	1	183	145	244	410	210	94	26	0	0	8730	4130	0	1	0
	564	57	78	14	1	185	148	245	400	200	94	25	0	27	0	0	0	1	59
	565	59	80	14	1	191	156	249	380	180	93	26	0	0	8270	3870	0	1	0
	566	64	85	14	1	196	162	254	360	170	94	22	0	18	8820	4170	0	1	20
	567	74	95	14	1	193	157	250	370	190	98	6	0	0	9550	4630	0	1	0
	568	76	96	14	1	192	157	250	370	180	98	8	0	12	0	0	0	1	0
	569	79	100	14	1	192	157	245	360	180	98	8	0	15	8920	4250	0	1	36
	570	86	107	14	1	186	150	246	390	200	94	25	0	20	8010	3810	0	1	41
	571	98	119	14	1	198	165	247	330	170	99	2	0	14	9740	4950	0	1	69
	572	115	136	14	1	186	147	246	400	210	98	7	0	12	9250	3940	0	1	26
	573	117	138	14	1	0	0	0	0	0	0	0	0	0	0	0	0	1	0

1. Area, drill hole and sample-interval*
2. Sample number
3. Drill hole collar footage (feet)
4. Radial distance from the working point (feet)
5. Rock unit code**
6. Rock type code
7. As-received density ($\text{gm/cc} \times 10^2$)**
8. Dry density ($\text{gm/cc} \times 10^2$)
9. Grain density ($\text{gm/cc} \times 10^2$)
10. Total porosity (percent $\times 10^1$)
11. Water content by wet weight (percent $\times 10^1$)
12. Saturation (percent)
13. Calculated air void content (percent $\times 10^1$)
14. Hydrostatic compression-permanent volume compaction after loading to 4 kb (percent by volume $\times 10^2$)
15. Uniaxial strain-permanent volume compaction after loading to 4 kb lateral stress (percent by volume $\times 10^2$)
16. Ultrasonic longitudinal velocity (feet per second)
17. Ultrasonic shear velocity (feet per second)
18. Rigidity modulus (kilobars)
19. Test Laboratory code***
20. Stress difference at 4 kilobars confining pressure during uniaxial strain loading (kilobars $\times 10^2$)

* This example is preshot. Postshot data have an asterisk preceding the area and drill hole designation.

** 1 - Bed 5 4 - Bed 4H 7 - Bed 4E 10 - Bed 4AB 13 - Bed 2
 2 - Bed 4K 5 - Bed 4G 8 - Bed 4CDE 11 - Bed 3BC 14 - Bed 3D
 3 - Bed 4J 6 - Bed 4F 9 - Bed 4CD 12 - Bed 3A

+ 1 - ashfall tuff 2 - reworked tuff 3 - tuffaceous sandstone 4 - welded tuff
 ** Figure "0" indicates no data was available.

*** 1 - Terra Tek, Inc. 2 - Waterways Experiment Station 3 - Nevada Testing Laboratories 4 - United States Geological Survey 5 - Holmes and Narver Test Lab

Figure 2. Example of computer data.

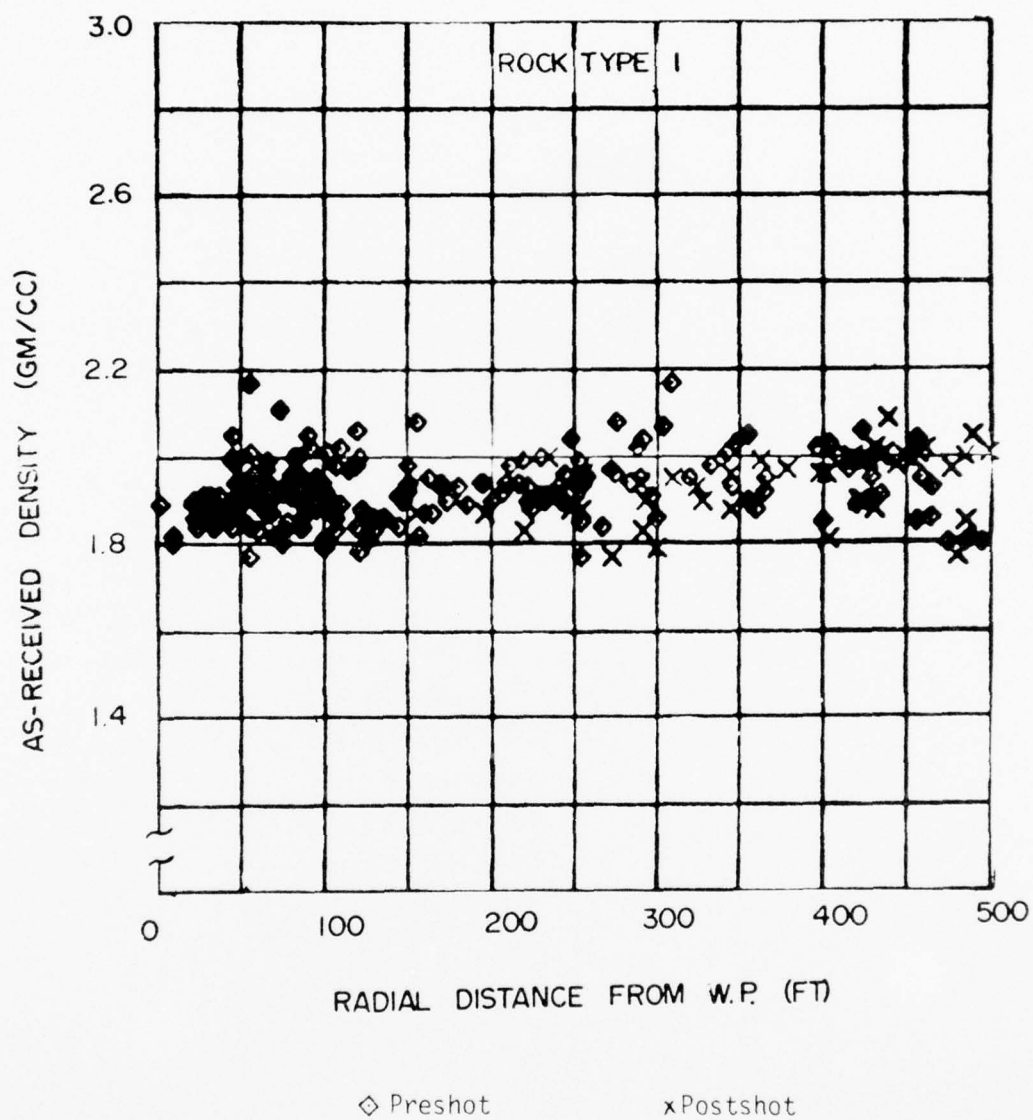


Figure 3a. Example of data plots (Rock Type 1).

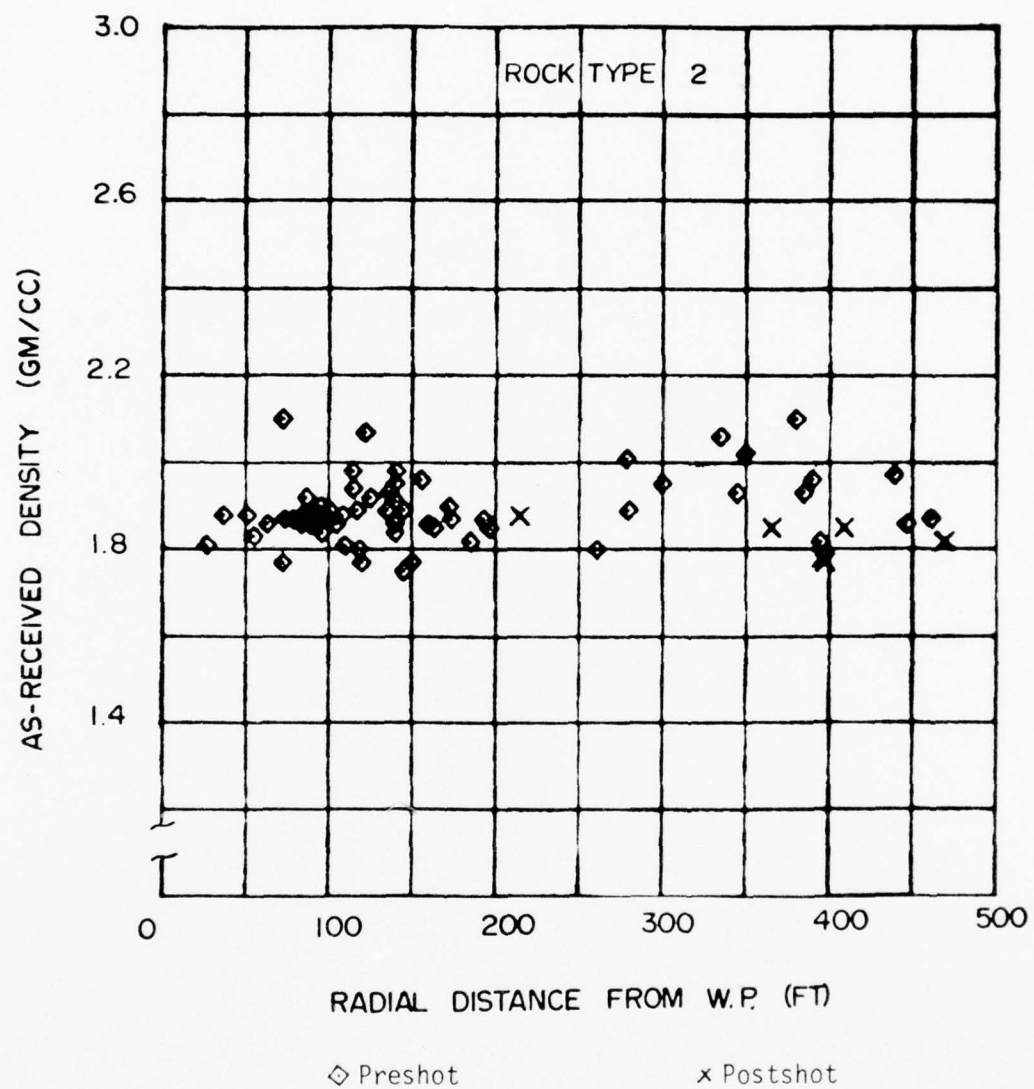


Figure 3b. Example of data plots (Rock Type 2).

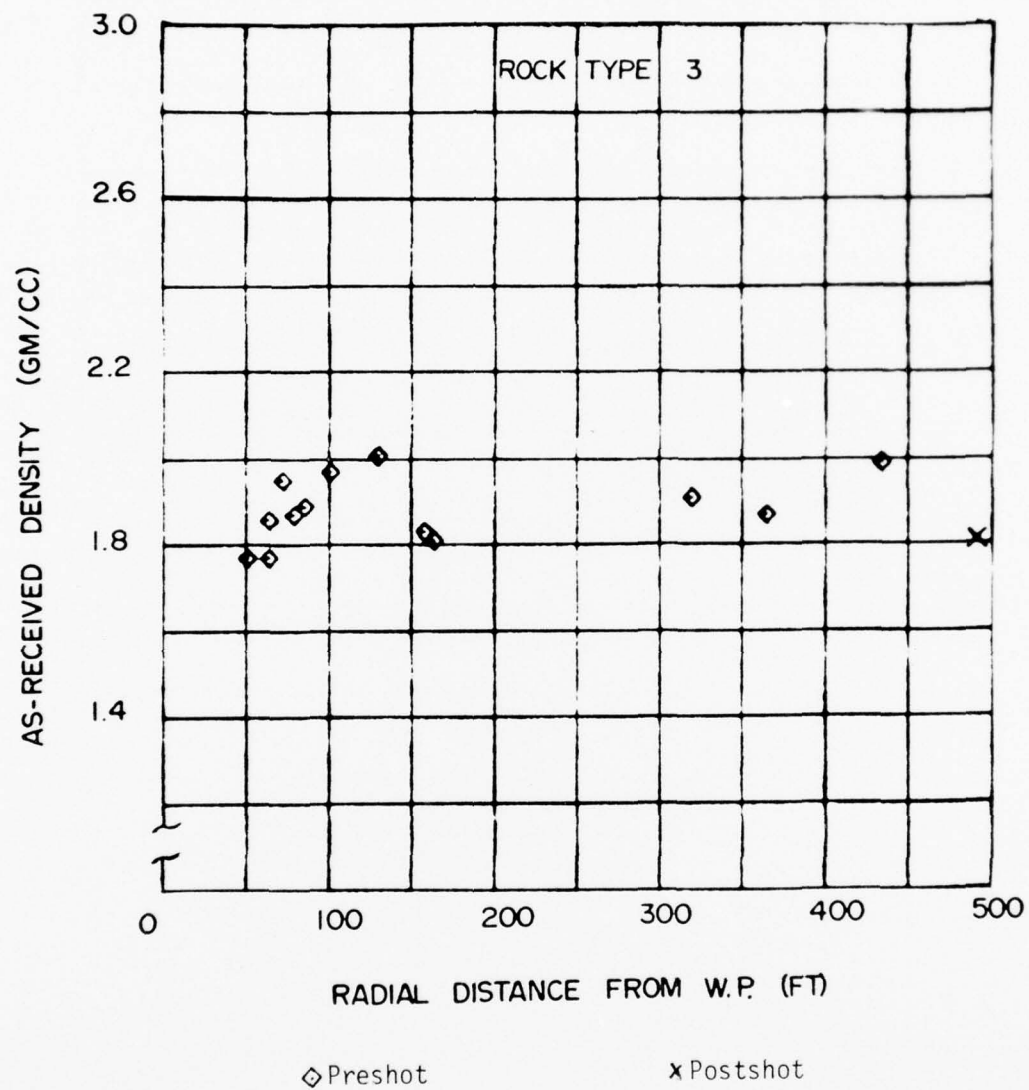


Figure 3c. Example of data plots (Rock Type 3).

DISCUSSION

In reviewing and analyzing the data plots and averages, the questions needed to be answered were "What magnitudes of change are relevant to containment evaluation?" and "Can these changes be resolved in this analysis?". The former question was addressed first since the answer would indicate what to look for in the preshot-postshot comparisons.

All of the material properties included in this analysis have been used as an indicator of the media's ability to contain the nuclear test. Expected low and high values for the media properties are listed in Table 2.

TABLE 2
Expected Low and High Values for Tough Media Properties

Property	Typical, Low & High Values
As-received density	1.75-2.05 gm/cc
Dry density	1.40-1.70 gm/cc
Grain density	2.30-2.50 gm/cc
Total porosity	30-40 percent
Water content by wet weight	15-25 percent
Saturation	90-100 percent
Calculated air void content(by total volume)	0-2 percent
Permanent compaction from hydrostatic compression test to 4 kb	0-2 percent
Permanent compaction from uniaxial strain test to 4 kb lateral stress	0-2 percent
Ultrasonic longitudinal velocity	7500-11,000 ft/sec
Ultrasonic shear velocity	3500-6000 ft/sec
Stress difference at 4 kilobars confining pressure during uniaxial strain loading	0.1-1.0 kilobars

Containment evaluation is based on a combination of the properties. Example: a core sample showing an as-received density of 1.70 gm/cc, which is out of the expected range, would suggest a high porosity. Further testing, however, indicated an ultrasonic longitudinal velocity of 9000 ft/sec, a high water content and, most importantly, a "permanent volume compaction" of 1.5 percent by volume. Properties such as as-received density, water content, and sound velocities (ultrasonic, sonic and seismic) are measured and reviewed as they often times will indicate the existence of tuff with a high GFVC. That property -- the GFVC of the *in situ* material -- is viewed most critical as it has been shown to have a direct affect on containment⁵. The most consistent method to date for an indication of the GFVC is to conduct a uniaxial strain test and measure the permanent volume compaction⁶. The range of acceptable values for the GFVC is from 0 (100 percent saturation) to about 2 percent by volume. The upper limit (2 percent) is simply a rule of thumb⁷ and GFVC's greater than 2 percent can be acceptable in view of factors such as lithology, fault zones, volume of material, relation to working point, etc.

There are over 3500 individual data points in the computer, 70 percent preshot and 30 percent postshot data. The preshot data is concentrated in the 0 to 300 foot range while the postshot data is from about 200 to 500 feet. The preshot data, however, need not be a function of the distance from the working point and can, therefore, be compared to the 200 to 500 foot postshot range. The plots shown in Figure 3 (and the appendix) were produced to allow a review for obvious differences and trends between the preshot and postshot data as a function of radial distance. The plots give excellent insight into the data scatter and where to look in more detail.

Physical Property Changes:

As seen in the plots, there is little noticeable difference between preshot and postshot data. One region, 200 to 300 feet from the working point, did show some lower than usual as-received densities and higher than usual porosities. In order to study this range more closely, it was necessary to eliminate as many variables as possible. That is, for the detailed comparisons to be meaningful, it was essential that they be made between samples of the same rock units and rock types.

The computer averaging routine was capable of selecting samples as a function of rock unit, rock type and radial distance from the working point with distinction between preshot and postshot. Table 3 shows a number of averages obtained for studying the 200 to 300 foot range. Note the closeness of the preshot to postshot data averages in the ranges 25 to 200 feet and 300 to 450 feet. In the 200 to 300 foot (bed 4AB) and 250 to 300 foot (bed 4F) ranges there are differences. The data indicates that even though the densities are low and porosities are high in the 200 to 300 foot range, the gas-filled void content decreased from an average of 2.5 percent to 1.1 percent by volume. It would suggest that void space was created and subsequently filled with water, which is possible, but unlikely. Obviously, trends and changes need to be based on averages for a larger number of data points.

TABLE 3
Selected Preshot and Postshot Material Property Averages

BED	ROCK TYPE	RANGE	PRESHOT				POSTSHOT			
			AS-REC. DENSITY	POROSITY	1-D PERMANENT COMPACTION	STRESS DIFFERENCE @ $\sigma_v = 4 \text{ kb}$	AS-REC. DENSITY	POROSITY	1-D PERMANENT COMPACTION	STRESS DIFFERENCE @ $\sigma_v = 4 \text{ kb}$
			UG#9 and Y-2				RE#2 (HORIZONTAL)			
3D	Ashfall	25-200	1.91(16)	37(16)	1.6(16)	0.40(14)	1.90(3)	38(1)	1.3(1)	0.16(2)
4AB	Ashfall	200-300	1.95(4)	35(4)	2.4(4)	0.53(4)	1.88(3)	42(2)	1.1(2)	0.22(2)
4E	Ashfall	330-450	1.91(7)	35(7)	0.3(1)	1.00(1)	1.91(5)	36(3)	1.0(3)	0.43(3)
							RE#1 (INCLINED)			
4F	Ashfall	250-300	1.88(14)	34(27)	---	---	1.81(6)	41(1)	2.0(3)	0.49(3)

Mechanical Property Changes:

Normally strength refers to the triaxial compression shear strength of samples. There was, however, a lack of available triaxial compression failure data. Recent observations of the uniaxial strain test stress difference data indicate that it can be used to give an estimate of the relative magnitudes of shear strength⁸. Since there have been quite a number of uniaxial strain tests conducted, it was this value (stress difference at 4 kilobars confining pressure) which was included in this analysis.

As shown in Table 3, the postshot material appears to be lower in strength. However, as shown in Figure 4, it is not uncommon to see large changes in the material strength of virgin tuff over tens of feet. Additional data is required before drawing conclusions on the shear strength of the postshot material.

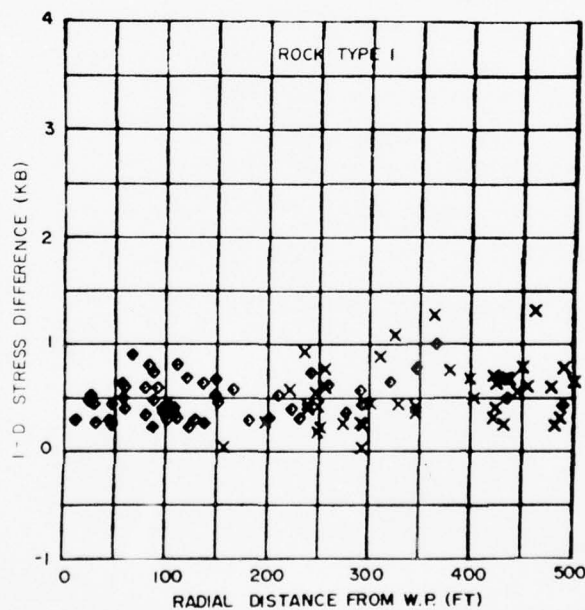


Figure 4. Stress difference at 4 kilobars confining pressure during uniaxial strain testing.

CONCLUSIONS

Regarding trends and changes as a function of distance from the working point, there was some indication of changes in the 200 to 300 foot range but these were based on very limited data. Most importantly, the changes were not of the magnitude which would be detrimental to the containment of subsequent nuclear events. Isolated postshot samples appear which show low densities, low velocities, high gas-filled void contents, etc., but they are no more prevalent in postshot cores than are seen in preshot cores.

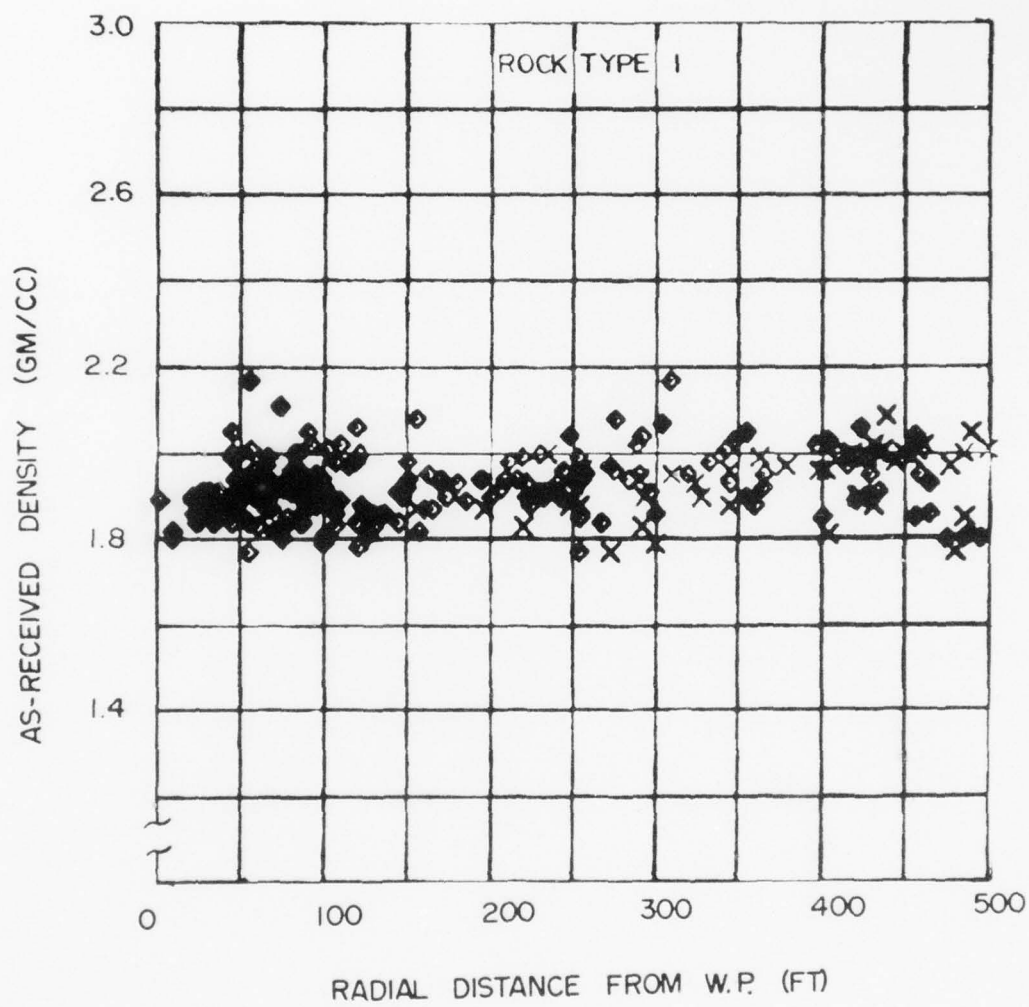
In more detail, there are indications that the strength of the tuff may have been decreased (20 to 50 percent) over the complete range of postshot data (~200 through 500 feet). Within the 200 to 300 foot range, some postshot data showed lower densities, higher porosities but lower gas-filled void contents.

It is recommended that the data base be continually updated to allow additional comparisons as events are executed. Emphasis should be placed on sampling. Preshot sampling has previously been concentrated around the working point (out to 200 to 300 feet) while postshot sampling cannot usually be closer than 200 feet from the working point. More meaningful comparisons could be realized if preshot core samples were taken near expected re-entry hole locations (within distances of feet to eliminate rock unit and rock type variations).

REFERENCES

1. Keller, C., Kent, G., and LaComb, J., "Close Siting in Rainier Mesa," (discussion draft), March 1975.
2. R. L. Bjork, Pacifica Technology, Personal communication, December 1976.
3. H. F. Cooper, Jr., "Emperical Studies of Ground Shock and Strong Motion in Rock," R & D Associates, RDA-TR-3601-002, October 1973.
4. Mr. Cliff Snow, Defense Nuclear Agency Field Command, Mercury, Nevada.
5. Bjork, R. L., "Late Time Containment, Progress Report for July, 1970," edited by R. E. Duff, 3SR-419 (August 14, 1970).
6. Butters, S. W., Dropek, R. K., Green, S. J. and Jones, A. H., "Material Properties in Support of the Nevada Test Site Nuclear Test Program," Terra Tek Final Report DNA 3870F-1, October 1975.
7. Mr. J. W. LaComb, Defense Nuclear Agency Field Command, Mercury, Nevada.
8. Butters, S. W., Stowe, R. L. and LaComb, J. W., "Characterization of Tuff and Development of Grouts for Mighty Epic Structures Program," Terra Tek, Inc. Report TR 76-21, April 1976.

APPENDIX



AD-A043 977

TERRA TEK INC SALT LAKE CITY UTAH

F/G 18/3

MATERIAL PROPERTIES OF NEVADA TEST SITE TUFF AND GROUT - WITH E--ETC(U)

NOV 76 S W BUTTERS, R K DROPEK, A H JONES

DNA001-75-C-0260

UNCLASSIFIED

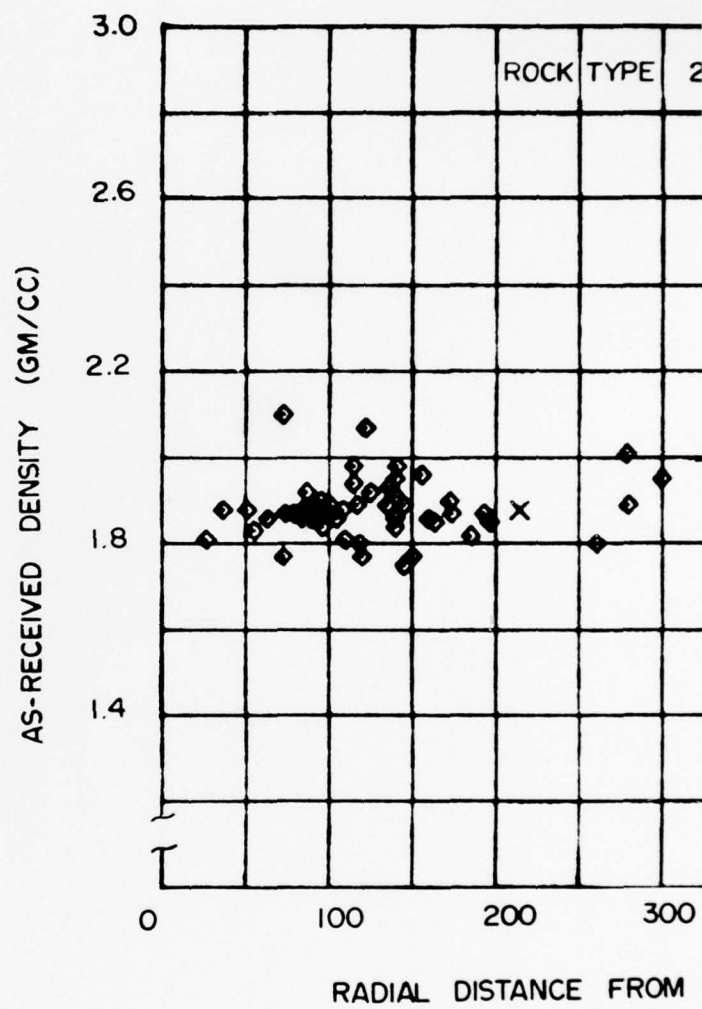
TR-76-63

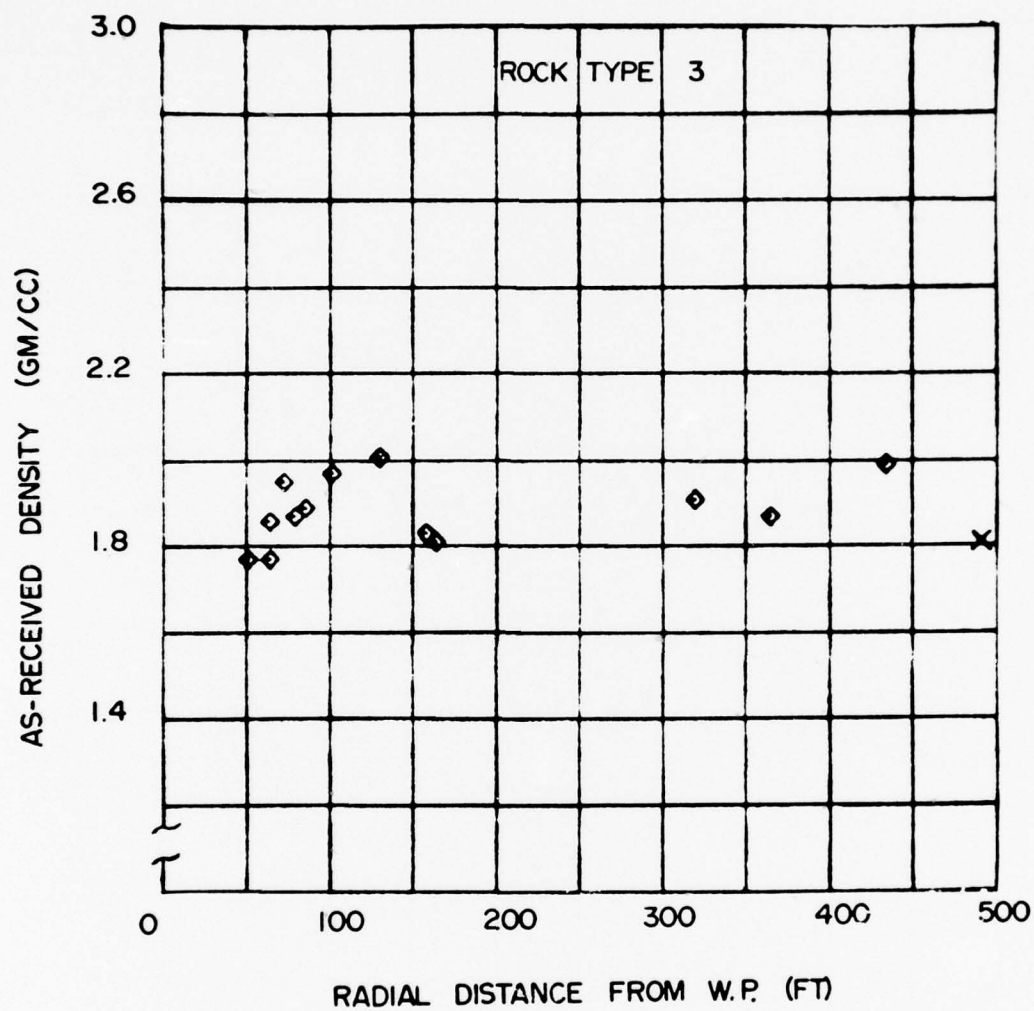
DNA-4235F

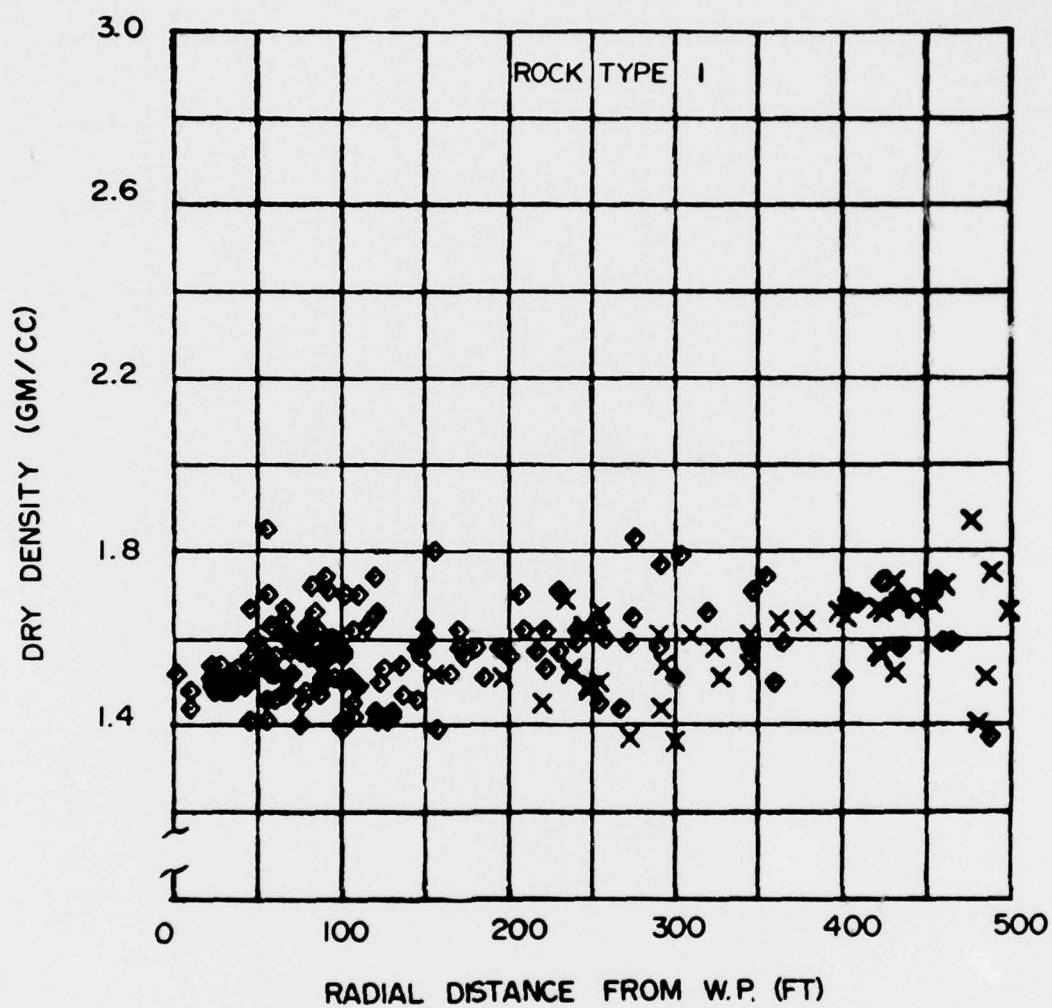
NL

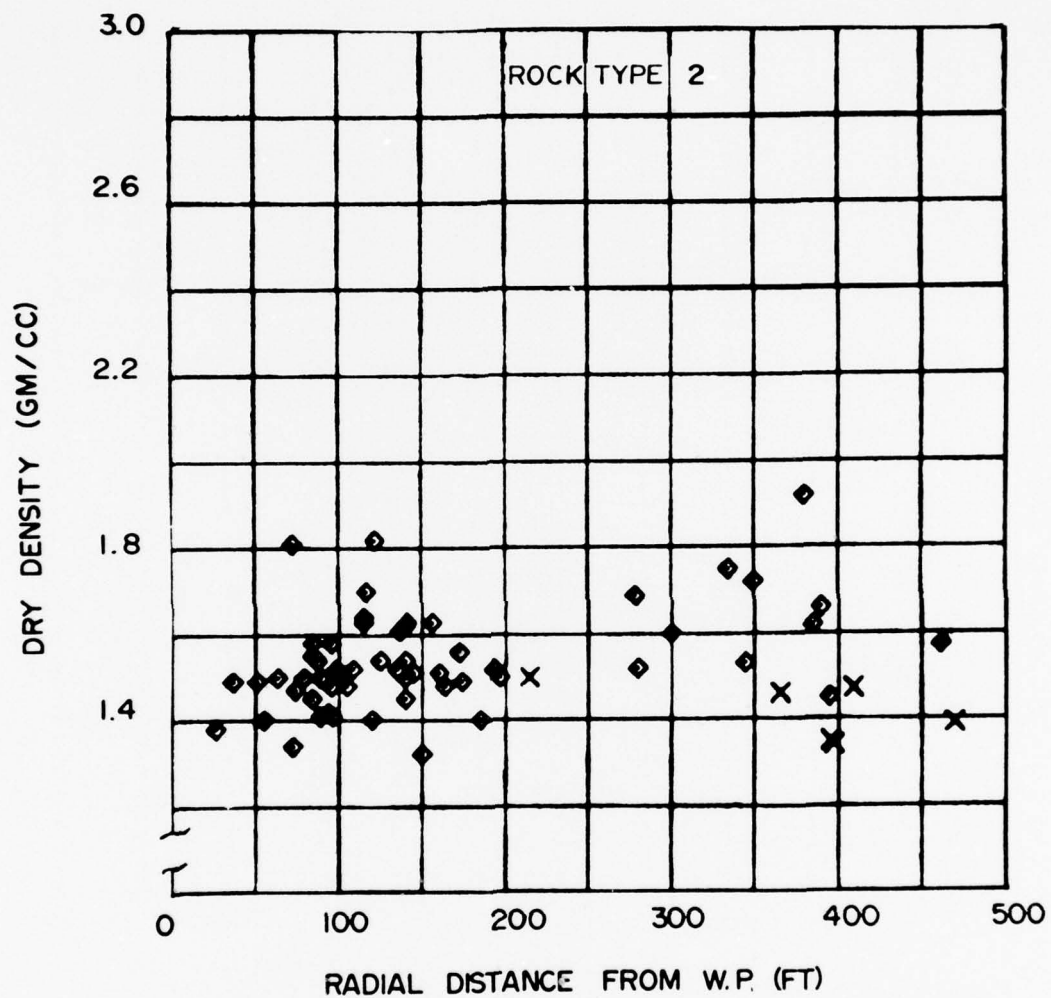
4 OF 5
AD
A043 977

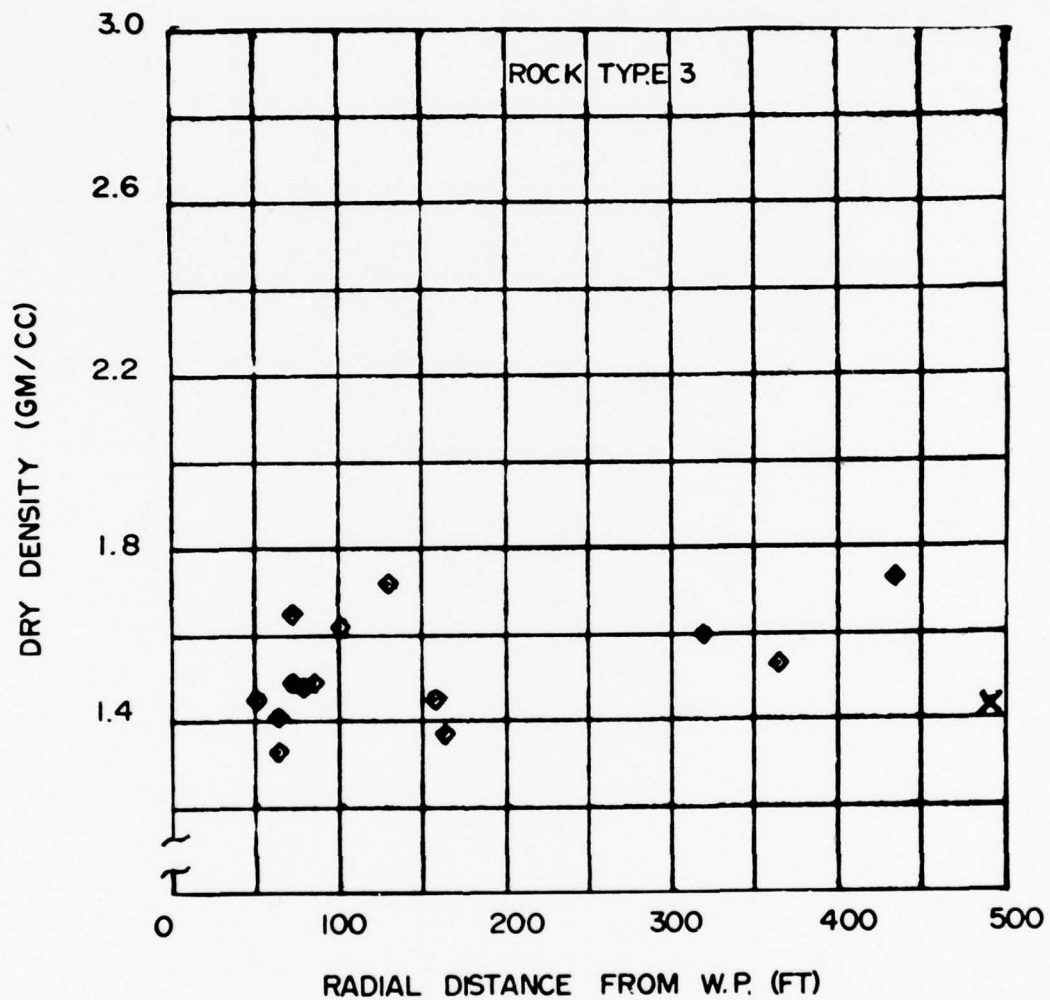


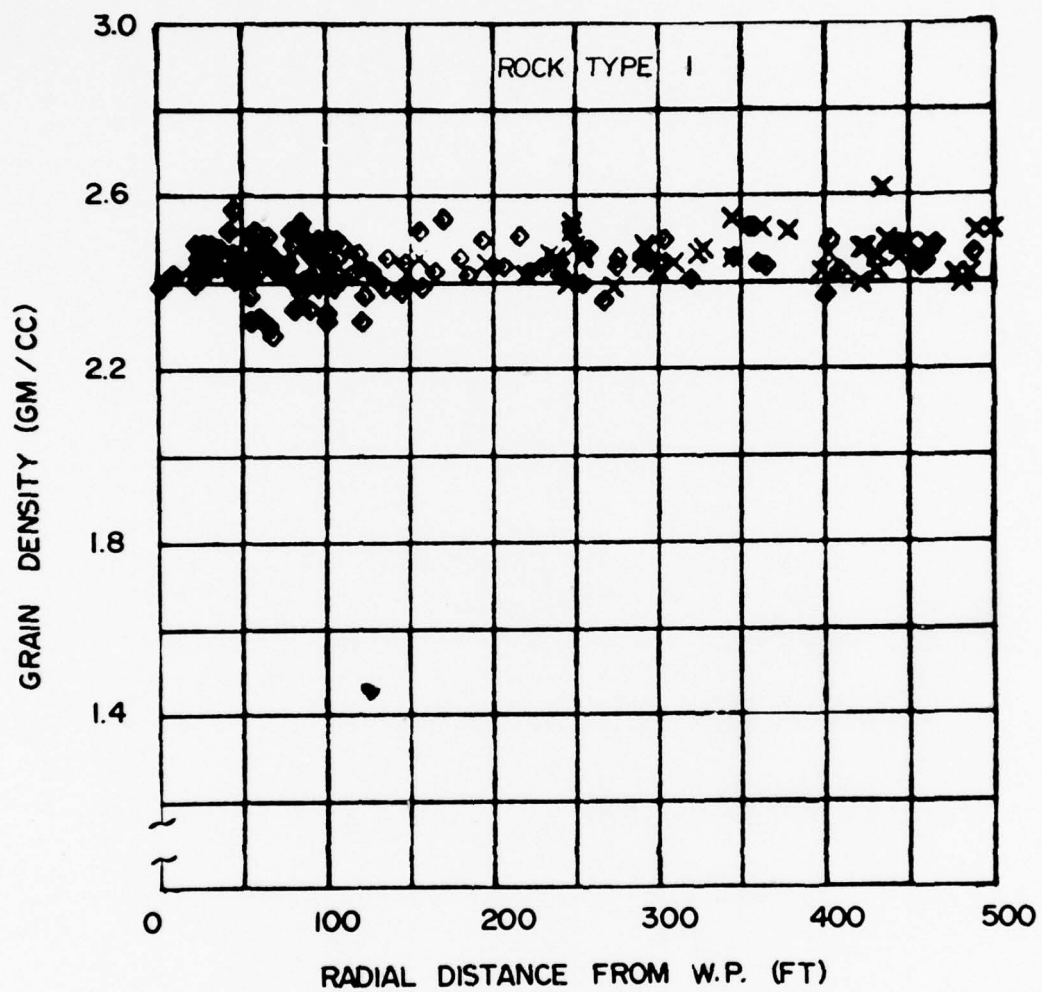


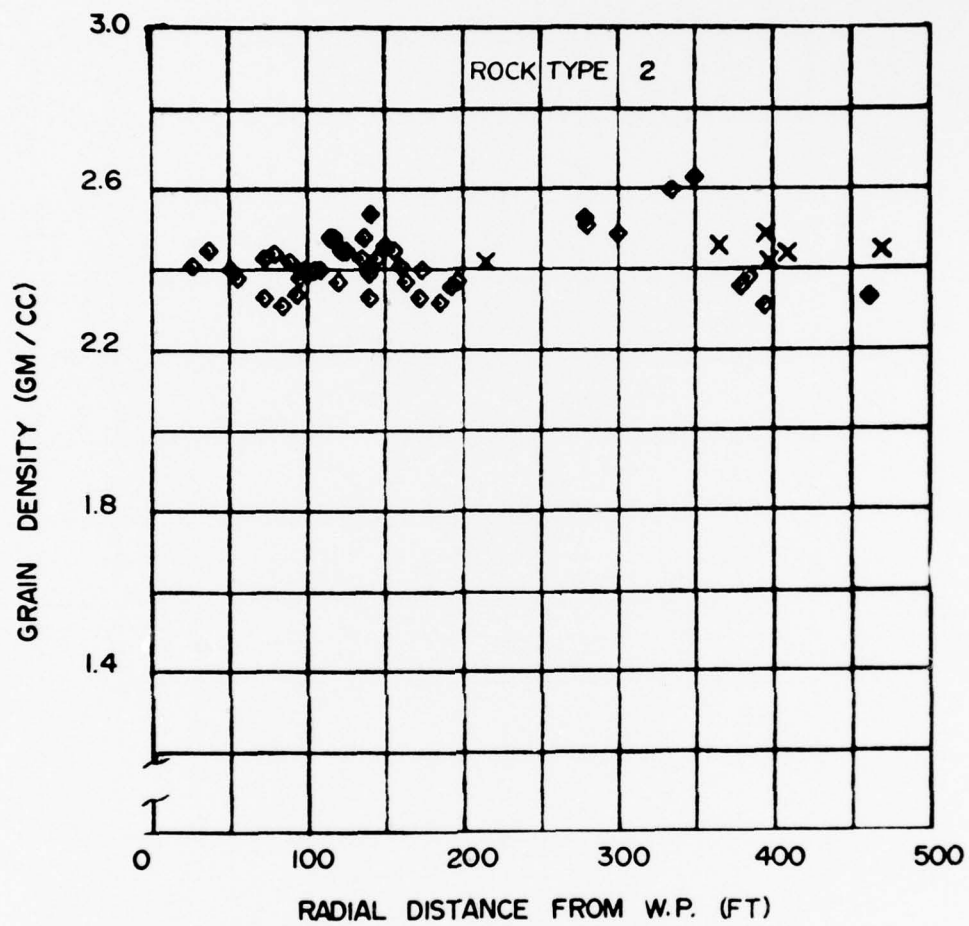


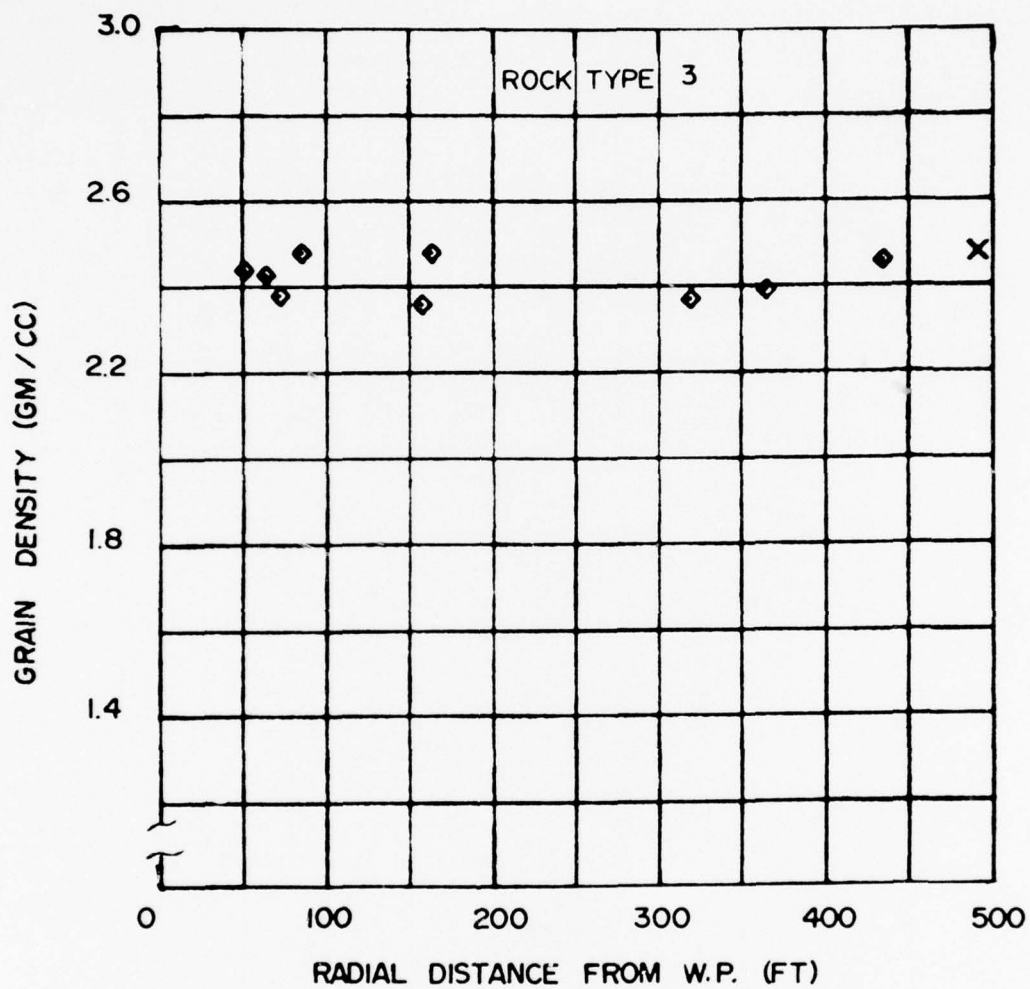


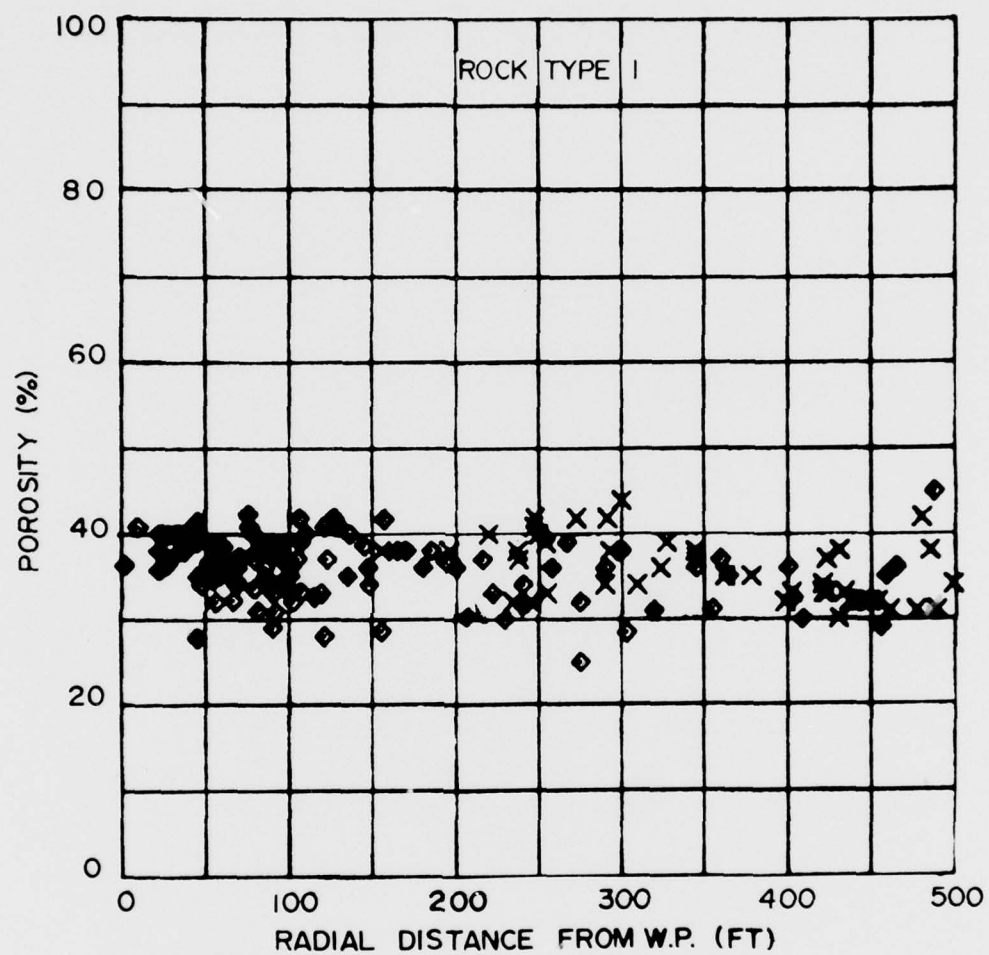


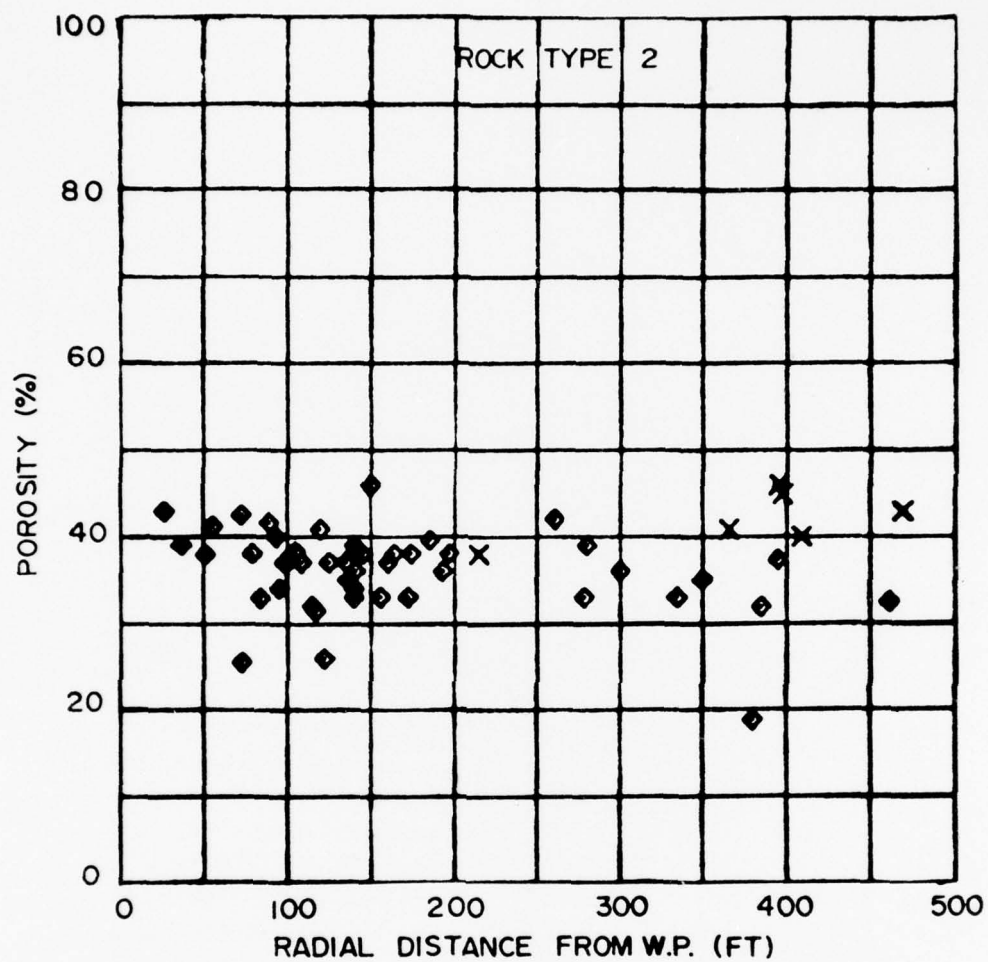


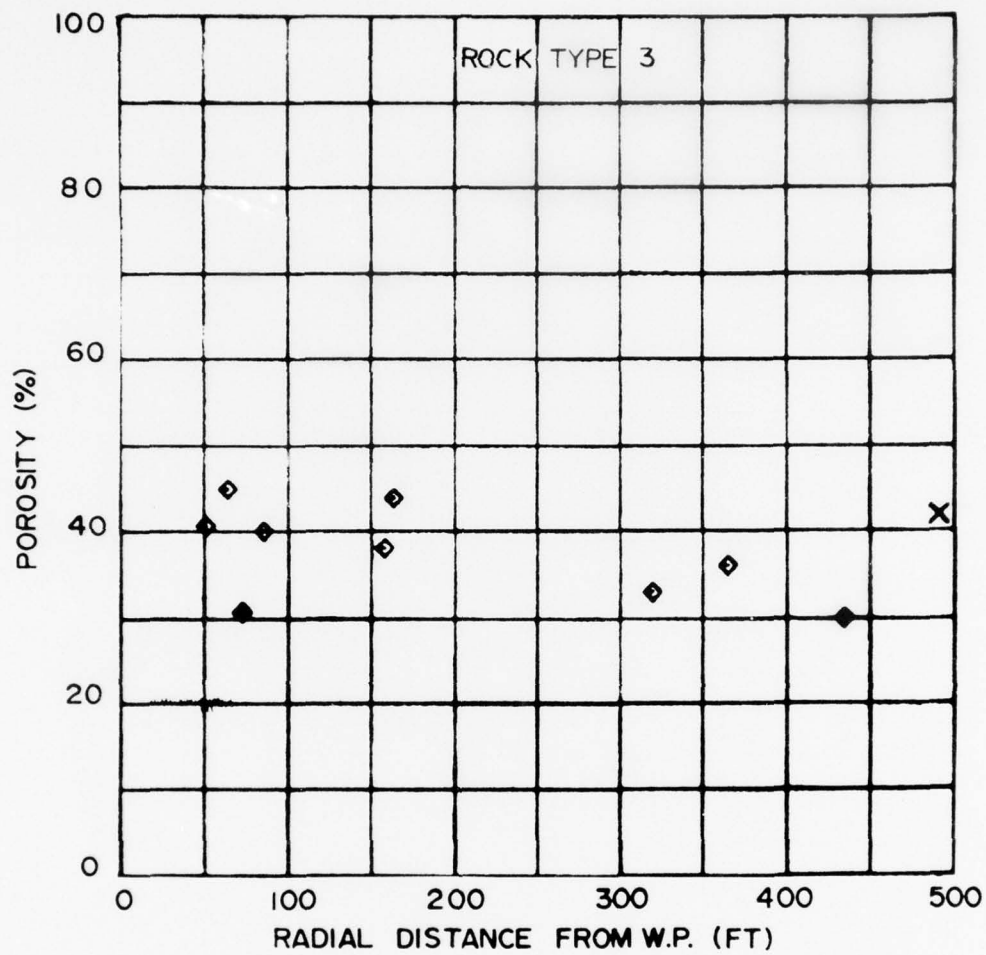


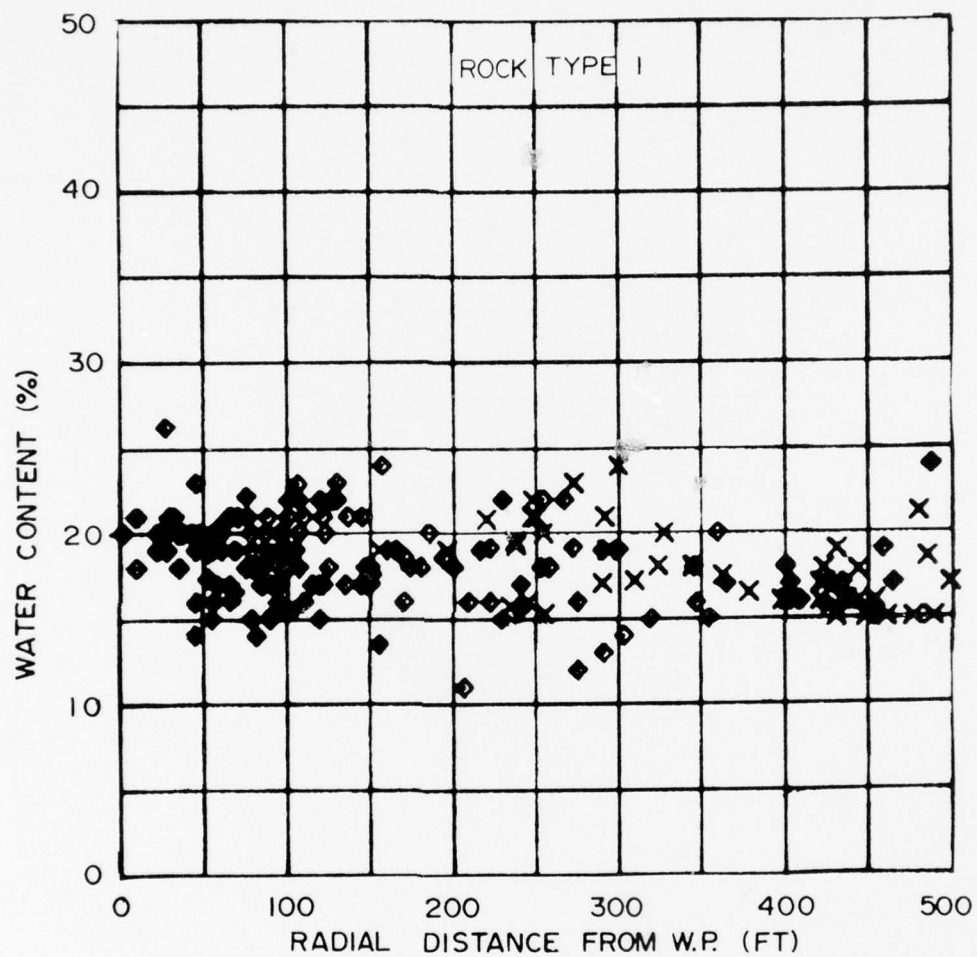


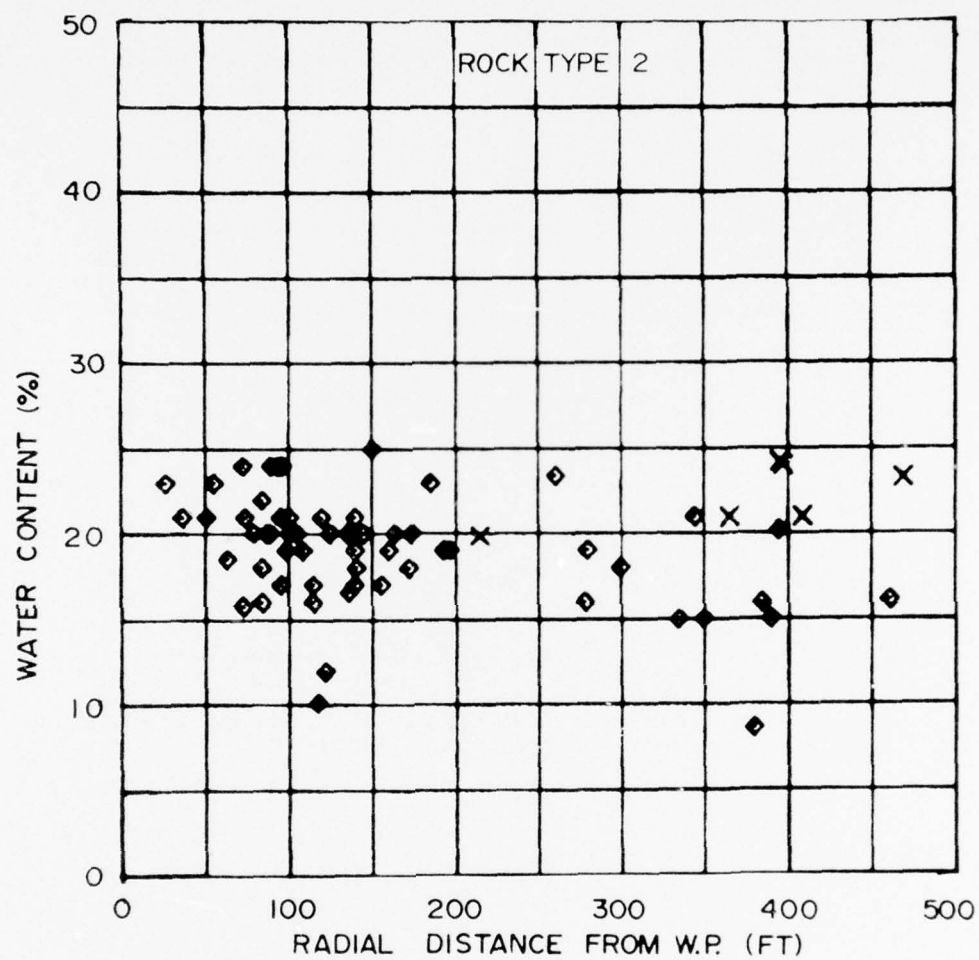


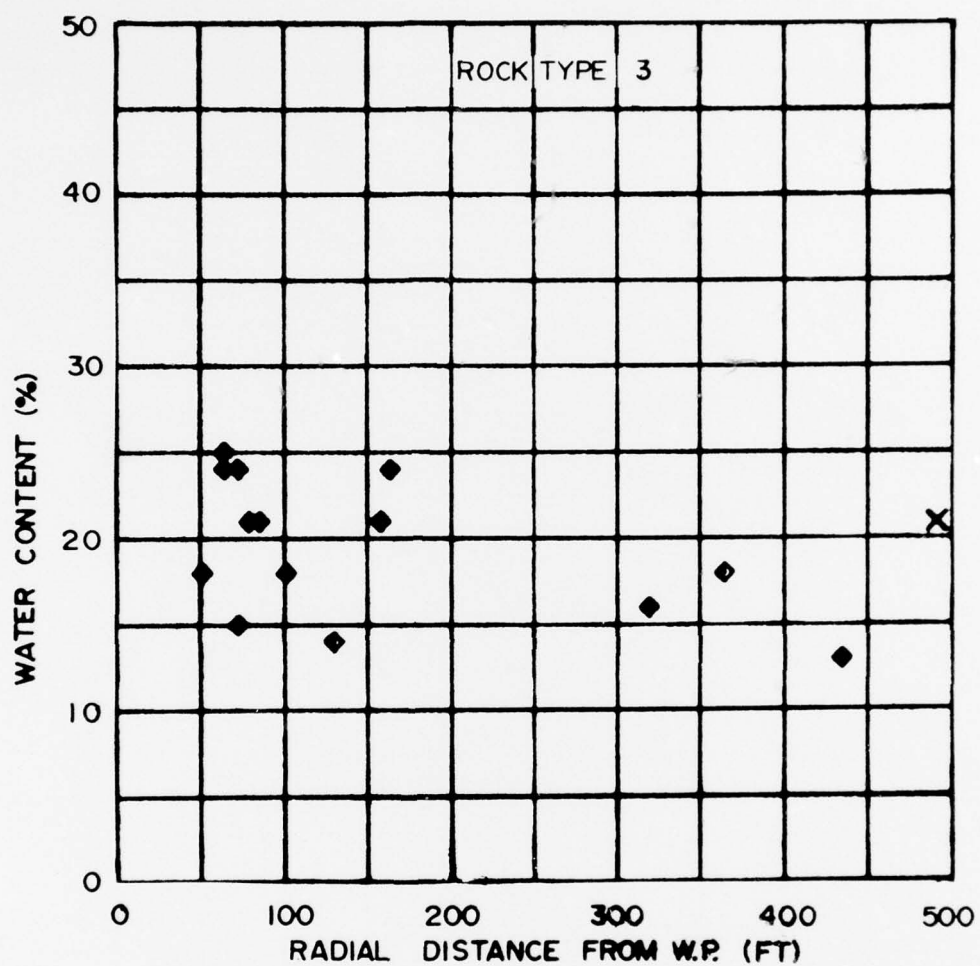


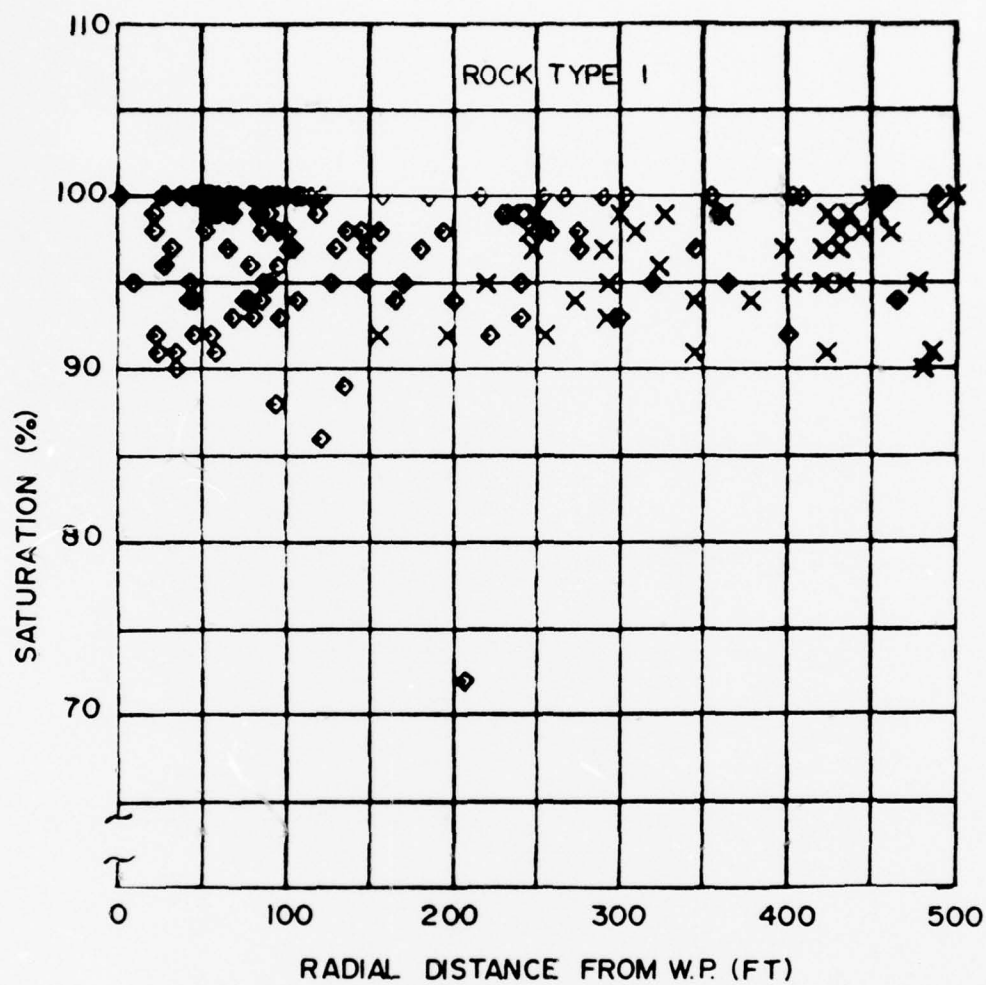


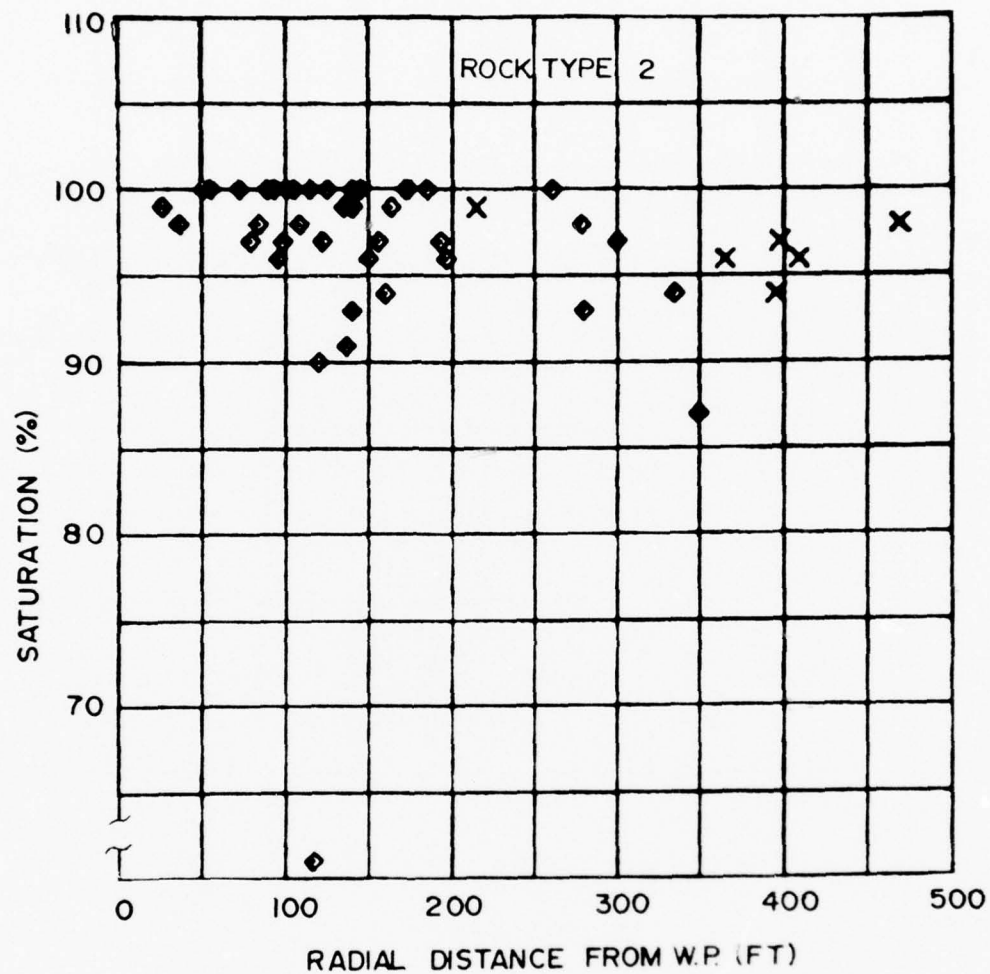


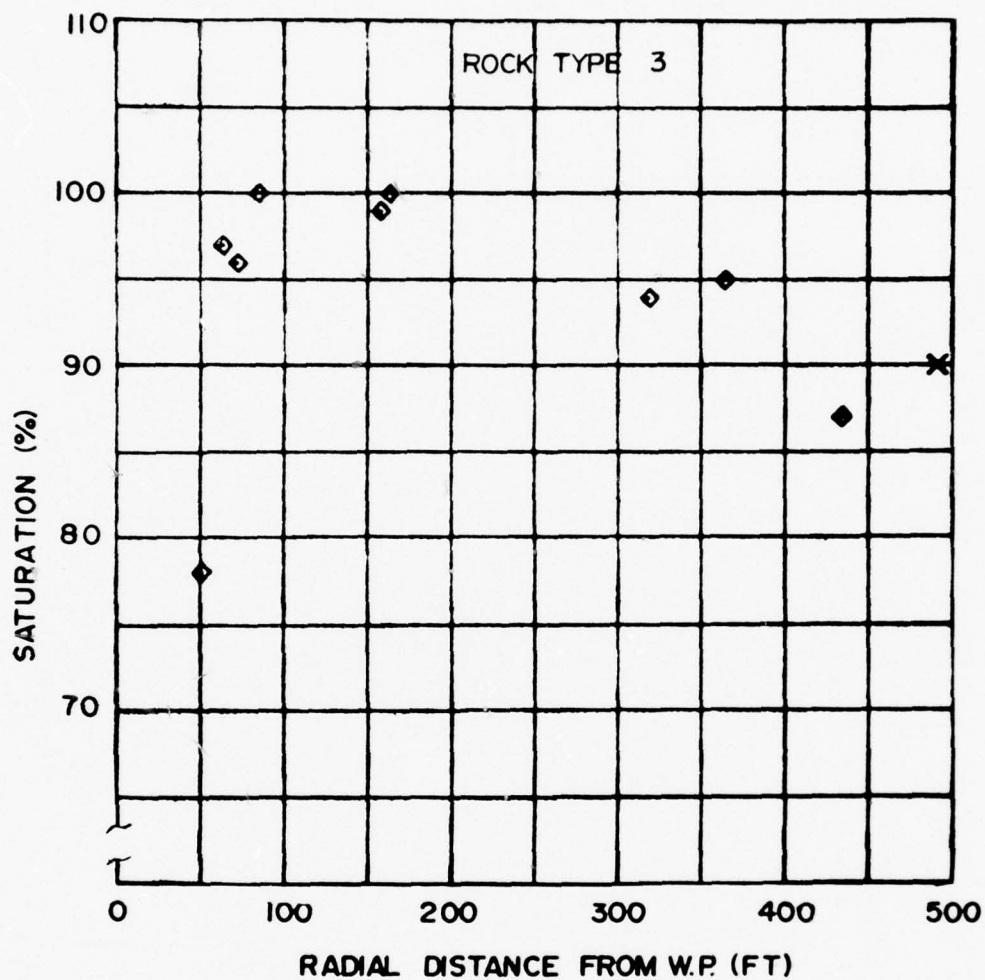


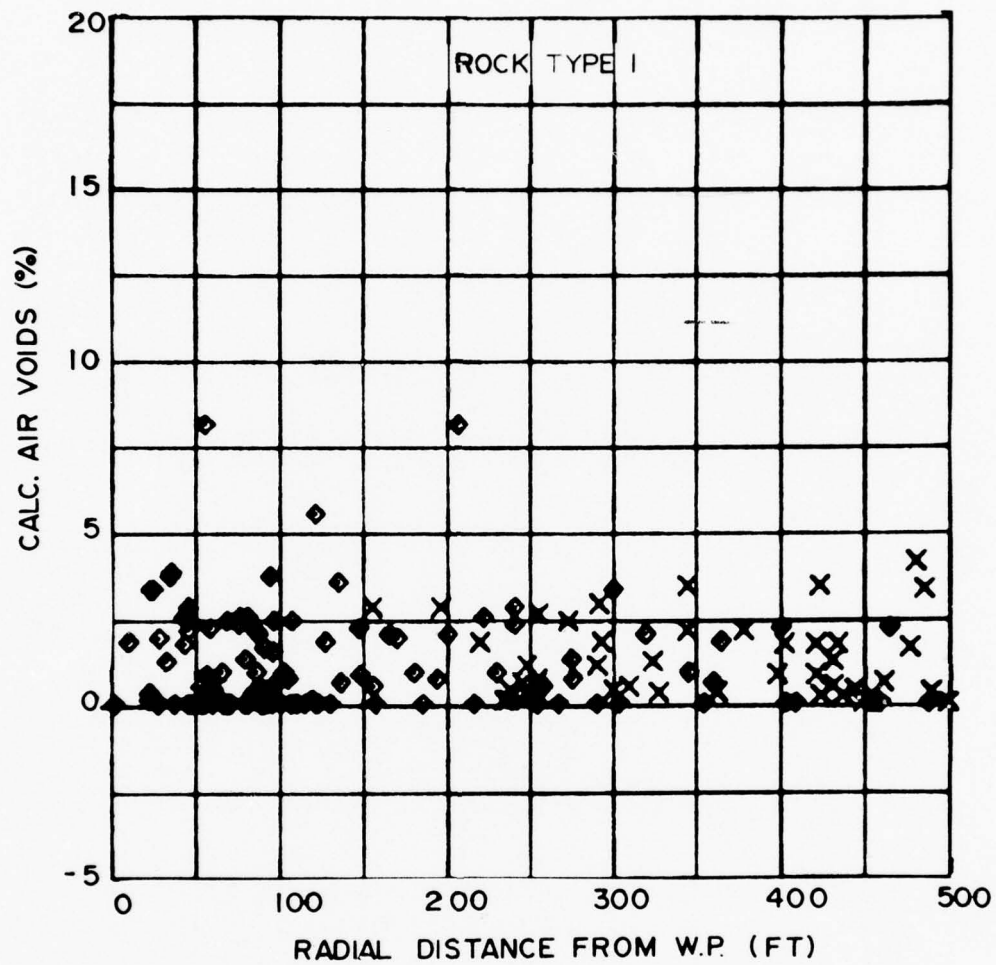


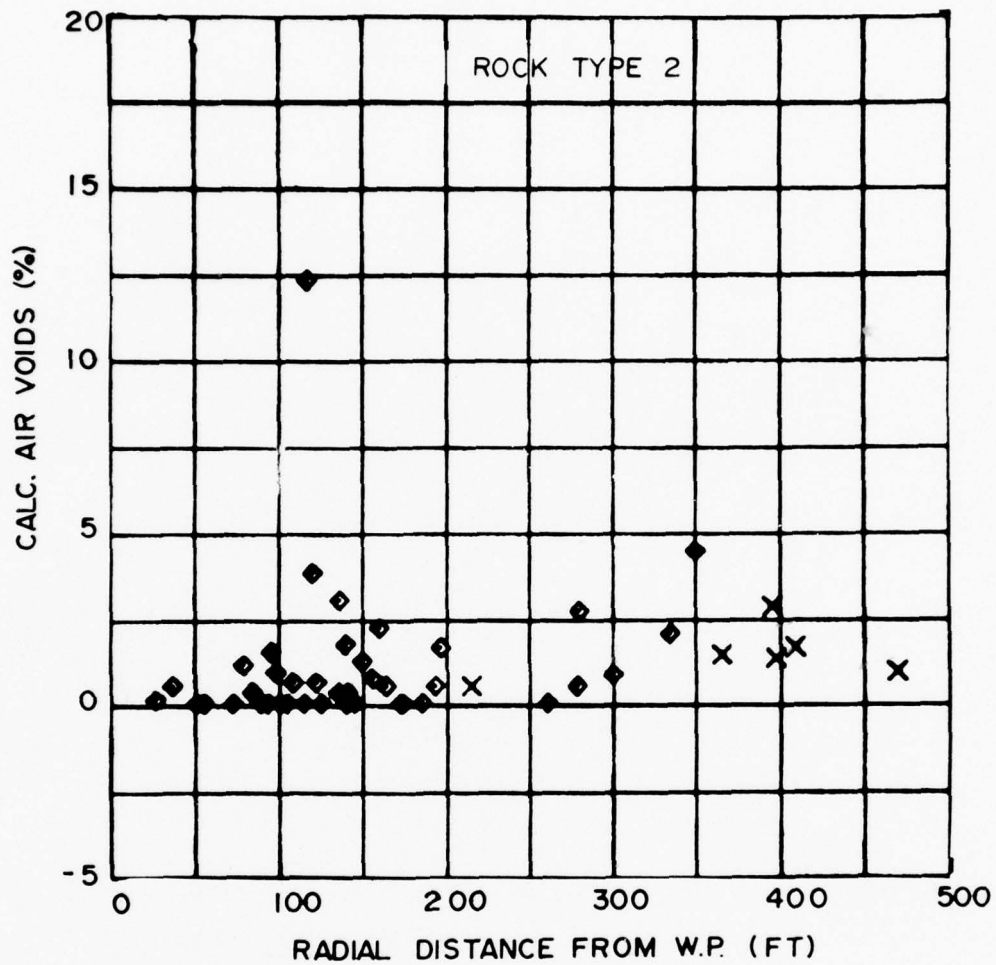


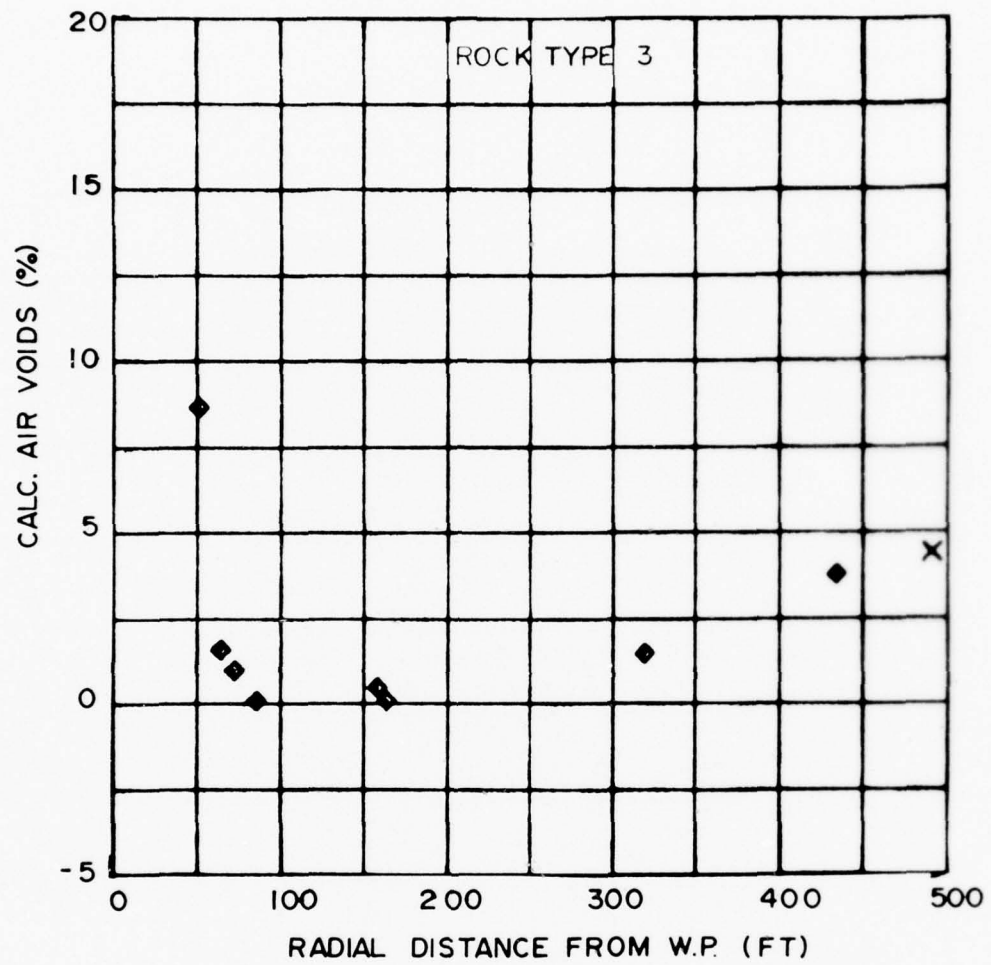


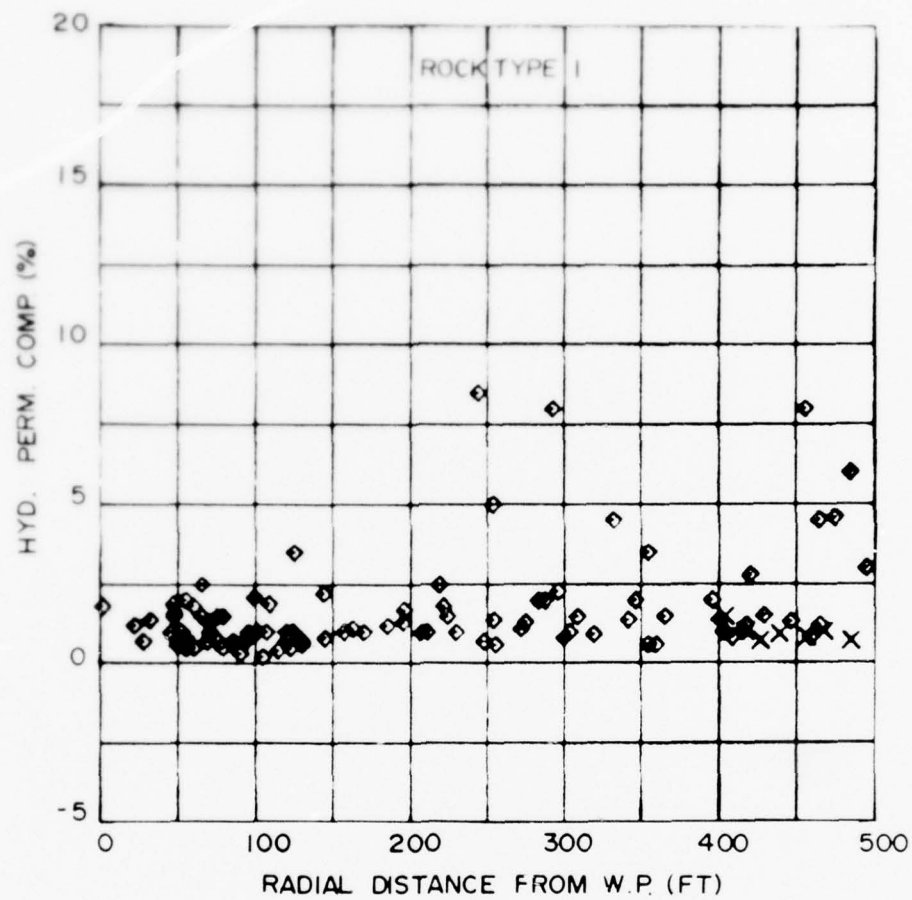


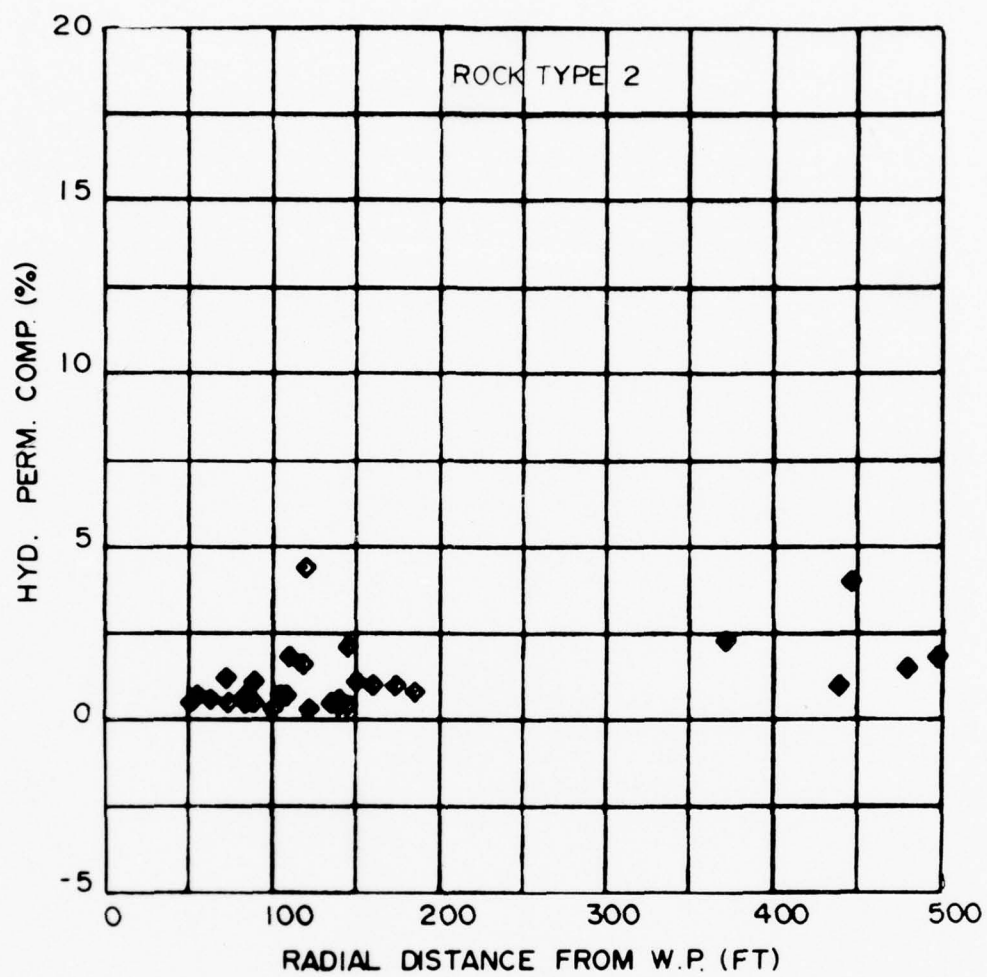


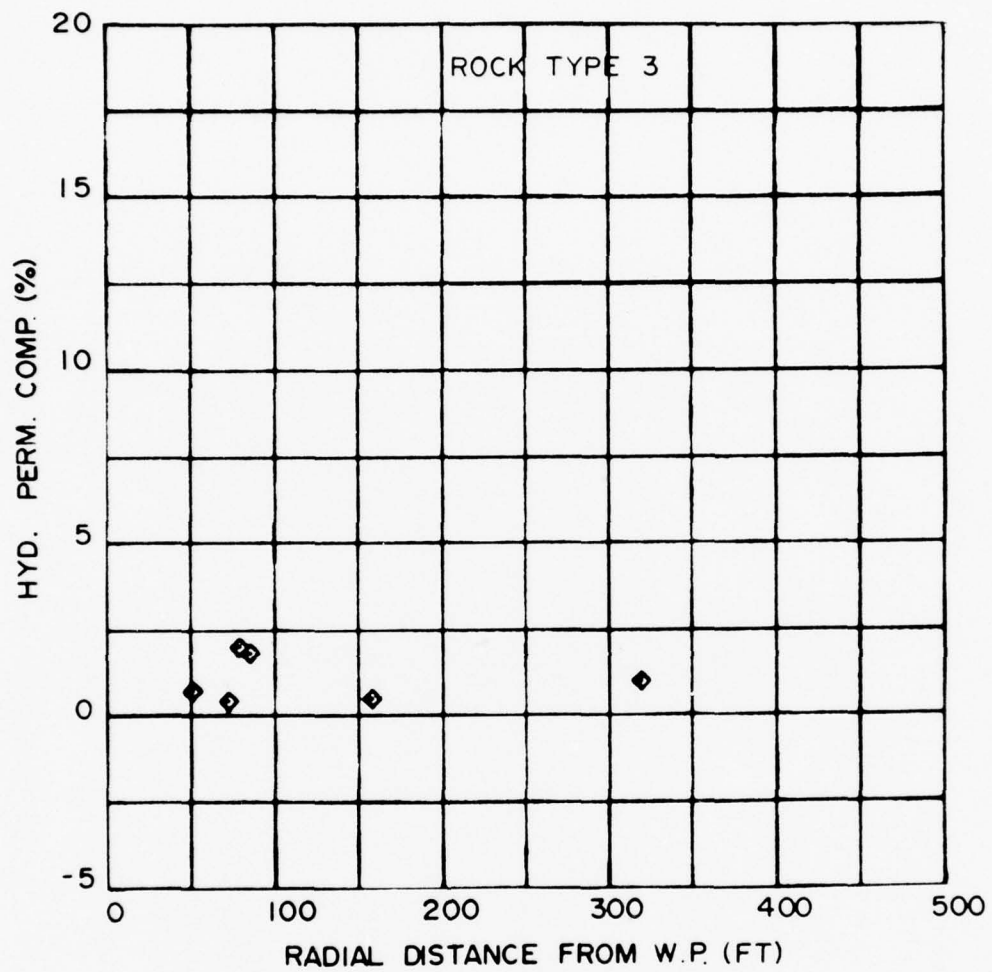


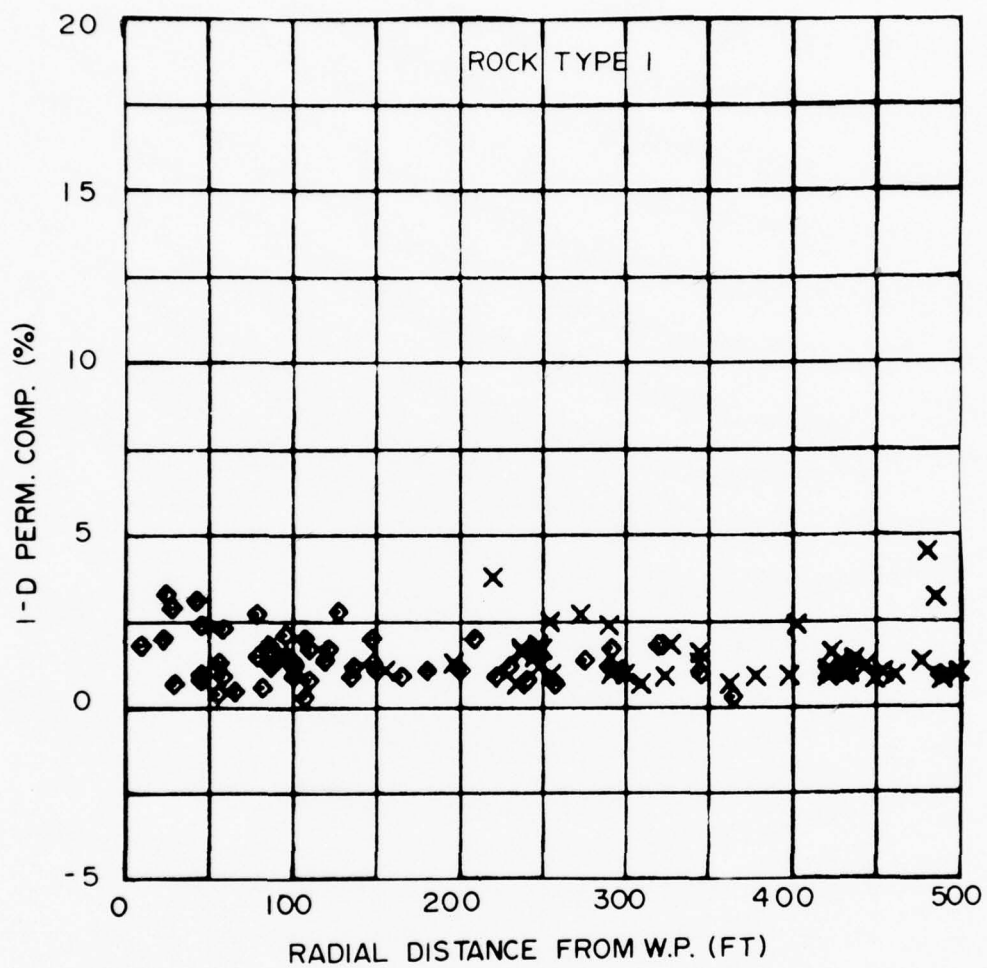


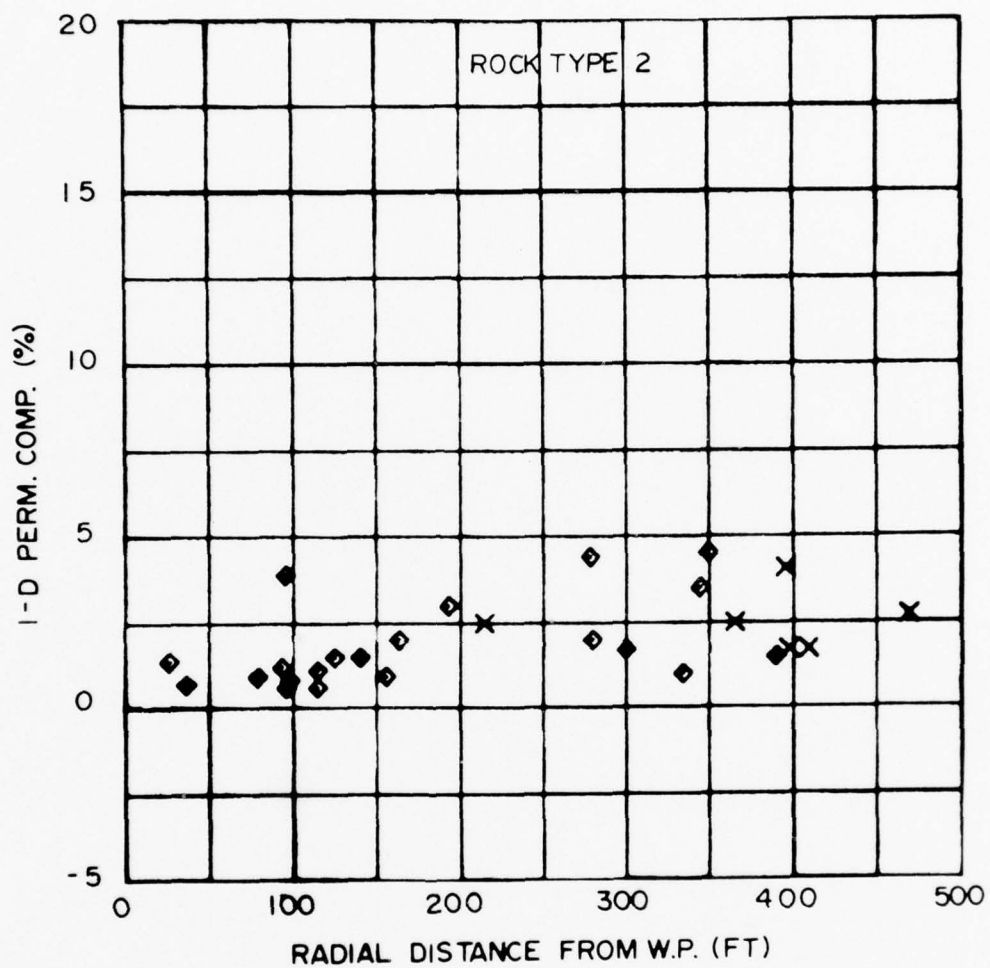


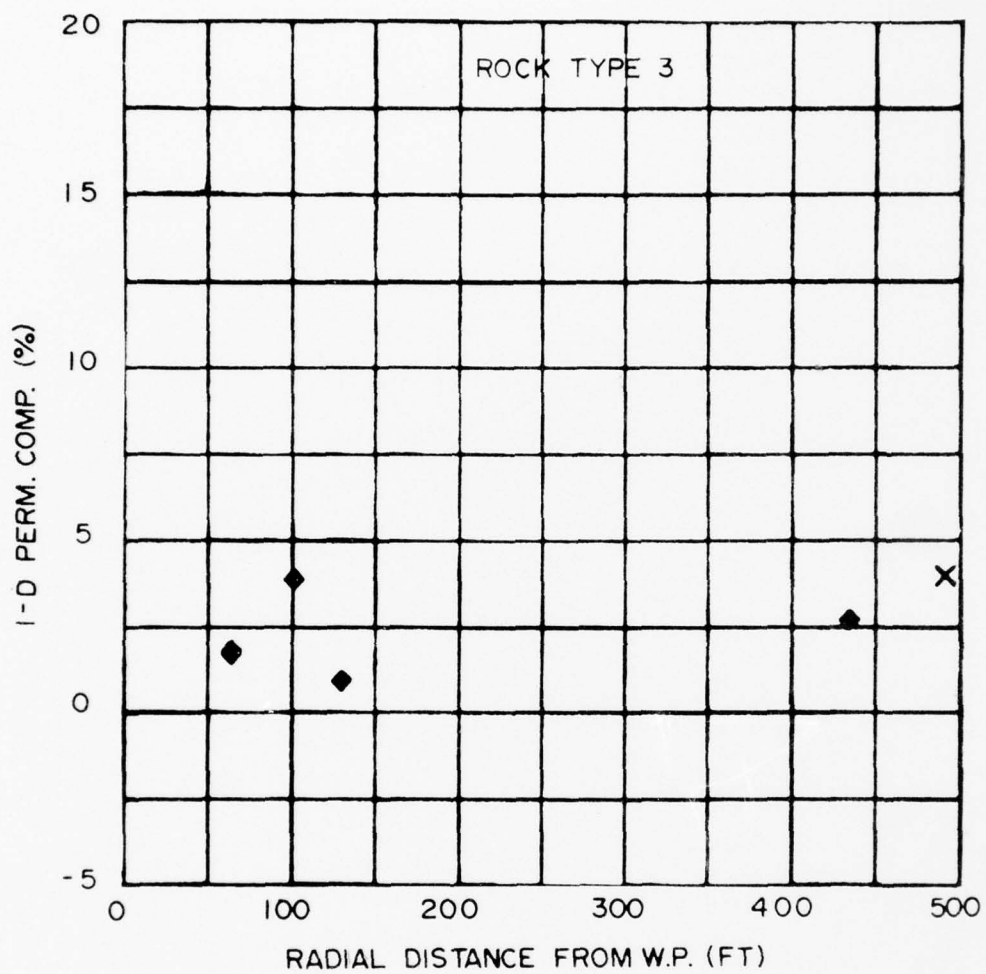


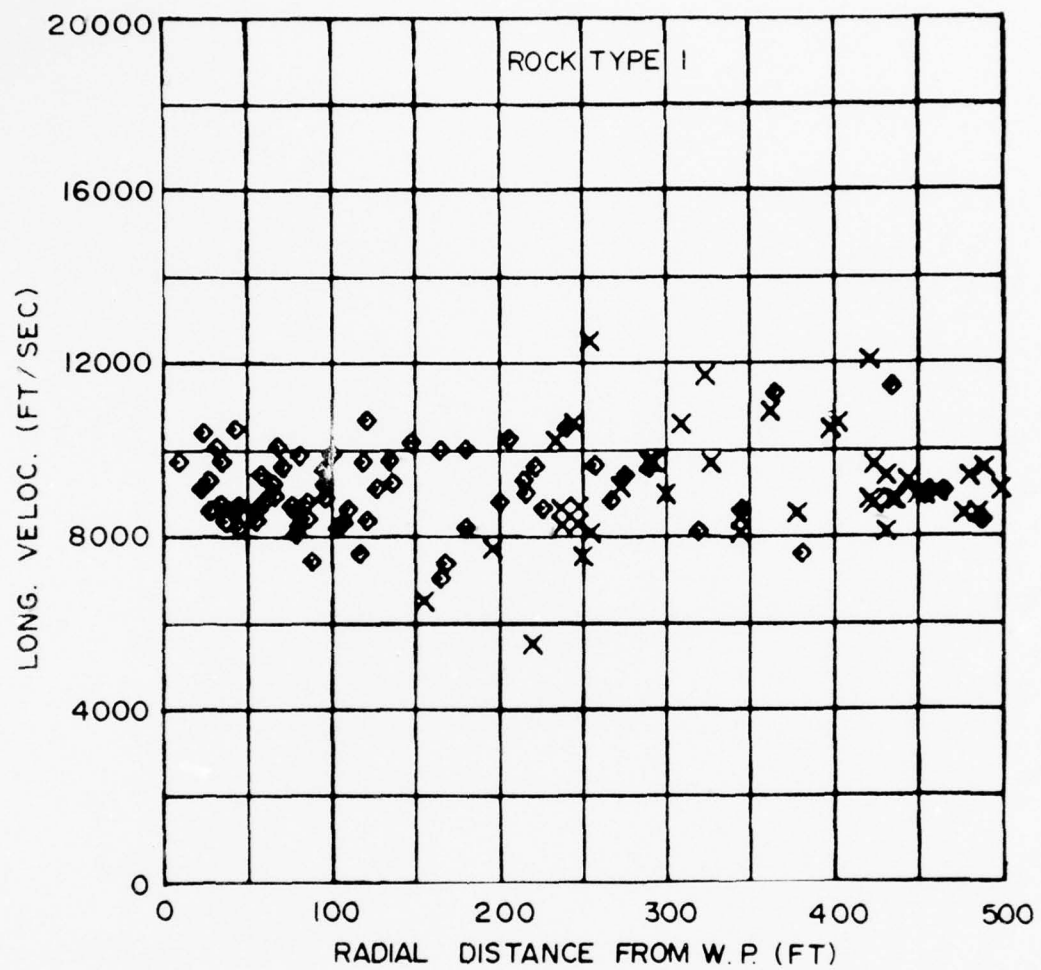


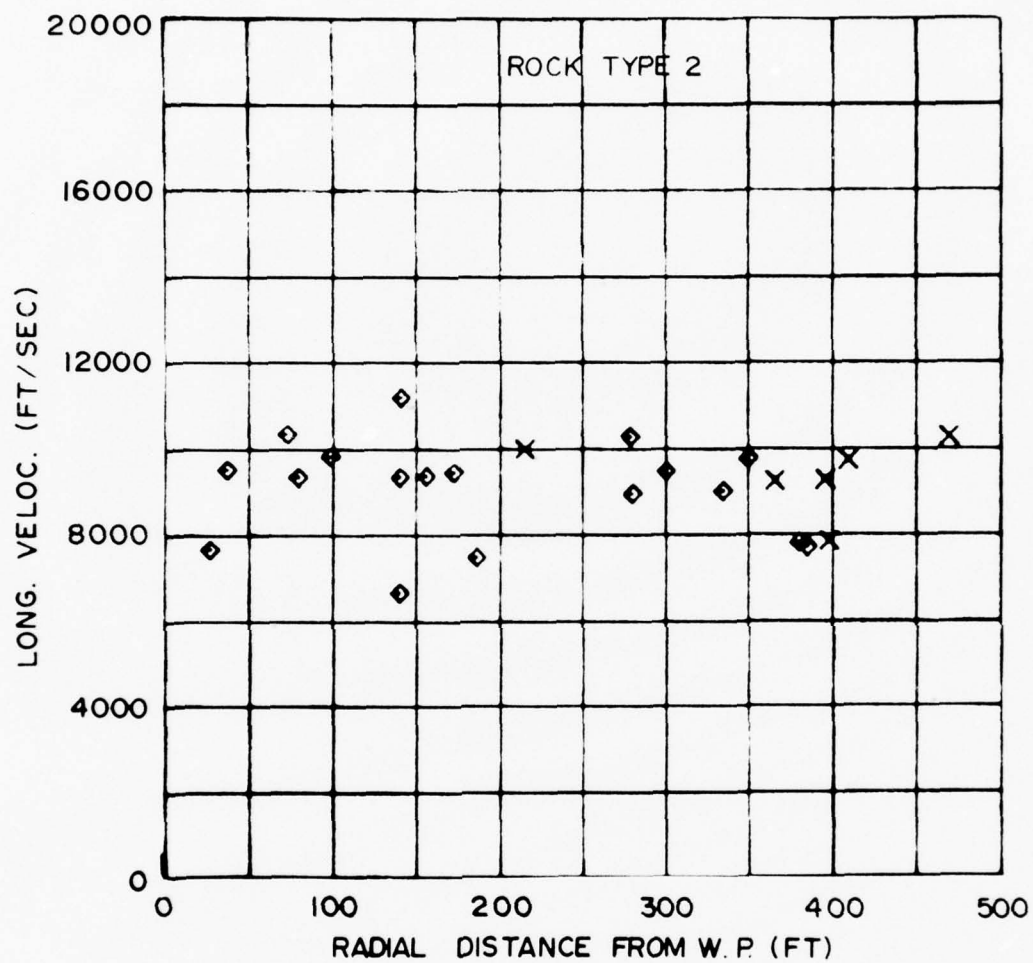


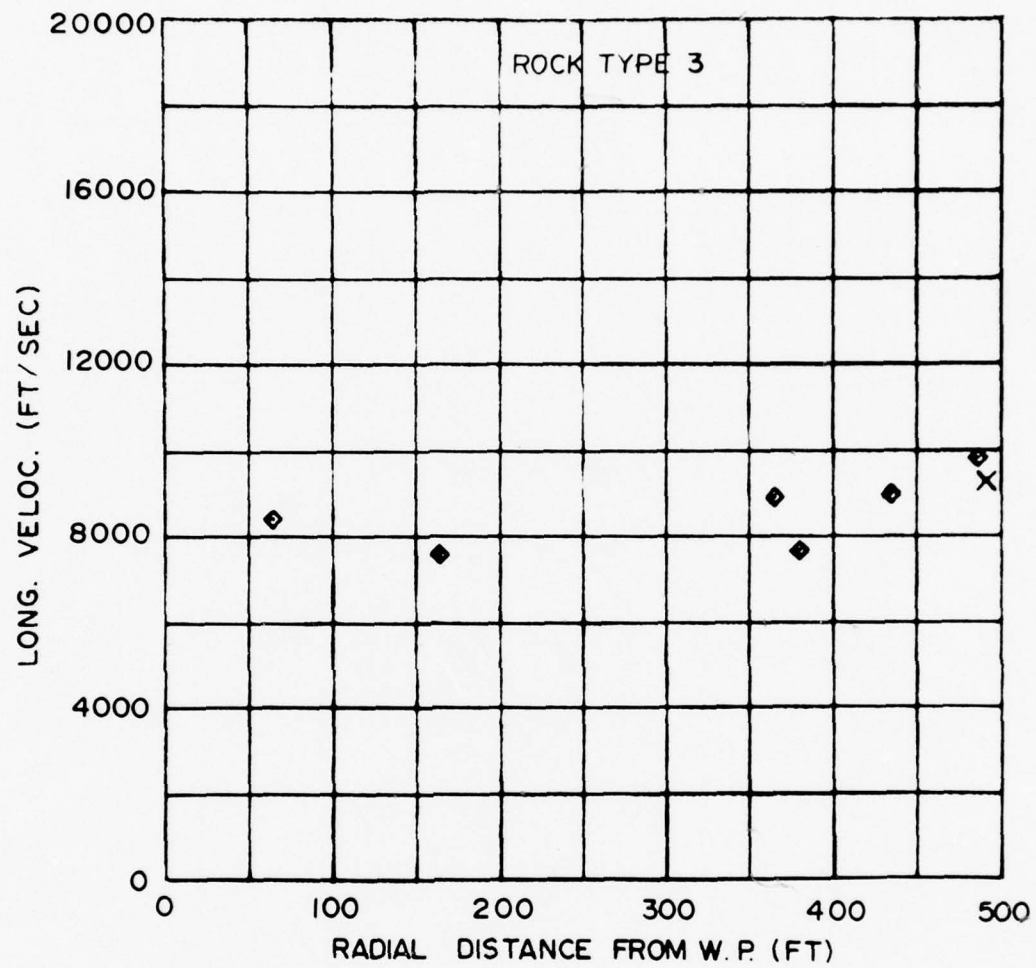


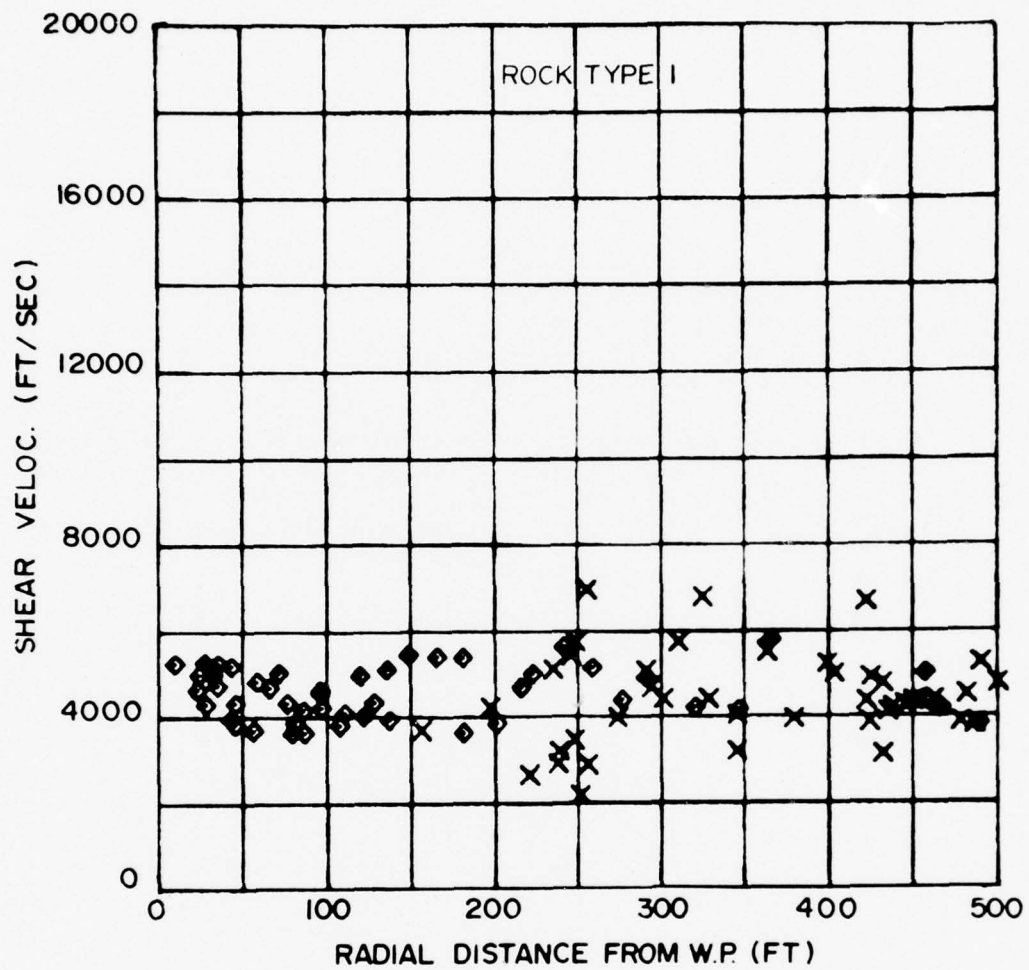


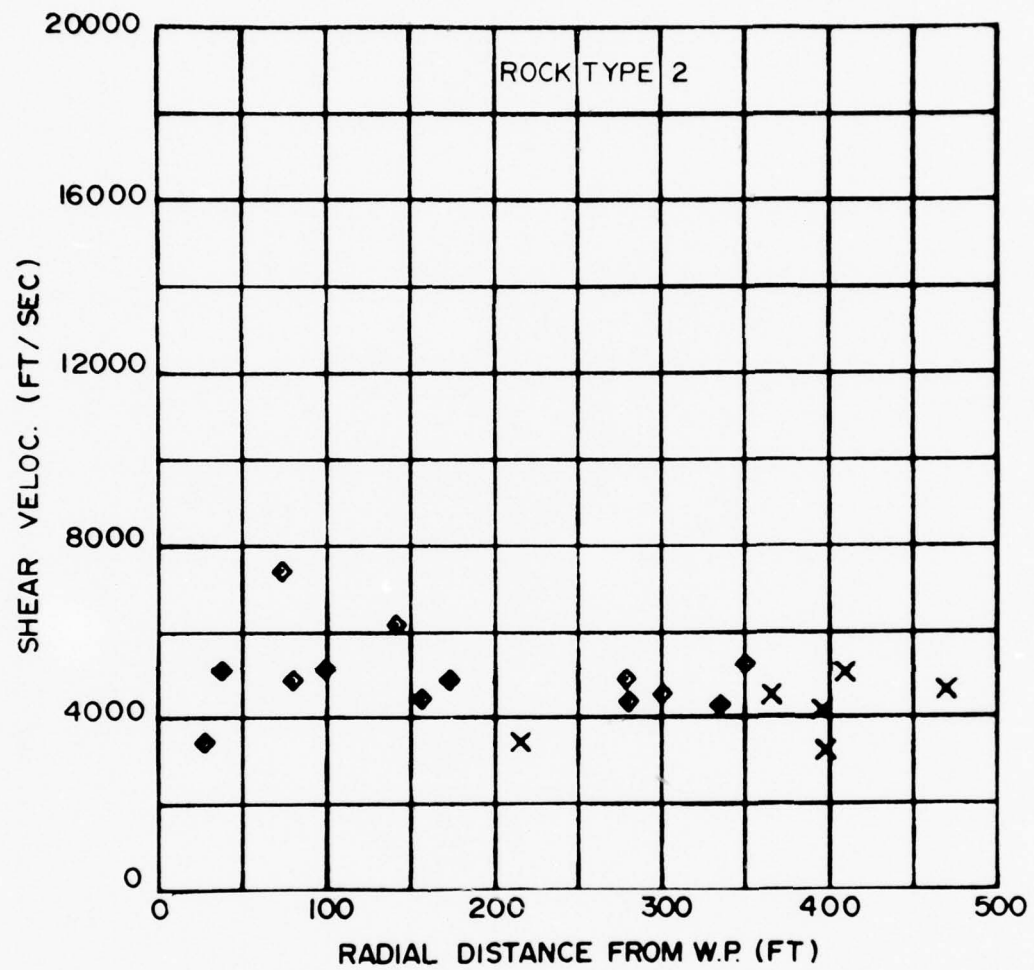


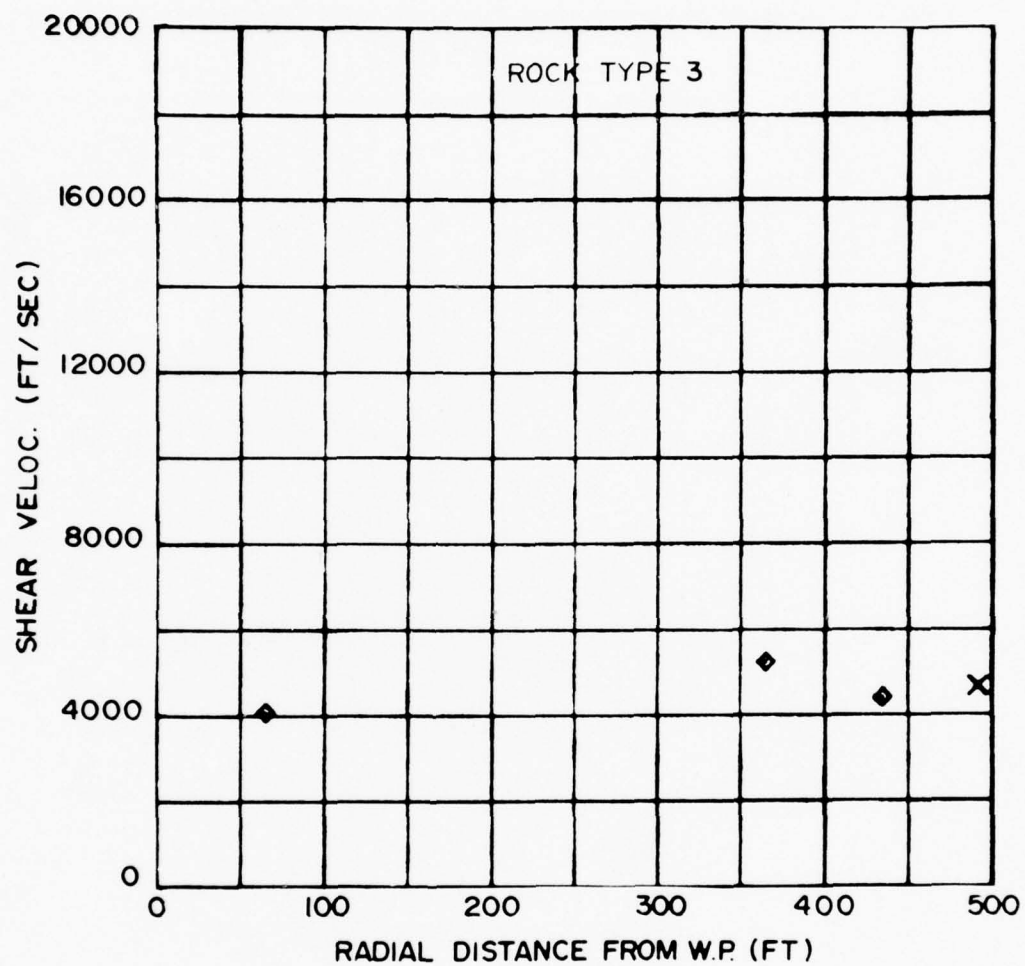


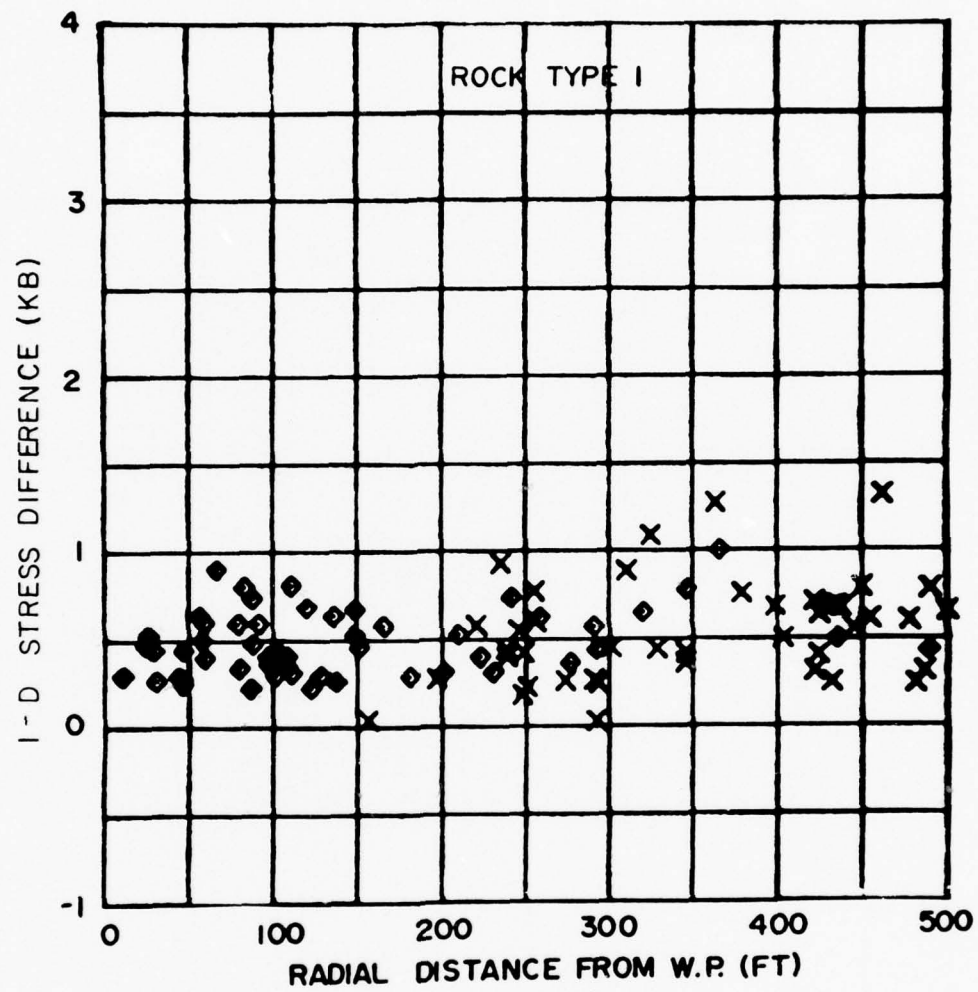


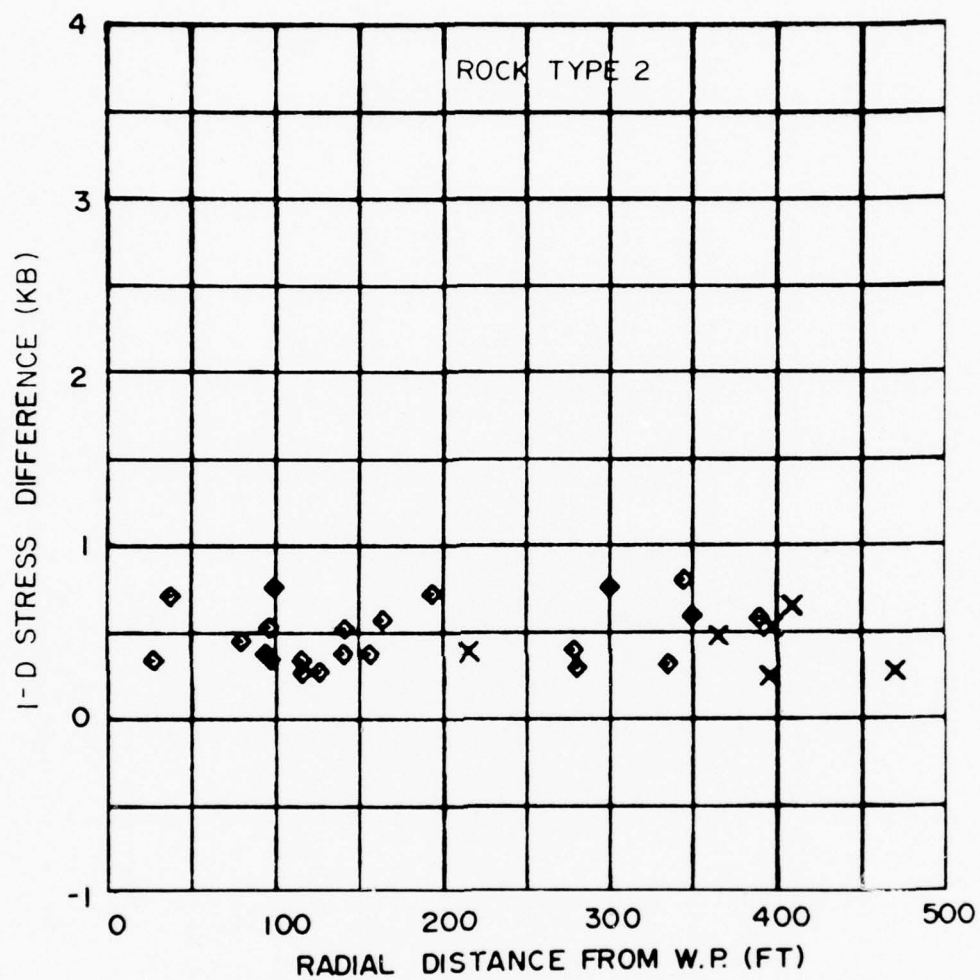


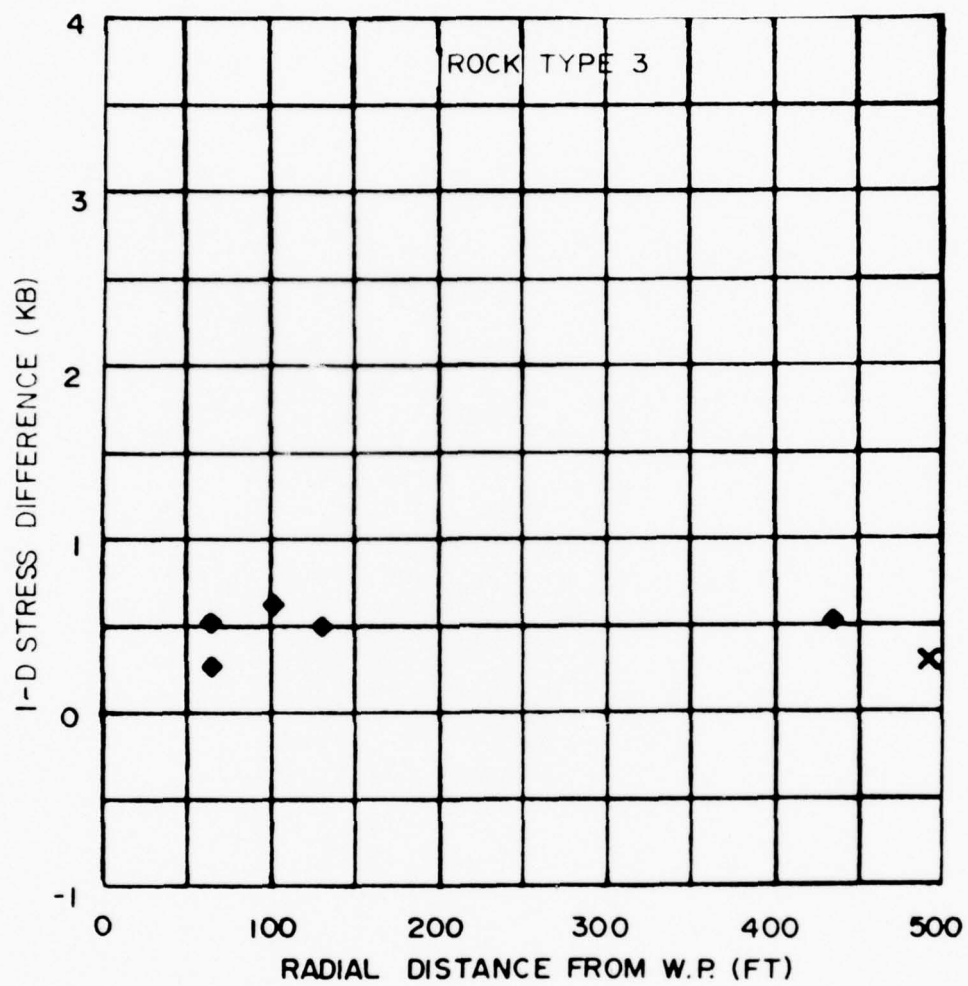












Preceding Page BLANK - NOT FILMED

DETERMINATION OF THE
ANGLE-OF-INTERNAL-FRICTION
FOR NTS TUFFS

by

W. F. Brace
S. J. Green
A. H. Jones
S. W. Butters

Submitted to
Defense Nuclear Agency
Nevada Test Site
Mercury, Nevada 89023

Attn: J. W. LaComb
Field Command

Contract No. DNA-001-75-C-0260

Submitted by
Terra Tek, Inc.
420 Wakara Way
Salt Lake City, Utah 84108

TR 75-38
July 1975

PREFACE

Discussions with Joe LaComb, DNA Field Command, and inquiries from those doing calculations for design for tunnel structures in the tuffs have lead to consideration of "Angle-of-Internal-Friction Models". That is, Terra Tek is called upon to provide the angle-of-internal-friction for the tunnel bed tuffs to be used presumably in a Coulomb model relating shear stress and normal stress at failure. Intuitive reasoning as well as data available indicate the ambiguity related to any estimate of angle-of-internal-friction for the intact tuffs. This brief write-up is an attempt to clarify the angle-of-internal-friction model for the tuffs and to help suggest what tests might be most suited to provide an adequate model.

INTRODUCTION

In compression, granular materials like soils fail in shear. From the stresses at failure, the shear and normal stresses, τ and σ respectively, can be calculated. Typically for soils¹, shear and normal stresses at failure are related by

$$\tau = \tau_0 + \mu \sigma_\eta \quad (1)$$

where τ_0 and μ are constants. τ_0 is the so-called cohesion and μ the coefficient of internal friction, or the arc tangent of the angle-of-internal-friction η . Ideally, granular materials are cohesionless, i.e. $\tau_0 = 0$. Similarly for ideally cohesive media the angle-of-internal-friction is zero. This linear relationship between τ and σ_η is equivalent to

$$\sigma_1 = a \sigma_3 + b \quad (2)$$

and to

$$\sigma_D = c \sigma_3 + b \quad (3)$$

where a , b and c are constants, σ_1 is the maximum and σ_3 the least compressive stresses, respectively; σ_D is the stress difference, $\sigma_1 - \sigma_3$. If (1) is linear for a particular material, then (2) and (3) will also be linear. These are standard concepts in soil mechanics, where (1) is called the Coulomb Law. Figure 1 depicts Equation 1 as the envelope to the Mohr's circles for the ultimate strength of a rock under different stress states. Individual circles are derived from the maximum stress (σ_1) and minimum stress (σ_3) at failure in a single test. The individual circles are centered at $(\sigma_1 + \sigma_3)/2$ with radius $(\sigma_1 - \sigma_3)/2$.

How valid are these ideas for rocks? Is there such a thing as a coefficient of internal friction (angle-of-internal-friction) for a rock? We will briefly discuss these questions below and also give some indication of the role of (a) intermediate principal stress, (b) pore pressure, (c) initial anisotropy (preexisting fractures), (d) *in situ* stress, and (e) effect of measurement technique.

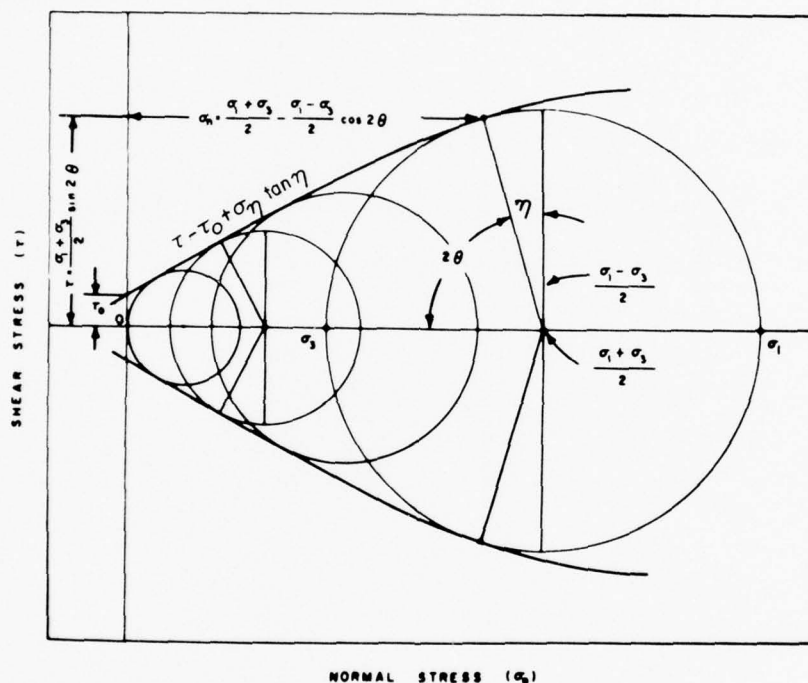


Figure 1. Typical Mohr envelope for ultimate strength of rock. Mohr stress circle with diameter $(\sigma_1 - \sigma_3)/2$ and center at $(\sigma_1 + \sigma_3)/2$ gives values of shear stress, τ , and normal stress, σ_n , on planes inclined at angles $\pm 2\theta$ to direction of σ_1 . Mohr envelope tangent to series of circles from data of triaxial compression tests gives values of cohesive strength, τ_0 , from zero normal stress intercept and coefficient of internal friction, $\tan \eta$, from slope. At tangent points $\theta = \pm 45 \mp \eta/2$. Envelope curves toward σ_n -axis, showing that $\tan \eta$ is not necessarily constant.³

GENERAL APPLICABILITY TO ROCKS

To begin with, failure of rocks is more complicated than failure of soils^{2,3}. Consider the suite of stress-strain curves for limestone in Figure 2. At low effective pressures, stress first peaks and then falls to a lower, or residual value. At the peak stress a fault or fracture is formed; at the residual stress the two parts of the fault slide on one another. The residual stress, therefore, is a measure of frictional resistance of the fault to sliding.

If the peak and residual values for one rock at different confining pressure are compared (Figure 3) two curves result, one for fracture and one for frictional-sliding. Here σ_n is the normal stress on the fracture and is not the principal stress as seen in Figure 1. The results shown

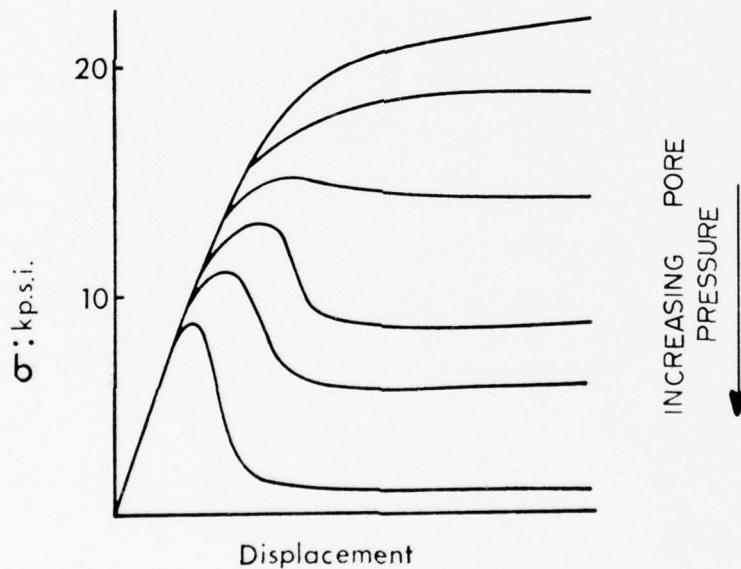


Figure 2. The effect of pore-pressure on the brittle-ductile transition in limestone at a confining pressure of 10 kpsi.²

in Figure 3 indicate that the frictional-sliding shear strength is always less than or equal to fracture strength (frictional-sliding shear strength is zero at zero confining pressure).

From Figure 3 the ambiguity of the failure stress for rocks is apparent. If we take failure to mean the maximum stress which can be maintained in a particular rock mass, then this maximum will depend on whether the rock is already fractured or not and the nature of the fracture. If the rock mass is intact the upper curve in Figure 3 will likely apply for the initial loading⁴; if the rock mass is already fractured, then the failure stress will be lower. It should be noted that slip of large blocks within a jointed rock mass is probably not represented by the lower curve since block interaction due to combined sliding on two intersecting inclined failure planes (joints or faults) complicates the mode of failure^{5,6}.

The failure curves in Figure 3 have the same general form as the Coulomb law (Figure 1) but the fracture curve is very nonlinear. Fracture curves of four other rocks are given in Figure 4 where it can be seen that they are also decidedly nonlinear. The frictional-sliding curves are not available for these rocks, but for most rocks they are closer to being linear, as suggested by the lower curve in Figure 3. For frictional-sliding Byerlee⁷ has found the slope μ has a relatively small range from about .55 to .65, more or less independent of mineralogy. Presumably these values are equivalent to the coefficient of internal friction as defined by the Coulomb law for soils.

The applicability of the Coulomb law is less clear for intact rock, inasmuch as the failure curves for intact rock (Figure 4) are nonlinear. One way around this nonlinearity is to consider only a limited range of

confining pressure. In Figure 4, for example, the failure curves for Mixed Company sandstone, granite and shale are nearly linear up to a pressure (σ_3) equal to the unconfined compressive strength, C_0 . Over that limited range we can define a slope which might be called an angle-of-internal-friction. As seen in Figure 4, this slope varies considerably from one rock to another (quite differently than the relatively constant value of the angle-of-internal-friction for frictional-sliding). This is seen in another way in Figure 5 which is a compilation of fracture

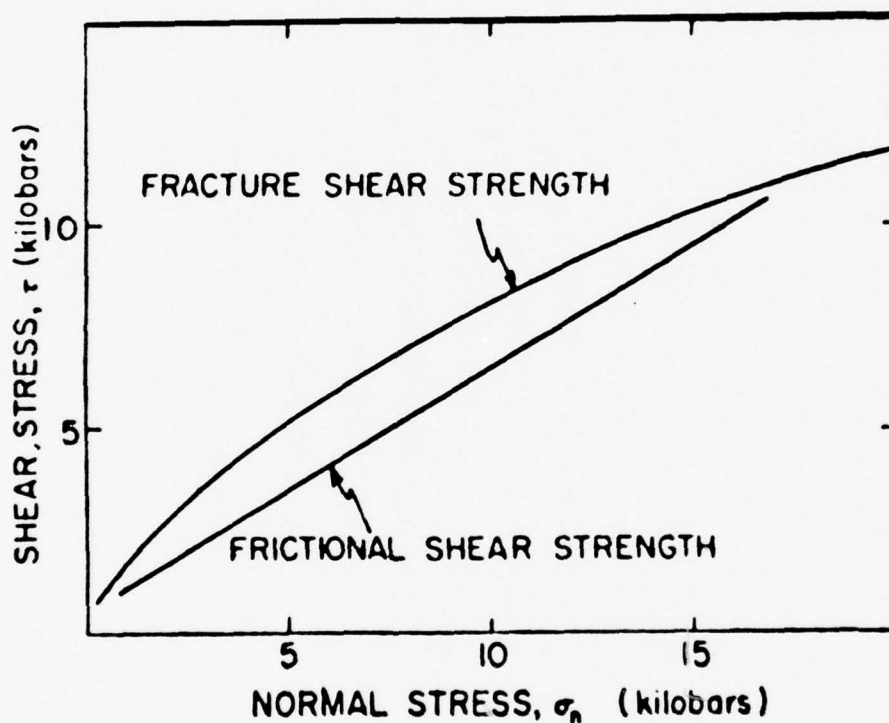


Figure 3. Fracture shear strength and frictional shear strength versus normal stress for westerly granite.⁷

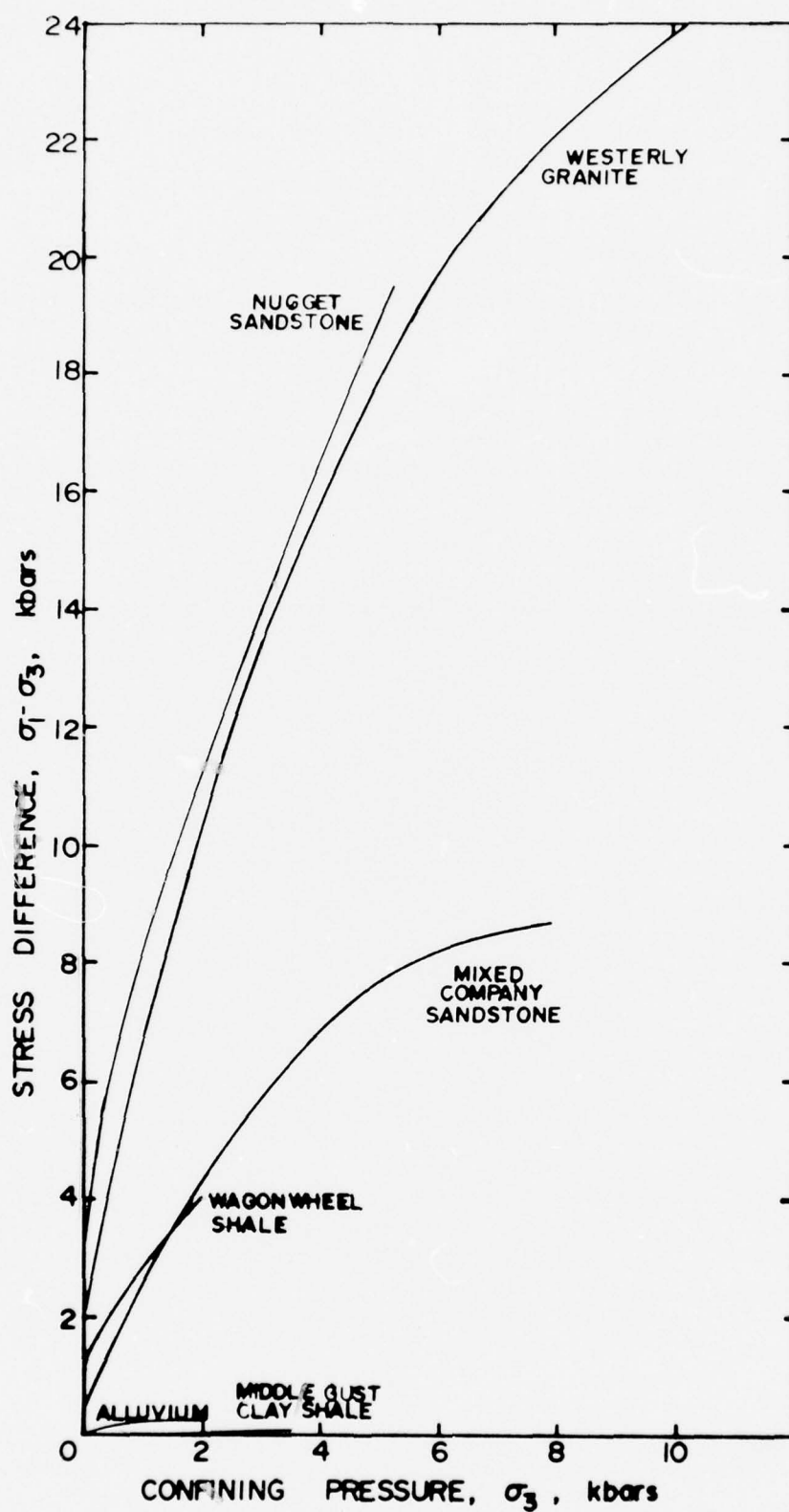


Figure 4. Failure Curves for Rocks and Soils

stresses, σ_1 , versus confining pressure, σ_3 , for 32 rocks where the data have been normalized by dividing by C_0 . The slopes (for fracture stress) range from about 0.5 to somewhat over 1.0.

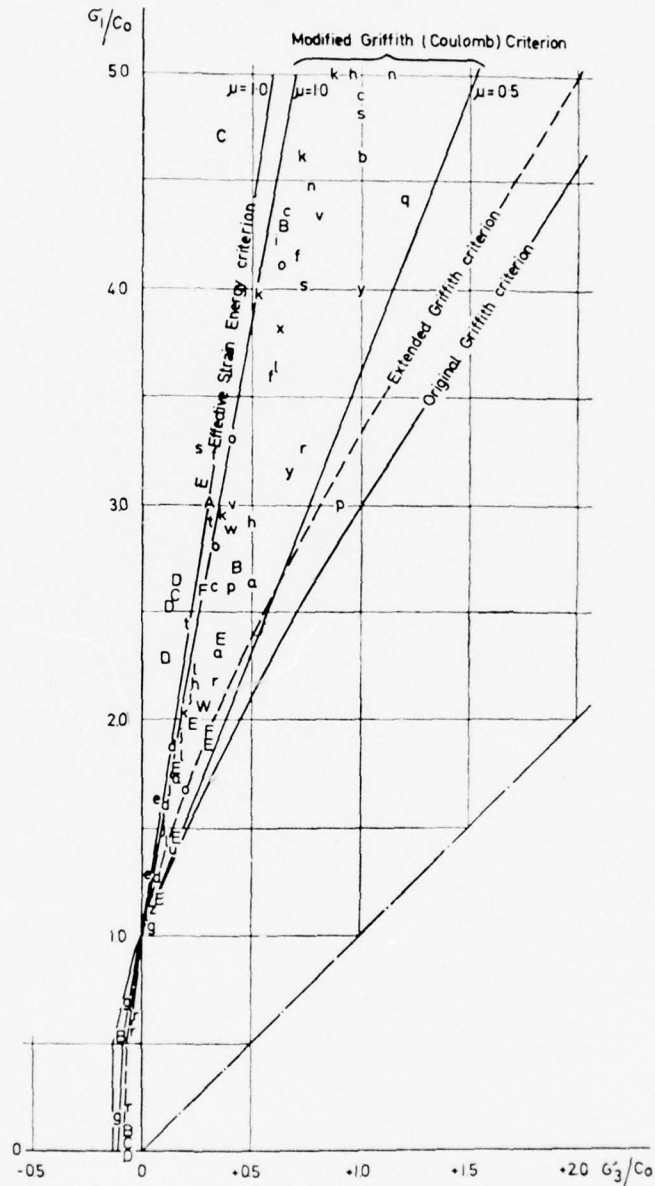


Figure 5. A comparison between the measured strengths of rock and various failure criteria.²

Other Considerations Affecting the Angle-of-Internal-Friction

Intermediate Principal Stress σ_2 : Byerlee⁷, Mogi⁸, Green, et al⁹, Swanson¹⁰ and Christensen, et al¹¹ have shown that the effect of σ_2 on the fracture stress is small and on the frictional-sliding stress negligible. For example, fracture strength is as much as 10 percent higher when $\sigma_2 = \sigma_3$; the effect on the slope of the fracture curve is even less noticeable for the one or two rocks for which this has been investigated.

Pore Pressure: The fracture strength of saturated rocks is considerably reduced in comparison to the dry rock strength even though the presence of fluids per se has little effect on the frictional-sliding coefficient. Additionally, elevated pore fluid pressure is known to have significant effect on fracture stress (see Figure 2) but its effect on frictional-sliding is unclear. The fracture stress has been found to be a function of the least effective stress. Therefore, other things being constant, an increase in the pore pressure will result in an increase in the apparent (fracture) coefficient of internal friction. This will probably not be the case with frictional-sliding shear strength, for, as noted above, its slope is not very dependent on the normal stress, σ_n .

Initial Anisotropy: Since most sedimentary and metamorphic rocks are anisotropic, the effect of anisotropy on failure is of importance. Determination of the mode of failure requires knowledge of the orientation of the principal stresses to the principal material directions. Little experimental work has been performed to delineate the complete failure surface for anisotropic materials, and frictional-sliding tests have normally been limited to determining shear strength along through going planes of weakness. More work is needed to understand the apparent coefficient of internal friction for either fracture or frictional-sliding for anisotropic materials.

In Situ Stress: *In situ* stress may also be an important factor, although it is not yet well understood. One approach, and it is the only one possible at present, is to add any known *in situ* ambient stress to the known applied stress, including the known *in situ* pore fluid pressures. This could cause changes in apparent coefficient of internal friction much as does change in pore pressure alone as noted above.

Effect of Measurement Technique: For soils, μ is usually determined in triaxial tests. Results from a direct shear test¹² should be nearly identical but the authors have seen no comparisons. For rocks, failure curves such as shown in Figures 2 and 3 are generally determined in triaxial tests, although Terra Tek¹³ has tested intact homogeneous rock to failure in a direct shear machine. Comparable failure stresses should, in principle, be obtainable; however, there are complicating factors such as inhomogeneous stress distribution due mainly to the nature of the loading.

To study the effect of nonhomogeneous stresses, Goodman¹⁴ performed finite element analysis of triaxial specimens containing inclined joints more compressible than the surrounding rock. The results indicated very uneven stress distributions along the joint and totally different concentrations of stress in the upper and lower walls of the joint. For these reasons Goodman concluded that the multistage triaxial is probably not a good test for seams or joints of shear origin.

Goodman has also discussed the problems of producing uniform stress distribution inside a direct shear box. He notes that due to joint thickness, the applied forces and reactions introduce turning moments to effect a nonuniform distribution of normal pressure along the sliding surface. Goodman also notes that the shear strength characteristics determined in direct shear tests are also dependent on the boundary conditions.

Neglecting the loading inhomogeneities, the major concerns are pore pressure and drainage conditions in triaxial versus direct shear tests. The pore pressure in triaxial tests is dependent on the rock permeability and the rate of loading. Material close to the shear surface in the direct shear tests will be drained except at very high loading rates, whereas it will likely remain undrained within the triaxial cell even at lower loading rates. This would cause a marked difference in effective stress at the failure surface and, at least for the fracture stress, a significant difference in the value of μ .

CONCLUSIONS

To sum up, then, the linear Coulomb relation (1) appears generally applicable to rocks when through going faults are already present; μ is $0.5 \pm .05$ for through going faults regardless of rock type. For intact rock, it is only applicable for a limited range of confining pressure, $\sigma_n/C_0 < 1$, and even then only for certain rocks. Within this pressure range, μ for fracture can be expected to vary from 0.5 to 1.5. Since there is such a wide range, it will have to be determined experimentally for any particular rock.

Since at the present time rock mechanics literature does not provide a comparison of coefficient of friction obtained from both triaxial and direct shear tests, there is a need to perform such a program over the normal stress range, σ_n , of interest. If the data appear sensitive to test conditions, a knowledge of how the data is to be used will allow selection of results best suited to meet the calculational needs here.

REFERENCES

1. R. F. Scott, *Principles of Soil Mechanics*, Addison-Wesley, 1963.
V. V. Sokolovskii, *Statics of Granular Media*, Pergamon Press, 1965.
2. J. C. Jaeger and N. G. W. Cook, *Fundamentals of Rock Mechanics*, Methuen, 1969.
3. S. P. Clark, Jr., *Handbook of Physical Constants*, The Geological Society of America, Inc., Memoir 97, 1966.
4. W. Wawersik, "Deformability and Strength of Singly- and Multiply-Jointed Sandstone," Terra Tek Report TR 74-4, January 1974
5. H. R. Pratt, W. F. Brace, A. D. Black and W. Brown, "A Technique for Measuring The Deformation and Frictional Properties of In Situ Rock," Terra Tek Report TR 73-15, April 1973.
6. H. R. Pratt, A. D. Black and W. F. Brace, "Friction and Deformation of Jointed Diorite," Terra Tek Report TR 74-13, March 1974.
7. J. D. Byerlee, "The Frictional Characteristics of Westerly Granite," Ph.D. Thesis, M.I.T., 1966.
8. K. Mogi, "Effect of Intermediate Principal Stress on Rock Failure," *J. of Geophys. Res.*, 72, 1967, pp. 5117-5131.
9. S. J. Green, J. D. Leasia, R. D. Perkins and A. H. Jones, "Triaxial Stress Behavior of Solenhofen Limestone and Westerly Granite at High Strain Rates," *J. of Geophys. Res.*, 77, 1972, pp. 3711-3724.
10. S. R. Swanson, "Representation of the Post-Fracture Mechanical Behavior of Nugget Sandstone," Terra Tek Report TR 71-13, March 1971.
11. R. Christensen, S. R. Swanson and W. Brown, "Torsional Shear Measurements of the Frictional Properties of Westerly Granite," Terra Tek Report TR 73-64, September 1973.
12. R. S. Rosso, E. R. Simonson, W. Wawersik and A. H. Jones, "Determination of the Properties of Jointed Oil Shale," Terra Tek Report TR 74-60 December 1974.
13. R. S. Rosso, "Rock Strength and Joint Property Data for the Mahoning Dam Site," Terra Tek Report TR 75-34, July 1975.
14. R. E. Goodman, "The Deformability of Joints," Winter Meeting American Society for Testing and Materials, Denver, Colorado, 2-7 February 1969. ASTM Special Technical Publication 477, Determination of the In Situ Modulus of Deformation of Rock.

PROGRESS REPORT II
WATER EXTRACTION FROM NEVADA TEST SITE TUFFS

by
R. K. Dropek
A. Levinson

Prepared for
Defense Nuclear Agency
Field Command
Albuquerque, New Mexico
Attn: Mr. J. W. LaComb

Sumbitted by
Terra Tek, Inc.
University Research Park
420 Wakara Way
Salt Lake City, Utah 84108

TR 75-52
September 1975

TABLE OF CONTENTS

Introduction	346
Phase I: Extraction Method Investigation	347
Phase II: Chemical Analysis Comparison	350
Phase III: Water Profile Development	354
Conclusions and Suggestions	356
References	357
Appendix A: Water Extraction Methods (Equipment and Procedures) . . .	358

LIST OF FIGURES

1.	Ion and SiO ₂ Concentration Comparison	352
2.	Loading Configuration Schematic for Compression Tests	360
3.	Jacketed Sample and Collection Chamber for Compression Methods	360
4.	Samples, End Caps, and Loading Frame for the Rigidly Confined Sample -- Argon Method	361
5.	Assembled Components for the Rigidly Confined Sample -- Argon Method	361
6.	Hydrostatically Confined -- Argon Method Showing Sample, Per- meability End Caps and Base Plug Connections	362
7.	Jacketed Sample and Collection Chamber for Centrifuging	362

LIST OF TABLES

1.	Results from Extraction Method Investigation	349
2.	Water Extraction Results for Chemical Analysis Comparison	350
3.	Water Extraction Results for Profile Development	355

INTRODUCTION

The hydrology of the Rainier Mesa, specifically the "T" tunnel area, at the Nevada Test Site is of interest to the nuclear test program. To pursue this interest, Terra Tek has been actively developing methods for extracting the water from core samples¹ for subsequent chemical and mineralogical analysis². The development of consistent water data is dependent upon both the method of water extraction and sanitary laboratory conditions. The extraction method is critical since various types of bound waters within the tuff may be extracted at different energy levels.

Water exists in the Rainier Mesa tuff in at least four forms. The water may reside in the pore structure of the material, it may exist as surface absorbed (interlayer) water on clay minerals, it may be an integral component of the clay mineral structure as OH^{-1} ions, or it may exist as zeolitic water within the tubular openings between elongated zeolitic clay structural units³. Consequently, extraction methods were sought which yielded only the type of water that was of particular interest for analysis.

The water extraction program thus far has consisted of three phases. The first phase was to experiment with several possible extraction methods and to analyze the total water yield from each, while the second phase concentrated on analyzing the extracted water for differences in chemical composition using the most efficient methods determined from Phase I². The final phase (which is in progress) has dealt with the extraction of water for hydrology studies using methods which proved satisfactory from the previous investigations. A discussion of each phase with results and conclusions will follow as well as suggestions to future testing procedures based on the present results.

PHASE I: EXTRACTION METHOD INVESTIGATION

In a preliminary investigation¹, water was extracted from tuff by cyclically loading to 2 kilobars hydrostatic pressure after which shear stresses were applied in order to "squeeze" the water from the sample. The volume of water obtained using this method ranged from about 5 cc to 25 cc depending upon sample moisture content. Microscopic analysis of the samples revealed considerable mineral fracture² suggesting locally high stresses on the mineral surfaces. A previous study⁴ had concluded that of the two adsorbed molecular water layers on a vermiculite clay, the layer furthest away from the clay particle required approximately 17,000 psi or 1.17 kilobars hydrostatic stress for removal. The closer water layer required about 76,000 psi or 5.24 kilobars for removal. Minimum stresses for water layer removal were determined theoretically using water adsorption curves with subsequent experimental agreement occurring when samples were hydrostatically stressed. Since adsorption energies for many clays are similar⁴, as a first approximation it may be assumed that the 2 kilobar stress level used in the initial study may well have exceeded the stress necessary to remove surface adsorbed water. Another consequence of this technique may be zeolitic water removal due to water pressure gradients within the sample aided by fracture and compaction of the tubular mineral structure. In order to eliminate these undesirable "destructive" characteristics, other extraction methods were sought.

Six methods subsequently were investigated, namely: 1) hydrostatic compression, 2) multiple cycle triaxial compression, 3) a rigidly confined sample - argon gas method, 4) a hydrostatically confined sample - argon gas method, 5) centrifuging, and 6) electro-osmosis. Methods 1 through 5 were

tested as shown in Table I. A detailed description of equipment and procedures for Methods 1 through 5 may be found in Appendix A. Literature describing Method 6 (electro-osmosis) indicated that this technique would not be practical since water extraction involved cation movement causing a change in the chemical composition of the water. Consequently, Method 6 was eliminated prior to experimentation.

Table 1 shows that the argon methods gave low water yields (from a trace to 3 cc). Centrifuging produced small quantities in most cases, but a few exceptions produced greater than 7 cc. The hydrostatic compression method produced water in quantities from 1 cc to 6 cc and the multiple cycle triaxial compression tests gave the largest yields with as much as 16 cc's being produced. Note that the 16 cc value is the sum of the yields from tests 15P and 13P since the water extracted due to the hydrostatic pressure would have also been extracted due to the hydrostatic-triaxial compression test.

Again, this "Phase I" was only intended to determine the water yields from several possible extraction methods.

TABLE I
RESULTS FROM EXTRACTION METHOD INVESTIGATION

Test No.	Sample I. D.	Test Type	Confining Pressure (kb)	Max. Axial Load (kb)	Vol. H ₂ O Extracted (cc)	Notes
1P	U12n.10 UG#1 600'	Argon Method I	0	0.10	1 cc	1" thick sample. Gas shorting through least resistance path.
2P	U12n.10 UG#1	Argon Method I	0	0.10	0 cc	1" thick sample. Gas shorting through least resistance path.
3P	U12n.10 UG#1 1323'	Argon Method I	0	0.10	0 cc	2" thick sample. Gas shorting through least resistance path.
4P	U12n.10 UG#1 600'	Argon Method I	0	0.10	~ 0.30 cc	1" thick sample. Gas shorting through least resistance path.
5P	U12n.10 UG#1 1323'	Argon Method I	0	0.10	~ 2 cc	Resaturated mtl. 2" thick sample. Gas shorting through least resistance path.
6P	U12n.10 UG#1 1050'	2 kb single cycle hydro.	2	0	5.6 cc (5 min)	---
7P	U12n.10 UG#1 1050'	Argon Method I	0	0.10	~ 0 cc	2" thick sample. Gas shorting through least resistance path.
8P	U12n.10 UG#1 926'	1 kb (single cycle)	1	0	0.76 cc	---
9P	U12n.10 UG#1 849'	Argon Method II	0.034 (effective)	0	1 cc	Jacket leaked.
10P	U12n.10 UG#1 507'	Argon Method II	0.034 (effective)	0	0.8 cc (10 min)	---
11P	U12n.10 UG#1 926'	Argon Method II	0.034 (effective)	0	~ 0.7 cc (5 min)	---
12P	U12n.10 UG#1 725'	Centrifuged 2,000 rpm	0	0.01	4.4 cc (1 hr)	---
13P	U12n.10 UG#1 725'	Centrifuged 2,000 rpm	0	0.01	1.3 cc (1 hr)	---
14P	U12n.10 UG#1 725' Reused test no. 12P samp.	3 kb (multi cycled)	3	1.45	9.1 cc (5 min)	Oven drying gave 17.05 cc water remaining.
15P	U12n.10 UG#1 725' Reused test no. 13P samp.	3 kb (multi cycled)	3	1.45	15 cc (5 min)	Jacket leaked after testing.
16P	U12n.10 UG#1 926'	3 kb (single cycle)	3	0	1.5 cc (5 min)	---
17P	UE12T#3 1079'	Centrifuge 2,000 rpm	0	0.01	0.10 cc	---
18P	UE12T#3 1079'	Centrifuge 2,000 rpm	0	0.01	2.77 cc	---
19P	ue12T#3 1079'	Centrifuge 2,000 rpm	0	0.01	0.10 cc	---
20P	UE12T#3 1059'	Centrifuge 2,000 rpm	0	0.01	No H ₂ O	Sample very dry.
21P	UE12T#3 1059'	Centrifuge 2,000 rpm	0	0.01	No H ₂ O	Sample very dry.
22P	UE12T#5 1488'	Centrifuge 2,000 rpm	0	0.01	No H ₂ O	---
23P	UE12T#5 1488'	Centrifuge 2,000 rpm	0	0.01	No H ₂ O	---
24P	U12n.10 UG#1 799.7'	Centrifuge 2,000 rpm	0	0.01	No H ₂ O	---
25P	U12n.10 UG#1 799.7'	Centrifuge 2,000 rpm	0	0.01	No H ₂ O	---
26P	UE12T#5 1464'	Centrifuge 2,000 rpm	0	0.01	0.50 cc	---
27P	UE12T#5 1464'	Centrifuge 2,000 rpm	0	0.01	0.40 cc	---
28P	UE12T#3 1079'	1/3 kb (single cycle)	0.333	0	6.29 cc	Sample dry but jacket leaked at end of test.
29P	UE12T#5 1464'	Centrifuged (2000 rpm)	-----	.01	None	crushed material
30P	UE12T#5 1464'	Centrifuged (2000 rpm)	-----	.01	None	crushed material
31P	UE12T#5 1488'	Centrifuged (6000 rpm)	-----	.11	1 cc	crushed material
32P	UE12T#5 1488'	Centrifuged (6000 rpm)	-----	.11	1 cc	crushed material
33P	UE12T#5 1488'	Centrifuged (6000 rpm)	-----	.11	1 cc	cut cylinder
34P	UE12T#5 1488'	Centrifuged (6000 rpm)	-----	.11	1 cc	cut cylinder
35P	UE12T#5 1488'	3 kb multi-cycled	2.75	-----	leaked	-----
36P	UE12T#5 1488'	3 kb multi-cycled	2.75	0	1 cc	-----

PHASE II: CHEMICAL ANALYSIS COMPARISON

As a result of the Phase I, which had indicated that sufficient water could be obtained via hydrostatic compression, triaxial compression and centrifuging, these three methods were then used in Phase II to determine their effects on the chemical analysis.

Fourteen water extraction tests were conducted for chemical analysis. Three different confining pressures (1/3, 1 and 3 kilobars) were used for both the hydrostatic and multiple cycle triaxial compression tests. All centrifuging was done at 2000 RPM.

Table II lists the water extraction results of the tests. Tests 1 through 10 were designed so that water could be chemically analyzed from the same sample under different loading conditions. For example, tests 1

TABLE II
WATER EXTRACTION RESULTS FOR CHEMICAL ANALYSIS COMPARISON

Test No.	Sample I. D.	Test Type	Confining Pressure (kb)	Deviatoric Load (kb)	Vol. H ₂ O Extracted (cc)*	Notes
1	UE12T#3 1079" Samp 1	1 kb single cycle hydro.	1.0	0	8.0	
2	UE12T#3 1079" Samp 1	1 kb multi cycle triax.	1.0	.36	4.4	
3	UE12T#3 1079" Samp 2	$\frac{1}{3}$ kb single cycle hydro.	.333	0	3.3	initially centrifuged at 2000 rpm as samp. 17P
4	UE12T#3 1079" Samp 2	$\frac{1}{3}$ kb multi cycle triax.	.333	.23	1.9	reused samp 2
5	UE12T#3 1079" Samp 3	2.75 kb single cycle hydro.	2.75	0	15.4	initially centrifuged at 2000 rpm as samp. 19P
6	UE12T#3 1079" Samp 3	2.75 kb multi cycle triax.	2.75	.36	4.6	reused samp 3
7	UE12T#3 1079" Samp 4	1 kb single cycle hydro.	1.0	0	5.1	
8	UE12T#3 1079" Samp 4	1 kb multi cycle triax.	1.0	.40	1.9	reused samp 4
9	UE12T#3 1079" Samp 5	Centrifuged (2000 rpm)	---	0.01	7.8	same as samp 18P
10	UE12T#3 1079" Samp 5	$\frac{1}{3}$ kb single cycle hydro.	.333	0	0.5	reused samp 5
11	U12n-10 UG#1 725" Samp 1	1 kb multi cycle triax.	3.0	1.45	9.1	
12	U12n-10 UG#1 725" Samp 2 + Samp 3	Centrifuged (2000 rpm)	---	0.01	5.7	combined the H ₂ O from samples 2 and 3
13	U12T-03 UG#3 1115" Samp 1	1 kb multi cycle triax.	3.0	0.65	7.7	
14	U12T-03 UG#3 1115" Samp 2	$\frac{1}{3}$ kb multi cycle triax.	.333	0.35	1.6	

*Prior to filtration

and 2 were conducted using the identical sample 1. Thus, water was first obtained from hydrostatic compression then from multiple cycle triaxial compression; the water from each test analyzed for ion and SiO_2 contents as shown in Figure 1*. Samples were used only once in tests 11 through 14. This was done to observe if trends in ion and SiO_2 content as seen in the multiply used samples were also observed in singly tested samples. For samples 1 through 10 Figure 1, the following may be observed:

- a) The ion concentrations for the hydrostatic compression tests were always higher than the multiple cycle triaxial compression tests.
- b) In general, the higher confining pressures gave lower ion concentrations.
- c) Ion concentrations for the centrifuged sample were observed to be about two times the average of the concentrations for the pressurized samples.

No repeatable trends were observed for the SiO_2 concentration. Tests 11 through 14 verified observations b) and c) even though the tests were conducted on samples from different holes and footages.

The change in ion concentration resulting from different test procedures is most likely due to the energy and time involved with each method. Thus, prior to hydrology analysis, it must be decided which extraction method best approximates the type of water to be retrieved for future correlation. For example, if water from a hydrostatic compression technique was used to develop the hydrology and water was later collected from well points (percolating water) then the correlation of the chemical analysis

* Ion and SiO_2 contents were analyzed by Water Resources Division, Desert Research Institute, Reno, Nevada.

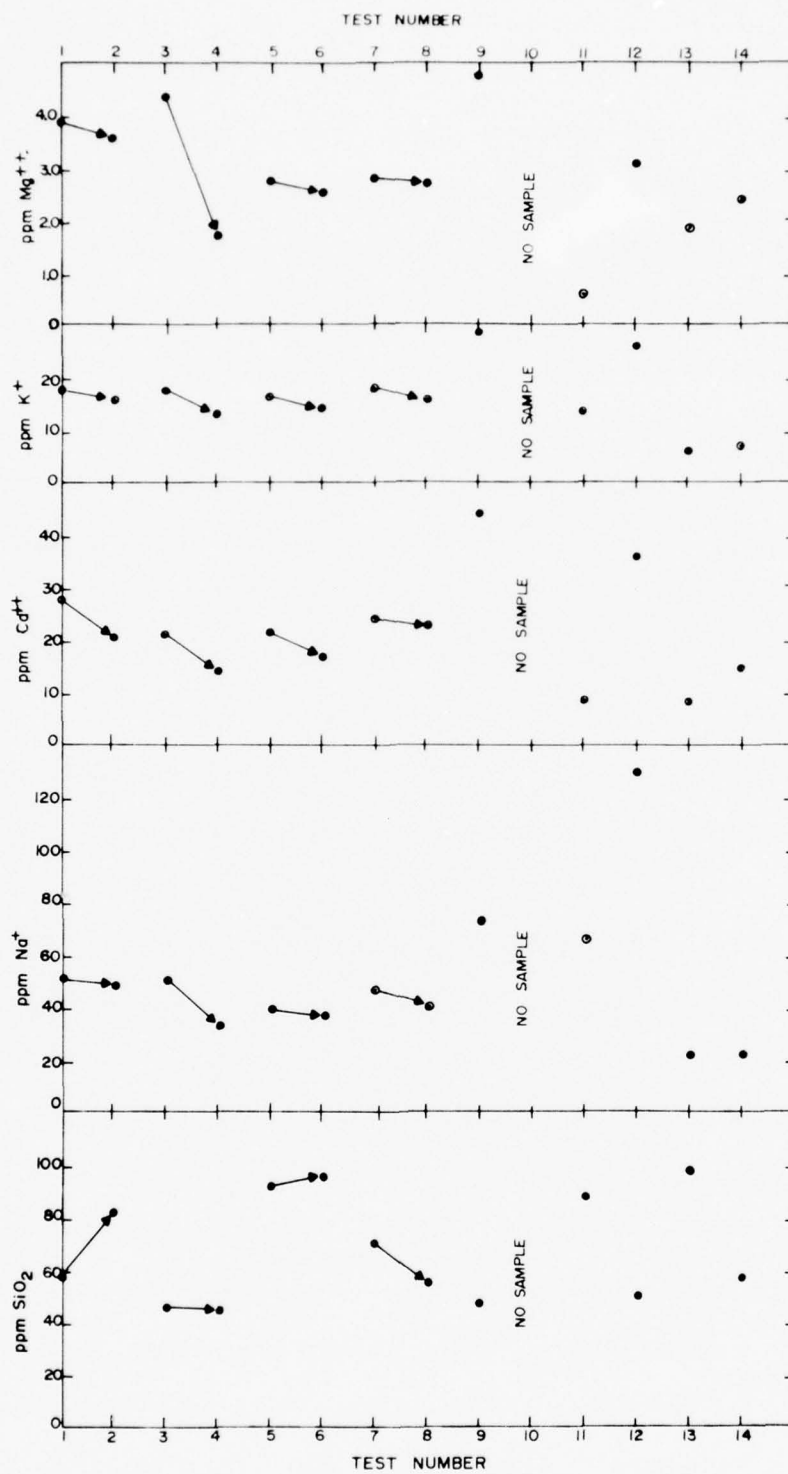


Figure 1: Ion and SiO_2 Concentration Comparison
(in parts per million, ppm)

would be difficult due to different extraction energies. It may be important then to answer questions relating to energies and rate of water removal associated with different extraction methods and thus determine the type of water being extracted (percolating, surface adsorbed, zeolitic or structural). The rate of water removal is important since the rates of reaction associated with the liquid-solid interface of the water-mineral system may cause changes in ion concentration.

PHASE III: WATER PROFILE DEVELOPMENT

As a step toward better understanding of the hydrology above the "T" tunnel area, water is being extracted from core samples from two vertical drill holes. The samples ranged from depths of 510' through 1642' and 441' through 2152' from drill holes UE12T#2 and UE12T#3, respectively. The "profile development" was started using the centrifuging technique on the non-zeolitic footages from holes UE12T#2 and UE12T#3. It was decided to initially use centrifuging because of its nondestructive character. The non-zeolitic footages were selected partly because of their higher permeability.

Table III lists the centrifuge results for both holes. A total of seven footages produced no water. Five of the nonproductive footages were very dry when first opened, while in only two instances did a moist footage not produce water. Quantities of extracted water ranged from 1 cc to as much as 143 cc with all samples being resealed with aluminum foil and beeswax for possible future testing.

In general, the centrifuging technique on non-zeolitic samples produced adequate water yields. Since the centrifuge water yield is closely related to the sample permeability, it may be desirable to investigate a flow rate relationship based on sample permeability to predict water production from future samples. However, zeolitic materials have a low permeability (microdarcies) and even though the centrifuge method may produce low water yields from the zeolitic footages, it may prove to be necessary for consistent profile development.

TABLE III
WATER EXTRACTION RESULTS FOR PROFILE DEVELOPMENT

UE12T #2

Footage (ft)	Test Type	Water Production (cc)	Storage	Zeolitic Content	Notes
510	Centrifuge	41	Polyethylene	None	Sample appeared very dry when first opened.
510	Centrifuge	67	Glass	None	
529	Centrifuge	0	- - -	None	
749					
756					
1004					
1008					
1246					
1262					
1509	Centrifuge	51	Polyethylene	None	
1509	Centrifuge	45	Glass	None	
1526	Centrifuge	6	Polyethylene	None	
1526	Centrifuge	6	Glass	None	
1642					

UE12T #3

Footage (ft)	Test Type	Water Production (cc)	Storage	Zeolitic Content	Notes
441	Centrifuge	58	Polyethylene	None	Very dry welded tuff
458	Centrifuge	26	Glass	None	
556	Centrifuge	59	Polyethylene	None	
559	Centrifuge	31	Glass	None	
653	Centrifuge	85	Polyethylene	None	
664	Centrifuge	36	Glass	None	
744					
756	Centrifuge	0	- - -	None	
845	Centrifuge	143	Polyethylene	None	
853	Centrifuge	98	Glass	None	
953					
954					
1051					
1052					
1054					
1151					
1152					
1253					
1349					
1351					
1448	Centrifuge	56	Polyethylene	None	Samples very dry when first opened
1451	Centrifuge	116	Glass	None	
1544					
1550					
1646					
1651					
1748					
1751					
1847	Centrifuge	0	- - -	None	Samples very dry when first opened
1851	Centrifuge	0	- - -	None	
1950	Centrifuge	1	Glass	None	Sample very dry when first opened
1957	Centrifuge	0	- - -	None	
2049					
2053					
2150	Centrifuge	0	- - -	None	Sample moist but did not produce
2152	Centrifuge	0	- - -	None	

CONCLUSIONS AND SUGGESTIONS

The extraction methods which yield the largest quantities of water are the hydrostatic compression, multiple cycle triaxial compression and centrifuging techniques. Ion concentrations vary depending on the extraction method. Thus it must be determined which extraction technique best approximates the type of water collection to be used during later analysis so that meaningful correlations can be made. Because of its nondestructive character, the centrifuge technique has been used thus far for profile development of the non-zeolitic footages in holes UE12T#2 and UE12T#3.

It is suggested that centrifuge extraction continue in the zeolitic footages (provided that adequate water yield occurs) to maintain ion concentration profile continuity. If the water yield is too low, low pressure (1/2 to 1 kilobar) hydrostatic compression tests could then be used to produce further water. A theoretical explanation for methodology induced ion concentration changes would be helpful in establishing a basis for future decisions.

REFERENCES

1. Butters, S. W., Dropek, R. K., Nielsen, R. R., "Water Extraction from Saturated Ash-Fall Tuffs from the Nevada Test Site," Terra Tek Report TR 75-16, 1975.
2. Benson, Larry, Desert Research Institute, Reno, Nevada, 1975.
3. Grim, R. E., 1968, Clay Mineralogy, McGraw-Hill Book Company, New York, pp. 234-352.
4. Van Olphen, H., "Compaction of Clay Sediments, Preceedings Eleventh National Conference on Clays and Clay Minerology", Macmillan Co., New York, 1962, pp. 178-187.

APPENDIX A

APPENDIX A

Water Extraction Methods

(Equipment and Procedures)

Hydrostatic and Triaxial Compression Methods: The hydrostatic and multiple cycle triaxial compression methods use the same test equipment. Figure 2 shows a schematic of the test configuration* while Figure 3 is a photograph of the sample and water collection system. The collection chamber was made of 431 stainless steel. A permeable stainless steel spacer, having a mean pore diameter of 30 microns, was used to prevent the sample from extruding into the water collection chamber. The sample rested on the collection chamber and both units were jacketed together with two wraps of polyurethane (25 mil. total thickness). The sample and chamber were sealed with rubber splicing compound and stainless steel lock wire as shown in Figure 3. Samples were approximately 2 inches long by 2.4 inches in diameter. Prior to use, all components contacting the sample were boiled in distilled water and thoroughly dried.

For the hydrostatic compression method, the sample was hydrostatically compressed and maintained at the desired stress level for a time of 5 to 10 minutes then hydrostatically unloaded. The sample and collection chamber were removed from the vessel and the extracted water drained into a suitable container. For the multiple cycle triaxial compression method, the sample was hydrostatically compressed and maintained at a given stress level while a deviatoric load was rapidly applied ten times to sample yield and back to zero followed by hydrostatic unloading. This total stress path was done three times in rapid succession with the total test time being 5 to 10 minutes.

* Figure taken from Reference 1.

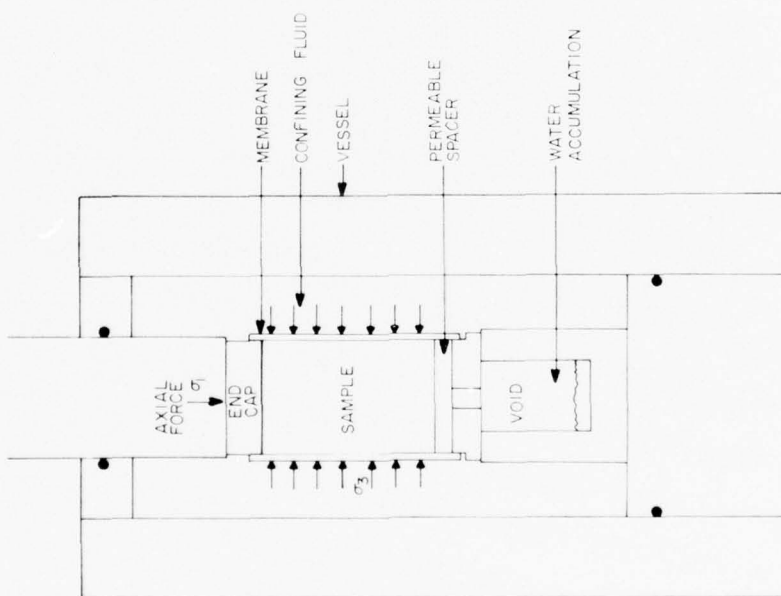


Figure 2: Loading Configuration Schematic For Compression Tests

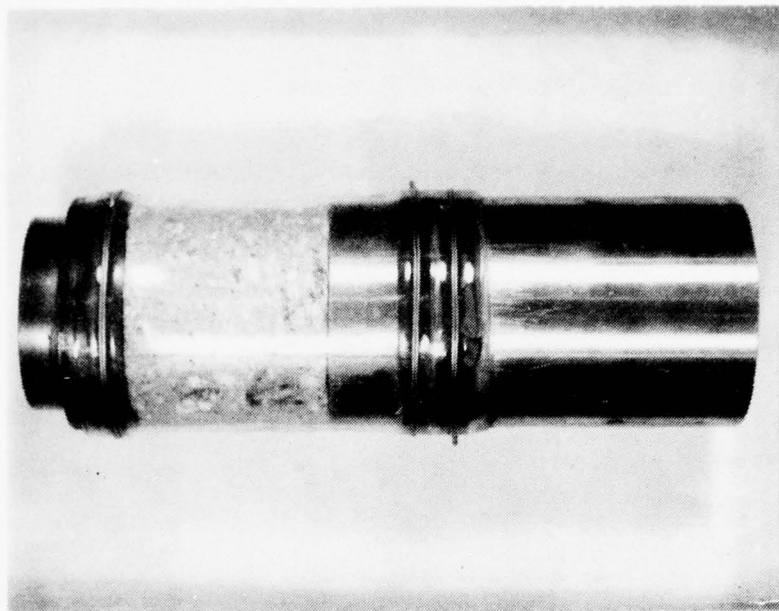


Figure 3: Jacketed Sample and Collection Chamber for Compression Methods

Argon Gas Methods: Two argon gas methods were analyzed for water extraction. The first method involved rigidly confining a 1 inch or 2 inch long by 1.85 inch diameter tuff sample by epoxying it to a 3/8 inch thick aluminum ring (Figure 4). The sample was then placed into a reaction frame with permeable end caps mounted at both ends. Argon gas was applied at 1500 psi pressure in the top cap with the water being collected at the lower cap (Figure 5).

The second method utilized a 2000 psi hydrostatic pressure for confinement. A 2 inch long by 1.85 inch diameter sample was mounted between two permeability end caps (Figure 6). The end caps were connected to the base plug with argon gas admitted to the top cap at 1500 psi while the lower cap collected the pore water.

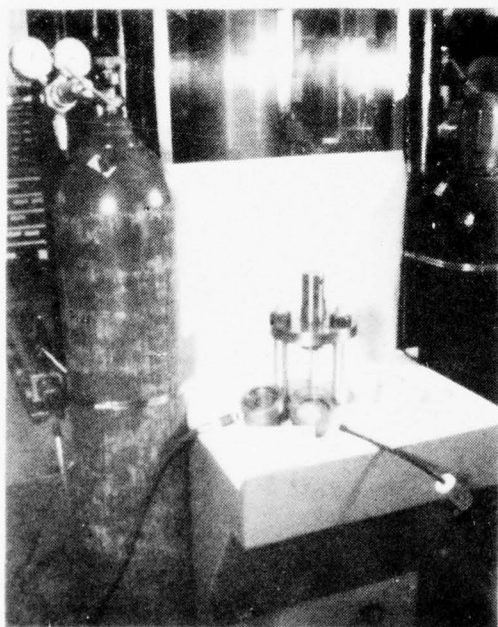


Figure 4: Sample, End Caps and Loading Frame for the Rigidly Confined Sample -- Argon Method ($\sigma_3 = 0$ psi)

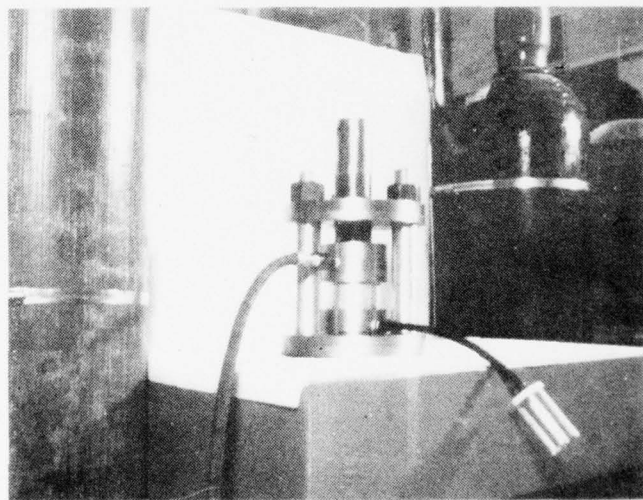


Figure 5: Assembled Components for the Rigidly Confined Sample -- Argon Method ($\sigma_3 = 0$ psi)

Centrifuge Method: The centrifuge method used a water collection system similar to that used in the hydrostatic compression method. The collection chamber was made of high density polyethylene. The sample rested on the water collection chamber and both units were jacketed with one wrap of polyurethane (5 to 10 mil. total thickness). The sample and collection chambers were sealed with rubber splicing compound and stainless steel lock wire, as shown in Figure 7. All samples were approximately 2 inches long by 2.4 inches in diameter. Prior to testing, all components in contact with the sample were boiled in distilled water and thoroughly dried. The prepared specimen was then placed into a centrifuge bucket and spun at 2000 RPM for one hour with the extracted water poured into suitable container for storage.

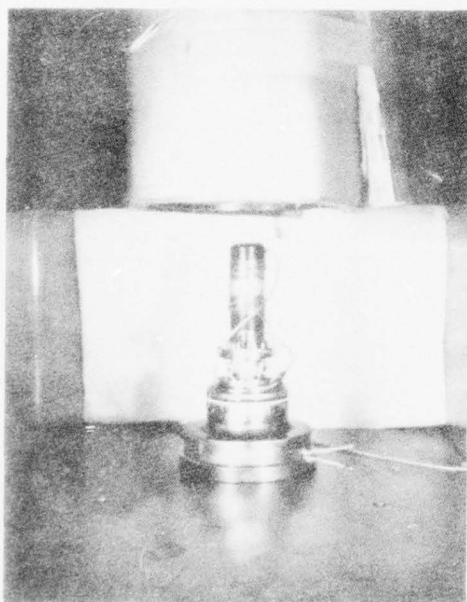


Figure 6: Hydrostatically Confined --
Argon Method Showing Sample,
Permeability End Caps and
Base Plug Connections

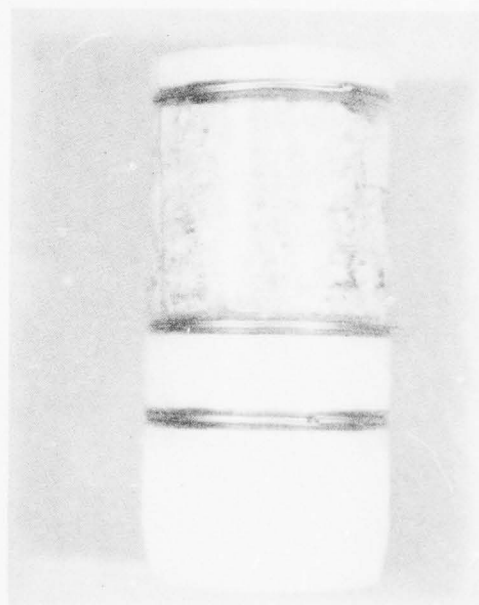


Figure 7: Jacketed Sample and Collection
Chamber for Centrifuging

Sample Preparation and Extracted Water Storage: Samples were prepared for the various extraction methods by first cutting them into 2 inch long cylinders from the core material. In order to prevent the diamond blade from seizing, a minimum flow of distilled water was used for coolant. This distilled cutting water was assumed not to effect the sample water since previous investigations at the Nevada Test Site had shown that water used during sample coring procedures essentially did not penetrate the rock. Cut samples were patted surface dry, sealed in aluminum foil and beeswax, and labeled.

After testing, the extracted water was emptied into either glass or polyethylene bottles depending upon the type of chemical analysis to be conducted. Polyethylene storage was used when ion and SiO_2 concentrations were to be determined while glass bottles were used for water destined for tridium dating. All bottles were cleaned with distilled water prior to use.

Preceding Page BLANK - NOT FILMED

HYDROSTATIC RESPONSE OF A WATER
SATURATED SAND

by

R. K. Dropek
S. W. Butters
A. H. Jones

to

Field Command
Defense Nuclear Agency
Nevada Test Site
Mercury, Nevada 89023

Attn: Mr. J. W. LaComb

March 1976
TR 76-9

INTRODUCTION

Sand-water slurries have applications where the mixture is subjected to varying magnitudes of shock waves. Mr. J. W. LaComb¹ requested that tests be conducted on a water saturated sand² to determine the condition of the mixture after hydrostatic loading (i.e., the possibility of causing cohesion due to grain "welding.")

The slurry density of interest was 1.69 gm/cm^3 . However, in a standard cylindrical static test sample, this bulk density would result in the sand settling to the bottom of the test cylinder leaving a layer of water at the surface. This problem was circumvented by drawing off the excess water creating a higher density water-sand mixture of about 2.18 gm/cm^3 . The test sample was therefore a mixture of water, and sand with grains touching in a loosely packed state.

Hydrostatic loading tests to stresses of 4 kilobars at loading rates of 66 bars per second were conducted to observe any cohesive properties due to welding of sand grains. Samples were tested in an undrained condition (i.e., the water was not allowed to migrate out of the sample). Pre and post test grain size analyses as well as visual examination of tested samples were used to determine the amount of cohesion.

Sample Description and Preparation

The slurry sand is called Monterey sand (manufacturer designation 20-40) and originates from Monterey Beach, California. It is tan in color having well rounded grains. It has no unconfined cohesion and is a clean, well washed material. The pre-test sand grain size distribution is shown in Figure 1 and listed in table 1. About 88 percent of the material has a grain size between 0.1 and 0.42 millimeters.

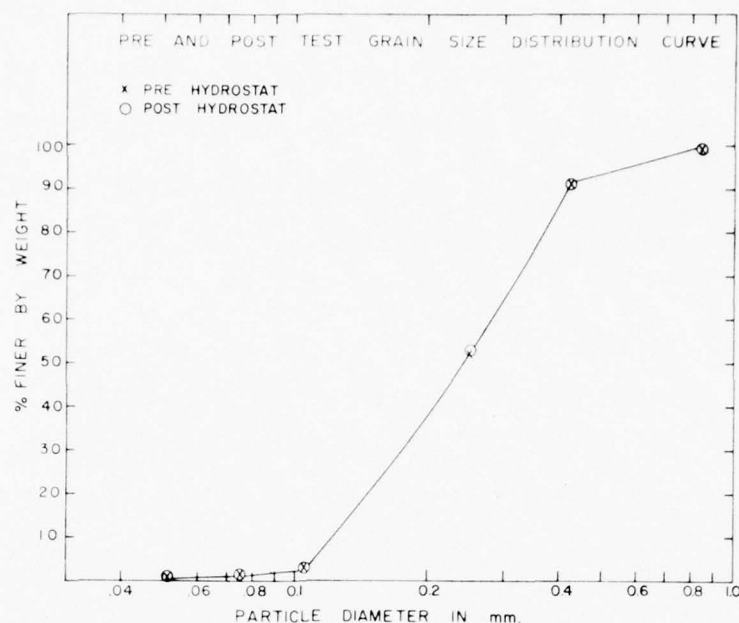


Figure 1: Pre and Post Hydrostatic testing grain size distribution curves.

TABLE 1
Sieve Analysis Results

SIEVE NO.	PERCENT PASSING	
	PRE-TEST	POST-TEST
20	99.86	99.85
40	91.33	91.52
60	52.71	53.98
140	3.11	3.13
200	0.73	0.68
270	0.35	0.30
Pan	0	0

Samples were prepared by forming them in a mold. The mold consisted of a two inch diameter polyurethane jacket attached to a circular steel end cap. The dry sand was poured into the mold to a height of 2.5" and then distilled water was added until a one inch layer of water existed above

the sand level. The mixture was then subjected to a vacuum until bubbling ceased. This was to insure that trapped air bubbles had been eliminated. Excess water was carefully removed and another steel end cap placed on top of the sample. Densities were determined by measuring and weighing the test samples and allowing for the size and weight of the urethane, end caps, etc. Test sample densities ranged from 2.1 to 2.3 gm/cm³.

Experimental Instrumentation

The fluid confining pressure was measured with a 350 ohm manganin wire pressure coil. The pressure coil was accurate to within 1 percent. Axial strains were measured using a four arm cantilever configuration accurate to within 0.05 percent strain. Figure 2 shows a sand-water sample in the test configuration.

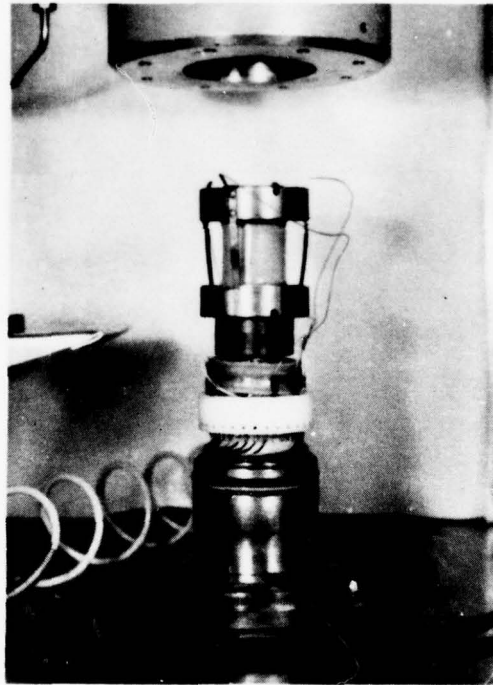


Figure 2: Sample configuration for hydrostatic compression testing.

Assuming a homogeneous isotropic material, approximate volume strains were calculated from the axial strain.

Experimental Results and Discussion

Both visual inspection and grain size distributions were conducted on the sand before and after testing to observe possible grain "welding" during hydrostatic loading. Figure 3 shows untested and tested samples as they were "poured" from their confining jackets. As apparent from Figure 3, no material cohesion could be observed as a result of the hydrostatic compression. Figure 1 and Table 1 show the pre and post test sieve analysis results which also indicates that "welding" on a small scale did not occur.



Figure 3: Pre and Post test sand/water samples.

The confining pressure versus volume strain curves are shown in Figure 4. Curve 1 is the average volume strain response for four sand samples with an initial average density of $2.18 \pm .02 \text{ gm/cm}^3$. For reference, curve 2 is

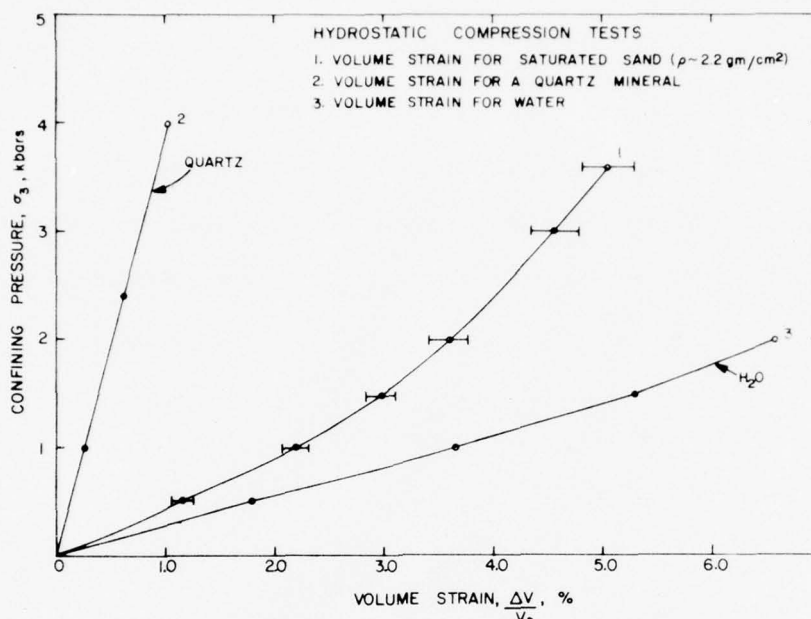


Figure 4: Hydrostatic compressibility curves for saturated sand, water and quartz.

the pressure-volume response for a α -quartz mineral³ while curve 3 shows the pressure-volume response of water at 25°C.⁴ Clearly, the saturated sand volume strain curve shows neither pure water nor quartz characteristics but a combination of both.

CONCLUSION

The sand grains showed no change in the grain size analyses as determined before and after loading to 4 kilobar hydrostatic pressure. The hydrostatically tested samples likewise showed no visual signs of cohesion when unjacketed. These facts suggest that both the high water content and undrained sample conditions resulted in a pore pressure buildup causing insufficient "welding" stresses to develop between grains (i.e., the sand grains were at a stress state lower than that of the vessel confining pressure). Pore pressures would have remained essentially zero during hydrostatic compression had the test sample water been vented to the atmosphere creating a drained sample condition (provided that allowances were made for permeability, test time and other pore pressure parameters). Consequently the sand grains would have experienced hydrostatic stresses equal to the vessel confining pressure; the result being possible grain welding at these higher stresses. An additional result of drained testing would have been larger volume strains. This effect has been observed in report TR 75-29⁵ for Mixed Company sandstone.

Finally, it is not anticipated that increasing the hydrostatic loading rate for the undrained tests reported herein would result in any significant increase in the cohesion of post test material.

REFERENCES

1. LaComb, J. W., DNA Field Command, Mercury, Nevada.
2. LaComb, J. W., Supplied Monterey Beach Sand.
3. Clark, S. P., ed., Handbook of Physical Constants, The Geological Society of American, Inc., New York, 1966.
4. Franks, Felix, ed., Water a Comprehensive Treatise, Plenum Press, New York, 1972, Vol. 1.
5. Johnson, J. N., Dropek, R. K., "Measurement and Analysis of Pore Pressure Effects in the Inelastic Deformation of Rocks," Terra Tek Technical Report TR 75-29, 1975.

LABORATORY DETERMINATION OF THE ELASTIC
MODULUS OF STRESS-RELIEF OVERCORES

by

R. K. Dropek (TTI)

A. Abou-Sayed (TTI)

W. L. Ellis (USGS, Denver)

Submitted to

Mr. J. W. LaComb
Defense Nuclear Agency
Nevada Test Site
Mercury, Nevada 89023

Contract DNA 001-75-C-0260

TR 76-33

PREFACE

The U. S. Geological Survey has used the borehole-overcore technique to determine *in situ* stresses at the Rainier Mesa, Nevada Test Site. Elastic constants were determined on site with the recovered overcores in order to calculate the *in situ* stresses from the deformations measured with the borehole gage. Terra Tek performed laboratory tests to evaluate the discrepancies in elastic moduli determined with the overcores (hollow cylinder) and standard triaxially loaded, solid, cylindrical samples. Elastic nonlinearity is the main cause for modulus discrepancy and is accounted for by evaluating moduli as a function of the mean and shear stresses. Errors generated by neglecting anisotropy are also discussed.

TABLE OF CONTENTS

	<u>Page</u>
Preface	374
Table of Contents	375
List of Figures	376
List of Tables	377
List of Units	378
Introduction	379
Elastic Theory and Anisotropy Considerations	382
Experimental Procedures and Results	384
Specimens and Sample Preparation	384
Apparatus Description and Testing Procedures	384
Experimental Results	389
Discussion	394
Modulus Comparisons	394
Modulus Selection	397
Laboratory Testing Recommendations	400
Concluding Remarks	402
References	403
Appendix A: Additional Experimental Results	404

LIST OF FIGURES

<u>Figure Number</u>	<u>Description</u>	<u>Page</u>
1	Three-component borehole deformation gage	379
2	Typical mean stress-borehole-deformation plot during a loading-unloading cycle	380
3	Test configurations	385
4	Biaxial testing apparatus	387
5	Terra Tek confined biaxial test configuration ($\epsilon_z \sim 0\%$)	387
6	Hydrostatic and deviatoric loading configuration	388
7	Stress trajectories during triaxial loading sequence	388
8	Typical radial-pressure-versus-borehole-deformation cycle which indicates nonlinear behavior	390
9	Pressure versus borehole deformation during unloading for the three test configurations.	390
10	Mean stress effect on the 5.1 cm-diameter core elastic modulus	393
11	Shear stress effect on the 5.1 cm-diameter core elastic modulus	393
12	Modulus curves for acrylic comparing tangent and secant moduli. Note little variation in moduli with mean stress	395
13	Modulus curves for ISS 4 overcore 5 comparing tangent and secant moduli. Note that moduli increase with mean stress	395
14	Modulus curves for ISS 9 overcore 4 comparing tangent and secant moduli. Note that moduli increase with mean stress	396
15	Tangent modulus comparison of the overcore and 5.1 cm (2 in) diameter samples when plotted against mean stress. The moduli were determined by triaxial loading from an initial hydrostatic state	396
16	Apparent elastic modulus discrepancy when comparing overcore secant moduli with 5.1 cm-diameter (solid) core modulus	398

<u>Figure Number</u>	<u>Description</u>	<u>Page</u>
17	Overcore secant modulus versus borehole deformation illustrating the selection of the secant modulus to be used for <i>in situ</i> stress calculations when radial <i>in situ</i> stresses are equal	399
18	Radial pressure versus borehole deformation during unloading for ISS 4 overcore 5 comparing the three test configurations	405
19	Radial pressure versus borehole deformation during unloading for ISS 6 overcore 2 comparing two test configurations	405
20	Radial pressure versus borehole deformation during unloading for ISS 7 overcore 2 comparing the three test configurations	406
21	Radial pressure versus borehole deformation during unloading for acrylic comparing the three test configurations	406

LIST OF TABLES

<u>Table Number</u>	<u>Description</u>	<u>Page</u>
I	Relations for Determining Young's Modulus for the Three Test Configurations	391
II	Secant Modulus Comparisons at 3.45 MPa Radial Pressure Using the Equations in Table I	391
III	Elastic Constants from Triaxial Tests	392
IV	Secant Modulus (GPa) Comparison During Hydrostatic Loading at 3.45 MPa and 6.9 MPa Pressure	400

LIST OF UNITS

1 MegaPascal = 10.0 bars

1 μm = 3.94×10^{-5} inches

INTRODUCTION

The USGS (U. S. Geological Survey), as part of the earth science support provided to DNA (Defense Nuclear Agency), determined *in situ* stresses in the Rainier Mesa at the NTS (Nevada Test Site). The standard method used in these stress determinations is the well documented USBM (U. S. Bureau of Mines) overcoring technique. This technique utilizes the three-component borehole deformation gage shown in Figure 1 (Merril, 1967; Hooker and Bickel, 1974) to determine deformational changes on the internal diameter as a cylindrical borehole is overcored free from the surrounding rock mass. To calculate stresses from borehole deformation data the elastic moduli of the rock in which the borehole deformation measurements are taken must be known.

Elastic moduli of the stress-relieved overcores are commonly determined by the use of a biaxial pressure chamber, (axial stress, $\sigma_z = 0.0$ MPa) and the three-component borehole deformation gage (Fitzpatrick, 1962).

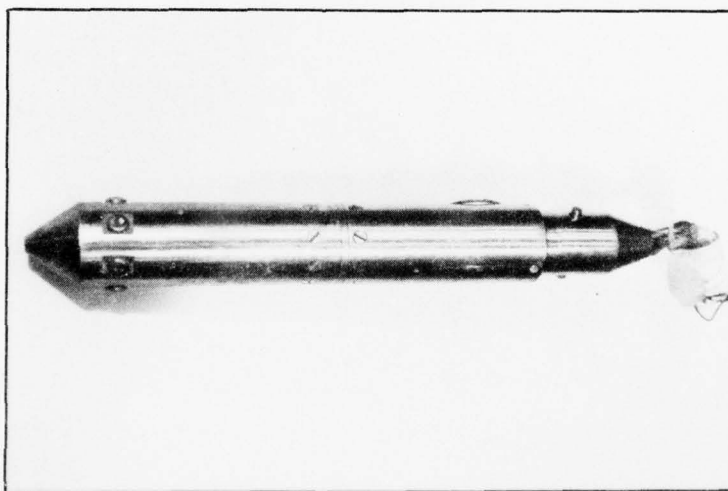


Figure 1. Three-component borehole deformation gage.

Briefly, the procedure involves application of an external radial pressure to the core and measurement of the corresponding inner-hole deformation. Such a procedure is simple and quick; however, it has been observed that overcore elastic moduli tested in the above manner do not agree with standard triaxially tested solid core elastic moduli (LaComb, 1976). Differences were on the order of 30 to 50 percent. Two possible sources for the discrepancies are: (1) the difference in elastic modulus definition (secant versus tangent) and (2) the effect of mean and shear stresses on the elastic moduli.

The problem in modulus definition is a result of the NTS tuffs exhibiting nonlinear elastic behavior (see Figure 2). Figure 2 also points out a shortcoming of the biaxial testing apparatus; that NTS tuff fails in extension at approximately 2.5 MPa mean stress.

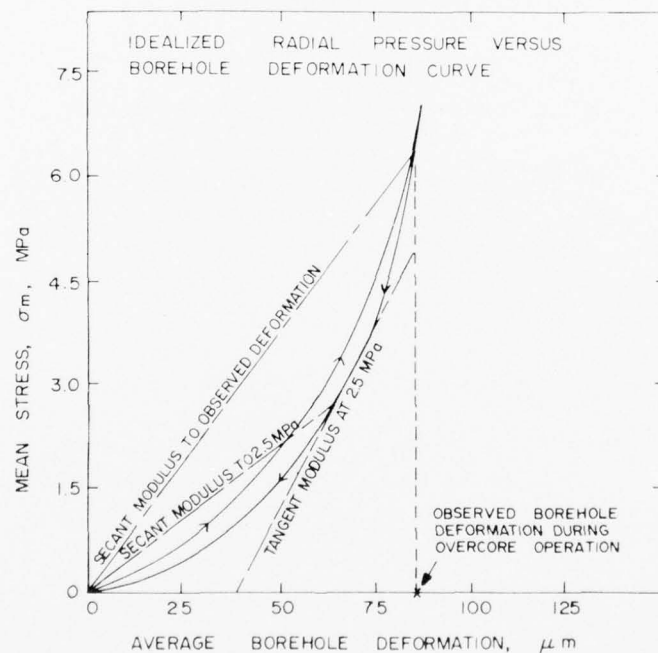


Figure 2. Typical mean stress--borehole-deformation plot during a loading-unloading cycle.

To evaluate these problems a five-point testing program was devised.

1. Overcore samples were tested biaxially as is normally done in the field. Radial pressure was applied along the middle 17.8 cm of the 38.1 cm long cores. Axial stress, σ_z , was kept equal to zero.
2. The overcores were tested in a constrained biaxial loading configuration. The radial pressure was applied along the entire sample length while zero axial strain, ϵ_z , was maintained.
3. The overcores were subjected to hydrostatic loading, i.e. equal radial and axial pressures.
4. The overcores were loaded axially under a uniform lateral confining pressure.
5. Solid cores obtained from the overcore samples were subject to axial loading under a uniform lateral confining pressure.

From these loading configurations the effect of the mean and shear stresses on the elastic moduli (E , ν) could be evaluated.

ELASTIC THEORY AND ANISOTROPY CONSIDERATIONS

The load-deformation relations for a linear elastic thick-walled cylinder subjected to radial pressure and axial strain have been derived previously (Obert, 1964). Only a brief statement of the equations which bear directly on the text will be given below (in what follows stress and strain are positive in compression).

The axial stress (σ_z)-strain (ϵ_z) relation for a hollow elastic cylinder subjected to external pressure P_o is

$$\sigma_z = \frac{2 \nu P_o b^2}{(b^2 - a^2)} + \epsilon_z E \quad (1)$$

while the borehole deformation, U_i at the inner radius, a , is related to Young's modulus of the rock, E , by the equation

$$U_i = \frac{4 (1-\nu^2) P_o b^2 a}{E (b^2 - a^2)} - 2 \nu \epsilon_z a \quad (2)$$

where ν is Poisson's ratio, and b is the sample outer radius. When axial stress is zero, equation 2 reduces to

$$U_i = \frac{4 a b^2 P_o}{E (b^2 - a^2)} \quad (3)$$

Similarly the external radial deformation U_o is given by

$$U_o = \frac{2 (1 + \nu) P_o}{E (b^2 - a^2)} [b^3 (1 - 2\nu) + a^2 b] - 2\nu \epsilon_z b. \quad (4)$$

Deviation from isotropy of each overcore (measured as the ratio of the maximum to minimum Young's moduli in the plane normal to the specimen

axis) is estimated by the development of a radial deformation ellipse from which a maximum and minimum Young's moduli may be calculated. For the Nevada Test Site tuff, the ratio of E_{\max} to E_{\min} is usually less than 1.5 while the ratio of the secondary *in situ* principal stresses is approximately 2.

Becker and Hooker (1967) theoretically analyzed the problem of anisotropy for thick-walled cylinders. Their results indicated that the error in *in situ* stress determination caused by a modulus ratio E_{\max} to E_{\min} of 1.5 and a stress ratio of 2 was small, i.e., the error induced by the assumption of isotropy was less than 10 percent. Thus, the remainder of the report shall deal with isotropy. Note that since three orthogonal overcore determinations are made at the Nevada Test Site, it is not necessary to assume that one of the axes of elastic symmetry is orthogonal to the borehole in order to compute the stress ellipse (Panek, 1966).

EXPERIMENTAL PROCEDURES AND RESULTS

Specimens and Sample Preparation

Four Nevada Test Site overcore samples from the U12n.10 drift complex were obtained from Mr. William Ellis (USGS, Denver). Three samples (ISS 6 overcore 2, ISS 7 overcore 2 and ISS 9 overcore 4) were wrapped in aluminum and coated with beeswax to preserve *in situ* moisture. The fourth sample (ISS 4 overcore 5) was received air dried and consequently immersed in water to bring it up to the assumed *in situ* saturation of 95 percent. Samples were prepared by saw cutting the ends of the overcores received from the field. External and internal sample diameters were measured to be within $13.97 \pm .1$ cm and $3.81 \pm .1$ cm, respectively. Hardened steel endcaps were attached to the sample ends using Ultra-Cal 30 grout. The endcaps were aligned before the grout hardened, and were maintained parallel to within $\pm .008$ cm over the 14 cm diameter. When necessary, samples were then sealed using a urethane jacket, rubber tape and steel lock wire.

Acrylic plastic samples of the same configuration and size as the NTS tuff were used to calibrate the test systems.

Apparatus Description and Testing Procedures

Overcore specimens were tested in four different loading configurations as listed below and shown schematically in Figure 3, as Cases I through IV:

Case I) $\sigma_z^a = 0$ MPa, ($0.0 \text{ MPa} < P_0 < 3.45 \text{ MPa}$)

Case II) $\epsilon_z^b = 0\%$ strain giving $\sigma_z^b \approx 2.16 \nu P_0$, ($0.0 \text{ MPa} < P_0 < 6.9 \text{ MPa}$)

Case III) $\sigma_z^c = P_0$, ($0.0 \text{ MPa} < P_0 < 6.9 \text{ MPa}$)

Case IV) $\sigma_z^d = P_0 + L$ (deviatoric loading)

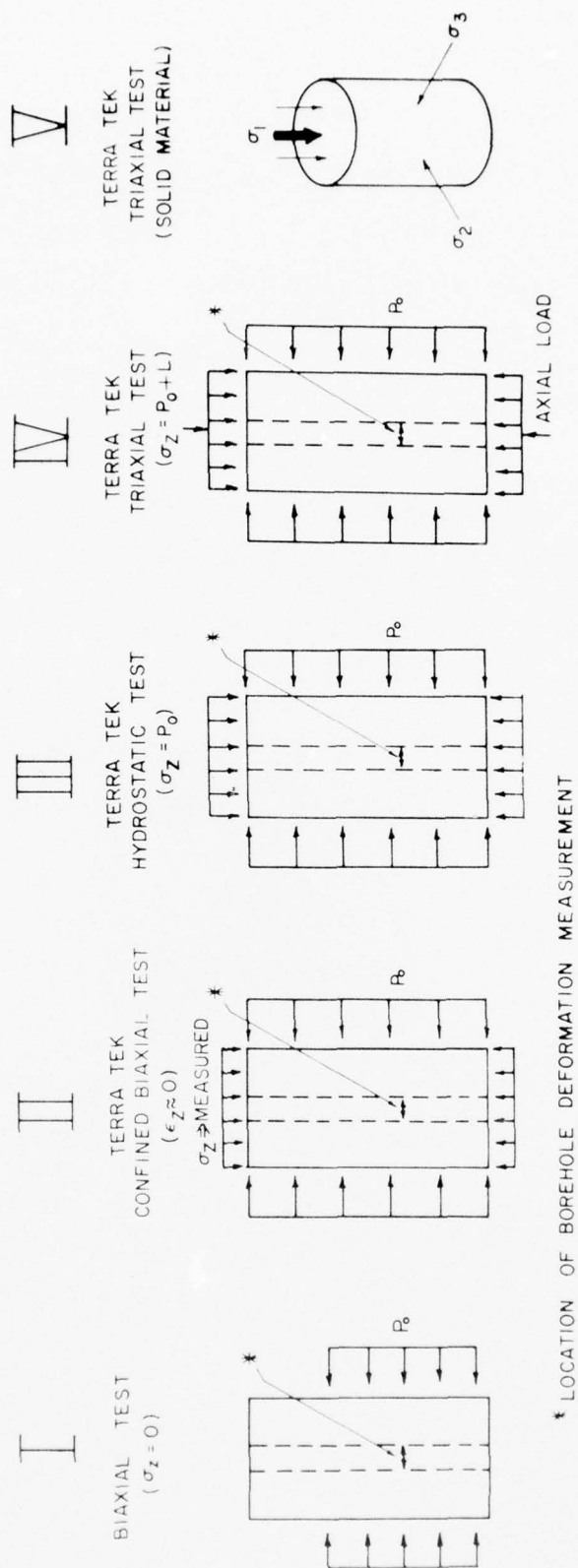


Figure 3. Test configurations.

where σ_z , ϵ_z , ν and P_0 are defined as before. The magnitude of the axial stresses for the four test configurations were such that $\sigma_z^a < \sigma_z^b < \sigma_z^c < \sigma_z^d$. Case I ($\sigma_z = 0.0$ MPa) was achieved using the standard biaxial testing apparatus, as shown in Figure 4. The apparatus simply consisted of a rubber bladder retained in a steel cylinder with a 14.5 cm internal diameter. Samples were tested by radial pressurization from 0.0 MPa to 3.45 MPa to 0.0 MPa with borehole deformations recorded after pressure increments to 0.69 MPa.

Figure 5 shows Case II configuration; sample endcaps and strain-gaged reaction column are visible. The sample is contained within the reaction column, 16.5 cm ID, 17.8 cm OD, which provided a measure of the axial load. The complete system was placed in a pressure vessel for radial pressurization.

Final overcore testing was conducted in both hydrostatic and deviatoric loading configurations, Cases III and IV, respectively, with only samples ISS 9 overcore 4, ISS 4 overcore 5 and Acrylic subject to Case IV loading. Figure 7 shows the stress trajectories used during Case IV loading. Axial and lateral strain transducers were attached to the sample as shown in Figure 6.

Axial and lateral strains were accurate to within ± 0.001 percent strain and ± 0.002 percent strain, respectively. Axial load was measured accurate to within ± 0.03 MPa.

Once the hydrostatic and deviatoric loading response had been determined for the overcores, 5.1 cm-diameter cores 6.4 cm long were obtained from selected overcores. These samples were triaxially tested (Case V) using the standard techniques and apparatus. Three cores from ISS 9 overcore 4 and ISS 4 overcore 5, were tested using the loading sequence shown in Figure 7. The tests showed how Young's modulus, E , varied with both mean and shear stresses.

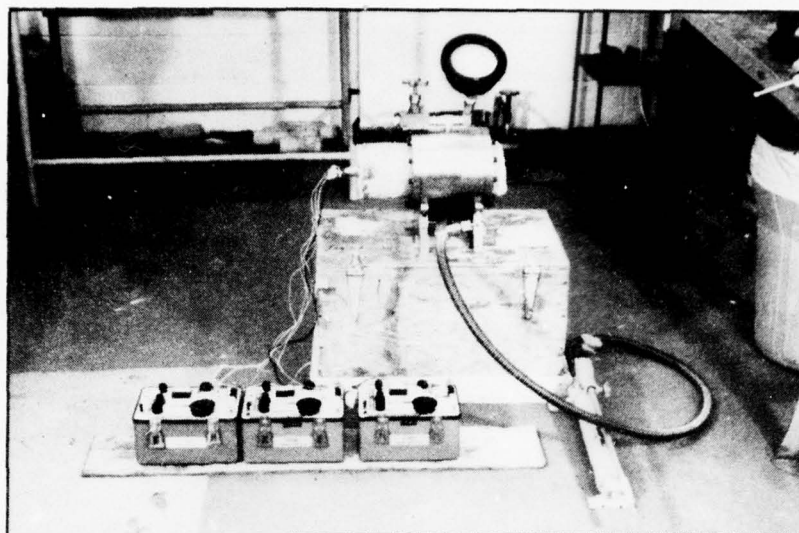


Figure 4. Biaxial testing apparatus.

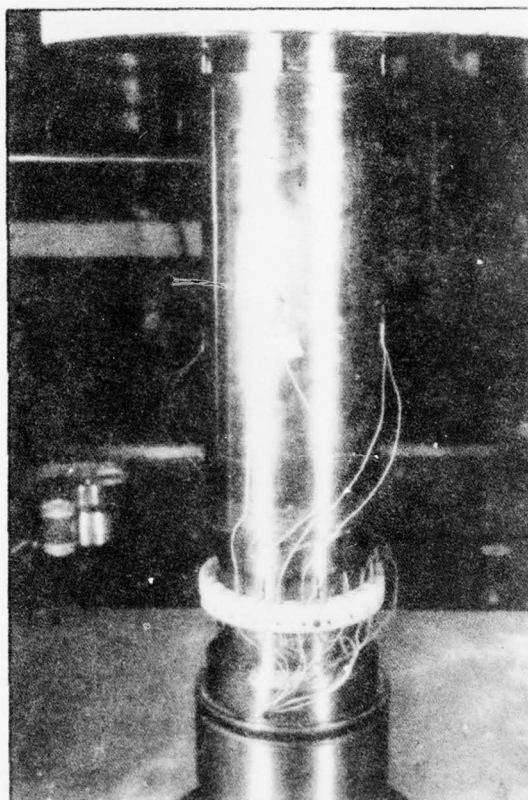


Figure 5. Terra Tek confined biaxial test configuration ($\epsilon_z \approx 0\%$).



Figure 6. Hydrostatic and deviatoric loading configuration.

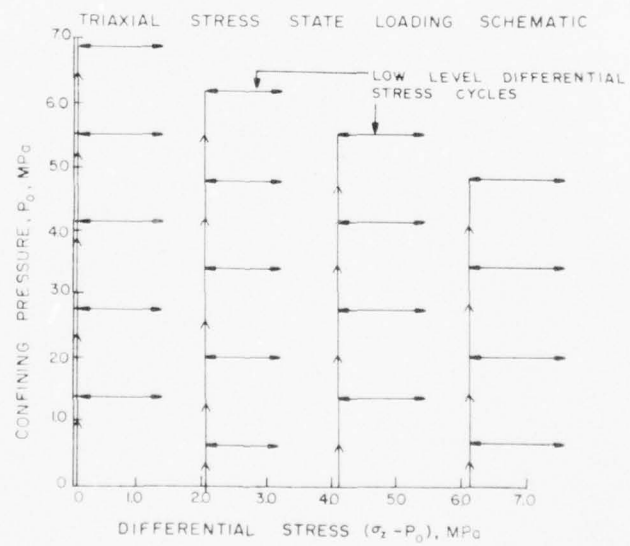


Figure 7. Stress trajectories during triaxial loading sequence.

Experimental Results

Figure 8 shows a typical result of the experimental program outlined above. It consists of the radial pressure - borehole deformation plot for sample ISS 9 overcore 4. The tested rock shows 95 percent deformation recovery upon unloading. Because the unloading phase best approximates the overcoring operation, only unloading curves will be analyzed throughout the remainder of the report. Figure 9 shows a typical borehole deformation result during unloading for sample ISS 9 overcore 4. Results for ISS 4 overcore 5, ISS 6 overcore 2, ISS 7 overcore 2 and acrylic may be found in Appendix A.

Table I summarizes the equations used for determining the secant modulus for each of the three test configurations (Cases I, II and III). These equations were obtained by substituting 1.91 cm and 6.99 cm for a and b , respectively, in equations 1 through 3. Table II lists the average values of the calculated secant moduli to 3.45 MPa radial pressure for the different test configurations. The results of the acrylic specimen are included for comparison.

Table III lists Young's modulus and Poisson's ratio for the overcore tests performed for configurations IV and V. Note that at each mean stress state the initial external differential load was zero. Figures 10 and 11 show typical results for the 5.1-cm diameter triaxially tested cores in which Young's modulus is plotted versus mean and shear stress respectively, (Case V).

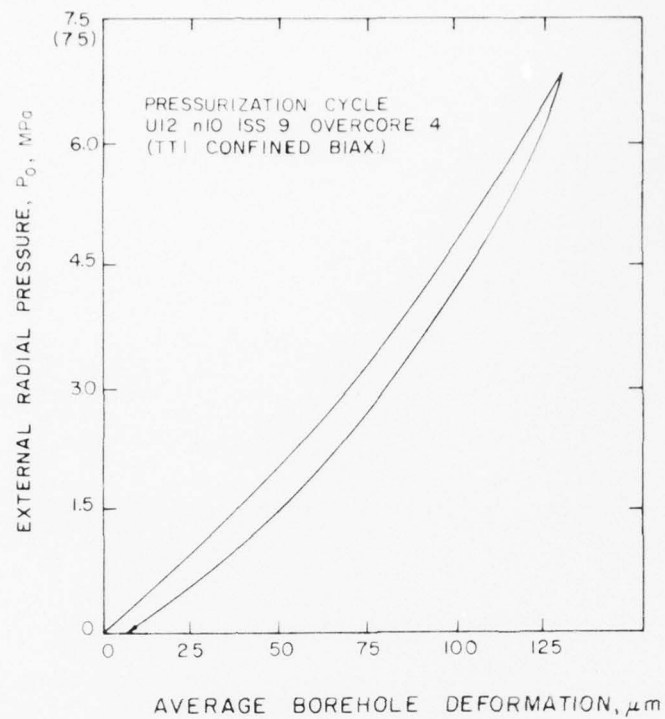


Figure 8. Typical radial-pressure-versus-borehole-deformation cycle which indicates nonlinear behavior.

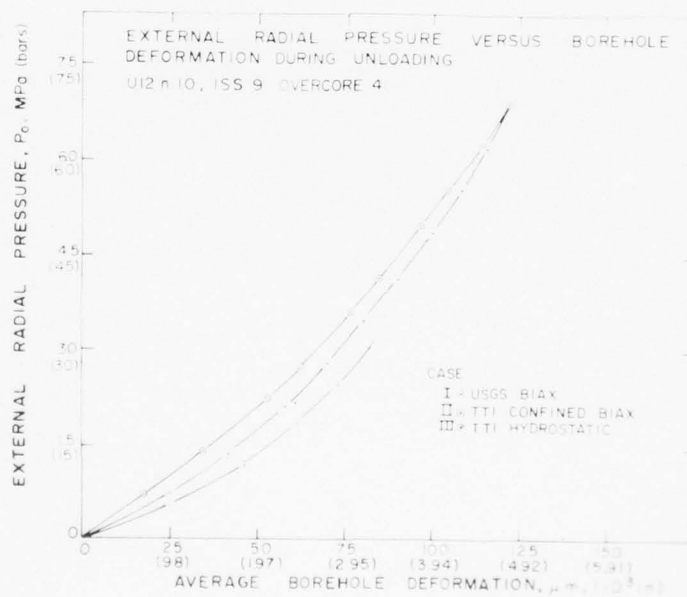


Figure 9. Pressure versus borehole deformation during unloading for the three test configurations.

AD-A043 977

TERRA TEK INC SALT LAKE CITY UTAH

F/G 18/3

MATERIAL PROPERTIES OF NEVADA TEST SITE TUFF AND GROUT - WITH E--ETC(U)

NOV 76 S W BUTTERS, R K DROPEK, A H JONES

DNA001-75-C-0260

UNCLASSIFIED

TR-76-63

DNA-4235F

NL

5 OF 5
AD
A043977



END
DATE
FILMED

10-77

DDC

TABLE I
Relations for Determining
Young's Modulus for the Three Test Configurations

Test Type	Elastic Modulus Equation
Case I	$E = 8.23 P_o/U_i$ (i)
Case II	$E = 8.23 P_o/U_i - 3.81 \nu \sigma_z/U_i$ (ii)
Case III	$E = P_o/U_i (8.23 - 3.81 \nu)$ (iii)

TABLE II
Secant Modulus Comparisons at
3.45 MPa Radial Pressure
Using the Equations in Table I

Material	Test Type		
	Case I	Case II	Case III
Acrylic	2.63 GPa	2.66 GPa	2.77 GPa
ISS 4 oc 5*	1.79 GPa	1.41 GPa	1.28 GPa
ISS 6 oc 2**	2.12 GPa	2.14 GPa	---
ISS 7 oc 2	8.90 GPa	7.86 GPa	8.07 GPa
ISS 9 oc 4	3.19 GPa	3.33 GPa	3.54 GPa

* Noted extensive fracture running the length of the overcore sample. It appears to have caused deviations in the characteristic rock deformation.

** Moduli compared at 2.41 MPa radial pressure due to core failure during Biax test.

TABLE III
Elastic Constants From Triaxial Tests
(initial slope at $P_0 = 1/3 J_1$ Case IV)

Sample	$1/3 J_1$ MPa	Overcore Young's Modulus GPa	Poisson's Ratio		Average Poisson's Ratio
			Case IV	Case V	
ISS 4 oc 5	1.38	2.05	0.15	0.17	0.16
	2.76	2.60	0.18	0.18	0.18
	4.14	3.41	0.22	0.19	0.21
	5.52	3.43	0.22	0.19	0.21
	6.90	4.06	0.23	0.19	0.22
ISS 7 oc 2*	0.0	--	--	0.08	0.08
	3.45	--	--	0.19	0.19
	6.90	--	--	0.20	0.20
ISS 9 oc 4	0.0	2.59	0.06	--	0.06
	1.38	3.81	0.10	0.12	0.11
	2.76	4.50	0.12	0.13	0.13
	4.14	5.13	0.11	0.13	0.12
	5.52	5.55	0.14	0.13	0.14
	6.90	6.21	0.16	0.14	0.15

* Triaxial test run on adjacent footage to overcore sample.

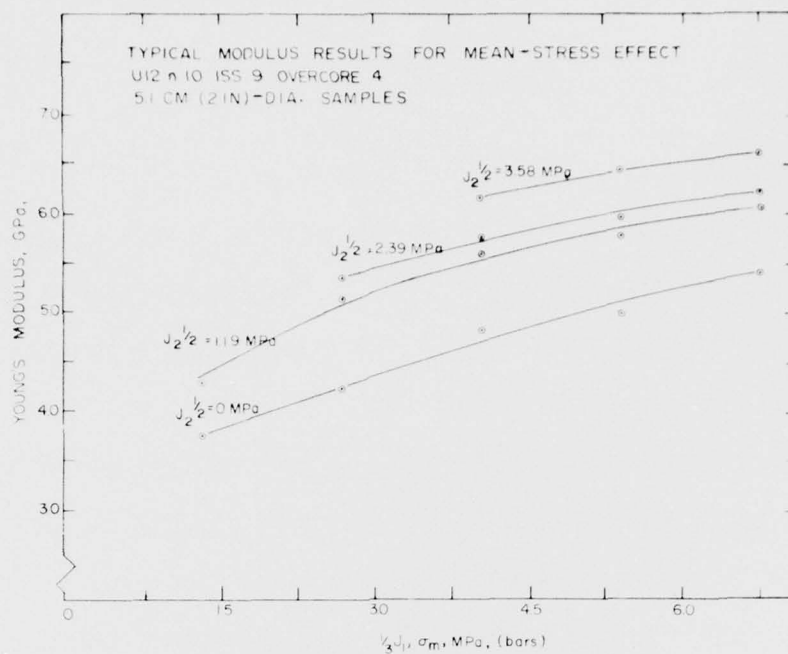


Figure 10. Mean stress effect on the 5.1 cm-diameter core elastic modulus.

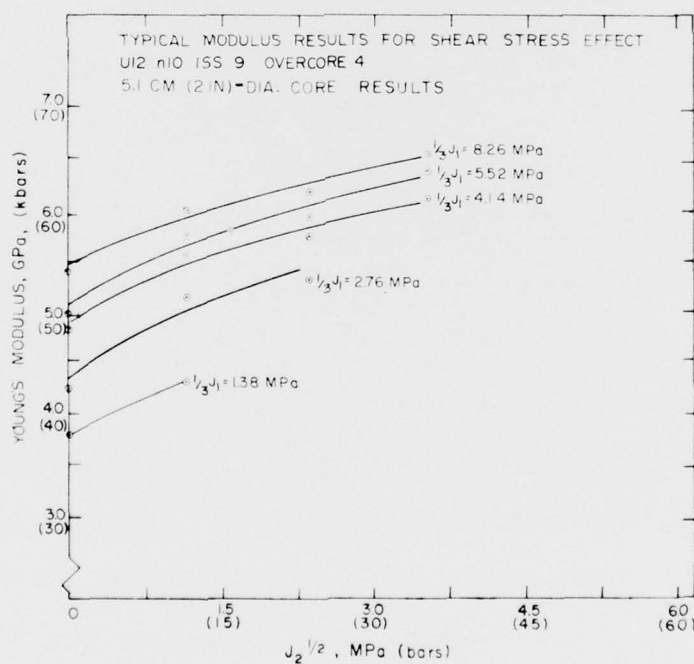


Figure 11. Shear stress effect on the 5.1 cm-diameter core elastic modulus.

DISCUSSION

Modulus Comparisons

The effects of mean stress and shear stress on the secant and tangent elastic moduli of Rainier Mesa Tuff are shown in Figures 12, 13 and 14. These figures show the moduli determined from test configurations III and IV. Figure 12 shows that mean stress has little effect on the acrylic sample and that the determined tangent moduli agree to within the experimental accuracy of 5 percent. Figures 13 and 14 show Young's modulus to increase as the mean stress increases, the tangent moduli increasing more than the secant moduli. The tangent moduli determined from different loading conditions agree to within 10 percent in both cases.

A comparison of Young's modulus between the triaxially loaded overcore sample (case IV) and the solid core (case V) is shown in Figure 15. Solid-core moduli were obtained from crossplotting Figure 10 ($J_2^{1/2} = 0.0$ MPa). Although the tangent moduli were determined for both solid sample and overcore at zero initial deviatoric load, the overcore, due to its geometry, maintained a shear stress which varied as the inverse of the radius squared. Thus at any given external hydrostatic load an average shear stress $\bar{J}_2^{1/2}$ defined by $(b-a)^{-1} \int_a^b J_2^{1/2} dr$ could be calculated. After calculating the average shear stress in the overcore, a correction was applied to the solid-core modulus, the correction being based on the results for solid core as shown in Figures 10 and 11. After shear-stress correction, Figure 18 shows a tangent Young's modulus agreement within 5 percent. It becomes apparent that to determine an overcore Young's modulus using standard "solid" specimens require that the shear and mean stresses experienced by the overcore be applied to the solid specimen.

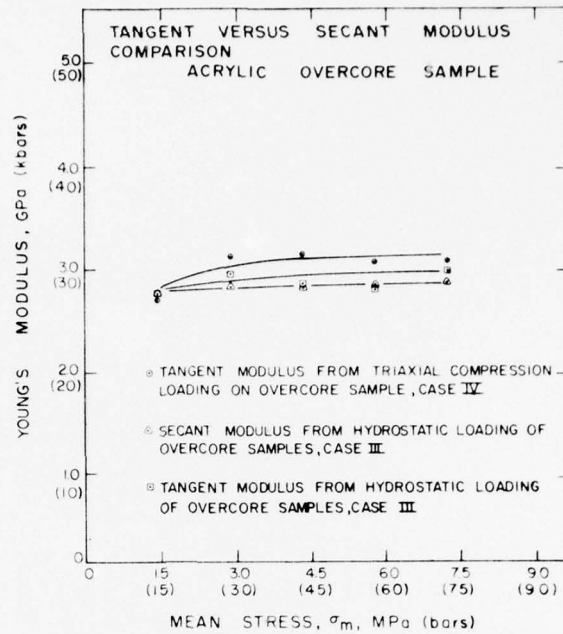


Figure 12. Modulus curves for acrylic comparing tangent and secant moduli. Note little variation in moduli with mean stress.

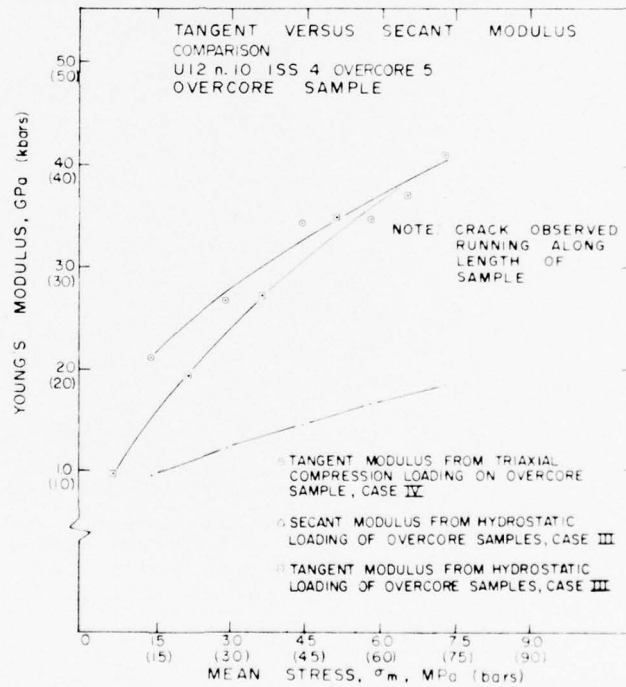


Figure 13. Modulus curves for ISS overcore 5 comparing tangent and secant moduli. Note that moduli increase with mean stress.

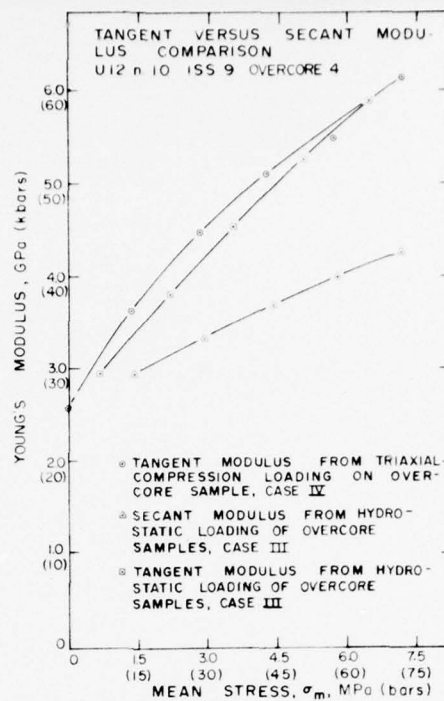


Figure 14. Modulus curves for ISS 9 overcore 4 comparing tangent and secant moduli. Note that moduli increase with mean stress.

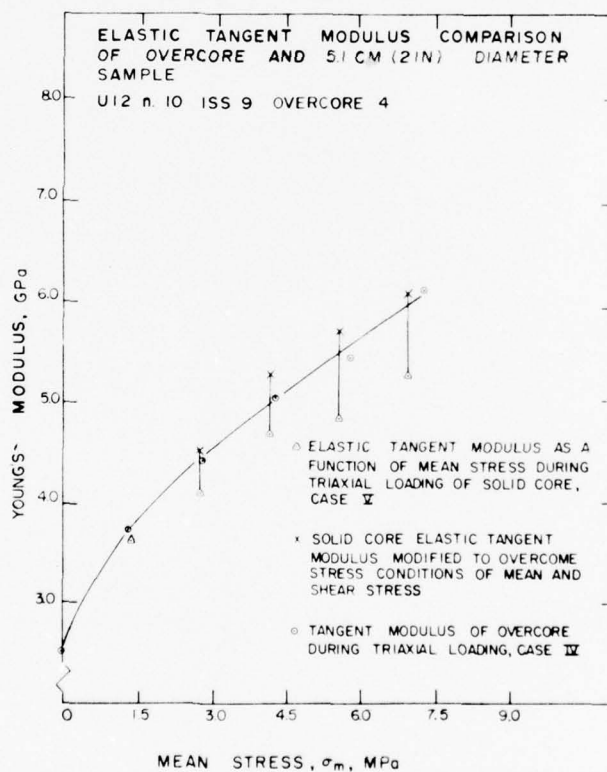


Figure 15. Tangent modulus comparison of the overcore and 5.1 cm (2 in) diameter samples when plotted against mean stress. The moduli were determined by triaxial loading from an initial hydrostatic state.

Another point of discussion concerns the comparison of biaxial secant moduli to standard (solid-core) tangent moduli. When comparing the tangent moduli of the 5.1 cm-diameter core with the overcore secant moduli as shown in Figure 16 an apparent discrepancy occurs; Figures 14 and 15 illustrate that by comparing tangent moduli and correcting for shear stresses one obtains a fair agreement. The apparent discrepancy lies in the modulus definition and the different stress states in which the samples were tested.

Modulus Selection

It is obvious from the idealized loading curve shown in Figure 2 that the secant Young's modulus at 2.5 MPa mean stress is less than the secant Young's modulus determined at higher radial pressures. Similar results may be obtained from Figures 9, 18, 19 and 20 as listed in Table IV. Table IV shows a secant modulus comparison at 3.45 MPa and 6.9 MPa radial pressure with the associated percent difference. As the degree of non-linearity increases so also does the percent difference in secant moduli. In order to select the secant modulus for *in situ* stress calculations it is necessary to generate a secant modulus versus borehole deformation plot as shown in Figure 17. The plot shows that for any observed *in situ* deformation, the corresponding secant modulus may be properly selected for calculation purposes. This assumes that the sample can be tested to high-enough radial pressures to achieve borehole deformations equal to or greater than that observed *in situ*, and that the principal *in situ* stresses perpendicular to the borehole axis are nearly equal. This type of plot would minimize errors caused by mean and shear stress effects on Young's

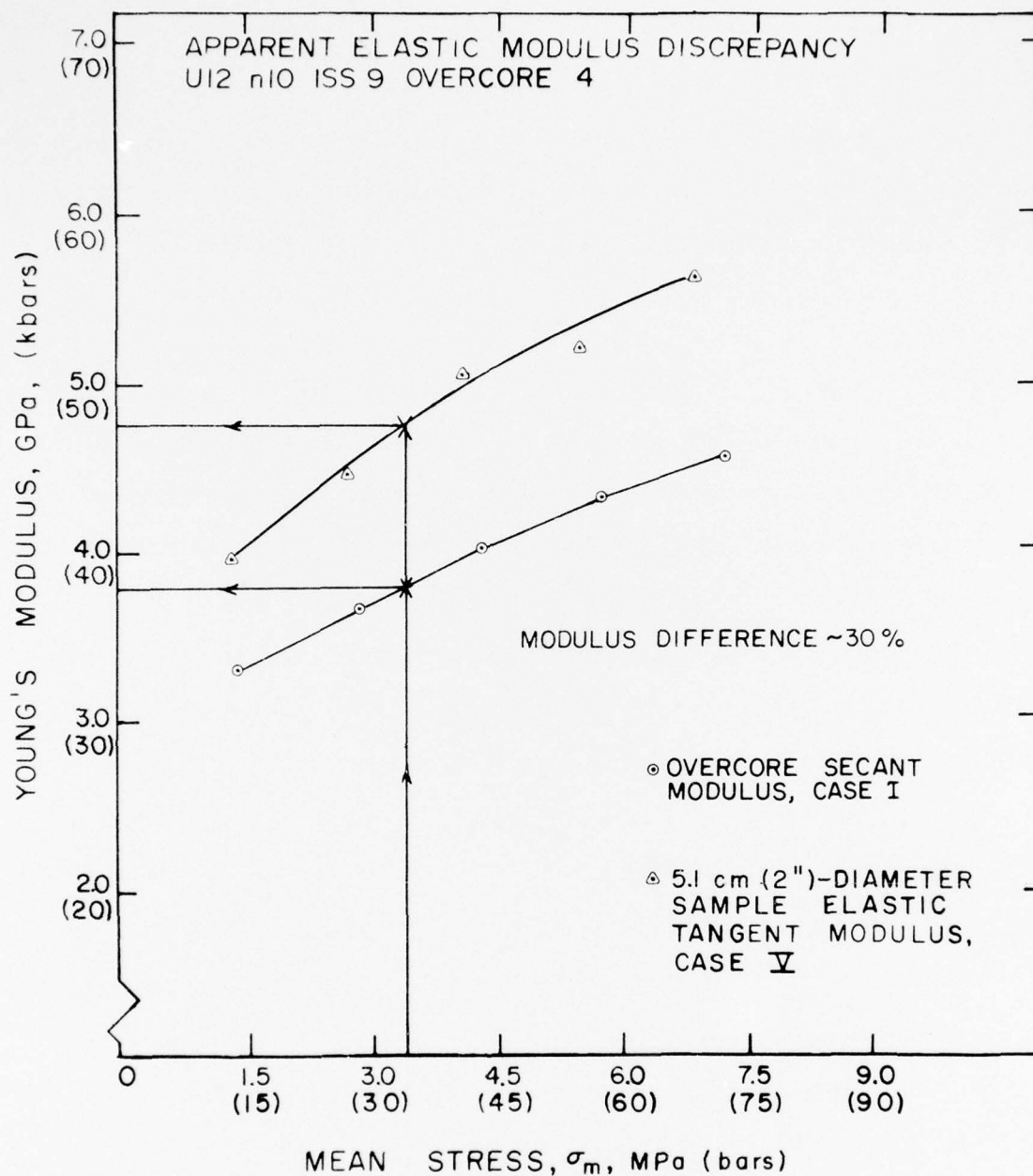


Figure 16. Apparent elastic modulus discrepancy when comparing overcore secant moduli with 5.1 cm-diameter (solid) core moduli.

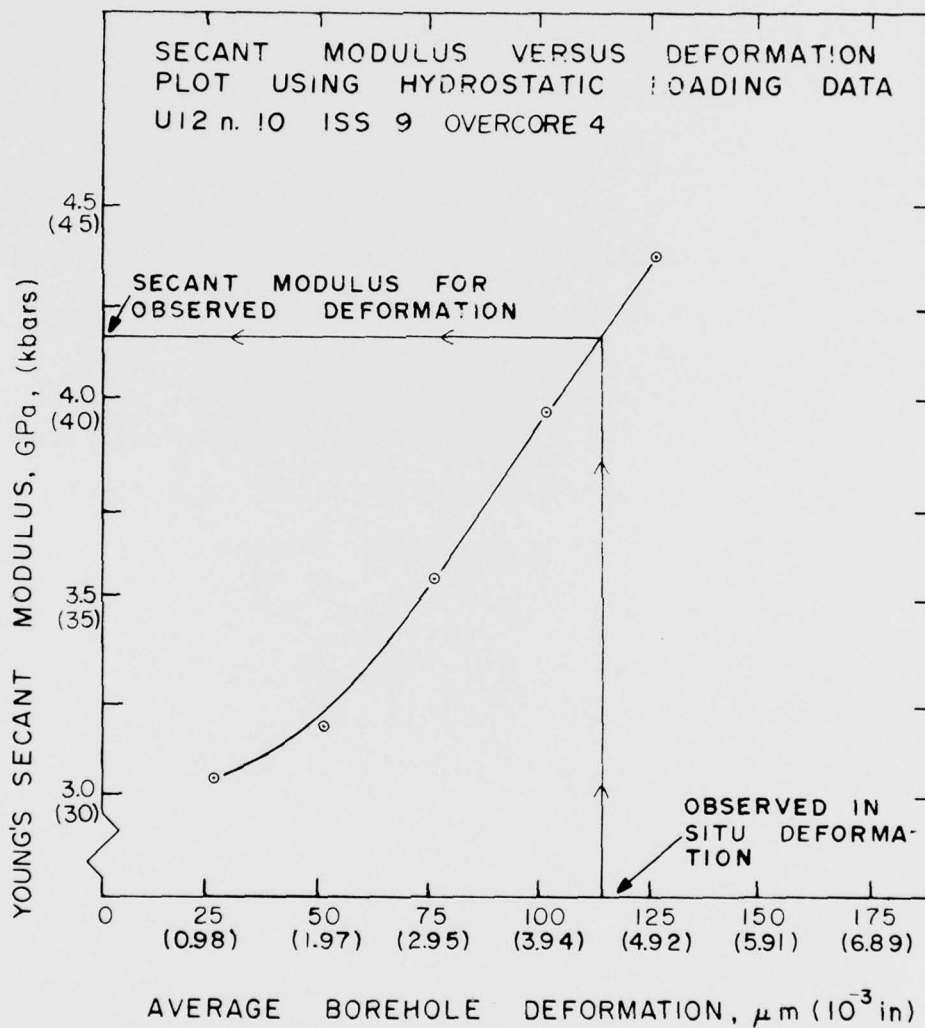


Figure 17. Overcore secant modulus versus borehole deformation illustrating the selection of the secant modulus to be used for *in situ* stress calculations when radial *in situ* stresses are equal.

TABLE IV
Secant Modulus (GPa) Comparison During
Hydrostatic Loading at 3.45 MPa and 6.9 MPa Pressure

Material	3.45 GPa	6.9 GPa	% Difference
Acrylic	2.77	2.79	0.8
ISS 4 oc 5	1.28	1.76	37.8
ISS 7 oc 2	8.07	9.45	17.1
ISS 9 oc 4	3.54	4.27	20.7

modulus when $\sigma_1 \approx \sigma_2 \approx \sigma_3$ *in situ*. The principal *in situ* stresses at Rainier Mesa have been shown to be approximately $\sigma_1 \approx \sigma_2 \approx 2\sigma_3$ (Haimson, et al., 1974) suggesting that for any overcoring operation the principal *in situ* stresses perpendicular to the axis of a vertical borehole would most likely be unequal. Under these conditions *in situ* mean stresses may be achievable, but *in situ* shear stress effects on Young's modulus could not be approximated since unequal radial stresses cannot be applied about the circular overcore specimens in the present test configurations. However, by obtaining moduli as a function of mean and shear stress the correct moduli can be defined.

Laboratory Testing Recommendations

As previously noted, the biaxial tester (Case I) often fails the NTS tuff at radial pressures slightly above 3.45 MPa due to extension failure. Because of the 3.45 MPa radial pressure limitation, the biaxial tester is often not able to obtain the average *in situ* borehole deformation. It has been shown that with either the rigid-end constraint condition (Case II) or the hydrostatic case (Case III), radial pressures in excess of 6.90 MPa

are attainable without sample failure. Ideally the applied axial stress during laboratory testing should approximate the *in situ* axial stress on the overcore sample during the overcoring procedure. This axial stress is unknown however and varies even as overcoring progresses past the gage point. It may be argued that an intermediate axial stress state, $0.0 < \sigma_z < P_0$, should be used during laboratory testing since it is likely that the axial stress during overcoring lies within this range. An intermediate axial stress may be approximated using the confined biaxial test in which axial strain was zero (Case II) giving $\sigma_z = \nu 2.16 P_0$. The Young's modulus and Poisson's ratio for this case become

$$E = 8.23 (1 - \nu^2) P_0 / U_i \quad (5)$$

and,

$$\nu = 0.463 \sigma_z / P_0 \quad (6)$$

using $a = 1.91$ cm and $b = 6.99$ cm. A desirable feature of this technique is that Poisson's ratio is independent of the elastic modulus. The additional field instrumentation for an $\epsilon_z = 0.0$ percent test would involve an axial loading frame with an axial loading piston and a means of measuring axial stress and strain.

CONCLUDING REMARKS

When triaxially testing standard 5.1 cm-diameter solid cores taken from the overcore samples, it was shown that mean and shear stress states should be adjusted to the average overcore stress state to obtain comparable Young's modulus values. It was also shown that agreement occurred between tangent moduli determined from radial and axial loading of the overcores suggesting material isotropy.

The tuff samples tested herein were nonlinearly elastic. Elastic nonlinearity requires that samples be tested to external radial pressures equal to or greater than those required to induce *in situ* deformation. With the radial pressurization schemes used here, *in situ* mean stresses were obtainable but not the shear stresses. Achieving *in situ* mean stresses may require axial load application to achieve radial pressures greater than 3.45 MPa (biaxial tester limitation due to sample failure). An intermediate axial stress during laboratory testing ($0.0 < \sigma_z < P_0$) is suggested as an approximation to the unknown *in situ* axial stress during overcoring. A convenient intermediate axial stress state ($0.0 < \sigma_z < P_0$) may be achieved using a zero axial strain loading scheme from which Poisson's ratio and Young's modulus are easily obtained.

REFERENCES

- Becker, R. M., Hooker, V. E., 1967, "Some Anisotropic Consideration in Rock Stress Determinations," *U. S. Bureau of Mines Rept. Inv.* 6955, pp. 1-23.
- Fitzpatrick, J., 1962, "Biaxial Device for Determining Modulus of Elasticity of Stress-Relief Cores," *U. S. Bureau of Mines Inv.* 6128, pp. 1-13.
- Haimson, B., LaComb, J. W., Jones, A. H., and Green, S. J., 1974, "Deep Stress Measurements in Tuff at the Nevada Test Site," *Terra Tek Technical Report* TR 74-11.
- Hooker, V. E. and Bickel, D. L., 1974, "Overcoring Equipment and Techniques used in Rock Stress Determination," *U. S. Bureau of Mines Inf. Circ.* 8618, pp. 1-32.
- LaComb, J. W., 1976, Personal Communication, Defense Nuclear Agency, Nevada Test Site, Mercury, Nevada.
- Merrill, R. H., 1967, "Three-component Borehole Deformation Gage for Determining the Stress in Rock," *U. S. Bureau of Mines Rept. Inv.* 7015, pp. 1-38.
- Obert, L., 1964, "Triaxial Method for Determining the Elastic Constants of Stress Relief Cores," *U. S. Bureau of Mines Rept. Inv.* 6490, pp. 1-22.
- Panek, L. A., 1966, "Calculations of the Average Ground Stress Components from Measurements of the Diametral Deformation of a Drill Hole," *U. S. Bureau of Mines Rept. Inv.* 6732, pp. 1-41.

APPENDIX A
Additional Experimental Results

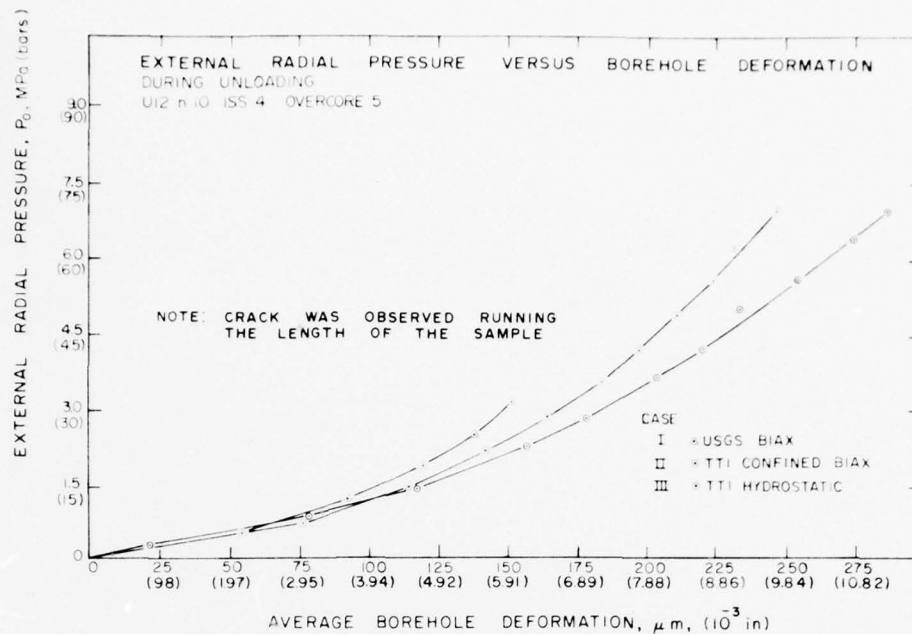


Figure 18. Radial pressure versus borehole deformation during unloading for ISS 4 overcore 5 comparing the three test configurations.

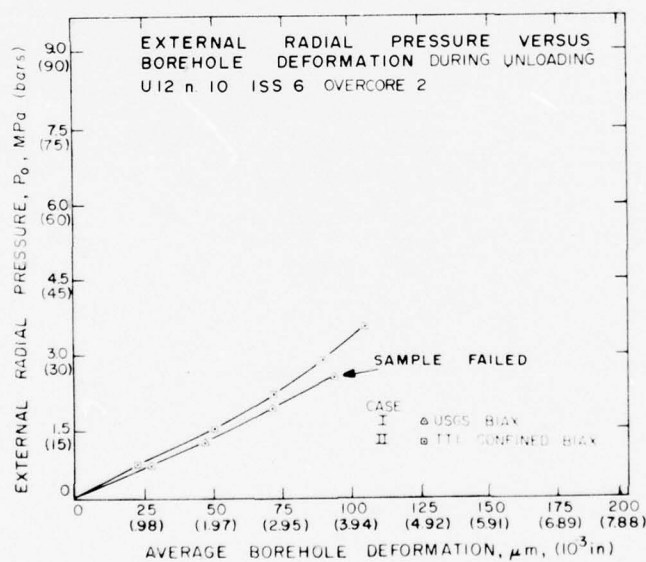


Figure 19. Radial pressure versus borehole deformation during unloading for ISS 6 overcore 2 comparing two test configurations.

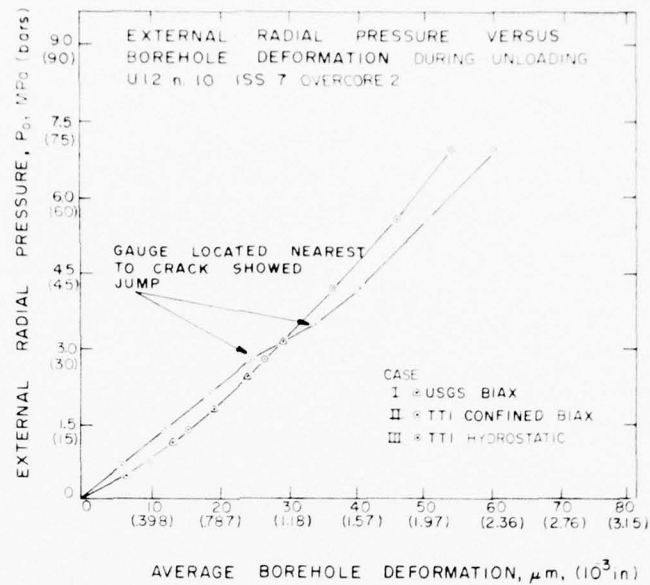


Figure 20. Radial pressure versus borehole deformation during unloading for ISS 7 overcore 2 comparing the three test configurations.

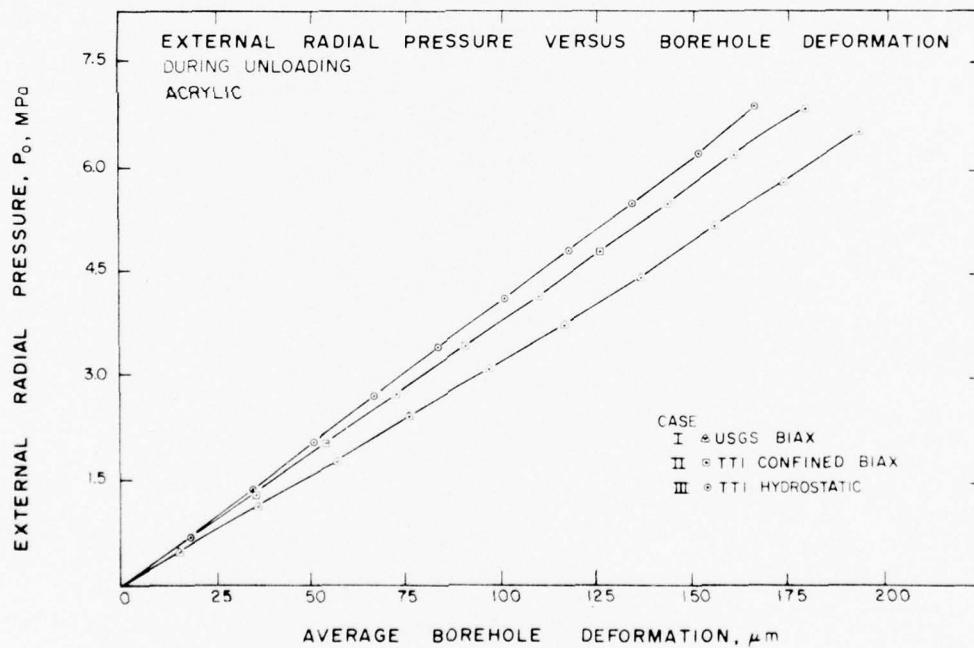


Figure 21. Radial pressure versus borehole deformation during unloading for acrylic comparing the three test configurations.

SPECIFIC MOISTURE RETENTION
OF NEVADA TEST SITE TUFFS

by

S. W. Butters
R. K. Dropek
A. H. Jones

Submitted to

Mr. J. W. LaComb
Defense Nuclear Agency
Nevada Test Site
Mercury, Nevada 89023

Contract DNA 001-75-C-0260

Submitted by

Terra Tek, Inc.
University Research Park
420 Wakara Way
Salt Lake City, Utah 84108

TR 76-35
July 1976

SUMMARY

Moisture was reintroduced into dry Nevada Test Site tuff core chips through placement in a high humidity (~95 to 100 percent) chamber at room temperature (~23°C) and atmospheric pressure (~650 mm). A minimum of 29 days was required for the dry samples to equal or exceed what was considered their *in situ* saturation levels (these *in situ* saturation levels were obtained from adjacent samples). Mechanical tests conducted subsequent to resaturation suggest that dried-resaturated samples can be used to obtain representative material properties for virgin saturated tuff.

Tuff samples, immediately sealed at the Nevada Test Site on removal from a core barrel, were subjected to the same environment to assist in analyzing the invasion of the drilling water. Tests results to date are inconclusive.

TABLE OF CONTENTS

	<u>Page</u>
Summary	408
Table of Contents	409
List of Illustrations	410
List of Tables	410
Introduction	411
Test Program	413
Experimental Results	414
Discussion	420
Conclusions	422
References	423

LIST OF ILLUSTRATIONS

<u>Figure</u>	<u>Title</u>	<u>Page</u>
1	Moisture gain versus time plots for dry samples, 0-30 days	414
2	Moisture gain versus time plots for dry samples, 25-30 days	415
3	Moisture gain versus time plots for sealed samples, 0-30 days	417
4	Moisture gain versus time plots for sealed samples, 25-30 days	418
5a	Mean normal stress versus volume strain for dry- resaturated and sealed-further moisturized sam- ples subjected to uniaxial strain load-unload . . .	419
5b	Differential stress versus confining pressure for dry-resaturated and sealed-further moisturized samples subjected to uniaxial strain load- unload	419

LIST OF TABLES

<u>Figure</u>	<u>Title</u>	<u>Page</u>
I	Core Location in UE12n#9	413
II	Physical and Mechanical Property Data on Dry- Resaturated Cores, As-Received Cores (Sealed) and the Further Moisturized "As-Received" Core Samples	416

INTRODUCTION

The complexity of the Nevada Test Site nuclear test program has increased considerably during the past several years. This increased demand requires "fine tuning" our knowledge of the material properties of the resident tuff at the site. To this end, Terra Tek conducted tests to evaluate the effect of drying and resaturation on the material properties of tuff core samples and to establish the likelihood of water invasion during field coring.

Drying-Resaturating: As the state-of-the-art of material properties evaluation, material models and ground-motion calculations have advanced, there is benefit to reanalyzing past nuclear events. The lack of preserved (sealed) core samples has presented limitations. A solution is to resaturate dry core samples and use them for obtaining the material properties. It was, therefore, necessary to verify that material properties measured on the dried-resaturated samples were representative of the properties of material in which the moisture had been maintained.

Several sets of dry and adjacent sealed tuff core samples were processed and tested to answer this question of the effect of the drying-resaturation cycle.

Field Coring Water Penetration: Pieces of the sealed core samples, discussed above, were also subjected to further moisturizing in a high humidity chamber. The purpose was to determine the probability of water invasion into the already "wet" samples. It has been reasoned¹ that measuring the loss or gain in weight of previously sealed cores while suspended in a high humidity chamber would provide an indication of whether

or not drilling water invaded the cores. Lost moisture would suggest water had invaded the tuff during coring. On the other hand, a gain in moisture would not provide conclusive evidence of drilling water invasion.

TEST PROGRAM

Dry core samples were resaturated in a high humidity environment (95 to 100 percent) at room temperature and atmospheric pressure. When the samples ceased to gain moisture, the physical and mechanical properties were measured and compared with those of adjacent samples which had been maintained at their original *in situ* moisture level.

Samples prepared to investigate water invasion during coring were received sealed. They were unwrapped on placement in the high humidity chamber.

Sample Preparation: Samples were retrieved from five sets of neighboring locations in drill hole UE12n#9 at the Nevada Test Site². The individual footages are listed in Table 1. With the exception of "Location 1", these cores are in close proximity to each other.

TABLE I
Core Location in UE12n#9

Location	Dry Samples	Sealed Samples	Sealed and Remoisturized Samples
1	147'	155'	155'
2	317'	319'	319'
3	455'	456'	456'
4	516'	515'	515'
5	589'	588'	588'

EXPERIMENTAL RESULTS

Drying-Resaturating: The moisture gain data for the dry samples are shown in Figure 1. The samples increased in moisture content very noticeably during the first eleven days with subsequent rapid stabilization to a lower moisture assimilation rate. The samples were still gaining moisture slightly, through the 30 days of the test, as shown in Figure 2. Physical properties of the dry-resaturated tuff are listed in Table II³. The measured permanent compactions, included in Table II, were obtained from cycling in uniaxial strain to 4 kilobars mean stress. Note the comparison of the physical properties of the dry-resaturated samples to the sealed samples.

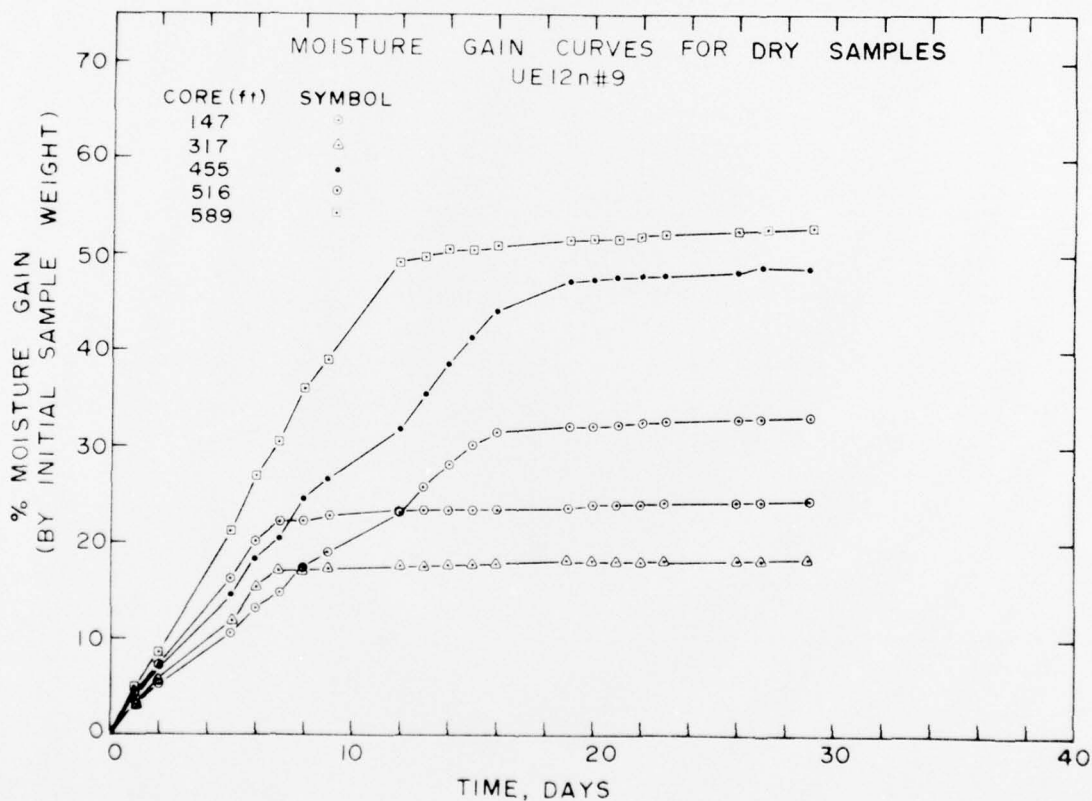


Figure 1. Moisture gain versus time plots for dry samples, 0-30 days.

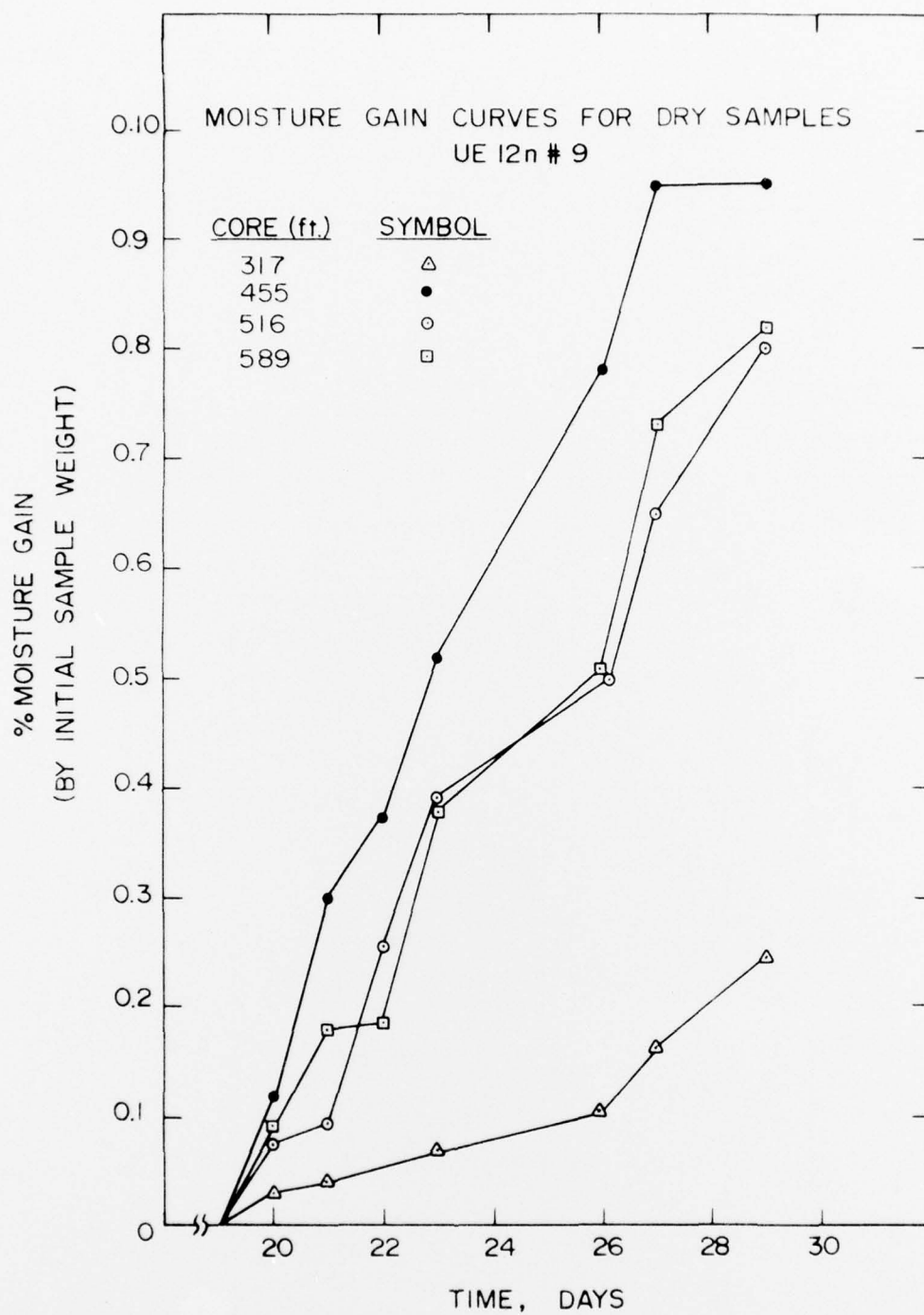


Figure 2. Moisture gain versus time plots for dry samples, 25-30 days.

TABLE II

Physical and Mechanical Property Data on Dry-Resaturated Cores,
As-Received Cores (Sealed) and the Further Moisturized "As-Received" Core Samples

FOOTAGE SAMPLE DESIGNATION	DENSITY (gm/cc)			WATER BY WET WEIGHT (%)	POROSITY (%)	SATURATION (%)	CALC. AIR VOIDS (%)	MEAS PERMANENT COMP (%)
	WET	DRY	GRAIN					
<u>147-155</u>								
Dry-Resat 1A	1.80	1.43	2.47	20.5	42	88	5.0	----
As-Received (Sealed) 1B	----	----	----	----	--	--	---	----
As-Received and Further Moisturized 1C	----	----	----	----	--	--	---	----
<u>317-319</u>								
Dry-Resat 2A	1.81	1.52	2.37	15.8	36	80	7.3	8.0
As-Received (Sealed) 2B	1.80	1.50	2.38	16.4	37	80	8.3	----
As-Received and Further Moisturized 2C	1.82	1.50	2.37	17.4	37	86	5.1	5.5
<u>455-456</u>								
Dry-Resat 3A	1.49	0.99	2.41	33.6	59	85	8.7	8.2
As-Received (Sealed) 3B	1.49	1.02	2.42	31.6	58	81	10.8	----
As-Received and Further Moisturized 3C	1.54	1.02	2.42	33.6	58	89	6.3	3.7
<u>515-516</u>								
Dry-Resat 4A	1.58	1.14	2.37	27.8	52	84	8.2	----
As-Received (Sealed) 4B	1.55	1.19	2.37	23.4	50	73	13.7	----
As-Received and Further Moisturized 4C	1.62	1.19	2.37	26.3	50	86	7.1	----
<u>588-589</u>								
Dry-Resat 5A	1.47	0.94	2.36	35.9	60	88	7.0	7.6
As-Received (Sealed) 5B	1.46	0.91	2.37	37.5	61	89	6.8	----
As-Received and Further Moisturized 5C	1.51	0.91	2.37	39.6	61	97	1.6	2.8

Field Coring Water Penetration: The moisture gain data for the sealed samples are shown in Figure 3. Note that the samples did gain moisture and were still gaining slightly after 30 days - Figure 4. The physical properties for these samples are also listed in Table II (see "as-received and further moisturized"). Uniaxial strain tests were conducted on these samples for comparison with the tests conducted on the dry-resaturated. The stress-strain and stress-stress curves for both groups are shown in Figure 5. Mechanical tests were not conducted at footages 147-155 and 515-516 due to the poor condition of the core samples following resaturation.

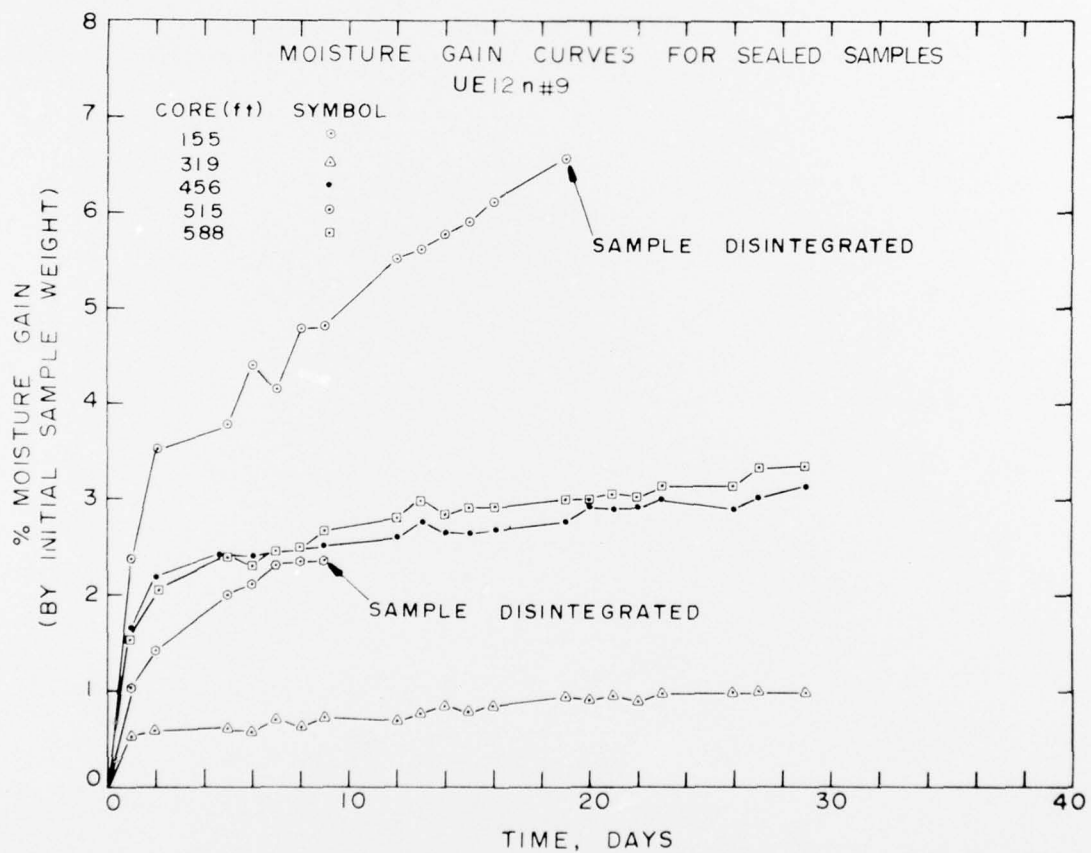


Figure 3. Moisture gain versus time plots for sealed samples, 0-30 days.

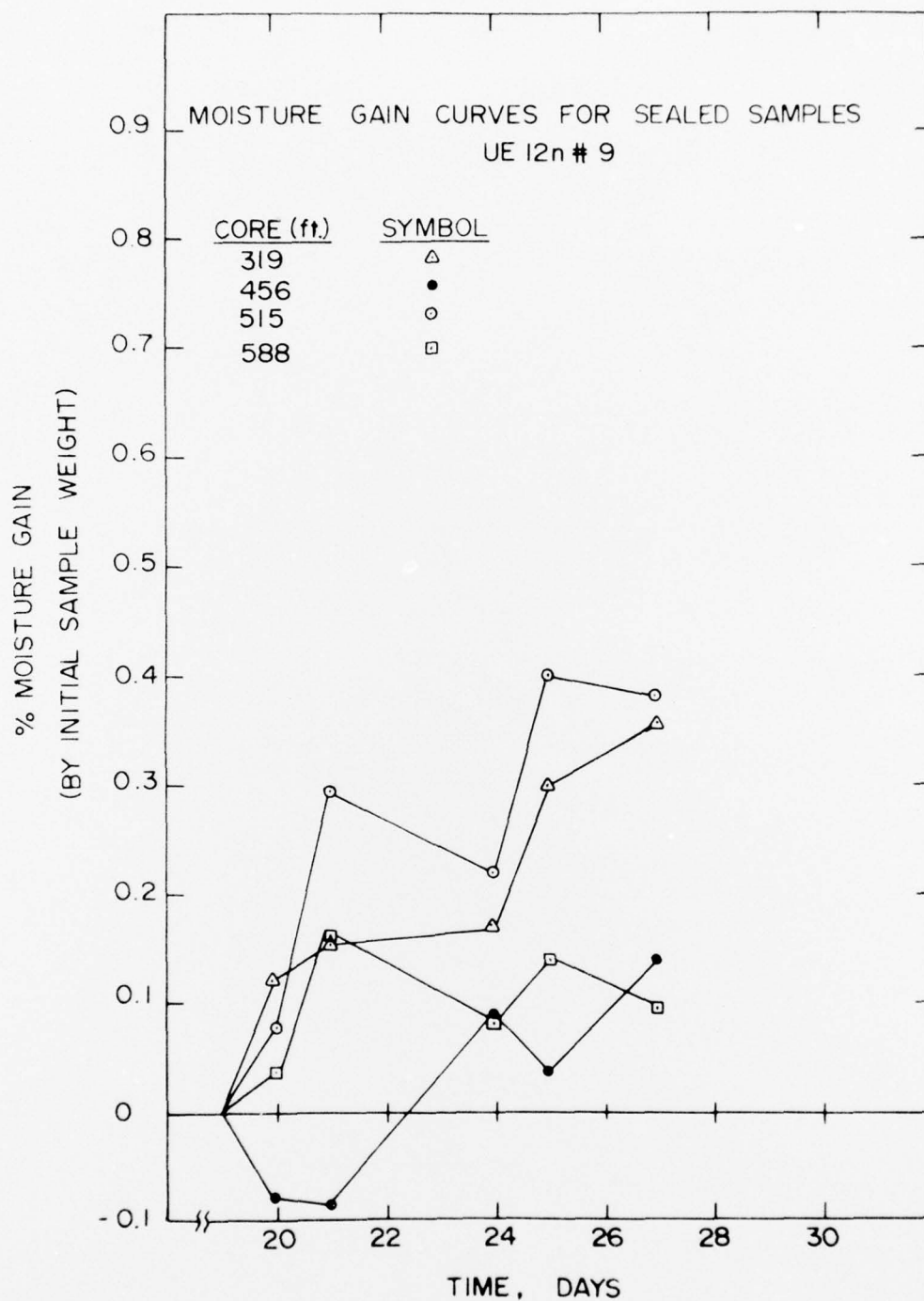


Figure 4. Moisture gain versus time plots for sealed samples, 25-30 days.

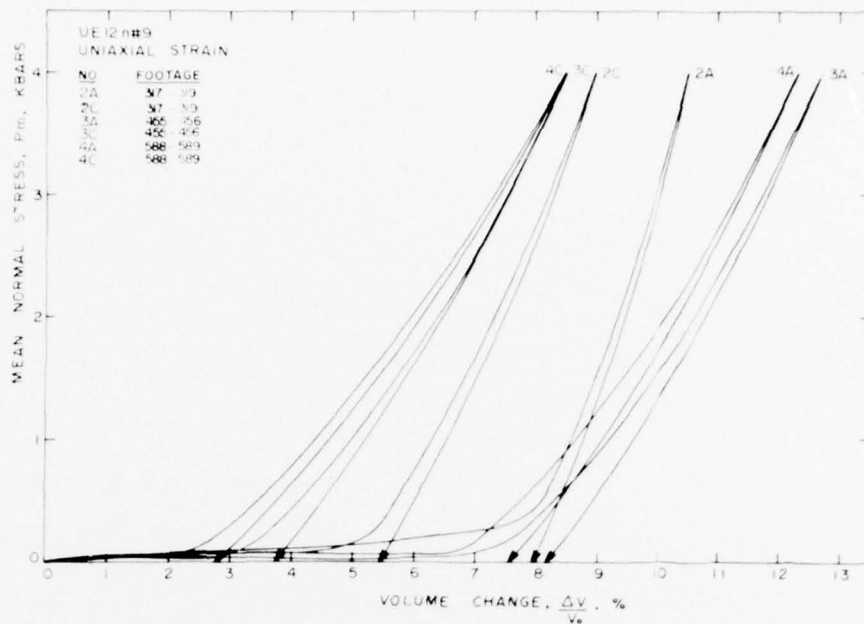


Figure 5a. Mean normal stress versus volume strain for dry-resaturated and sealed-further moisturized samples subjected to uniaxial strain load-unload.

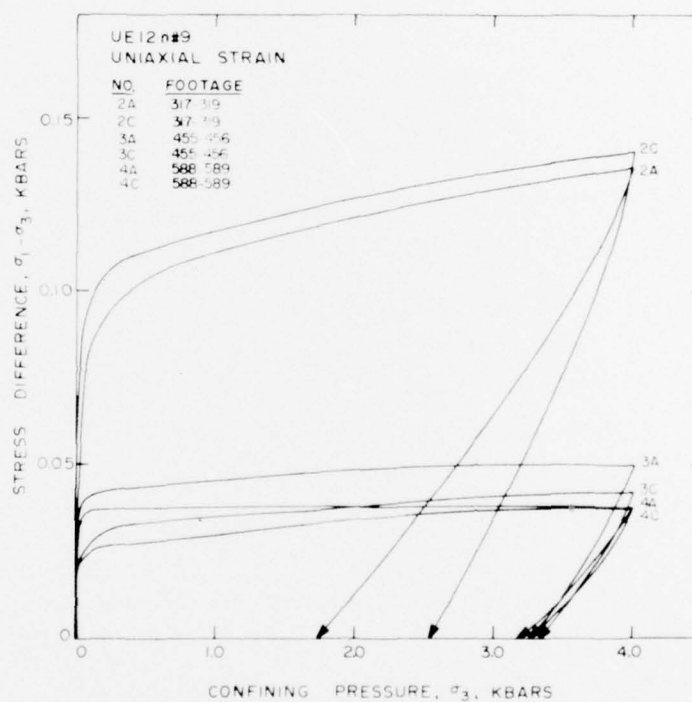


Figure 5b. Differential stress versus confining pressure for dry-resaturated and sealed-further moisturized samples subjected to uniaxial strain load-unload.

DISCUSSION

Drying-Resaturating: As seen in Table II, there are considerable differences in the material properties between the samples from different locations. An example is the porosities -- 38 percent in the set of samples at 317'-319' and 59 percent in the samples at 455'-456'. Nonetheless, the dry samples all showed increases in moisture content of several percent per day through the first 6 to 16 days with gains then changing to tenths of a percent per day through 30 days. The lower porosity samples, expectedly, showed a rapid decrease in rate of gain in moisture at an earlier date than the higher porosity samples.

The moisture contents on the dry tuff samples, after 30 days, had exceeded the moisture contents of the adjacent sealed samples. This would suggest that the dry samples could be resaturated but the questions would be -- "to what moisture content". If only the strength properties are required, the resaturation process and the final moisture content do not appear to have a noticeable effect, (Figure 5b). However, the moisture content is critical if the material properties requirements include the gas-filled void content, (Figure 5a).

Heretofore, the *in situ* moisture content has been obtained from sealed core samples. Since sealed core is not always available, however, a means for identifying the original *in situ* moisture content of the dry core is necessary. One possible means is the use of the inflection point on the moisture gain versus time curves for the dry samples (i.e., the intercept of the tangents to the high and low rates). The exact meaning of this inflection point is not presently understood although it is most likely a function of the water in a sample (i.e. pore water, molecular water, etc.).

An indication of the significance of the inflection point on the curves is that when using the inflection point moisture content for comparison with the moisture content of the sealed samples, there were two previously dry (2A and 5A) which had exceeded the moisture content of the sealed samples (2B and 5B) and two previously dry samples (3A and 4A) with moisture contents less than those of the sealed samples (3B and 4B). Further analysis, therefore, could prove that the inflection points are indeed a good indicator of the original *in situ* moisture content of the samples.

Field Coring Water Penetration: The moisture gains on the sealed samples were somewhat surprising and did not allow any conclusions to be made concerning the intrusion of water during field coring. One problem in analyzing the data is the lack of moisture gain measurements during the first 24 hours. Obviously, further analysis should include measurements at much shorter time history. The experimental setup should also better simulate the actual field coring conditions such as fluid (mud) pressure and viscosity.

CONCLUSIONS

The dry tuff core samples from the Nevada Test Site can be returned to a nearly saturated state. Given that saturation state, the resaturated cores can be used to obtain material properties representative of those of a sample in which the moisture had been preserved. That is, the drying-resaturation cycle itself does not appear to affect the material properties, but, the final resaturated moisture content will affect certain properties. For example, the shear strength of the tuff was not affected by the drying/resaturating cycle or the final moisture content. The gas-filled void contents (both calculated and from the uniaxial strain tests), on the other hand, were affected very noticeably by the final moisture content. The answer to using the dry core then, lies in having available the correct *in situ* moisture content, heretofore represented by the sealed core samples. Since adjacent sealed core is not always available, however, a means for identifying the original *in situ* moisture content of the dry core is necessary.

As discussed previously, the moisture gain curve inflection point appears to show some possibility for obtaining this needed *in situ* moisture content. Further analysis should include drying several core samples which are presently sealed. This would eliminate the unavoidable discrepancy which existed in this reported work -- that of having to compare sample properties from adjacent cores.

Further analysis on the coring water intrusion would require simulated field coring conditions such as the correct fluid (mud) pressure and viscosity.

REFERENCES

1. March 16, 1976 meeting at the Denver Federal Center with W. S. Twenhofel, J. W. LaComb, W. L. Ellis, S. W. Butters, *et al.*
2. LaComb, J. W., 1976, Supplied Nevada Test Site Tuff Samples, Mercury, Nevada.
3. Dropek, R. K. Butters, S. W., Jones, A. H., 1975 "Methods for Determination of Physical Properties of Rock Materials," Terra Tek, Inc., Technical Report TR 75-13.

Preceding Page BLANK - NOT FILMED

DISTRIBUTION LIST

DEPARTMENT OF DEFENSE

Defense Documentation Center
Cameron Station
12 cy ATTN: TC

Director
Defense Nuclear Agency
ATTN: STSI
3 cy ATTN: STTL
ATTN: DDST
ATTN: SPSS, Dr. Sevin
ATTN: SPSS, T. Kennedy
ATTN: SPSS, K. L. Goering
ATTN: SPSS, LTC Burgess

Commander
Field Command
Defense Nuclear Agency
ATTN: FCTMO
ATTN: FCTMC, Mr. Tibbetts
ATTN: FCT, Captain J. T. Lewis
ATTN: FCTME, Colonel L. G. Langseth
10 cy ATTN: FCTMC, Carl Keller

Chief
Livermore Division, Field Command, DNA
Lawrence Livermore laboratory
ATTN: FCPRL
ATTN: Document Control

Chief
Test Construction Division
Field Command Test Directorate, DNA
10 cy ATTN: NTS, Joe LaComb

Dir. of Defense Research & Engineering
Department of Defense
ATTN: S&SS (OS)

DEPARTMENT OF THE ARMY

Dep. Chief of Staff for Research Dev. & Acq.
Department of the Army
ATTN: NBC Division

Director
Explosive Excavation Research Laboratory
Lawrence Livermore Laboratory
ATTN: Document Control

Commander
Harry Diamond Laboratories
ATTN: DRXDO-NP

Commander
US Army Engineer Center
ATTN: ATSEN-SV-L

DEPARTMENT OF THE ARMY (Continued)

Director
US Army Engineer Waterways Experiment Station
ATTN: Don Day
ATTN: J. Zelasko
ATTN: W. Flathau
ATTN: Research Center Library
ATTN: Leo F. Ingram
ATTN: P. Hadala
ATTN: J. G. Jackson
ATTN: John Ehr Gott
ATTN: Ralph Bendinelli

DEPARTMENT OF THE NAVY

Chief of Naval Research
Department of the Navy
ATTN: Chief of Naval Research

Officer In Charge
Civil Engineering Laboratory
Naval Construction Battalion Center
ATTN: J. Allgood
ATTN: Code L31
ATTN: Warren Shaw
ATTN: John Crawford

Director
Naval Research Laboratory
ATTN: Code 1065
ATTN: Control Branch

Commander
Naval Surface Weapons Center
ATTN: Navy Nuclear Programs Office

DEPARTMENT OF THE AIR FORCE

AF Geophysics Laboratory, AFSC
ATTN: Ken Thompson, LNW

AF Weapons Laboratory, AFSC
ATTN: DE-I
ATTN: J. Bratton
ATTN: DEV, M. A. Plamondon
ATTN: DEV, Robert Henny
ATTN: SUL
ATTN: N. H. Froula

ENERGY RESEARCH & DEVELOPMENT ADMINISTRATION

Los Alamos Scientific Laboratory
ATTN: J. McQueen
ATTN: R. Sharp, Jr.
ATTN: Al Davis
ATTN: Report Library
ATTN: A. N. Cos
ATTN: R. R. Brownlee
ATTN: Barbara Germain

ENERGY RESEARCH & DEVELOPMENT ADMINISTRATION
(Continued)

Sandia Laboratories

ATTN: C. Gulisk
ATTN: W. E. Vollendorf
ATTN: C. Broyles
ATTN: W. Weart

US Energy Research & Development Admin.
Nevada Operations Office

ATTN: R. Newman
ATTN: Technical Library

University of California
Lawrence Livermore Laboratory

ATTN: J. R. Hearst
ATTN: V. W. Wheeler
ATTN: L. D. Ramspott
ATTN: H. C. Rodean
ATTN: L-18, L. W. Germain
ATTN: David Oakley

Holmes & Narver, Incorporated
ATTN: K. Dye

Reynolds Electrical & Engineering Co., Inc.
ATTN: Doc. Con. Facility for W. Flangas

OTHER GOVERNMENT AGENCIES

Bureau of Mines
Twin Cities Research Center
ATTN: T. Ricketts
ATTN: T. C. Atchison

Department of the Interior
US Geological Survey
Special Projects Center
ATTN: R. Carroll
ATTN: W. Twenhofel

Department of the Interior
Bureau of Mines
ATTN: L. A. Obert

DEPARTMENT OF DEFENSE CONTRACTORS

Agbabian Associates
ATTN: Document Control
ATTN: C. F. Bagge

Applied Theory, Incorporated
2 cy ATTN: J. Trulio

EG&G Incorporated
San Ramon Operations
ATTN: R. G. Preston

General Electric Company
TEMPO-Center for Advanced Studies
ATTN: DASIAC

University of Illinois
ATTN: N. M. Newmark
ATTN: William Hall

DEPARTMENT OF DEFENSE CONTRACTORS (Continued)

Massachusetts Institute of Technology
ATTN: W. F. Brace

University of Michigan
ATTN: R. McLaughlin

Physics International Company
ATTN: C. Vincent

Electromechanical Systems of New Mexico, Inc.
ATTN: R. A. Shunk

R&D Associates
ATTN: J. Whitener
ATTN: H. L. Brode
ATTN: H. Cooper
ATTN: Jerry Stockton

Stanford Research Institute
ATTN: George Abrahamson
ATTN: H. E. Lindberg

Systems, Science & Software, Incorporated
ATTN: Russ Duff
ATTN: Document Control
ATTN: Donald R. Grine
ATTN: T. Cherry

Weidlinger Associates, Consulting Engineers
ATTN: Melvin L. Baron

University of Wisconsin
Milwaukee Department of Geological Services
ATTN: D. Willis

Pacifica Technology
ATTN: R. Bjork
ATTN: J. Kent

Merritt Cases, Incorporated
ATTN: J. L. Merritt

Engineering Design Analysis Company, Incorporated
ATTN: R. P. Kennedy

Terra Tek, Incorporated
ATTN: S. Green
25 cy ATTN: Janet Grant
ATTN: S. W. Butters
ATTN: R. K. Dropek
ATTN: A. H. Jones

Ken O'Brien & Associates
ATTN: D. Donegan

California Research & Technology
ATTN: K. N. Kreyenhagen

Boeing Aerospace Company
ATTN: James Wooster
ATTN: Ken Friddell